

Oxysterol-LXR signalling in the triple negative breast cancer microenvironment

Alex Websdale

Submitted in accordance with the requirements for the degree of Doctor of
Philosophy

The University of Leeds
School of Food Science and Nutrition

April 2022

Supervised by Associate Professor James L. Thorne¹, Associate Professor
Thomas A. Hughes², Associate Professor Hanne Røberg-Larsen³ and Dr
Giorgia Cioccoloni¹.

School of Food Science and Nutrition, University of Leeds¹, School of Medicine,
University of Leeds² and Department of Chemistry, University of Oslo³.

Declaration

The candidate confirms that the work submitted is his/her own and that appropriate credit has been given where reference has been made to the work of others.

.....

Alex Websdale
April 2022

Acknowledgements

I would first like to thank my main supervisor, Dr James Thorne, for his mentorship throughout my PhD. I would also like to acknowledge my co-supervisors, Dr Thomas A. Hughes, Dr Hanne Røberg-Larsen and Dr Giorgia Cioccoloni for the support they have provided. I would also like to thank all members of the Thorne group, past and present, for their help in experimental work and making time in the lab more enjoyable. Finally, I would like to thank Breast Cancer UK and the School of Food Science and Nutrition, University of Leeds Study Scholarship for funding my PhD.

Abstract

Triple negative breast cancers (TNBCs) are difficult to treat successfully due to the lack of targeted therapies. Instead, cytotoxic chemotherapy and radiotherapy are the most efficient treatments available. A common issue with chemotherapy is the development of multi-drug resistance in tumours, reducing the long-term efficacy of treatments. Studies have shown that elevated circulating cholesterol in TNBC patients associates with an increased risk of treatment failure. Liver x receptors (LXRs) are transcription factors activated by the cholesterol derivatives, oxysterols. Their primary function is the regulation of cholesterol homeostasis but they also regulate expression of chemotherapy resistance protein, P-glycoprotein (Pgp), in non-cancer tissue. Previous work from the Thorne Lab has demonstrated that oxysterol-LXR signalling can induce Pgp expression in TNBC cells and subsequently enhance resistance to chemotherapy.

My first aim was to demonstrate whether intratumour oxysterol content and the proteins responsible for their production correlated with Pgp expression in TNBC tumours, finding this to be true. As oxysterols can be sourced from a variety of cells in the tumour microenvironment (TME), I then investigated whether the fibroblasts of the TME contribute to LXR-mediated upregulation of epithelial Pgp expression. Here, cancer-associated fibroblasts (CAFs) were shown to be potent activators of LXR signalling in epithelial cells through *in silico*, *in vitro* and *in vivo* work in TNBC. CAFs were also shown to upregulate epithelial Pgp expression. Finally, the role of cholesterol esterification was also investigated as this can reduce intratumour oxysterol levels. To achieve this, I performed a meta-analysis that demonstrated how cholesterol esterification enhanced cancer progression through many mechanisms, one of which being through increased intratumour oxysterol content.

In summary, LXR ligands and the enzymes that produce them positively associate with Pgp in TNBC tumours. Furthermore, CAFs are able to secrete oxysterols that activate LXR and induce expression of Pgp in epithelial cells. Finally, I have demonstrated that other cholesterol modifications, such as esterification also influence cancer progression.

Table of Contents

| | |
|--|-----------|
| CHAPTER 1: OVERVIEW | 15 |
| 1.1 RATIONALE | 15 |
| 1.2 OVERALL AIM AND HYPOTHESIS..... | 16 |
| 1.3 OUTPUTS FROM THIS PHD | 16 |
| 1.3.1 <i>Poster presentations</i> | 16 |
| 1.3.2 <i>Oral presentations</i> | 16 |
| 1.3.3 <i>Published peer-reviewed journal articles</i> | 17 |
| 1.3.4 <i>Prizes</i> | 18 |
| 1.3.5 <i>Supervision of BSc/MSc student projects</i> | 18 |
| CHAPTER 2: INTRODUCTION | 19 |
| 2.1 BREAST CANCER..... | 19 |
| 2.1.1 <i>Stage/grade</i> | 19 |
| 2.1.2 <i>Breast cancer subtypes</i> | 20 |
| 2.1.2.1 Luminal A/B | 20 |
| 2.1.2.2 HER2-enriched..... | 21 |
| 2.1.2.3 TNBC/Basal-like/Claudin-low | 21 |
| 2.1.3 <i>Breast cancer treatment</i> | 22 |
| 2.1.3.1 Surgery..... | 22 |
| 2.1.3.2 Radiotherapy | 22 |
| 2.1.3.3 Receptor targeting therapy | 22 |
| 2.1.3.4 Chemotherapy..... | 23 |
| 2.1.4 Prognostic factors for TNBC | 24 |
| 2.1.4.1 Clinical | 24 |
| 2.1.4.2 Lifestyle | 25 |
| 2.1.4.3 Intrinsic..... | 26 |
| 2.2 CHOLESTEROL HOMEOSTASIS AND LXR | 28 |
| 2.2.1 <i>Oxysterols</i> | 30 |
| 2.2.1.1 LXR-oxysterol interaction | 31 |
| 2.2.1.2 Transactivation of LXR | 33 |
| 2.2.2 <i>Esterification</i> | 35 |
| 2.2.3 <i>Sulphation</i> | 36 |
| 2.2.4 <i>Summary</i> | 37 |
| 2.3 STEROLS AND BREAST CANCER | 38 |
| 2.3.1 <i>Expression and regulation of LXRα and LXRβ activity in breast cancer</i> | 38 |
| 2.3.2 <i>Oxysterols</i> | 39 |
| 2.3.2.1 Synthesis and function of 24OHC in breast cancer | 39 |
| 2.3.2.2 Synthesis and function of 25OHC in breast cancer | 39 |
| 2.3.2.3 Synthesis and function of 26OHC in breast cancer | 40 |
| 2.3.3 <i>Esterification</i> | 41 |
| 2.3.3.1 Cholesteryl esters | 41 |
| 2.3.3.2 SOAT | 41 |
| 2.3.3.3 LCAT | 42 |
| 2.4 TUMOUR MICROENVIRONMENT AND OXYSTEROLS | 42 |
| 2.4.1 <i>Autocrine, juxtacrine and paracrine signalling</i> | 43 |
| 2.4.2 <i>TME cells, chemoresistance and oxysterol synthesis</i> | 44 |
| 2.4.2.1 Macrophages | 44 |
| 2.4.2.2 Adipocytes | 46 |
| 2.4.2.3 Fibroblasts | 47 |
| 2.4.2.4 T-cells..... | 48 |
| 2.4.2.5 Other cells..... | 49 |
| 2.4.3 <i>Summary</i> | 51 |
| CHAPTER 3: OXYSTEROL SIGNALLING CAUSES CHEMOTHERAPY RESISTANCE IN TRIPLE NEGATIVE BREAST CANCER..... | 52 |
| 3.1 INTRODUCTION | 52 |

| | |
|--|----|
| 3.2 HYPOTHESIS AND AIMS | 55 |
| 3.3 MATERIALS AND METHODS | 57 |
| 3.3.1 <i>Cell culture</i> | 57 |
| 3.3.2 <i>Drugs and reagents</i> | 57 |
| 3.3.3 <i>Cell culture assays</i> | 57 |
| 3.3.3.1 MTT..... | 57 |
| 3.3.3.2 siRNA knockdowns | 58 |
| 3.3.4 <i>Quantification of gene expression</i> | 58 |
| 3.3.4.1 Extraction of RNA | 58 |
| 3.3.4.2 Conversion of RNA to cDNA | 59 |
| 3.3.4.3 Assessment of gene expression | 59 |
| 3.3.5 <i>Immunohistochemistry</i> | 59 |
| 3.3.5.1 Assessment of antibody accuracy using immunofluorescence | 59 |
| 3.3.5.2 Immunohistochemical staining | 60 |
| 3.3.5.3 Quantification of immunohistochemical staining | 61 |
| 3.3.5.4 Generation of tissue microarray | 62 |
| 3.3.6 <i>TCGA dataset analysis</i> | 63 |
| 3.3.7 <i>Analysis of oxysterol content in tumour</i> | 64 |
| 3.3.7.1 Liquid chromatography with tandem mass spectrometry analysis of tumour oxysterol content ... | 64 |
| 3.3.7.2 Tissue RNA extraction and gene expression analysis..... | 65 |
| Three tumour 5 mg slices were taken from different areas of the breast tumour tissue for gene expression analysis. Tumour tissue was homogenised in LBA + TG buffer to inactivate resident tissue ribonucleases. Following this step, RNA extraction was continued following section 3.3.4.1 “Extraction of RNA”. cDNA synthesis and gene expression was performed following section “3.3.4.2 Conversion of RNA to cDNA” and | 65 |
| 3.3.4.3 “Assessment of gene expression”..... | 65 |
| 3.4 RESULTS..... | 66 |
| 3.4.1 <i>LXR-mediated chemotherapy resistance is mediated by Pgp in triple-negative breast cancer cells</i> | 66 |
| 3.4.2 <i>CH25H correlates with ABCB1 at mRNA level in primary TNBC samples</i> | 67 |
| 3.4.3 <i>Oxysterol synthesising enzymes correlate with expression of Pgp in triple negative breast tumours at protein level</i> | 68 |
| 3.4.4 <i>The intratumour correlation between 24OHC and Pgp is decoupled in ER-negative, No Event patients</i> | 70 |
| 3.4.5 <i>High expression of CYP46A1 and CH25H associate with reduced disease-free survival in triple-negative breast cancer</i> | 71 |
| 3.4.6 <i>High concentrations of 24OHC, 25OHC and 26OHC associate with reduced disease-free survival in ER-negative tumours</i> | 73 |
| 3.5 DISCUSSION | 75 |
| 3.6 CONCLUSION..... | 78 |

CHAPTER 4: OXYSTEROLS FROM CANCER-ASSOCIATED FIBROBLASTS IMPACT LXR SIGNALLING IN TRIPLE NEGATIVE BREAST CANCER..... 80

| | |
|---|----|
| 4.1 INTRODUCTION | 80 |
| 4.2 HYPOTHESIS AND AIMS..... | 82 |
| 4.3 MATERIALS AND METHODS | 83 |
| 4.3.1 <i>Systematic review</i> | 83 |
| 4.3.1.1 Search strategy | 83 |
| 4.3.1.2 Study selection | 83 |
| 4.3.2 <i>TCGA and METABRIC dataset analysis</i> | 84 |
| 4.3.2.1 Data extraction and analysis | 84 |
| 4.3.2.2 Generation of heatmaps | 86 |
| 4.3.3 <i>Cell culture assays</i> | 86 |
| 4.3.3.1 Cell lines..... | 86 |
| 4.3.3.2 Co-culture | 86 |
| 4.3.3.3 Conditioned media | 87 |
| 4.3.3.4 DMEM acidity assessment..... | 87 |
| 4.3.3.5 Luciferase assay..... | 87 |
| 4.3.3.6 siRNA knockdowns | 87 |

| | |
|---|------------|
| 4.3.4. Immunohistochemistry | 88 |
| 4.3.4.1 Quantification of immunohistochemical staining | 88 |
| 4.3.5 Quantification of gene expression | 88 |
| 4.4 RESULTS | 90 |
| 4.4.1 Expression of multiple CAF marker genes associate with canonical LXR targets | 90 |
| 4.4.1.1 Determining the TNBC-specific CAF marker gene panel | 90 |
| 4.4.1.2 Expression of CAF-marker genes correlates with expression of a subset of LXR target genes in TNBC and BLCL tumours | 96 |
| 4.4.2 Oxysterols secreted by CAFs activate LXR in epithelial cells | 99 |
| 4.4.2.1 Comparison of oxysterol producing enzyme expression and oxysterol concentration in cancer cells and CAFs | 99 |
| 4.4.2.2 CAFs require oxysterol synthesising enzymes to activate LXR in adjacent TNBC cells | 102 |
| 4.4.2.3 CAF conditioned media activates LXR in TNBC cells | 104 |
| 4.4.3 Stromal oxysterol synthesising enzymes associate with epithelial Pgp expression | 106 |
| 4.4.3.1 Stromal expression of oxysterol producing enzymes associates with DFS and epithelial Pgp expression | 106 |
| 4.4.3.2 Combining stromal expression of oxysterol producing enzymes and stromal proportion strengthens the association with epithelial Pgp expression | 108 |
| 4.5 DISCUSSION | 110 |
| 4.6 CONCLUSION | 115 |
| CHAPTER 5: PHARMACOLOGIC AND GENETIC INHIBITION OF CHOLESTEROL ESTERIFICATION IMPAIRS CANCER PROGRESSION – A SYSTEMATIC REVIEW AND META-ANALYSIS OF PRECLINICAL MODELS ... | 116 |
| 5.1 INTRODUCTION | 116 |
| 5.2 HYPOTHESIS AND AIMS | 120 |
| 5.3 MATERIALS AND METHODS | 121 |
| 5.3.1 Search strategy | 121 |
| 5.3.2 Study selection | 121 |
| 5.3.3 Data extraction | 122 |
| 5.3.4 Statistical analysis | 122 |
| 5.3.5 Publication bias | 122 |
| 5.3.6 Risk of bias | 123 |
| 5.4 STUDY CHARACTERISTICS | 124 |
| 5.4.1 Records returned | 124 |
| 5.4.2 Cancer sites | 124 |
| 5.4.3 Interventions and dosing | 124 |
| 5.5 RESULTS | 127 |
| 5.5.1 Cholesteryl esters are concentrated in tumour tissue | 127 |
| 5.5.2 SOAT promotes tumour growth | 128 |
| 5.5.2.1 Brain cancer | 129 |
| 5.5.2.2 Liver cancer | 130 |
| 5.5.2.3 Pancreatic cancer | 131 |
| 5.5.2.4 Prostate cancer | 132 |
| 5.5.2.5 Skin cancer | 133 |
| 5.5.2.6 Other cancers | 134 |
| 5.5.3 SOAT expression is associated with enhancement of cancer hallmarks | 135 |
| 5.5.3.1 SOAT inhibition prolongs survival | 135 |
| 5.5.3.2 Sustained proliferative signalling | 136 |
| 5.5.3.3 Resisting cell death | 137 |
| 5.5.3.4 Evasion of immune detection | 138 |
| 5.5.3.5 Activating invasion and metastasis | 140 |
| 5.6 RISK OF BIAS | 141 |
| 5.6.1 Study criteria | 141 |
| 5.6.2 Heterogeneity | 142 |
| 5.6.3 Publication bias | 142 |
| 5.7 DISCUSSION | 144 |
| 5.8 CONCLUSION | 149 |
| CHAPTER 6: DISCUSSION | 150 |

| | |
|---|------------|
| 6.1 CHOLESTEROL METABOLISM PATHWAYS ARE LINKED | 150 |
| 6.2 CHOLESTEROL METABOLISM DETERMINES THE TME COMPOSITION | 151 |
| 6.3 FUTURE PROSPECTS | 153 |
| 6.4 CONCLUSION..... | 155 |
| APPENDICES | 156 |
| APPENDIX A SUPPLEMENTARY DATA FOR CHAPTER 3 | 156 |
| APPENDIX B SUPPLEMENTARY DATA FOR CHAPTER 4 | 169 |
| APPENDIX C SUPPLEMENTARY DATA FOR CHAPTER 5 | 176 |
| REFERENCES | 188 |

List of Abbreviations

| Abbreviation | Definition |
|---------------------|--|
| 2,3(S):22(S)23DOS | 2,3;22,23-dioxidosqualene |
| 2,3(S)OS | 3S-squalene-2,3-epoxide |
| 24(S)25EL | 24(S),25-epoxycholesterol |
| α -SMA | α -smooth muscle actin |
| EC | epoxycholesterol |
| OHC | hydroxycholesterol |
| ABCA1 | ATP Binding Cassette Subfamily A Member 1 |
| ABCB1 | ATP Binding Cassette Subfamily B Member 1 |
| ABCG1 | ATP Binding Cassette Subfamily G Member 1 |
| ABCG5 | ATP Binding Cassette Subfamily G Member 5 |
| ABCG8 | ATP Binding Cassette Subfamily G Member 8 |
| AC-T | doxorubicin/ cyclophosphamide/ paclitaxel |
| AF1 | activation function 1 |
| AKR | aldo-keto reductase |
| APOE | apolipoprotein E |
| BCSD | breast cancer-specific death |
| B-cell | bone marrow cell |
| BCN | bicyclononyne |
| BLCL | basal-like and claudin-low |
| BRCA | breast cancer type susceptibility protein |
| Breg | B regulatory cell |
| CAA | cancer associated adipocyte |
| CAF | cancer-associated fibroblast |
| CAM | cancer-associated macrophage |
| CAR | chimeric antigen receptor |
| CCL2 | chemokine (C-C motif) ligand |
| CE | cholesteryl ester |
| CETP | cholesteryl ester transfer protein |
| CH25H | Cholesterol 25-Hydroxylase |
| ChIP-seq | chromatin immunoprecipitation-sequencing |
| CI | confidence intervals |
| CM | conditioned media |
| CML | chronic myelogenous leukaemia |
| CSF-1 | colony stimulating factor |
| CYP11A1 | cytochrome P450 family 11 subfamily A member |
| CYP27A1 | cytochrome P450 family 27 subfamily A member |
| CYP46A1 | cytochrome P450 family 46 subfamily A member |
| CXCL | chemokine (C-X-C motif) ligand |
| DBD | DNA binding domain |
| DC | dendritic cell |
| DCIS | ductal in-situ carcinoma |
| DDA | dendrogenin A |
| DFS | disease-free survival |
| DMEM | Dulbecco's Modified Eagle's Medium |

| | |
|-----------|--|
| DMSO | dimethyl sulphoxide |
| Dr | doctor |
| EPI | epirubicin |
| ER | oestrogen receptor |
| FAP | Fibroblast activation protein |
| FBS | fetal bovine serum |
| FDR | false discover rate |
| FF-MAS | follicular fluid meiosis-activating sterol |
| FFPE | formalin-fixed, paraffin-embedded |
| FSP-1 | fibroblast-specific protein |
| GW | GW 3965 |
| GzmB | granzyme b |
| HER2 | human epidermal growth factor receptor 2 |
| HPRT1 | Hypoxanthine Phosphoribosyltransferase 1 |
| HR | hazard ratio |
| IFN | interferon |
| IG | intra gastric |
| IL | interleukin |
| IP | intraperitoneal |
| IT | intratumoural |
| IV | intravenous |
| KC | ketocholesterol |
| LCAT | lecithin-cholesterol acyltransferase |
| LC-MS/MS | liquid chromatography-tandem mass spectrometry |
| LBD | ligand binding domain |
| LBRTB | Leeds Breast Research Tissue Bank |
| LDL-C | low-density lipoprotein cholesterol |
| LLC | Lewis lung carcinoma |
| LPL | lipoprotein lipase |
| LSS | lanosterol synthase |
| LTHT | Leeds Teaching Hospitals Trust |
| LXR | liver x receptors |
| LXRE | LXR response element |
| MCF7 | michigan cancer foundation 7 |
| MD | mean difference |
| MDA-MB- | M.D.Anderson-metastatic breast |
| METABRIC | Molecular Taxonomy of Breast Cancer International Consortium |
| MHC | major histocompatibility complex |
| MLXIPL | MLX Interacting Protein Like |
| MMTV-PyMT | mammary specific polyomavirus middle T antigen overexpression mouse model |
| NCOR | nuclear receptor corepressor |
| NCT | national clinical trial |
| NGS | normal goat serum |
| NK | natural killer |
| PDGFR | platelet-derived growth factor receptor |
| PDX | patient derived xenograft |

| | |
|---------|---|
| Pgp | permeability-glycoprotein |
| PI3K | phosphatidylinositol 3-kinase |
| PLB | passive lysis buffer |
| PO | per oral |
| PR | progesterone receptor |
| qPCR | quantitative polymerase chain reaction |
| ROB | risk of bias |
| ROC | receiver operating characteristic |
| RNA-seq | RNA-sequencing |
| RR | risk ratio |
| RXR | retinoid X receptor |
| SCC | squamous cell carcinoma |
| SERM | selective oestrogen receptor modulator |
| SMD | standardised mean difference |
| SOAT | sterol-O acyltransferase |
| SREBP1c | sterol regulatory element-binding transcription factor 1c |
| SULT | cytosolic sulfotransferase |
| SQLE | squalene |
| T090 | T0901317 |
| T-cell | thymus cell |
| TCGA | the cancer genome atlas program |
| TGF | transforming growth factor |
| TLR | toll-like receptor |
| TME | tumour microenvironment |
| TNBC | triple negative breast cancer |
| TNF | tumour necrosis factor |
| Tre | tetrazine |
| Treg | T regulatory cell |
| V20 | verapamil |
| VC | vehicle control |
| VEGF | vascular endothelial growth factor |

List of Figures

| | |
|---|-----|
| Figure 2.1 Multiple cholesterol metabolites are LXR ligands. | 29 |
| Figure 2.2 LXR recruitment to the LXRE. | 32 |
| Figure 2.3 Relative transactivation of LXR agonists. | 34 |
| Figure 2.4 Graphical representation of the tumour microenvironment. | 43 |
| Figure 3.1 Natural and synthetic ligands of LXR reduce the efficacy of epirubicin. | 54 |
| Figure 3.2 Graphical Abstract - Can oxysterols confer chemotherapy resistance through LXR-mediated upregulation of Pgp? | 56 |
| Figure 3.3 Intraclass correlation coefficient. | 62 |
| Figure 3.4 LXR confers chemoresistance to epirubicin exclusively through P-glycoprotein. | 66 |
| Figure 3.5 Pgp correlates with LXR α and CH25H at mRNA level in TNBC..... | 67 |
| Figure 3.6 Protein expression of oxysterol producing enzymes, CYP46A1, CH25H and CYP27A1 in stroma correlate with Pgp expression in TNBC epithelial cells. | 69 |
| Figure 3.7 24OHC associates with <i>ABCB1</i> mRNA expression in patients that have suffered an event. | 71 |
| Figure 3.8 High expression of CYP46A1 and CH25H is predictive of reduced disease-free survival. | 72 |
| Figure 3.9 High concentrations of oxysterols are predictive of reduced disease-free survival. | 74 |
| Figure 4.1. Graphical hypothesis: Cancer associated fibroblast transactive LXR signalling in triple negative breast cancer epithelial cells through secreted oxysterols. | 82 |
| Figure 4.2 Decision tree for identifying TNBC-specific CAF marker genes. | 84 |
| Figure 4.3 Study discovery and distribution. | 91 |
| Figure 4.4 Correlations between triple negative breast cancer-specific cancer associated fibroblast markers. | 95 |
| Figure 4.5 Triple negative breast cancer-specific cancer associated fibroblast marker genes correlate with canonical LXR marker genes in triple negative breast tumours. ... | 98 |
| Figure 4.6 CAFs and epithelial cells have differential expression of oxysterol producing enzymes. | 99 |
| Figure 4.7 CAFs contain higher intracellular concentrations of oxysterols than MDA.MB.468s. | 100 |
| Figure 4.8 CAFs secrete higher concentrations of 24OHC and 25OHC than MDA.MB.468s. | 101 |
| Figure 4.9 CAF secretions induce LXR signalling in MDA.MB.468s. | 102 |
| Figure 4.10 Knockdown of oxysterol producing enzymes in CAFs may impair ability to induce LXR. | 103 |
| Figure 4.11 CAF conditioned media induces expression of ABCA1 and ABCB1. | 105 |
| Figure 4.12 High expression of oxysterol producing enzymes in stroma are predictive of reduced disease-free survival and associate with epithelial Pgp expression. | 107 |
| Figure 4.13 Increased tumour stroma associates with likelihood of event and Pgp expression. | 108 |
| Figure 4.14 Stromal expression of oxysterol producing enzymes works synergistically with stromal proportion to improve association with epithelial Pgp expression. | 109 |
| Figure 5.1 Mechanisms of cholesterol esterification..... | 117 |

| | |
|---|-----|
| Figure 5.2 Graphical abstract: How does SOAT inhibition impair cancer progression? | 120 |
| Figure 5.3 Study discovery and distribution. | 126 |
| Figure 5.4 Cholesteryl ester concentration in tumour tissue and matched-normal tissue from control littermates. | 128 |
| Figure 5.5 Change in tumour size following disruption of SOAT in brain cancer. | 129 |
| Figure 5.6 Change in tumour size following disruption of SOAT in liver cancer. | 130 |
| Figure 5.7 Change in tumour size following disruption of SOAT in pancreatic cancer. | 131 |
| Figure 5.8 Change in tumour size following disruption of SOAT in prostate cancer. | 132 |
| Figure 5.9 Change in tumour size following disruption of SOAT in skin cancer. | 133 |
| Figure 5.10 Change in tumour size following disruption of SOAT. | 134 |
| Figure 5.11 Forest plot showing changes in risk of arrival at maximal tumour volume following disruption of SOAT. | 135 |
| Figure 5.12 Forest plots showing changes in proliferation. | 137 |
| Figure 5.13 Forest plots showing changes in apoptosis. | 137 |
| Figure 5.14 Forest plots of change in immune responses following disruption of SOAT. | 139 |
| Figure 5.15 Forest plot showing changes in metastasis. | 140 |
| Figure 5.16 Risk of publication bias. | 143 |

List of Tables

| | |
|--|-----|
| Table 3.1 Table of siRNA used..... | 58 |
| Table 3.2 Taqman assays..... | 59 |
| Table 3.3 List of antibodies. | 61 |
| Table 3.4 Patient characteristics | 63 |
| Table 3.5 Cohort characteristics | 63 |
| Table 3.6 Patient characteristics | 64 |
| Table 4.1 Patient characteristics | 85 |
| Table 4.2 Patient characteristics | 85 |
| Table 4.3 Table of siRNA used..... | 88 |
| Table 4.4 Taqman assays..... | 89 |
| Table 4.5. TNBC-specific CAF marker genes..... | 92 |
| Table 4.6 Table of LXR target genes..... | 96 |
| Table 5.1 SOAT inhibitors assessed in clinical trials..... | 119 |

Chapter 1: Overview

1.1 Rationale

Patients with triple negative breast cancer (TNBC) are unable to benefit from effective receptor-targeting therapies such as tamoxifen and trastuzumab as their tumours lack the cellular receptors that are targeted by these drugs. Therefore, they are treated with non-specific, cytotoxic chemotherapy agents, which cause severe side effects. Resistance to chemotherapy is common, rendering these treatments ineffective. Previous work from the Thorne Lab has demonstrated how chemotherapy resistance can be induced *in vitro* in TNBC through Liver X receptor (LXR) transactivation by cholesterol derivatives called oxysterols (Hutchinson et al., 2021). However, whether this relationship exists in patients is unclear.

Fibroblasts are one of the predominant cells of the tumour microenvironment (TME). Within the TME, fibroblasts receive signals from epithelial cells to induce their conversion from normal fibroblasts to cancer-associated fibroblasts (CAFs), that then induce chemotherapy resistance in TNBC (Farmer et al., 2009; Broad et al., 2021). CAF co-culture with TNBC cell lines increased expression of canonical LXR target gene, *ABCA1* (Camp et al., 2011), however whether this was induced through CAF oxysterol secretions was unclear. Normal fibroblasts produce oxysterols (Kannenberg et al., 2013; Lange et al., 2009; Saucier, S. E. et al., 1985). Therefore, CAFs may contribute to epithelial LXR transactivation and chemotherapy resistance through LXR-mediated upregulation of Pgp.

Oxysterols can also undergo modifications such as esterification (Cases et al., 1998). Subsequently, inhibition of esterification leads to increased intratumour content of unesterified oxysterols in pre-clinical models (Lu, Ming et al., 2013). Cholesterol is also a target of esterification. Furthermore, the role of cholesteryl esters (CEs) in cancer progression is more greatly understood than oxysterol esters. Therefore, CEs have been proposed as a potential target for anticancer therapy (de Gonzalo-Calvo et al., 2015). There are many pre-clinical studies investigating inhibition of cholesterol/oxysterol

esterification in cancer, which can aid the decision to progress potential anti-cancer therapies to clinical trials.

1.2 Overall aim and hypothesis

This project aimed to investigate the oxysterol-LXR axis within TNBC tumours. The hypotheses tested in this project were:

- LXR-mediated Pgp upregulation drives chemotherapy resistance in TNBC tumours (**Chapter 3**).
- CAFs can transactivate epithelial LXR through oxysterol secretions to induce expression of LXR target genes (**Chapter 4**).
- Inhibition of cholesterol and oxysterol esterification in pre-clinical animal models of cancer leads to reduced tumour volume (**Chapter 5**).

1.3 Outputs from this PhD

1.3.1 Poster presentations

1. **Websdale A.**, Hutchinson S.A., Lianto P., Røberg-Larsen H., Wastall L.M., Williams B., Rose A., Sharma N., Hughes T.A. and Thorne J.L. Cholesterol side-chain hydroxylation is associated with expression of P-glycoprotein and disease-free survival in triple negative breast cancer patients. *The 7th PhD conference Food Science and Nutrition*. November 2020.
2. **Websdale A.**, Hutchinson S.A., Lianto P., Røberg-Larsen H., Wastall L.M., Williams B., Rose A., Sharma N., Hughes T.A. and Thorne J.L. Cholesterol side-chain hydroxylation is associated with expression of P-glycoprotein and disease-free survival in triple negative breast cancer patients. *The British Association for Cancer Research (BACR)*. November 2020.

1.3.2 Oral presentations

1. **Websdale A.**, Hutchinson S.A., Lianto P., Røberg-Larsen H., Wastall L.M., Williams B., Rose A., Sharma N., Hughes T.A. and Thorne J.L. Cholesterol Side-Chain Hydroxylation is Associated with Expression of P-glycoprotein and Disease-Free

Survival in Oestrogen Receptor Negative Breast Cancer Patients. *Proceedings of the Nutrition Society*. July 2020.

2. **Websdale A.**, Chalmers P., Chen X., Kiew Y., Luo X., Mwarzi R., Wu R., Cioccoloni G., Røberg-Larsen H., Hughes T.A., Zulyniak M.A. and Thorne J.L. Sterol esterification by SOAT1 increases cancer progression in pre-clinical animal models: a systematic review and meta-analysis. *Proceedings of the Nutrition Society*. July 2021.
3. **Websdale A.**, Chalmers P., Chen X., Kiew Y., Luo X., Mwarzi R., Wu R., Cioccoloni G., Røberg-Larsen H., Hughes T.A., Zulyniak M.A. and Thorne J.L. Pharmacologic and genetic inhibition of cholesterol esterification reduces tumour burden: a pan-cancer systematic review and meta-analysis of preclinical models. *European Network for Oxysterol Research (ENOR)*. September 2021.

1.3.3 Published peer-reviewed journal articles

1. Cioccoloni G., Soteriou C., **Websdale A.**, Wallis L., Zulyniak M.A. and Thorne J.L. Phytosterols and phytostanols and the hallmarks of cancer in model organisms: A systematic review and meta-analysis. *Critical Reviews in Food Science and Nutrition*. **1**, pp. 1-12. Reference (Cioccoloni et al., 2020)
2. Hutchinson S.A.*, **Websdale A.***, Cioccoloni G., Røberg-Larsen H., Lianto P., Kim B., Rose A., Soteriou C., Pramanik A., Wastall L.M., Williams B., Henn M.A., Chen J.J., Ma L., Moore J.B., Nelson E., Hughes T.A. and Thorne J.L. Liver x receptor alpha drives chemoresistance in response to sidechain hydroxycholesterols in triple negative breast cancer. *Oncogene*. **40**, pp. 2872-2883. Reference (Hutchinson et al., 2021)
3. **Websdale A.**, Kiew Y., Chalmers P., Chen X., Cioccoloni G., Hughes T.A., Luo X., Mwarzi R., Piorot M., Røberg-Larsen H., Wu R., Xu M., Zulyniak M.A. and Thorne J.L. Pharmacologic and genetic inhibition of cholesterol esterification enzymes reduces tumour burden: A systematic review and *meta*-analysis of preclinical models. *Biochemical pharmacology*. **144**, pp.108-119. Reference (Websdale et al., 2021)

* denotes co-authorship.

1.3.4 Prizes

1. BACR Executive Committee Choice Poster Prize. *The British Association for Cancer Research (BACR)*. November 2020.
2. Flash Talk Award First Place. *European Network for Oxysterol Research (ENOR)*. September 2021.

1.3.5 Supervision of BSc/MSc student projects

1. Laura Windel - Predicting the response to chemotherapy in breast cancer. 2019 MSc.
2. Xinyu Chen - Modifying activity of sterol O-acyltransferase differentially regulate tumour volume and metastasis compared to unexposed controls: A systematic review and a meta-analysis of pre-clinical animal models. 2020 MSc.
3. Rufaro Mwarazi - Cholesterol esterification and Immune Response in pre-clinical cancer Models: A systematic Review & meta-analysis. 2020 MSc.
4. Ruoying Wu - Cholesterol esterification and sulfation with tumour growth: A meta-analysis of animal models. 2020 MSc.
5. Yi Kiew - Systemic Review & Meta-analysis: Intracellular cholesterol esterification in tumour and non-tumour pre-clinical models. 2021 BSc.
6. Elinor Bally - Cancer associated fibroblasts drive xenobiotic detoxification through secretion of oxysterols in triple negative breast cancer. 2022 MSc.

Chapter 2: Introduction

2.1 Breast cancer

Breast cancer is the most frequently diagnosed cancer worldwide in women, affecting one in eight women (Howlader, 2020). The disease comprises of heterogenous tumours that typically arise from the epithelial cells of the milk ducts or lobules of the breast. In the earliest form of ductal breast cancer, abnormal epithelial cells of the milk duct grow to form ductal carcinoma in situ (DCIS). As these cells grow inside the milk duct and have not yet spread into the breast tissue, DCIS is considered as non-invasive. Once abnormal cells have disseminated from the ducts into the breast tissue, they are now classed as an invasive carcinoma. Carcinomas are the most commonly occurring breast cancer and are divided into multiple subgroups (described in “**2.1.2 Breast cancer subtypes**”). Breast cancers possess a unique microenvironment, typically one rich with hormone secreting adipocytes, fibroblasts that provide structure to the tissue and immune cells, which all have potential to interact with cancer cells.

2.1.1 Stage/grade

Tumour stage describes how far the cancer has progressed, with stages ranging from 0-4. Stage 0 breast cancer denotes that the rapidly proliferating epithelial cells in the breast duct have yet to spread into the surrounding breast, otherwise known as DCIS. Stages 1-3 denote the tumour size and its presence within lymph nodes, with stage 3 classed as the most severe. Stage 4 describes the dissemination of breast cancer beyond the breast to other organs of the body, otherwise rereferred to as metastatic cancer. Diagnosis of tumours into stages provides insight into the most effective course of therapy to take. Furthermore, the abnormality and proliferative rate of cancer cells can be classified through tumour grading. The tumour grade can be measured by quantifying tubule formation, nuclear pleomorphism and mitotic rate (Elston, 1984). Tumours can be classified into low (grade 1), moderate (grade 2) and high (grade 3). Grade 1 tumours tend to grow slowly, whereas grade 3 typically grow faster and are more likely to metastasise.

2.1.2 Breast cancer subtypes

Breast cancer is a highly heterogeneous disease, composed of a variety of subtypes with their own unique features. In a clinical setting, tumour classification relies on immunohistochemical assessment of the oestrogen receptor (ER), progesterone receptor (PR), Ki67 and human epidermal growth factor receptor 2 (HER2). These receptors enable the subgrouping of tumours into luminal A, luminal B, HER2-enriched and triple negative breast cancer (TNBC) subtypes. These receptors are targets for certain anti-cancer therapies. Therefore, classification of breast cancer into subtypes can enable informed treatment decisions to optimise the efficacy of anti-cancer therapy. However, diagnoses based on this 4-protein classification alone can lead to inaccurate prognoses and ineffective therapy selection through intratumour variation in subtype marker expression (Lindström et al., 2018; Rye et al., 2018). Furthermore, variable interpretations of histological subtypes can lead to large differences in predictive prognosis (Parker et al., 2009). To enhance predictive capabilities of subtype prognoses, an array of 50 genes, referred to as PAM50, was employed (Parker et al., 2009). The PAM50 method also considers the tumour size and the nodal status. Clinical subtypes remain within this categorisation method; however, they are not solely bound by receptor status of ER, PR and HER2. Furthermore, the TNBC subtype is replaced with basal-like and claudin-low subtypes (Prat et al., 2010).

2.1.2.1 Luminal A/B

Luminal breast cancers account for 80% of breast cancers (Acheampong et al., 2020). When assessed using immunohistochemistry, luminal A tumours are denoted through the expression of ER and PR, with low Ki67 expression. Luminal B tumours have similar expression profiles for ER and PR to luminal A tumours but have high Ki67 expression. As luminal cancers share expression of ER, they are commonly grouped together as ER-positive breast cancers. When compared to luminal A, luminal B tumours exhibit an increased chance of recurrence (Soliman and Yussif, 2016), metastasis (Viale et al., 2019) and death (Cheang et al., 2009). However, both subtypes are less severe when compared to HER2-enriched and TNBC (Hennigs et al., 2016). For example, over 95% of luminal A patients and 89% of luminal B patients survived five years after diagnosis,

whereas this dropped to 85% in HER2-enriched patients and 78% in TNBC patients (Hennigs et al., 2016).

2.1.2.2 HER2-enriched

Tumours that are negative for hormone receptors (ER and PR) and express high levels of HER2 are classed as HER2-enriched. HER2-enriched tumours account for 15-20% of breast cancers. The subtype has a poor prognosis compared to luminal breast cancers but is favourable in comparison to TNBCs (Hennigs et al., 2016).

2.1.2.3 TNBC/Basal-like/Claudin-low

Tumours expressing neither ER, PR nor HER2 are classified as TNBC and account for approximately 10-15% of breast cancers. Due to the lack of ER expression, TNBC and HER2-enriched tumours are commonly grouped together as ER-negative breast cancers. Of the four subtypes, TNBC has the worst prognosis for overall survival (Onitilo et al., 2009) and metastasis (Kennecke et al., 2010; Dent et al., 2007). If TNBC has metastasised, the chances of survival fall. Median survival time has been reported to be 13.3 months (Kassam et al., 2009) compared to a median of 4.2 years for all TNBC (Dent et al., 2007). Using the PAM50 classification method, tumours may be classified as basal-like or claudin-low, rather than TNBC. However, these two subgroups are not direct derivatives of TNBC, with 5% of basal-like tumours expressing ER (Parker et al., 2009). Furthermore, claudin-low tumours are reported to express ER and PR in low levels (Prat et al., 2010). Claudin-low tumours can be distinguished from basal-like tumours by their low claudin status. Furthermore, claudin-low tumours exhibit comparably high genomic stability and high immune cell infiltration and low proliferative rate compared to basal-like tumours (Fougner et al., 2020; Sabatier et al., 2014). Despite these differences, the subtypes exhibit markedly similar relapse frequencies (Fougner et al., 2020) and prognosis for disease-free survival (DFS) (Sabatier et al., 2014).

2.1.3 Breast cancer treatment

2.1.3.1 Surgery

Surgery is commonly used to remove breast cancers. Patients will either undergo breast-lumpectomy or mastectomy. Lumpectomy is more commonly used to treat stage 1 and 2 tumours (61% of surgery for stage 1 and 2 cancers), whereas mastectomy is typically reserved for stage 3 (68% of cancer treatments for stage 3). Occasionally, stage 4 cancers will be treated with either lumpectomy or mastectomy (5% and 12% of cancer treatments for stage 4, respectively) (DeSantis et al., 2019), however this is rare due to the spread of cancer beyond the breast. Lumpectomy and mastectomy are typically performed in combination with other therapies to prevent the growth of residual tumour cells and reduce the chance of recurrence.

2.1.3.2 Radiotherapy

Radiotherapy is used against all stages, typically in combination with other treatments. Radiation is used to destroy cancer cells that remain after surgical resection of tumours or to target secondary, metastatic tumours that cannot be removed by surgery. Patients can receive either external beam radiation or internal radiation therapy for local treatments. Adjuvant radiotherapy was shown to reduce incidence of locoregional breast cancer recurrence in luminal and TNBC tumours, however does not elicit a significant reduction in HER2-enriched tumour recurrence (Sjöström et al., 2017). This finding appears to be contested, with replacement of adjuvant radiotherapy with chemotherapy resulting in an increased risk of locoregional recurrence in HER2 enriched patients from other studies (Stål et al., 1995; Rakovitch et al., 2012). Furthermore, radiotherapy incites the strongest increase in overall survival in TNBC (Sjöström et al., 2017).

2.1.3.3 Receptor targeting therapy

The expression of ER in breast cancer enables the use of systemic drugs that impair ER function. ER-targeting treatment is termed hormone or endocrine therapy. Tamoxifen is a selective oestrogen receptor modulator (SERM) that prevents the canonical induction of ER activity by blocking oestrogen binding. Tamoxifen is commonly taken as

adjuvant therapy for five years, with the benefits such as reducing the risk of an event or death (HR = 0.59) and reducing the likelihood of treatment failure (Fisher et al., 1989; Colleoni et al., 2006). Furthermore, extended follow up of these patients demonstrated the importance of continued use of tamoxifen post-surgery of up to ten years (Fisher et al., 1996). However, tamoxifen itself is a carcinogen and is linked with increased risk of uterine cancers (Lavie et al., 2008). In post-menopausal women, oestrogen production by the ovaries is significantly reduced (Vermeulen, 1976). Instead, the hormone is predominantly produced from androgen in other tissues, notably adipose tissue. The conversion of androstenedione to oestrone via aromatase activity is the rate-limiting step in androgen-derived oestrogen production. Aromatase inhibitors (AI) were designed to impair the production of oestrogen by aromatase. AIs are taken daily and typically as adjuvant therapy, however some studies suggest that AIs are effective as neoadjuvant therapy (Smith et al., 2005; Dowsett et al., 2006). Comparisons between the AI, anastrozole and tamoxifen showed that anastrozole significantly increased DFS (HR = 0.83) and reduced distant metastases (HR = 0.86) (Howell et al., 2005) and reduced Ki67 positivity (Dowsett et al., 2006) compared to tamoxifen. Furthermore, patients undergoing anastrozole therapy reported fewer side effects than tamoxifen treatment (Howell et al., 2005). Common side effects of these treatments are hot flashes, myalgias and arthralgias (Group et al., 2009). Trastuzumab is a monoclonal antibody that binds to HER2, which is used to treat either HER2 enriched or luminal tumours that express high levels of the HER2 receptor (Nahta et al., 2006).

2.1.3.4 Chemotherapy

Due to the lack of ER or HER2 expression in TNBC, treatments such as tamoxifen, aromatase inhibitors and trastuzumab are ineffective. Instead, cytotoxic chemotherapy and radiotherapy are the most efficient treatments available. As such, the vast majority of TNBC patients are treated with chemotherapy rather than with receptor targeting therapy. Chemotherapy can also be used in conjunction with receptor-specific therapies, such as in patients with ER-positive or HER-enriched cancers, however these patients may also be treated solely with receptor targeting therapies. Chemotherapy is the systemic treatment of patients with cytotoxic agents designed to target the rapid proliferation of cancer cells. Chemotherapy can be performed as adjuvant to surgery to

destroy remaining cancer cells or as neoadjuvant to additionally reduce tumour size before surgery. The most commonly used cytotoxic chemotherapy treatments are doxorubicin/ cyclophosphamide/ paclitaxel (AC-T), docetaxel/ cyclophosphamide and doxorubicin/ cyclophosphamide. The combination of docetaxel and cyclophosphamide was more effective at increasing overall survival in breast cancer patients than doxorubicin and cyclophosphamide (HR = 0.69) (Jones, S. et al., 2009). Nevertheless, the inclusion of doxorubicin in chemotherapy regimens rather than its absence is beneficial (Casper et al., 1987). Furthermore, the addition of taxanes to doxorubicin/cyclophosphamide combination therapy, such as paclitaxel and docetaxel, were found to improve DFS compared to their exclusion (HR = 0.83) (Qin et al., 2011). These treatments have a high risk of nausea and sensory neuropathy (Jones, S.E.S., Michael A et al., 2006).

2.1.4 Prognostic factors for TNBC

2.1.4.1 Clinical

Many tumour and patient characteristics have been identified as useful in predicting patient outcome, with these characteristics termed prognostic factors. Typically, prognostic factors will predict the risk of relapse, metastasis or death from disease, providing patients with an estimated survival time (Hagerty et al., 2004) and allows for evaluation of optimal treatment for the patient (Steyerberg et al., 2013). Prognostic factors can be either modifiable or non-modifiable. Non-modifiable prognostic factors include tumour size (Carter et al., 1989), tumour grade (Rakha et al., 2010), node status (Carter et al., 1989), age (Brandt et al., 2015), heterogeneity of the tumour microenvironment (TME) (Dirat et al., 2011; Mahmoud et al., 2012; Hasebe et al., 2000), mammographic density and response to chemotherapy. Nodal status, tumour size, age at diagnosis and oestrogen receptor status were the most commonly assessed non-modifiable prognostic factors in predicting overall survival, recurrence or both (Phung et al., 2019).

Furthermore, the high heterogeneity of TNBC and limited success of neoadjuvant chemotherapy against the subtype led to further subclassification to enable the identification of target-specific therapies (Lehmann et al., 2011). Analysis of

transcriptome data from 894 TNBC tumours revealed that the subtype could be classified into seven subgroups. Of these seven subgroups, six of them would be classed as basal-like if using the PAM50 classifier, with one subgroup classed as “non-basal” (Masuda et al., 2013). A follow up study assessed these subgroups for their pathological complete response rates to neoadjuvant chemotherapy reporting that some tumour subtypes were significantly more susceptible to chemotherapy treatments than others (Masuda et al., 2013). Two subtypes, basal-like 2 and mesenchymal, were highlighted as associative with an increased chance of relapse and death, whereas tumours of the luminal androgen receptor subtype associated with favourable prognosis (Masuda et al., 2013). However, there was no investigation into the mechanisms behind the reduced sensitivity exhibited by some subgroups.

2.1.4.2 Lifestyle

There is a growing interest amongst breast cancer patients in whether changes to lifestyle can improve prognosis. For example, some modifiable prognostic factors for breast cancer include physical inactivity (Friedenreich, 2010), sleep (Costa, A.R. et al., 2014) and alcohol consumption (Kabat et al., 2011). One area of large interest is the effect of diet and obesity on the risk of breast cancer development and prognosis. A meta-analysis of 43 studies investigating the association between obesity and breast cancer survival demonstrated that overweight patients have an increased risk of death (HR = 1.33; 95% CI: 1.19 to 1.50) (Protani et al., 2010). Increased risk of breast cancer-specific death (BCSD) in overweight patients may be driven through the increased risk of obese women developing triple negative tumours (Vona-Davis et al., 2008). Current evidence suggests that maintaining pre-diagnosis weight minimises risk of early BCSD. Weight loss in patients with a history of cancer was shown to reduce risk of developing breast cancer, irrespective of the intention to lose weight (Luo, J. et al., 2019). However, weight loss post-breast cancer diagnosis is associated with reduced overall survival (Shang et al., 2021) but this was likely unintentional weight loss through cachexia. The influence of intentional weight loss post-breast cancer diagnosis is currently under investigation. Significant weight gain in both pre-menopausal and post-menopausal women the year before breast cancer diagnosis is associated with a 2-fold increased risk of BCSD (Cleveland et al., 2007). Furthermore, weight gain of $\geq 10.0\%$ post-diagnosis

associated with an increased risk of mortality compared to weight maintenance (HR = 1.23; 95% CI: 1.09 to 1.39; $p < 0.001$). However, increased risk of BCSD was not significant (Playdon et al., 2015).

Components of the diet that contribute to obesity have also been identified as modifiable prognostic factors. For example, dietary intake of cholesterol is associated with an increased risk of developing breast cancer (RR = 1.29; 95% CI: 1.06 to 1.56; $p = 0.001$) (Li, C. et al., 2016). Women with high serum cholesterol levels post-diagnosis of breast cancer had significantly worse chances of five-year DFS. Furthermore, when obesity and serum cholesterol levels were combined, the risk of reduced DFS increased further (Tartter et al., 1981). The importance of maintaining low serum cholesterol in risk of breast cancer development and survival is highlighted through studies assessing the influence of statins. Statins are a class of drugs typically prescribed with the intent to reduce patients' circulating LDL-C levels. Statins have been shown to significantly lower risk of diseases linked with high cholesterol levels, such as cardiovascular disease and breast cancers. Regular use of statins pre cancer diagnosis was associated with a reduced risk of breast cancer related death (HR = 0.77; 95% CI: 0.63 to 0.95; $p = 0.014$) (Borgquist et al., 2019). Furthermore, use of statins was significantly associated with a reduced risk of secondary tumour occurrence (HR = 0.68; 95% CI: 0.53 to 0.87; $p = 0.002$) (Wu, C.-Y. et al., 2012). Kumar et al., performed analysis on the development of ER-negative breast tumours in response to statin intake. The study found that patients on statins for over a year before diagnosis had proportionally fewer cases of ER-negative breast cancer (Kumar et al., 2008).

2.1.4.3 Intrinsic

Mutations within oncogenes or tumour suppressor genes are also useful prognostic tools. Breast cancer type susceptibility protein (BRCA) 1 and 2 are tumour suppressors that are commonly mutated in breast cancers and associate with an increased risk of developing breast cancer (Antoniou et al., 2003). BRCA1 mutation-associated breast cancers are more often triple-negative, whereas BRCA2 mutations are more commonly found in luminal cancers (Mavaddat et al., 2012). In TNBC, BRCA1 mutation carrying tumours are associated with more aggressive tumour characteristics than BRCA2-

mutated tumours (Krammer et al., 2017), however there is no difference in DFS or BCSD (De Talhouet et al., 2020). BRCA1 associated breast cancers are often associated with favourable prognosis in pan-breast cancer datasets (De Talhouet et al., 2020), however the evidence is conflicting when stratified by TNBC (Maksimenko et al., 2014; Lee, L.J. et al., 2011; Bayraktar et al., 2011; De Talhouet et al., 2020). Furthermore, mutations to p53 associates with poor prognosis but only in TNBC (Chae et al., 2009). In its normal form, p53 is a tumour suppressor that regulates the cell cycle, DNA repair and apoptosis. Mutations to the p53 gene can result in cells avoiding apoptosis, leading to malignancy. A common missense mutation leads to the production of a truncated p53 protein, which can lead to gain of function properties that promote tumourigenesis. Truncated p53 protein can be assessed by immunohistochemistry. Elevated p53 is associated with higher histological grade and an increased risk of recurrence (Pan, Y. et al., 2017).

During treatment of cancer, tumours may become less responsive to chemotherapy. This occurrence is deemed “chemoresistance” and can be elicited through a variety of methods to inactivate or redistribute drugs. Chemotherapy resistance can occur with both targeted therapies and non-targeted, cytotoxic therapy. Resistance to tamoxifen therapy in luminal A/B cancers is associated with changes in expression of transcriptional coactivators and corepressors that influence ER function at its target promoters. For example, reduced expression of nuclear receptor corepressor (NCOR) 1, abolishes tamoxifen SERM activity and instead, tamoxifen binding encourages canonical agonistic action of ER α both *in vitro* and *in vivo* (Lavinsky et al., 1998; Lu, Renquan et al., 2016). Unlike targeted treatments, mechanisms behind chemoresistance against cytotoxic agents are usually more general. Multidrug resistance proteins present a significant challenge for cytotoxic chemotherapy efficacy. These proteins are transmembrane pumps that perform efflux of xenobiotics from the cell through an ATP-dependent mechanism. Many multidrug resistance proteins are more frequently overexpressed in TNBC when compared to other breast cancer subtypes (Yamada et al., 2013) and are upregulated following neoadjuvant treatment (Guestini et al., 2019; Kim, B. et al., 2013). Multidrug resistance proteins are prognostic markers for reduced DFS (Park, S. et al., 2006; Yamada et al., 2013) and each have nuances in their drug exports (K Tiwari et al., 2011). P-glycoprotein (Pgp), also known as ATP-binding cassette sub-

family B member 1 (ABCB1) or multidrug resistance protein 1, is capable of exporting drugs from cells. Like many multidrug resistance proteins, Pgp is commonly overexpressed in cancers and increased expression in breast cancers is associated with reduced DFS (Linn et al., 1995; Gregorczyk et al., 1996; Tsukamoto et al., 1997). Pgp is more commonly overexpressed in ER-negative cancers (12% of TNBC and 11% of HER2+) than ER-positive cancers (5% for luminal A and B) (Millis et al., 2015).

2.2 Cholesterol homeostasis and LXR

Cholesterol is essential for membrane fluidity and hormone synthesis. Anomalous membrane cholesterol content is associated with various diseases and as such, intracellular cholesterol is highly regulated. To control cholesterol levels, most cells express proteins that regulate its transport, metabolism and storage. Cholesterol derivatives can modulate cholesterol homeostasis by influencing signalling pathways. Furthermore, they can act as allosteric activators or inhibitors of proteins, as found in cholesterol storage pathways (Cases et al., 1998). There are three modifications cholesterol can undergo: esterification, hydroxylation and sulphation. Hydroxylation products of cholesterol, called oxysterols, can also be esterified, sulphated and further hydroxylated. The production and metabolism of oxysterols is summarised in **Figure 1.1**.

2.2.1 Oxysterols

Oxysterols are derivatives of cholesterol produced by hydroxylation of the carbon-hydrogen bonds. Hydroxylation of cholesterol requires either an enzymatic reaction or reactive oxygen species. There are many hydroxylation sites on cholesterol and each site has biological relevance. As such, different enzymes are responsible for the hydroxylation at different sites to regulate oxysterol production. Cholesterol derived oxysterols can be further classified as side-chain and carbon-ring hydroxycholesterols (OHCs). There are five side-chain hydroxycholesterols generated through enzymatic reactions: 20OHC, 22OHC, 24OHC, 25OHC and 26OHC. These are produced by enzymes CYP11A1 (20OHC and 22OHC) (Strushkevich et al., 2011; Morisaki et al., 1985), CYP46A1 (Lund, E.G et al., 1999), CH25H (Lund, E. G. et al., 1998) and CYP27A1 (Andersson et al., 1989), respectively (**Figure 2.1**). Side-chain hydroxylation is the first step of the metabolism of cholesterol into bile acids and as such, subsequent modifications follow this initial oxidation step. The exception to this is CYP11A1, where production of 22OHC is an intermediary step within a three-step sequential reaction to cleave the side chain and produce pregnenolone (Strushkevich et al., 2011). This may explain the relatively low levels of 22OHC in the circulation and tumours compared to other side-chain hydroxycholesterols (Stiles et al., 2014; Solheim et al., 2019). Side-chain hydroxycholesterols can undergo secondary hydroxylation to form di-hydroxycholesterols. CYP27A1 can perform secondary hydroxylation events on 24OHC, 25OHC (Norlin et al., 2003b) and 26OHC (Pikuleva et al., 1998). CYP7A1 is also capable of hydroxylating C7 of 24OHC (Norlin et al., 2000) and CYP7B1 can hydroxylate 25OHC and 26OHC (Yantsevich et al., 2014), producing di-hydroxycholesterols. Additionally, 24OHC can also be hydroxylated at C7 by CYP39A1 (Li-Hawkins et al., 2000) (**Figure 2.1**). CYP7A1 also hydroxylates cholesterol at the C7 position to produce 7 α OHC (Griffiths et al., 2016a). CYP27A1 can hydroxylate 7 α OHC at C26 to produce 7 α ,26OHC (Griffiths et al., 2016a) and CYP3A4 can hydroxylate at C25 to produce 7 α ,25OHC (Griffiths et al., 2019). CYP3A4 can also hydroxylate cholesterol to produce 4 β OHC (Diczfalusy et al., 2011), which can be hydroxylated at C7 by CYP7A1 (Bodin et al., 2002) (**Figure 2.1**). The relative concentration of oxysterols in circulation can vary massively, likely due to a range of factors. First, differential expression of these catalysing enzymes and their preference for different targets can alter the rate of metabolism of cholesterol into bile acids.

Oxysterols also appear to exhibit different half-lives (Bodin et al., 2002). Furthermore, enzymes can become saturated by the concentration of one metabolite (Mast et al., 2017a), impairing their metabolism of other targets. Oxysterols can be generated from mechanisms other than cholesterol hydroxylation, such as in the case of epoxycholesterols. For example, 24,25EC can be generated both through a shunt in the mevalonate pathway, or by CYP46A1-mediated hydroxylation of desmosterol (Griffiths et al., 2016a).

2.2.1.1 LXR-oxysterol interaction

Originally classified as an orphan nuclear receptor due to the unknown mechanisms behind its activation (Apfel et al., 1994), liver x receptor (LXR) is now known to be primarily activated by oxysterols to varying degrees of potency (Janowski et al., 1999; Lehmann et al., 1997). There are two isoforms of LXR, LXR α and LXR β , which share 77% sequence homology (Bennett et al., 2008). LXR α is found in high levels in the liver, with lower expression levels found in other tissues (Auboeuf et al., 1997), whereas LXR β is more ubiquitously expressed but at consistently low levels (Repa and Mangelsdorf, 2000). The primary function of LXRs is to mediate cellular cholesterol levels through cholesterol export or metabolism (Repa and Mangelsdorf, 2000).

Structurally, LXRs resemble canonical nuclear receptors, with an activation function-1 (AF1), which is involved in coregulator binding, DNA binding domain (DBD), hinge region and ligand binding domain (LBD) (**Figure 2.2A**). The N-terminal domain is the most heterogeneous between the two isoforms, while the DNA binding domain remains highly conserved (Hoerer et al., 2003). The receptors can localise to both the nucleus and cytoplasm (Sevov et al., 2006), suggesting they can shuttle between the two. When unbound to ligand, both LXR α and LXR β are complexed with co-repressors NCOR1 and NCOR2, however LXR β shows considerably weaker attraction to these co-repressors (Hu, X. et al., 2003). Once activated by an oxysterol, LXR displaces its co-repressors, forms a heterodimer with retinoid X receptor α (RXR α) and binds the LXR response element (LXRE) in the promoter regions of LXR target genes (Lou et al., 2014) (**Figure 2.2B**). Alternatively, the LXR/RXR heterodimer can also be initiated by binding of RXR to 9-cis-13,14-dihydroretinoic acid, an RXR agonist (Rühl et al., 2015).

The LXRE consists of two direct hexanucleotide repeats, split by four nucleotides (Apfel et al., 1994). Comparison of LXREs within LXR target gene promoters indicates that while some nucleotides in each half site are subject to variability, others are conserved (Edwards et al., 2002) (**Figure 2.2B**). The biological relevance of LXRE sequence variation for the binding specificity of either LXR α or LXR β is not understood. However, despite the high sequence homology between the DBD of the LXR isoforms, there appears to be differential binding of LXR target promoters.

Cellular LXR α protein levels can be selectively reduced over LXR β due to its significantly shorter half-life by blocking all protein synthesis with cycloheximide. Selective reduction of LXR α shows the distinctions in promoter binding between the LXR isoforms. For example, the *ABCA1* promoter recruits similar levels of LXR α and LXR β but the *SREBP1* promoter favours LXR α recruitment (Ignatova et al., 2013a).

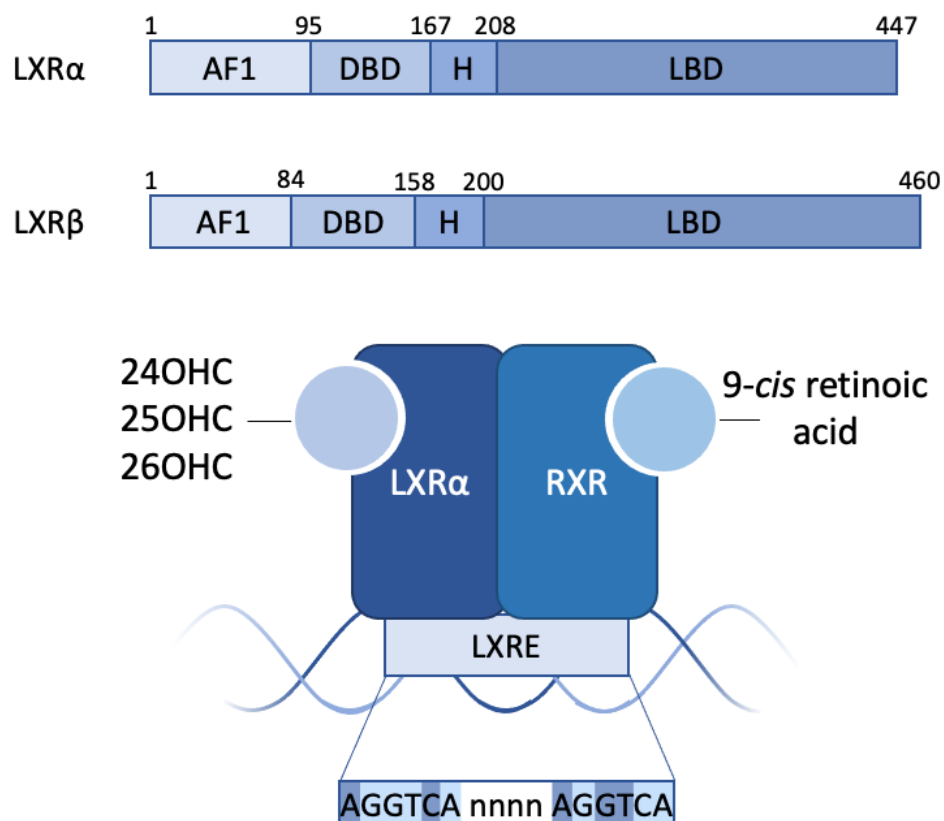


Figure 2.2 LXR recruitment to the LXRE.

(A) Schematic diagrams of LXR α and LXR β . (B) LXR bound to the LXRE in complex with RXR. LXRE is represented with conserved nucleotides in light blue and variable nucleotides in dark blue as reported in literature (Edwards et al., 2002).

2.2.1.2 Transactivation of LXR

Oxysterols can bind and activate LXRs, however the capacity of these oxysterols to activate the receptor appears to be different. 24OHC and 24,25EC are the most efficient LXR ligands for upregulating expression of LXR target genes, whereas 25OHC and 26OHC are 6-fold less potent (Janowski et al., 1999; Hutchinson et al., 2019b; Lehmann et al., 1997) (**Figure 2.3A-B**). X-ray crystallography of LXR α complexed with 22OHC, 24OHC or 26OHC demonstrated variance in receptor contact between the tested oxysterols (Svensson et al., 2003), which may explain their differential potency as LXR α ligands. LXR α and LXR β exhibit similar degrees of activation when treated with oxysterols of different agonistic potencies (Lehmann et al., 1997; Janowski et al., 1999), which may be attributed to the complete conservation of the LBD between the two isoforms (Hoerer et al., 2003). In addition to variable oxysterol ability to activate LXR α , their relative concentration in blood is also different. Mean 26OHC concentration across 3,230 samples was 158-fold higher than 22OHC, the lowest reported concentration of the LXR α ligands (Stiles et al., 2014).

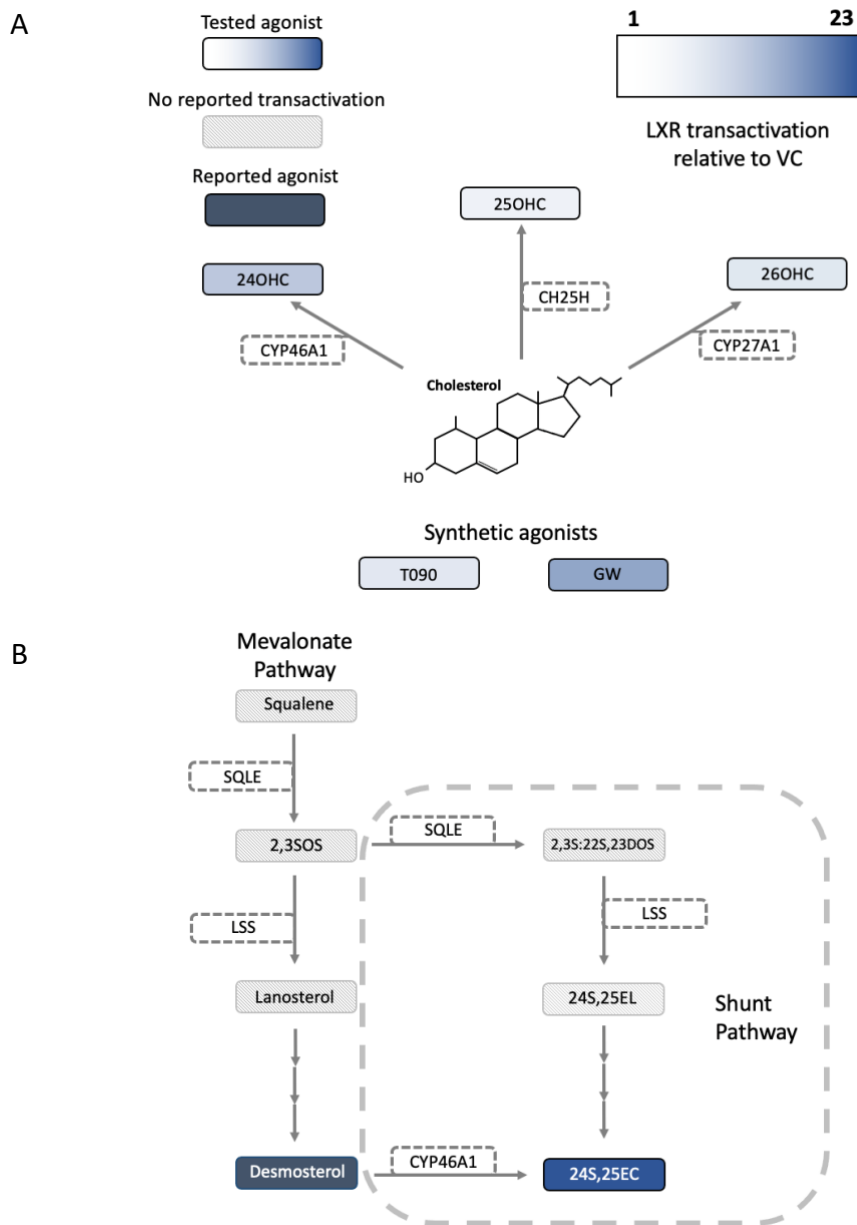


Figure 2.3 Relative transactivation of LXR agonists.

MDA-MB-468 cells were stably transfected with luciferase reporter constructs under the control of the ABCA1 promoter (a canonical LXR α target gene) and treated with known LXR agonists. Cells were treated with 1 μ M of ligand and luciferase signal normalised to vehicle control (VC). Luciferase signal for each agonist tested has been represented as a colour gradient with warmer and cooler shades representing low and high transactivation of LXR respectively. (A) Hydroxylation of cholesterol at either C7, C24, C25 and C26 of cholesterol to produce 24OHC, 25OHC and 26OHC. Additionally, panel A also shows LXR inductive potentials of T090, GW and GSK. (B) Generation of 24,25EC through two individual shunts from the mevalonate pathway. LXR transactivation data has been adapted from Hutchinson et al., (Hutchinson et al., 2019b). Metabolic pathways have been adapted from Griffiths et al., (Griffiths et al., 2016a). T090 = T0901317, GW = GW 3965, 2,3(S)OS = 3S-squalene-2,3-epoxide, 2,3(S):22(S)23DOS = 2,3;22,23-dioxidosqualene, 24(S)25EL = 24(S),25-epoxylanosterol, SQLE = squalene, LSS = lanosterol synthase.

7-ketocholesterol (7KC) transactivates LXR to a similar degree as 25OHC in MDAMB-468 cells (Hutchinson et al., 2019b). Moreover, intermediates of 24,25EC production display moderate LXR agonist function. For example, follicular fluid meiosis-activating sterol (FF-MAS), the subsequent intermediate of cholesterol biogenesis following lanosterol synthesis, reduced viability in squamous cell carcinoma 61 (SCC61) cells overexpressing LXR α . Treatments of FF-MAS matched the reduction in viability elicited by 22OHC treatment and also induced the expression of LXR targets (Gabitova et al., 2015). Desmosterol, another 24,25EC precursor, displays agonistic activity in cells but only where other LXR ligands are absent (Yang, C. et al., 2006). Additionally, dendrogenin A (DDA) can transactivate both LXR isoforms but has a four-fold preference for LXR β . DDA-LXR β signalling upregulates proteins associated with autophagy to induce cell death. However, 22OHC-LXR β signalling represses these proteins, suggesting DDA acts as a selective modulator of LXR (Segala et al., 2017). 5,6EC is an LXR antagonist and reduces efficacy of synthetic LXR ligand, T0901317 (T090), in co-treatments (Berrodin et al., 2010). Frequently used synthetic ligands for LXR are T090 and GW3965 (GW). Additionally, synthetic antagonist GSK2033 is commonly used to assess inhibition of LXR.

Metabolism of oxysterols alters their potency as LXR agonists. For example, hydroxylation at the 7C position of 25OHC to form 7 α ,25OHC impairs its ability to induce expression of canonical LXR target genes. Furthermore, co-treatments of T090 with 7 α ,25OHC impairs the efficacy of T090 treatment on LXR transactivation (Huang, J. et al., 2020). Additionally, 7 α ,26OHC is unable to induce LXR and instead transactivates ROR γ (Soroosh et al., 2014).

2.2.2 Esterification

Cholesterol esterification is a tightly regulated component of homeostatic cholesterol control and enables packaging of cholesterol inside lipid droplets. Lipid droplets act as cholesterol reservoirs and provide an accessible store for hormone production and plasma membrane synthesis in cells. Cholesteryl ester side chain length can vary in size, as can localisation of double bonds in unsaturated side chains (Ren, J. et al., 2017), however the effects this has on cholesterol packaging within lipid droplets are unclear. Esterification of cholesterol can be carried out by acyltransferases. Membrane-bound

O-acyltransferases are a family of endoplasmic reticulum proteins that modify lipids and proteins through the breakdown of acyl-CoA. Sterol-O-acyltransferases (SOAT), SOAT1 and SOAT2, are capable of esterifying cholesterol at the C3 position through incorporation of an acyl group. Each esterification enzyme exhibits preferences over acyl-CoA substrate, with SOAT1 prioritising oleoyl ester production (Qian et al., 2020; Cases et al., 1998), whereas SOAT2 favours palmitoyl ester production (Cases et al., 1998). Lecithin cholesterol acyltransferase (LCAT) also esterifies cholesterol by transferring a fatty acid chain from lecithin to form both monoesters and diesters, depending on the substrate (Szedlacsek et al., 1995). LCAT is expressed highly in the liver and is secreted into plasma, where it circulates in a reversible complex with high density lipoprotein. LCAT preferentially generates oleoyl esters over linoleoyl esters (Szedlacsek et al., 1995). Esterification is not exclusive to cholesterol, with both SOAT1 and SOAT2 shown to esterify side chain hydroxycholesterols 24OHC, 25OHC and 26OHC in H5 insect cells (Cases et al., 1998) (**Figure 1.1**). 24OHC is the preferred substrate of SOAT1 and SOAT2 of the side-chain hydroxycholesterols, with 25OHC being esterified the least. Additionally, other oxysterols were esterified by the SOATs including 7 α OHC, 7KC and 24,25EC (Cases et al., 1998), while purified LCAT can esterify 24OHC (La Marca et al., 2016), 25OHC and 26OHC (Szedlacsek et al., 1995) (**Figure 1.1**). Many of these esterified oxysterols are found in human serum (Yamamuro et al., 2020) and tumour tissue (Solheim et al., 2019). In patients with LCAT deficiencies, there is a significant reduction of esterified 7 α OHC, 24OHC, 25OHC and 26OHC, highlighting the importance of LCAT in esterification in the systemic circulation (Yamamuro et al., 2020). Despite the abundance of esterified oxysterols within organisms, there is no evidence of oxysterol esterification affecting LXR induction. There is no evidence of cholesteryl esters being hydroxylated to become esterified oxysterols.

2.2.3 Sulphation

Sulphation inactivates oxysterols as signalling molecules, particularly in their roles as ligands to LXR (Chen, W. et al., 2007). Reduction of oxysterols through the addition of a sulphate group at C3 by SULT2B1b impairs the ability of 22OHC, 24OHC, 25OHC and 24,25EC to activate LXR (Chen, W. et al., 2007). Cholesterol and oxysterol sulphation is regulated through LXR signalling, with both natural and synthetic agonists inducing an

increase in SULT2B1b expression in CHK cells (Jiang, Y.J. et al., 2005). Cytosolic sulfotransferases (SULTs) mediate the sulphation of a variety of compounds such as hormones, steroids and sterols. Within the SULT superfamily, SULT2 is responsible for the sulphation of steroids and sterols. Cholesterol sulphation is primarily mediated by SULT2B1b, however its isoform, SULT2B1a is capable of cholesterol sulphation but pregnenolone is its preferred substrate (Fuda et al., 2002). SULT2A1 can also mediate cholesterol sulphation, although its preferred substrate is DHEA (Kong et al., 1992). Sulphation of sterols involves the addition of a sulphate moiety at the C3 position. Additionally, SULTs catalyse sulphation of oxysterols. Purified SULT2B1b produces both cholesterol and 26OHC sulphates, at significantly higher levels than SULT2A1 and SULT2B1a (Javitt et al., 2001). The levels of 22OHC, 25OHC and 24,25EC were higher in damaged livers of SULT2B1^{-/-} mice compared to the damaged livers of WT mice (**Figure 1.1**), suggesting that SULT2B1a and SULT2B1b may also be sulphating these oxysterols (Wang, Z. et al., 2017). Purified SULT2A1 and SULT2B1b have demonstrated the ability to sulphate 24OHC (**Figure 1.1**), however SULT2A1 seems to favour the production of disulphates (Cook et al., 2009). Furthermore, purified SULT2B1b catalyses the sulphation of non-side-chain hydroxycholesterols such as 7 α OHC, 7 β OHC, 7KC and several ECs (Fuda et al., 2007).

2.2.4 Summary

Here, the mechanisms of cholesterol homeostasis have been summarised, be it through hydroxylation, esterification or sulphation and how these events are linked. Oxysterols are generated through cholesterol hydroxylation and are LXR agonists. These cholesterol derivatives induce LXR signalling, which in turn regulates components of the cholesterol homeostasis pathway. Each oxysterol has its own potency for LXR transactivation. Further hydroxylation events or sulphation of oxysterols impair their ability to transactivate LXR, however the effect of esterification is unclear. Furthermore, cholesterol esterification allows for cholesterol storage inside intracellular lipid droplets, maintaining cholesterol levels in preparation for processes of high cholesterol requirement, such as plasma membrane synthesis. This process reduces the pool of accessible cholesterol for oxysterol production (Lu, Ming et al., 2013), which may explain the SOAT-inhibitory function demonstrated by some oxysterols (Cases et al., 1998).

2.3 Sterols and breast cancer

2.3.1 Expression and regulation of LXR α and LXR β activity in breast cancer

The LXR α gene, *NR1H3* is predicted to generate 62 transcript variants through alternate splicing (Annalora et al., 2020). LXR α isoforms 1, 4 and 5 produced from these transcript variants act as prognostic markers in TNBC (Lianto et al., 2021). The receptor can be found in both the nucleus and cytoplasm (Sevov et al., 2006). High cytoplasmic LXR α was linked with reduced overall survival in patients with early stage breast cancer (Shao et al., 2021). The concentration of different LXR co-repressor proteins within tumours also have prognostic value. High numbers of functionally deleterious mutations within the *NCOR1* gene associated with poor prognoses and high expression of *NCOR1* associated with improved prognoses in breast cancers (Noblejas-López et al., 2018). Furthermore, *NCOR2* downregulation occurs in triple negative invasive ductal carcinomas compared to normal breast tissue (Kurebayashi et al., 2000). Additionally, expression of LXR α corepressors is significantly lower in ER-negative breast cancers when compared to less LXR α -sensitive, ER-positive breast cancers (Hutchinson et al., 2019b). Once activated by an oxysterol, LXR α displaces these co-repressors, forms a heterodimer with RXR and binds the LXRE (Lou et al., 2014). LXR α negatively regulates its own expression through upregulation of miR-613, which binds to the 3'-untranslated region of *NR1H3* mRNA and prevents its translation into protein (Ou et al., 2011). In TNBC, miR-613 is downregulated when compared to luminal A/B tumours and normal breast (Xiong, H. et al., 2018), again indicating a role for LXR α signalling in the TNBC subtype. There is limited investigation into the role of LXR β in breast cancer. In TNBC, expression of *NR1H2* mRNA was associated with reduced DFS, however this was not the case in ER-positive cancers. High expression of the two LXR β isoforms found in TNBC associated with reduced DFS (Lianto et al., 2021).

2.3.2 Oxysterols

2.3.2.1 Synthesis and function of 24OHC in breast cancer

CYP46A1 is an endoplasmic reticulum protein belonging to the P450 superfamily (Juhasz et al., 2005). The primary function of CYP46A1 is to hydroxylate cholesterol to produce 24OHC (Lund, E.G et al., 1999). Within breast cancer, 24OHC has been shown to induce expression of chemotherapy efflux protein, Pgp, in TNBC cell lines. 24OHC-mediated upregulation of Pgp increases resistance to chemotherapy in TNBC cells (Hutchinson et al., 2021). ER-negative breast tumours contain higher levels of 24OHC than ER-positive (Solheim et al., 2019). CYP39A4, the enzyme responsible for 24OHC metabolism, is downregulated in incidences of ER-positive breast cancer compared to normal tissue (Kloudova et al., 2017) resulting in accumulation of 24OHC in breast tissue. There has been little investigation into CYP46A1 in breast cancers. However, alternate splicing events of CYP46A1 have been related to poor prognosis (Du et al., 2021) but whether these were loss or gain of function splicing events is unclear.

2.3.2.2 Synthesis and function of 25OHC in breast cancer

CH25H resides in the mitochondrial membrane and its sole reported function is the production of 25OHC from cholesterol (Andersson et al., 1989). In addition to agonistic binding to LXR α , 25OHC also activates ER in MCF7 cells (Lappano et al., 2011), exhibiting a similar stimulatory response to oestrogen. CH25H is upregulated in cases of pathological angiogenesis in breast cancer (Guarisch-Sousa et al., 2019), however no mechanistic association was established. There is contrasting data between patient cohorts regarding *CH25H* mRNA and 25OHC metabolite, with low levels of *CH25H* being suggested as a marker for increased distant metastasis in breast cancer (Mittempergher et al., 2013) but the metabolite showing no association (Kloudova-Spalenkova et al., 2020). 25OHC induces expression of Pgp in TNBC cells, however whether this led to resistance to chemotherapy was not shown (Hutchinson et al., 2021). There was no difference between intratumoural content of 25OHC between ER-positive and ER-negative breast tumours.

2.3.2.3 Synthesis and function of 26OHC in breast cancer

CYP27A1, a mitochondrial member of the cytochrome P450 superfamily of enzymes, forms 26OHC from cholesterol (Lund, E. G. et al., 1998). Much like CYP46A1, CYP27A1 has multiple substrates, including cholesterol (Mast et al., 2017b) and is capable of further metabolising both 24OHC and 25OHC (Norlin et al., 2003a). In addition to 26OHC action as an LXR agonist, the ligand acts as a SERM in ER-positive breast cancer cells through alternate cofactor recruitment (DuSell et al., 2008), which has led to a vast amount of research in ER-positive breast cancers. Two separate studies have investigated the role of 26OHC on the ER-positive MCF7 xenograft progression, finding increased tumour weight (Wu, Qian et al., 2013) and volume (Nelson, Erik R et al., 2013) in response to 26OHC treatment. Additionally, 26OHC is present in higher levels in tumour tissue when compared to normal breast tissue (Wu, Qian et al., 2013) and high expression CYP27A1 is associated with a higher tumour grade (Nelson, Erik R et al., 2013), which has been validated in two other cohorts (Kimbung et al., 2017). Contrastingly, high CYP27A1 predicts favourable prognosis for recurrence free survival and overall survival in ER-positive cancers but has no prognostic value in ER-negative cancers (Inasu et al., 2021). 26OHC has also been associated with increased tumour size (Kloudova-Spalenkova et al., 2020). Furthermore, 26OHC treatments increased metastasis to the lung in MMTV-PyMT mice and induced upregulation of metastasis markers (Nelson, Erik R et al., 2013). Following publication of these studies, inhibitors of CYP27A1 have been examined for treatment of ER positive breast cancers (Mast et al., 2015). A subsequent study in TNBC, demonstrated that 26OHC treatment in both E0771 and Met1 cells reduced cytotoxic lymphocyte infiltration into both tumours and metastatic lesions of the lungs (Baek, Amy E et al., 2017). Furthermore, chronic exposure of TNBC cells with 26OHC selects for cells with increased capacity to proliferate and metastasise (Liu, W. et al., 2021). 26OHC has also been shown to induce chemotherapy resistance in TNBC cells through LXR-mediated Pgp upregulation (Hutchinson et al., 2021). Moreover, CYP27A1-positive tumours have also been shown to associate with higher p53 expression compared to CYP27A1-negative (Le Cornet et al., 2020). When compared to ER-positive breast cancer, 26OHC was found at higher levels in both ER-negative breast tissue (Solheim et al., 2019) and cells (Roberg-Larsen et al., 2017).

2.3.3 Esterification

2.3.3.1 Cholesteryl esters

Hydroxylation of cholesterol to oxysterols is not the only mechanism through which cholesterol enhances cancer progression, with cholesteryl esters also associated with poor prognosis. Within breast cancer patients, cholesteryl ester rich tumours associate with higher histological grade and Ki67 positivity (de Gonzalo-Calvo et al., 2015). Furthermore, TNBC tumours contain higher intratumoural cholesteryl ester content than luminal A (de Gonzalo-Calvo et al., 2015). TNBC cell lines exhibit enhanced capacity to produce cholesteryl esters than luminal A and have higher expression of genes essential for lipid droplet formation (Giudetti et al., 2019). TNBC models using UCI-082014 and MDA-MB-231 xenografts found that primary xenografts exhibited higher lipid droplet number than lung metastases from matched models (Wright et al., 2017), suggesting that cholesteryl ester storage is not essential for metastasis.

2.3.3.2 SOAT

Inhibiting both SOAT1 and SOAT2 with CP113,818 results in reduced proliferative (Antalis and Buhman, 2010) and migrative (Antalis et al., 2011) abilities in ER-negative breast cancer cell lines that have been treated with LDL-C. Furthermore, these studies found that MCF7 cells were unresponsive to SOAT inhibition. This may be due to the significantly lower levels of SOAT1 and cholesterol esters in the cells (Antalis et al., 2008) and tumours (Antalis et al., 2011) than that found in ER-negative cells, suggesting a reduced reliance on cholesterol esterification in ER-positive cancers. Enhanced cholesterol ester content in ER-negative breast cancers has been attributed to higher levels of SOAT1 (de Gonzalo-Calvo et al., 2015). Currently, SOAT inhibitors have been studied in human studies as both cancer (Naing et al., 2015; Smith, David C et al., 2020a) and non-cancer treatments (Chang, C. et al., 2006; Tardif et al., 2004). SOAT inhibitor, avasimibe, has been suggested for use in combination with doxorubicin therapy in cancer. Due to the efficacy of avasimibe and doxorubicin co-treatment, the doxorubicin dose could be reduced with no loss in anti-cancer potency, reducing the risk of side effects in patients (Bai et al., 2020). However, the requirement for combination therapy

may be negated in luminal A/B cancer patients, with tamoxifen inhibiting SOAT (de Medina et al., 2004).

2.3.3.3 LCAT

Radiotherapy reduces plasma LCAT, which has been suggested to cause cell membrane dysfunction and impair lipid metabolism in breast cancer patients (Özmen and Askin, 2013). Cholesteryl esters in plasma are lower in breast cancer patients compared to healthy individuals (Subbaiah et al., 1997). Interestingly, there appears to be a greater reliance on LCAT-mediated esterification in aggressive breast tumours, with high LCAT expression associating with reduced overall survival in grade 3 tumours but not in grade 1 or 2 (Park, H.-M. et al., 2020). Basal-like xenograft models express significantly higher levels of LCAT compared to luminal xenograft models (Moestue et al., 2010).

2.4 Tumour microenvironment and oxysterols

The tumour mass and surrounding area is typically heterogeneous and formed from an array of non-cancer cell types together with cancer cells to generate the tumour microenvironment (TME) (Albini and Sporn, 2007). The non-cancer 'host' portion of the tumour comprises immune cells, fibroblasts and adipocytes that secrete factors into the TME impacting molecular signalling pathways of tumour cells (Gouirand et al., 2018) (**Figure 2.4**). Many non-cancer cell types such as macrophages, fibroblasts and adipocytes produce and secrete OHCs. Each of the cell types of the TME exhibit their own potential for oxysterol production through their differential expression of metabolising and catabolising enzymes (Babiker et al., 1997). Within TNBC, high levels of macrophages, fibroblasts and adipocytes are associated with poor prognosis (Yamaguchi et al., 2021; Yuan et al., 2014; Zhou et al., 2018), with one mechanism behind this possibly being paracrine/juxtacrine loading of oxysterols to cancer cells. Furthermore, these cell types have been previously implicated inducing chemotherapy resistance in cancer through alternate mechanisms.

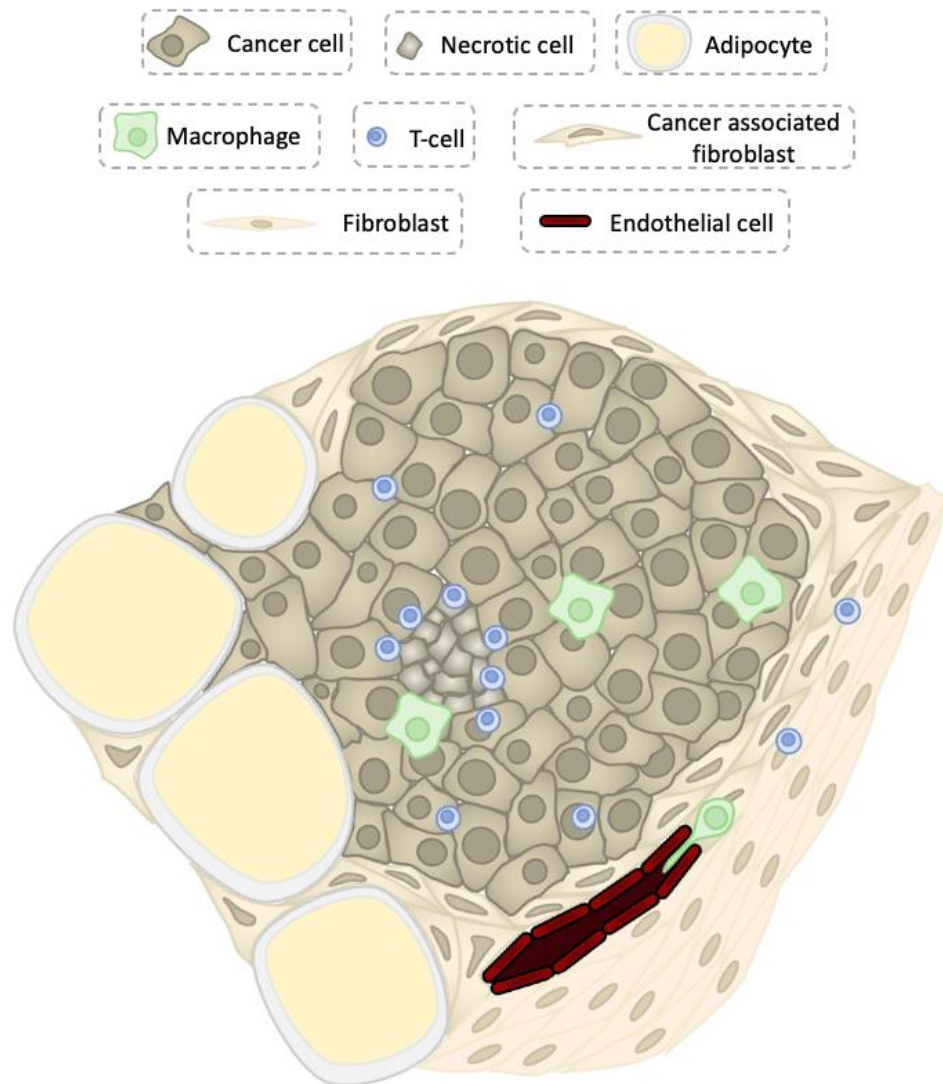


Figure 2.4 Graphical representation of the tumour microenvironment.

2.4.1 Autocrine, juxtacrine and paracrine signalling

Cells of the TME are constantly communicating with each other. The bidirectional signalling between epithelial cells and surrounding non-cancer cells of the TME heavily influences cancer progression. These interactions are mediated through paracrine and juxtacrine signalling, which change and develop throughout the maturation of the TME. Juxtacrine signalling requires cell-cell contact to initiate signalling, for example through gap junctions that allow the transfer of signalling molecules between cells. This mechanism allows for continued signalling between cells by successive cellular interactions. Contrastingly, paracrine signalling does not require contact between communicating cells but instead occurs through intracellular diffusion of signalling

molecules. Furthermore, autocrine signalling may be employed by cells of the TME. Autocrine signalling is the production and secretion of a signalling molecule, which then activates receptors on the same cell to initiate signal transduction.

2.4.2 TME cells, chemoresistance and oxysterol synthesis

2.4.2.1 Macrophages

Macrophages are members of the immune system characterised through their primary function of phagocytosis but also act as antigen presenting cells to activate T-cells. Macrophages are recruited by various chemoattractant protein signals, such as chemokines and growth factors, secreted by resident cells (Varol et al., 2015). Prior to signal stimulation, macrophages exist in the systemic circulation in their undifferentiated state, as monocytes. Upon recognition of a chemoattractant signal, monocytes extravasate from the circulation to the signal origin where they undergo maturation into macrophages. Typically, there are two sub-types that exist under normal conditions, the classically activated M1 macrophages or the alternatively activated M2 macrophages, which have been further subcategorised into M2a, M2b and M2c (Mantovani et al., 2004). M1 macrophages are involved in the defence against invasive pathogens and have also been shown to display anti-tumour properties. M2 macrophages express greater numbers of angiogenic factors, anti-inflammatory cytokines and are generally perceived to be pro-tumourigenic (Mantovani et al., 2002). Macrophages of the TME are termed cancer associated macrophages (CAMs) due to their differences from the traditional subtypes. CAMs are understood to resemble the pro-tumorigenic M2 phenotype, however, differences in secretome and cell surface proteins of CAMs from M2 macrophages has led to the establishment of the M2d subtype.

Triple negative tumours with high CAM infiltration have a significantly reduced rate of pathological complete response (Ye et al., 2021), suggesting macrophage involvement in chemotherapy resistance. There are many CAM-mediated mechanisms that may be driving the association between CAM infiltration and decreased tumour sensitivity to chemotherapy, one such being the secretion of CCL2. Macrophage-derived CCL2 has been found in the lysates of MMTV-PyMT breast tumour models treated with

doxorubicin. The same study established that recruitment of macrophages driven through this mechanism, lead to decreased vascular leakage and thus, reduced doxorubicin distribution to tumour through macrophage MMP9 secretion (Nakasone et al., 2012). Furthermore, treatment of MMTV-PyMT mice with paclitaxel induced an increase in CSF-1 production, enhancing macrophage recruitment to the tumour and increasing vascular density via macrophage secreted VEGF, again disturbing drug diffusion to the tumour. Blockade of CSF-1 signalling through inhibitor PLX-3397 reversed this effect (DeNardo et al., 2011). These findings were replicated in MCF7 mouse xenografts treated with CSF-1 antibodies, resulting in increased sensitivity to 5-fluorouracil, cyclophosphamide and methotrexate (Paulus et al., 2006). The phenotype of CAMs appears to impact chemotherapy resistance. Conditioned media from M2 CAMs compared to M1 induces a significant increase in resistance to doxorubicin treatment (Li, Y. et al., 2018)

In addition to their roles in the immune response, macrophages are adept in oxysterol production. CYP27A1 is expressed in high levels across both M1 and M2 subtypes (Hansson et al., 2003) allowing for 26OHC production. Monocyte 25OHC and 26OHC production is relatively low compared to M1 and M2 macrophages. Expression of CH25H is 90-fold higher after M0 polarisation to M1, with M2 cells having similar levels of CH25H as M0 (Kimura et al., 2016). In the same study, levels of 22OHC and 24OHC were not detected by liquid chromatography-mass spectrometry. Despite this, CYP46A1 is expressed in macrophages infiltrating the spinal cord during early stages of an autoimmune encephalomyelitis (Chu et al., 2018). Furthermore, intracellular 24OHC (in addition to 25OHC and 26OHC) is found in TPH-1 monocytes, suggesting that CYP46A1 expression may be inversely regulated upon differentiation to the M1 and M2 phenotype. Additionally, 24,25EC production has also been established in macrophages (Rowe et al., 2003). Monocytes, M1 and M2 macrophages express significantly higher levels of CYP27A1 and CYP7B1 than ER-positive and ER-negative breast cancer cells. Treatments of TPH-1 monocytes with either ER-positive or ER-negative breast cancer cell conditioned media induces monocyte polarisation to M2 macrophages, which secrete the highest 26OHC of the macrophage subtypes (Shi et al., 2019).

2.4.2.2 Adipocytes

The primary function of adipocytes is the storage of triacylglycerides and cholesterol. The size of these cells is highly variable and dependent on the amount of lipid stored in the cytoplasm. Adipocytes secrete a range of signalling proteins termed adipokines, with their function being involved in energy expenditure (Kajimura, 2017). Within the TME, adipocytes residing nearby a tumour are smaller than those more distal *in vivo*, suggesting that these proximal adipocytes possess a lower density of lipid stores (Nieman et al., 2013). In the TME, adipocytes first undergo a primary dedifferentiation into cancer-associated adipocytes (CAA), subsequently becoming fibroblast-like cells that contribute to the cancer-associated fibroblast (CAF) population (Bochet et al., 2013). This phenotypic change occurs in a Wnt-dependent manner (Bochet et al., 2013). Exosomes produced by cancer cells can also induce this cell line shift (Cho et al., 2012).

Adipocytes have recently been reported to aid cancer progression and specifically chemoresistance. Sheng et al. established that adipocytes not only possess the capability to sequester a chemotherapy drug of the anthracycline family, daunorubicin, but also expresses aldo-keto reductase (AKR) genes, the enzymes involved in the drug's metabolism. Interestingly, fibroblasts could not sequester and metabolise daunorubicin (Sheng et al., 2017), suggesting that this process may be lost following cancer-induced dedifferentiation of the adipocyte. Furthermore, adipocyte CM treated MDA-MB-231s exhibited reduced sensitivity to 48 h treatment with doxorubicin (Mentoor et al., 2021), suggesting that adipocytes can impair anthracycline efficacy through two mechanisms. Additionally, adipocytes derived from obese women impair the anti-proliferative effect of tamoxifen on MCF7s in co-culture. MCF7s treated with adipocyte conditioned media also showed impaired tamoxifen efficacy (Bougaret et al., 2018).

Upon differentiation from adipocyte precursor, pre-adipocytes, CYP27A1 is upregulated and CYP7B1 is downregulated (Li, J. et al., 2014). The same study also established that following adipocyte maturation, CYP11A1 is upregulated, suggesting that adipocytes are capable of 20OHC and 22OHC production (Li, J. et al., 2014). Furthermore, expression of CH25H has been identified in both pre-adipocytes (Guo et al., 2018) and mature adipocytes (Russo et al., 2020), however no study has compared changes in expression

pre and post adipocyte maturation. CYP46A1 expression was recently shown to be positively regulated by calorie intake in adipocytes (Franck et al., 2011). Currently, there appears to be little evidence that suggests adipocyte can produce 24,25EC, however, with the oxysterols' role in cholesterol metabolism, it may be likely it has just yet to be identified.

2.4.2.3 Fibroblasts

The main function of fibroblasts is the production of extracellular matrix and collagen, providing support and segregation for surrounding cells. Fibroblasts exhibit an irregularly branched cytoplasm and possess migratory capabilities, with the cells commonly found in connective tissue. CAF markers are readily expressed in fibroblasts and myofibroblasts but overexpressed in CAFs, such as α -smooth muscle actin (α -SMA), fibroblast activation protein (FAP), caveolin-1, CD29, β -type platelet-derived growth factor receptor (PDGFR β) and fibroblast-specific protein-1 (FSP-1) (Costa, A. et al., 2018). Recently four CAF subtypes using the aforementioned markers were identified, being CAF-S1, 2, 3 and 4. Additionally, these CAF subtypes are specific to breast cancer subtype, with TNBC accumulating CAF-S1 and CAF-S4 in high numbers (Costa, A. et al., 2018). Morphologically, CAFs differ from normal fibroblasts; fibroblasts grown in MCF7 conditioned media increased in length by almost 50% (Vandermoere et al., 2005).

High expression of fibroblast marker genes correlates with a reduced response to treatment with 5-fluorouracil, cyclophosphamide and epirubicin in ER-negative breast cancer (Farmer et al., 2009). Furthermore, CAF co-culture protected claudin-low breast cancer cells (MDA-MB-231 and MDA-MB-157) but not basal-like cells (MDA-MB-468) from epirubicin treatment through IFN β 1 secretion (Broad et al., 2021). CAF conditioned media desensitises MDA-MB-468s to cisplatin therapy (Cosentino et al., 2020). Furthermore, CAFs have also been implicated in inducing chemotherapy resistance in ER-positive cancers. CAF conditioned media reduces efficacy of combination therapy containing doxorubicin, fluorouracil and cisplatin in ER-positive T47D and ZR-75-1 cells (Louault et al., 2019) and CAF IL-6 secretions induce tamoxifen resistance in MCF7 cells (Sun et al., 2014).

Fibroblasts taken from the foreskin have been shown to produce 24OHC, 25OHC and 26OHC, with oxysterols secreted in significantly greater numbers than they are retained within cells (Lange et al., 2009). This finding was confirmed within hip skin fibroblasts; however, variation was found with cellular concentration between the oxysterols (Kannenberg et al., 2013). Interestingly, breast cancer CAFs expressed a mean fold decrease of 0.34 in CH25H expression when compared to normal fibroblasts from healthy donors (Pasanen et al., 2016), suggesting a reduced output for 25OHC production. Fibroblasts have been shown to exhibit 7-hydroxylase capabilities of both 26OHC and 25OHC through the expression of CYP7B1 (Zhang, J. et al., 1995). Furthermore, 24,25-epoxycholesterol (24,25EC) has been demonstrated to be produced in a sufficient concentration to regulate HMG-CoA reductase activity (Saucier, Sandra E et al., 1985).

2.4.2.4 T-cells

T-cells play a role in modulating the adaptive immune response. These cells can be subcategorised into CD4+, CD8+ and Treg cells. CD4+ cells assist in activation of CD8+ cells, which possess the capability to destroy both infected and tumour cells. These cells perform this action through recognition and binding of major histocompatibility complex (MHC) class 1 proteins present on target cells through the T-cell receptor. Binding of MHC proteins stimulates the secretion of cytotoxins to induce apoptosis in the target cell. Treg cells inactivate T-cell-mediated immunity (Santana and Esquivel-Guadarrama, 2006). There is no proposed mechanism behind T-cells altering chemosensitivity in breast cancer. Nevertheless, ER-negative tumours with high T-cell gene markers respond better to neoadjuvant chemotherapy (Rody et al., 2009). Furthermore, low Treg tumour infiltration is associated with pathological complete response after neoadjuvant chemotherapy (Oshi et al., 2020). Additionally, high CD8+ T-cell infiltration associates with increased response to anthracyclines compared to an absence of CD8+ T-cell infiltration in ER-negative breast cancer (Ali et al., 2014).

T-cells possess oxysterol producing properties; however, this ability differs highly between the cell types. CD4+ subtypes, Th1 and Th2, express very low levels of CYP11A1 (Oka et al., 2000), CH25H, CYP27A1 and CYP46A1 (Vigne et al., 2017), allowing for little

production of oxysterols. In terms of CD8+ cells, CYP11A1 very lowly expressed, however when differentiated in the presence of IL-2 and IL-4, this expression was increased massively (Jia, Y. et al., 2013). CYP27A1 is absent in the CD8+ T-cells, suggesting their ability to produce 26OHC is minimal (Sigmundsdottir et al., 2007). Treg cells can produce high levels of 25OHC due to their greatly increased expression level of CH25H over the other T-cells. However, their expression of CYP27A1 and CYP46A1 is equally as low as in CD4+ subtypes (Vigne et al., 2017).

2.4.2.5 Other cells

Dendritic cells (DCs) are members of the adaptive immune system with the primary function of antigen presentation to activate T-cells. These cells exist in two developmental stages; immature and mature. Immature DCs exist in the peripheral tissues, collecting antigens and possess low potential for T-cell activation. Once in contact with an antigen, they are able to migrate to the lymph nodes and mature where they can activate T-cells (Granucci et al., 2005). There are two main subtypes of mature DCs, myeloid DCs and plasmacytoid DCs. DC function is frequently dysregulated in the TME, nullifying their anti-cancer potential. Tumour infiltrating DCs exhibit impaired ability to mature, resulting in a reduced capacity to mount the adaptive immune response towards cancer. Many studies have shown that DC aberration in the TME is due to their retention in an immature state (Bell et al., 1999). Tumour infiltrating DCs also accumulate lipids, leading to complications in antigen presentation (Herber et al., 2010), perhaps explaining why DCs in breast tumours show decreased antigen presentation (Gabilovich et al., 1997). The infiltration of immature DCs associates with higher breast cancer stage (Almand et al., 2000). However, infiltration of DCs using a general DC marker, positively associates with infiltration of CD4 and CD8 T-cells in TNBC. Furthermore, high infiltration also associates with increased overall survival in patients with lymph node metastasis (Lee, H. et al., 2018). Although, infiltration of plasmacytoid DCs is associated with reduced overall survival and relapse-free survival in general breast cancer (Treilleux et al., 2004). Investigation of DCs in the development of breast cancer chemotherapy resistance is limited. However, the maturation of dendritic cells improves the likelihood of pathological complete response in HER2-enriched cancers (Dieci et al., 2016). Nevertheless, a panel of chemotherapy drugs have been shown to

slow the maturation of DCs (Hu, J. et al., 2013). The stage of cancer has also been shown to correlate with DC efficacy, with aggressive cancers containing a higher level of immunosuppressive DCs (Scarlett et al., 2012). With regards to their oxysterol production, DCs are competent producers of 26OHC through high levels of expression of CYP27A1 but are unable to express 25OHC without TLR4 stimulation (Liu et al., 2011b).

Natural killer (NK) cells are cytotoxic lymphocytes that are part of the innate immune response (Rosenau and Moon, 1961; Yang, Q. et al., 2006), with some features of the adaptive immune response (O'Leary et al., 2006; Björkström et al., 2011). Studies have implicated multiple factors involved in NK cell recruitment such as CXCL10 and IL-2 (Albertsson et al., 2003; Wendel et al., 2008) Once stimulated by IL-2, NK cells become reliant on the cytokine and without continued stimulation, they will begin apoptosis within 24 h (Basse et al., 1994). NK cell infiltration into the TME is generally considered to bring a favourable prognosis, with studies showing NK cell depleted tumours develop faster (Guerra et al., 2008). High numbers of activated NK cells are present in HER2-enriched tumours that achieve a pathological complete response to chemotherapy treatment (Muraro et al., 2015). These findings were replicated in a cohort of general breast cancer patients (Kim, R. et al., 2019), suggesting their importance to chemotherapy success. NK cells are proven producers of oxysterols. Murine NK cell expression of CYP7B1 is the greater than that in DCs, macrophages and B-cells but expression is still generally low. Furthermore, murine NK cells do not express CH25H but exhibit high levels of expression of CYP27A1, comparable to that of macrophages. However, TLR4 activation stimulates CYP7B1 and CH25H expression but downregulates CYP27A1 (Liu et al., 2011b). Invariant NK cells, NK cells with an enhanced ability to respond to pro-inflammatory cytokines, express CYP27A1, CYP7A1 and CYP7B1 (Nong et al., 2020). CH25H expression appears to be variable depending on NK derivatives. NK cells sourced from the uterine mucosa have 10-15-fold greater expression of CH25H than endometrial derived NK cells (Kopcow et al., 2010).

B-cells are members of the adaptive immune system and encompass the main subtypes; plasma cells, memory cells and B regulatory (Breg) cells. These cells are all derived from

B-cells and their differentiation is induced through both T-cell dependent and independent responses. Plasma cells act as the main source of antibodies in the body, memory cells are long-lasting B-cells that retain their ability to mount an immune response to a specific antigen and Breg cells are an immunosuppressive cell type (Hoffman et al., 2016). ER-negative tumours with high B-cell gene markers respond better to neoadjuvant chemotherapy (Rody et al., 2009). Additionally, evidence of B-cell clonal selection in triple negative tumours associates with improved response to chemotherapy treatment (Shepherd et al., 2021). B-cells express approximately 3-fold less CYP27A1 than macrophages, DCs and NK cells, suggesting their capacity to produce 26OHC is poor (Liu et al., 2011b). However, B-cells express CH25H but express no CYP7B1, indicating that further metabolism of 25OHC and 26OHC will be minimal (Liu et al., 2011b).

2.4.3 Summary

Cells of the TME have very different roles in cancer progression. However, despite their nuances, all appear to contribute oxysterols to the TME, potentially leading to LXR signalling in epithelial cells. Macrophages, adipocytes and fibroblasts have been shown to induce chemotherapy resistance in epithelial breast cancer cells through a range of mechanisms and their presence in TNBC tumours associate with poor prognosis. Alternatively, T-cells, dendritic cells, NK cells and B-cells appear to offer favourable prognosis and do not have links to induction of chemotherapy resistance. Potentially, distinct oxysterol production between cell types may be a mechanism driving chemotherapy resistance in epithelial cells through paracrine or autocrine signalling.

Chapter 3: Oxysterol signalling causes chemotherapy resistance in triple negative breast cancer

3.1 Introduction

Increased intake of dietary cholesterol is linked to breast cancer development and high circulating LDL-C has been associated with reduced overall survival (Dos Santos et al., 2014). Furthermore, dietary interventions assessing reduced cholesterol intake in breast cancers lead to reduced cancer recurrence (Chlebowski et al., 2006; Toledo et al., 2015) and LDL-C-lowering drug class, statins, can reduce incidence of recurrence (Kwan et al., 2008). Specific enzymes are responsible for the hydroxylation of the cholesterol side chain, for example CYP46A1, CH25H and CYP27A1 produce 24OHC, 25OHC and 26OHC, respectively. Of these oxysterols, 26OHC has been the most robustly investigated in breast cancers and induces metastasis in TNBC (Nelson, Erik R et al., 2013; Baek, Amy E. et al., 2017; Liu, W. et al., 2021).

Within TNBC, pro-cancer actions of oxysterols may be mediated through their transactivation of LXR. Breast cancer cells (Roberg-Larsen et al., 2017) and tumours (Solheim et al., 2019) are capable of producing a variety of oxysterols, however vast differences are found regarding oxysterol content between exosomal and cytoplasmic extracts for Luminal A and TNBC cells. TNBC cells possess a higher proportion of oxysterols retained in the cytoplasm compared to Luminal A, where much of their oxysterol content is released into exosomes. With TNBC cells also having been demonstrated to exhibit a higher sensitivity to LXR signalling than Luminal A cells (Hutchinson et al., 2019b), this may be a symptom of TNBC's enhanced reliance on LXR signalling. However, when assessing tumour tissue, there was no difference in oxysterol concentrations between ER-negative and ER-positive tumours (Solheim et al., 2019). The proficiency of LXR signalling has been demonstrated for ER-negative breast cancer in both cell lines (Hutchinson et al., 2019a) and mouse models (Nelson, E. R. et al., 2013).

TNBC lack the receptors to allow for receptor targeting therapies, leading to use of non-targeted cytotoxic chemotherapy that is accompanied by severe side effects. A common issue with non-targeted therapies is the development of multi-drug chemotherapy resistance in tumours, reducing the long-term efficacy of treatments. Resistance can arise through various mechanisms such as overexpression of the drug metabolising proteins (Van Emburgh et al., 2008), enhancing the DNA repair response (Balko et al., 2014) or through overexpression of chemotherapy efflux pumps that export drugs out of cancer cells (Leonessa and Clarke, 2003). Expression of the chemotherapy efflux pump, Pgp, is positively regulated by LXR in the blood brain barrier by both natural (Saint-Pol et al., 2013) and synthetic LXR ligands (ElAli, Ayman and Hermann, Dirk M, 2012). Furthermore, ChIP-Seq data indicate that treatment of mouse macrophages with synthetic LXR ligand, GW, leads to LXR α recruitment to the Pgp promoter (Oishi et al., 2017). Interestingly, Pgp is most commonly found to be overexpressed in TNBC compared to other subtypes (Millis et al., 2015). LXR is more responsive to ligand in TNBC than other subtypes (Hutchinson et al., 2019b), leading me to examine whether Pgp expression in TNBC may be in part regulated by the oxysterol-LXR pathway.

Previous work from the group indicated that pre-treating MDA-MB-468s with the oxysterols produced by CYP46A1, CH25H and CYP27A1 or synthetic LXR agonist, GW3965, induced resistance (**Figure 3.1A**) to a major Pgp substrate, epirubicin (Wielinga et al., 2000). Oxysterols also improved long-term survival of breast cancer cells following epirubicin insult through colony forming assays. *ABCB1*, the gene that codes for Pgp, was shown to be upregulated in cells treated with a panel of oxysterols or synthetic LXR ligands and suppressed in cells treated with LXR antagonists. Furthermore, gene expression of chemotherapy efflux pumps, *ABCC1* and *ABCG2*, were demonstrated to not be influenced by LXR-signalling in TNBC. To verify whether LXR-mediated resistance to epirubicin was through Pgp, the rate of epirubicin efflux was assessed following treatment with oxysterols and in co-treatment with verapamil, a Pgp inhibitor (**Figure 3.1B**). Furthermore, treatments with LXR ligands were investigated within a preclinical model using a TNBC 4T1 allograft model. Mice were treated every two days with either 30 mg/kg GW3965 or vehicle control for 24 h pre-graft and then after tumour

graft with 2.5 mg/kg epirubicin or vehicle control every 48 h for 12 days. At the end of the 12-day treatment, mice pre-treated with GW exhibited tumours with enhanced resistance to epirubicin treatment, growing to a significantly greater size than tumours from epirubicin treated mice (**Figure 3.1C**). Gene expression of *Abcb1b*, the murine Pgp gene and canonical LXR target, *Abca1*, were assessed, finding that GW3965 significantly upregulated expression of both genes when compared to the control (Hutchinson et al., 2021). These data suggest that in TNBC patients, the enzymes responsible for oxysterol production and the oxysterols they produce may be associated with chemoresistance and cancer relapse through Pgp upregulation. Therefore, this chapter will validate whether LXR induced chemotherapy resistance in cancer cells is driven through LXR-mediated increased expression of Pgp using the MTT assay. Furthermore, IHC, LC-MS/MS and prognostic data will be used to elucidate whether this relationship exists *in vivo*.

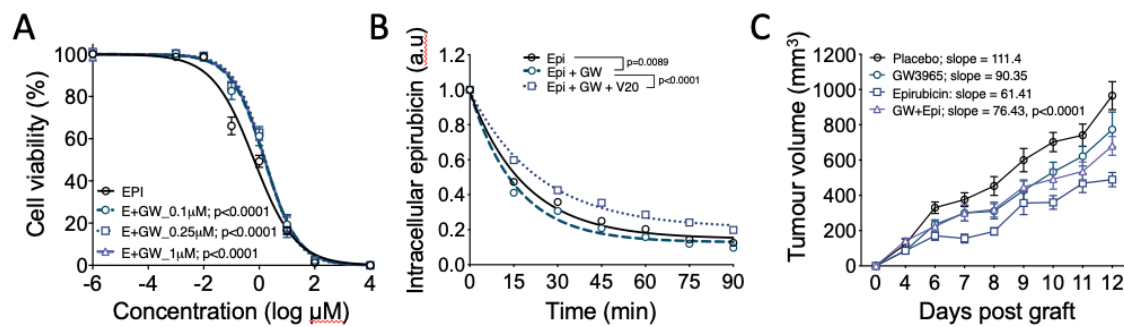


Figure 3.1 Natural and synthetic ligands of LXR reduce the efficacy of epirubicin.

(A) MTT assay of epirubicin dose response following 24 h pre-treatment of GW3965 in MDA-MB-468 cells. Experiments and data analysis performed by Dr Priscilia Lianto. (B) Chemotherapy efflux assay of MDA-MB-468 cells pre-treated with GW3965 or vehicle for 16 h and Pgp inhibitor, V20 (verapamil) or vehicle for 30 minutes before loading with 50 μM epirubicin. Experiments performed by Dr Samantha A. Hutchinson. (C) change in tumour volume of 4T1 allograft model that was treated daily with GW3965 (30 mg/kg), epirubicin or vehicle control. Daily treatments of epirubicin or vehicle control began 48 h post graft. Experiment performed by the group of Erik Nelson (Hutchinson et al., 2021).

3.2 Hypothesis and Aims

Activation of the oxysterol-LXR axis can lead to induction of *ABCB1*/P-glycoprotein expression in blood-brain-barrier, in mouse models of breast cancer and in cell lines. Elevated Pgp is also linked to reduced disease-free survival. Here I tested the hypothesis that in TNBC, expression of enzymes that synthesise endogenous LXR ligands and concentrations of ligands themselves, positively correlate with expression of P-glycoprotein and are prognostic for disease-free survival.

The aims of this chapter were to:

- Validate whether LXR-mediated cancer resistance to epirubicin was mediated by Pgp.
- Establish if oxysterol concentrations and/or expression of oxysterol producing enzymes correlate with P-glycoprotein mRNA and protein expression in TNBC tumours.
- Examine whether protein levels of oxysterol producing enzymes and oxysterol content associate with disease-free survival in ER-negative tumours.

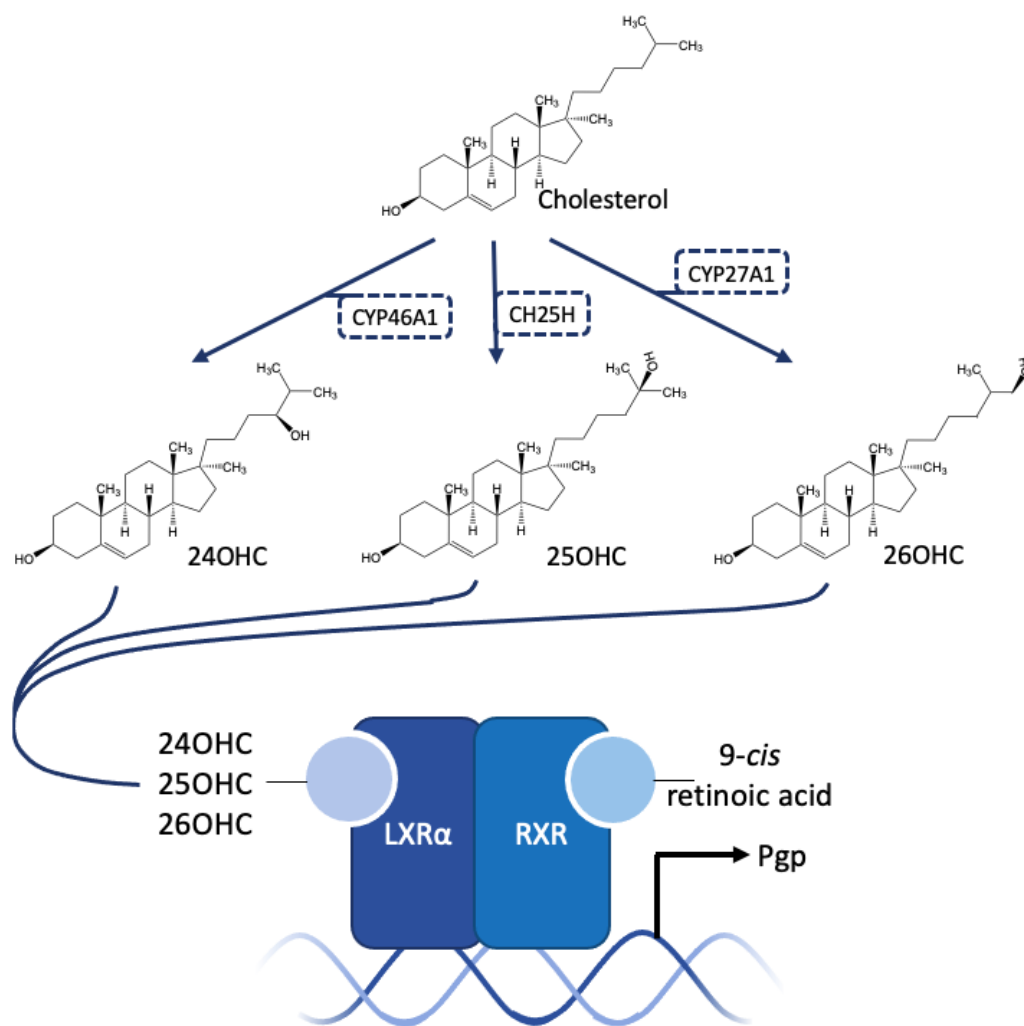


Figure 3.2 Graphical Abstract - Can oxysterols confer chemotherapy resistance through LXR-mediated upregulation of Pgp?

Cholesterol can be modified to form oxysterols through hydroxylation of the cholesterol side chain by CYP46A1, CH25H and CYP27A1 to form 24OHC, 25OHC and 26OHC. I hypothesise that oxysterols can induce resistance to chemotherapy drugs through upregulation of Pgp, a chemotherapy efflux pump, via their agonistic action on LXR α .

3.3 Materials and methods

3.3.1 Cell culture

HepG2, MDA-MB-468 and MCF7 cell lines were sourced from Dr Thomas Hughes and originally from ATCC. Cells were cultured in Dulbecco's Modified Eagle Medium (DMEM) GlutaMAX (31966047, Thermo Fisher Scientific, UK) supplemented with 10% Fetal Bovine Serum (FBS) (11560636, Thermo Fisher, UK) at 37°C, 5% CO². Cells were passaged at 80% confluence and re-plated at 1x10⁶ cells in T75 flasks (10364131, Thermo Fisher Scientific, UK). Cell lines were routinely checked for mycoplasma every 6 months and their identities were authenticated at the start of the project.

3.3.2 Drugs and reagents

Epirubicin (12091, Cambridge bioscience, UK) and GW (2474, ToCris, UK) were stored at -20°C and diluted in nuclease free water and nitrogen flushed ethanol, respectively. 24OHC (700061P), 25OHC (700019P) and 26OHC (700021P) and the deuterated internal standard mixture of 22OHC-d7 (700052P), 25OHC-d6 (700053P) and 26OHC-d6 (700059P) were stored at -20°C in nitrogen flushed ethanol. All oxysterols or deuterated oxysterols were sourced from Avanti Polar Lipids, US.

3.3.3 Cell culture assays

3.3.3.1 MTT

MDA-MB-468s were seeded onto 96 well plates at a density of 2x10⁴ cells per well. Cells were left for 24 h before media was replaced with 200 µL fresh media with VC (1% ethanol) or 1 µM GW dilution in DMEM supplemented with 10% FBS. Cells were incubated a further 24 h before a 0.1 µM of epirubicin was added for 48 h. Cells were washed with PBS and media replaced with 90 µL of phenol red free DMEM (11880036, Thermo Fisher Scientific, UK) with 10 µL solubilised MTT reagent (M2128, Sigma-Aldrich, UK; final concentration 0.5 mg/mL). Cells were incubated for 3 h, media removed and cells washed once with PBS before adding 200 µL of isopropanol, respectively. Absorbance was read using CLARIOstar Plus plate reader (BMG LABTECH, Germany) at 540 nm.

3.3.3.2 siRNA knockdowns

Knockdowns were achieved through transfection with Origene duplexes, USA and scrambled RNA negative control listed (**Table 3.1**). Cells were seeded at a starting cell number of 1.5×10^5 in 2.25 mL of DMEM GlutaMAX in 6-well plates. 24 h after seeding, 250 μ L of OptiMEM (31985062, Thermo Fisher Scientific, UK) containing 30 nM of siRNA duplexes and 3 μ L lipofectamine RNAiMAX (13778030, Thermo Fisher Scientific, UK) were added to the wells. siRNA containing media was replaced with DMEM GlutaMAX after 20 h of exposure. Total siRNA incubation time for assessment of gene and protein expression was 48 and 72 h, respectively. siRNA duplexes used in this chapter are listed in **Table 3.1**.

Table 3.1 Table of siRNA used

Gene names and product codes for siRNA tri-silencers used.

| Gene name | siRNA ID |
|---------------|----------|
| ABCB1 | SR303486 |
| Scrambled RNA | SR322981 |

3.3.4 Quantification of gene expression

3.3.4.1 Extraction of RNA

RNA extraction was performed using the ReliaPrep™ RNA Miniprep System (Z601, Promega, UK). In summary, cells were lysed with 250 μ L BL-TG buffer (Guanidine Thiocyanate + 1-Thioglycerol) and 85 μ L of isopropanol. Cell lysates were transferred to spin columns placed inside collection tubes and centrifuged for 30 seconds at 14,000 rpm. Lysate was washed with 500 μ L of RNA wash buffer and spun at 14,000 rpm for 30 seconds. Lysates then incubated for 15 minutes in DNase 1 incubation mix at room temperature to digest DNA before washing with 150 μ L column wash solution. 15 μ L nuclease free water was used to elute RNA and samples stored at -80°C . RNA yield was measured on LVis Plate (BMG LABTECH, Germany) using CLARIOstar Plus plate reader (company details) with 2 μ L RNA. RNA was assessed for quality absorption at 260/280 nm and quantity through absorption at 260 nm.

3.3.4.2 Conversion of RNA to cDNA

cDNA was generated from 2 µg RNA using the GoScript™ Reverse Transcriptase kit (A5003, Promega, UK). 2 µg RNA was mixed with 0.5 ng random primer per reaction and heated to 70°C for 5 minutes before cooling on ice for a further 5 minutes. 15 µL of master mix solution (5 µl nuclease-free water, 4 µl MgCl₂ (25mM), 4 µl GoScript™ 5x Reaction Buffer RNA, 1 µl PCR nucleotide mix (0.5mM) and 1 µl GoScript™ Reverse Transcriptase) was added to each reaction to reach a final volume of 20 µL per tube. Tubes were then heated at 25°C for 5 min, at 42°C for 59 min, then 70°C for 15 min. Once the cycle is complete, cDNA was diluted in 80 µL nuclease-free water and stored at -20°C.

3.3.4.3 Assessment of gene expression

Gene expression assessment was performed using Taqman Fast Advanced Mastermix (4444557, Thermo Fisher, UK,) with Taqman assays (4331182, Thermo Fisher, UK) with PCR-mediated amplification quantified on a QuantStudio Flex 7 (Applied Biosystems Life Tech, Thermo Scientific, UK) using MicroAmp optical 96-well reaction plates (4306737, Thermo Fisher, UK). The cycling conditions were as follows: two hold stages of 2 minutes at 55°C and then 95°C, followed by 40 cycles at 95°C for 1 second and 60°C for 20 seconds. Gene expression was analysed using $\Delta\Delta CT$ method normalised to Hypoxanthine Phosphoribosyltransferase 1 (HPRT1). Gene expression assays were stored at -20°C and displayed in **Table 3.2**.

Table 3.2 Taqman assays.

Gene names and product codes for Taqman qPCR assays used.

| Gene Name | Taqman ID |
|-----------|------------|
| HPRT1 | Hs02800695 |
| ABCB1 | Hs00184500 |

3.3.5 Immunohistochemistry

3.3.5.1 Assessment of antibody accuracy using immunofluorescence

For protein expression analysis, 150,000 HepG2 or MCF7 cells were seeded onto 22x22 mm coverslips (631-0125, VWR International, UK), treated with siRNA and fixed in 100

µL of 3.7% paraformaldehyde for 15 minutes and washed twice in PBS, at 72 h following siRNA exposure. Cells were incubated in PBS-Tween20 2% (PBS-T) for 30 minutes and blocked with 10% normal goat serum (NGS) (50197Z, Thermo Fisher Scientific, UK) for a further 30 minutes. Primary antibodies were added in optimised concentrations stated in **Table 3.3** in 2% NGS in PBS-T and incubated for 1 h at room temperature. Cells were washed 2 times in PBS-T and incubated for 30 minutes at room temperature with Alexa 647-conjugated secondary antibody against rabbit IgG (A11004, Thermo Fisher Scientific, UK) at 1:1000. Coverslips were washed 4 times with PBS and mounted onto SuperFrost Plus slides (10149870, Menzel-Glaser, Germany) with one drop of Prolong Gold Antifade Mountant with DAPI (P36941, Thermo Fisher Scientific, UK) and imaged using Zen-Imaging software (Zeiss, UK) on an LSM 880 with Airyscan (Zeiss, UK). Knockdown efficiencies were analysed through imaging three fields on each slide, drawing around the perimeter of all cells in the image and quantifying pixel intensity via the Mean Gray Value function in Fiji macOS (LOCI, USA). Optimisation for antibodies targeting CYP46A1, CH25H and CYP27A1 can be found in **Appendix Figure A.1-3**.

3.3.5.2 Immunohistochemical staining

Formalin-fixed, paraffin-embedded (FFPE) sections were dewaxed in 100% xylene (10784001, Fisher Scientific, UK) 3 times for 5 minutes each followed by dehydration in 100% ethanol (32221, Thermo Fisher Scientific, UK) 3 times for 5 minutes each. For anti-Pgp, anti-CYP46A1 and anti-CH25H antibodies, antigen retrieval was not performed. For anti-CYP27A1 antibody, slides were heated in citrate buffer (2.1 g citric acid monohydrate (C1909, Sigma-Aldrich, UK), 700 mL H₂O and 13 mL of 2M NaOH) via microwave for 10 minutes, followed by a cooling period of 20 minutes. Activity of endogenous peroxidase was blocked with 0.3% H₂O₂ (10736291, Fisher Scientific, UK) in methanol (32213, Thermo Fisher Scientific, UK) for 10 minutes. For anti-Pgp, anti-CYP46A1 and anti-CH25H, a further block step was carried out using Blocker™ Casein in TBS (37532, Thermo Fisher Scientific, UK) for 30 minutes. Slides were incubated with antibodies at optimal concentrations (**Table 3.3**, optimisation process shown in **Appendix Figure A.4-7**) for 1 h at room temperature. Staining was visualised using secondary antibodies against rabbit (8114, Cell Signalling Technology, US) and mouse (7076, Cell Signalling Technology, US) primary antibodies for 30 minutes and SignalStain

DAB substrate kit (80595, Cell Signalling Technology, US) kit for 3 minutes at room temperature. Nuclei were stained with Mayer's haematoxylin and washed with Scott's tap water. Sections were dehydrated with ethanol, washed with xylene and mounted onto coverslips with DePeX (Fluka). All antibody stain assays were optimised using tumour samples obtained through ethical approval from Leeds Breast Research Tissue Bank (LBRTB) (reference number: 15/HY/0025).

Table 3.3 List of antibodies.

Antibody name, species that the antibody was generated in, product codes and respective concentrations of antibodies for immunofluorescence and immunohistochemistry.

| Antibody target | Species origin | Product code | Concentration IF | Concentration IHC |
|-----------------|----------------|------------------------------|------------------|-------------------|
| Pgp | Mouse | sc-73354, Santa Cruz Biotech | N/A | 1:500 |
| CYP27A1 | Rabbit | ab126785, Abcam | 1:100 | 1:100 |
| CYP46A1 | Rabbit | ab198889, Abcam | 1:100 | 1:100 |
| CH25H | Rabbit | bs-6480R, Bioss | 1:100 | 1:150 |

3.3.5.3 Quantification of immunohistochemical staining

Positive staining of Pgp, CYP27A1, CH25H and CYP46A1 was assessed semi-quantitatively using a weighted histoscore system. Each tumour was scored in triplicate, with three cores embedded in the tissue microarray (TMA) per tumour. Histoscores between 0-300 were determined, with this value calculated with the formula (1 x % of tumour cells weakly stained) + (2 x % of tumour cells moderately stained) + (3 x % of tumour cells strongly stained). For scoring of TMA sections, whole cores were scored. Tumours were ignored if two or more duplicate cores were missing. Accuracy of primary observer histoscores were verified using the intraclass correlation coefficient (ICC), with 10 triplicate cores selected at random for secondary scoring by an independent observer (either BW or LW [both histopathologists]). ICCs of double scored tumour cores ranged between 0.81 and 0.99 (**Figure 3.3**), all representing an almost perfect agreement (Barry et al., 2010). Parametric correlations analysed through one-tailed Pearson's rank and non-parametric correlations analysed through one-tailed Spearman's rank to a significance of 0.05. Difference of medians was calculated through Welch's t-test or Man-Whitney test depending on whether the groups were normally or not normally

distributed, respectively. To compare survival curves, log rank test was used. Statistical analyses were performed using Prism 8 (GraphPad Software Inc, USA).

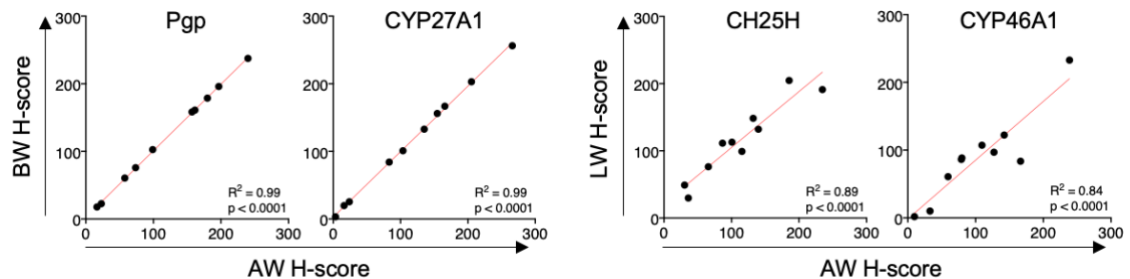


Figure 3.3 Intraclass correlation coefficient.

Intraclass correlation between two independent observers (Alex Websdale [AW] and one of either Dr Bethany Williams [BW] or Dr Laura Wastall [LW], both histopathologists) for Pgp, CYP27A1, CH25H and CYP46A1. Scores given by AW are plotted against secondary scorers, with intraclass correlation coefficient calculated using Pearson’s correlation.

3.3.5.4 Generation of tissue microarray

Ethical approvals were obtained from Leeds (East) REC (reference numbers: 06/Q1206/180, 09/H1306/108). The patient cohort consisted of TNBC tumours as determined by immunohistochemistry from Leeds Teaching Hospitals Trust (LTHT) between 1/01/2008 and 01/10/2012. Further selection criteria for these tumours were that patients had not undergone neoadjuvant therapy, tumour contained sufficient stroma, avoiding heavily necrotic or inflammatory cell rich regions and whether resection blocks were available for normal tissue. Areas suitable for TMA were identified from slides stained with haematoxylin/eosin, with three separate cores of 0.6mm taken and transferred into recipient wax blocks on grid by Dr Laura Wastall (Broad et al., 2021). Clinicopathological features of the cohort are summarised (**Table 3.4**). TMA Blocks were sectioned to 5 μ m onto SuperFrost Plus slides (Menzel-Glaser; Braunschweig, Germany).

Table 3.4 Patient characteristics

Clinicopathological features of the TMA cohort (n = 146).

| Characteristic | Category | TMA No. of patients = 146 (%) |
|-------------------|----------|-------------------------------|
| Tumour Grade | 1 | 2 (2) |
| | 2 | 19 (13) |
| | 3 | 3 (2) |
| Tumour size | ≤ 35 mm | 66 (45) |
| | ≥ 35 mm | 18 (12) |
| | N/A | 64 (43) |
| Survival status | Alive | 101 (68) |
| | Deceased | 47 (32) |
| Recurrence status | None | 102 (69) |
| | Present | 46 (31) |

3.3.6 TCGA dataset analysis

mRNA expression z-scores relative to diploid samples of our gene cohort was obtained from <http://cBioportal.org> (Cerami et al., 2012). Breast cancer gene expression databases provided by The Cancer Genome Atlas (TCGA) used. Expression data were stratified by clinical and PAM50 subtypes, TNBC. To generate TNBC cohorts, clinical information was obtained and filtered for negativity of ER, PR and HER2 status for both TCGA. Clinicopathological features are summarised in **Table 3.5**.

Table 3.5 Cohort characteristics

Clinico-pathological features of the TCGA breast cancer cohort separated by TNBC subtype (n = 123) by hormone receptor status or Basal and Claudin low subtype (n = 85) by PAM50 method.

| Characteristic | Category | TCGA TNBC No. of Patients = 123 (%) |
|-----------------|-------------|-------------------------------------|
| Tumour Stage | 0 | 0 (0) |
| | 1 | 26 (21) |
| | 2 | 82 (66) |
| | 3 | 11 (9) |
| | 4 | 2 (2) |
| | N/A | 2 (2) |
| Survival Status | Alive | 104 (85) |
| | Deceased | 19 (15) |
| PAM50 Subtype | Basal | 76 (62) |
| | HER2 | 5 (4) |
| | Luminal A | 4 (3) |
| | Luminal B | 1 (1) |
| | Normal | 2 (2) |
| | Claudin-low | 0 (0) |
| | N/A | 35 (28) |

3.3.7 Analysis of oxysterol content in tumour

Ethical approvals were obtained from LBRTB through 15/HY/0025 for 47 breast tumours (31 TNBC, 16 HER2 enriched). These samples were cut into nine consecutive slices of 5 mg, with three slices used for assessment of mRNA expression, three for protein expression, and the final three for analysing total, free, and esterified oxysterol concentration. Clinicopathological features of this cohort are summarised in **Table 3.6**.

Table 3.6 Patient characteristics

Clinicopathological features of the LBRTB breast tumour cohort (n = 47).

| Characteristic | Category | LBRTB No. of patients = 47 (%) |
|-------------------|----------|--------------------------------|
| Tumour Grade | 1 | 1 (2) |
| | 2 | 9 (19) |
| | 3 | 37 (79) |
| Tumour size | ≤ 35 mm | 27 (57) |
| | ≥ 35 mm | 20 (43) |
| Survival status | Alive | 25 (53) |
| | Deceased | 22 (47) |
| Recurrence status | None | 23 (49) |
| | Present | 24 (51) |
| HER2+ status | Positive | 16 (34) |
| | Negative | 31 (66) |

3.3.7.1 Liquid chromatography with tandem mass spectrometry analysis of tumour oxysterol content

5 mg tumour slices were homogenised in 500 µL internal standard solution using an IKA T10 Ultra-Turrax homogenizer (VWR). Internal standard solution comprised of 1.5 nM of deuterated 22OHC, 25OHC and 26OHC each in isopropanol and 30 µL of 6 µM cholesterol-25,26,27-13C (for autoxidation monitoring). For assessment of total oxysterol content, alkaline hydrolysis was performed by adding 35 µL of 2M potassium hydroxide in methanol to 100 µL of homogenized sample solutions at heated for 60°C for 120 minutes. Sterols were extracted from sample solution using liquid-liquid extraction with 300 µL of n-hexane and type 1 water solution (1:1), retaining the light phase. Liquid-liquid extraction was repeated a further two times, adding 150 µL of n-hexane. Samples were evaporated in an Eppendorf concentrator plus and resuspended in 100 µL isopropanol. Samples were added to an Oasis PRiME HBL 1 cc (30 mg) SPE cartridge and eluted with methanol, evaporated and resuspended in 20 µL isopropanol.

Samples were treated with cholesterol oxidase 50 mM phosphate buffer pH 7 and heated at 37°C for 60 minutes. Samples were derivatized with a solution of 15 mg Girard's reagent T (G900, Sigma-Aldrich UK), 15 µL glacial acetic acid and 500 µL methanol and left at room temperature overnight. Derivatized samples were stored at 4°C and measured within a week. Sample oxysterol content was measured using a Dionex UltiMate 3000 UHPLC system connected to a TSQ Vantage triple quadrupole mass spectrometer operated in multiple reaction monitoring (MRM) mode. Excess Girard P waste was removed by an on-line HotSEP C18 SPE column (1 mm ID x 5 mm, (Teknolab, Norway)) and subsequently separated on an ACE UltraCore Super PhenylHexyl column (2.1 mm ID x 100 mm, particle diameter 2.5 µm (Advanced Chromatography Technologies LTD, UK)). Peaks were quantified with Xcalibur software (Thermo Fischer Scientific, UK).

3.3.7.2 Tissue RNA extraction and gene expression analysis

Three tumour 5 mg slices were taken from different areas of the breast tumour tissue for gene expression analysis. Tumour tissue was homogenised in LBA + TG buffer to inactivate resident tissue ribonucleases. Following this step, RNA extraction was continued following section 3.3.4.1 "Extraction of RNA". cDNA synthesis and gene expression was performed following section "3.3.4.2 Conversion of RNA to cDNA" and 3.3.4.3 "Assessment of gene expression".

3.4 Results

3.4.1 LXR-mediated chemotherapy resistance is mediated by Pgp in triple-negative breast cancer cells

Previous work had already established that Pgp expression was inducible by LXR ligands (Hutchinson et al., 2021). To establish whether Pgp was mediating the LXR α dependent chemotherapy resistance, cells were treated with epirubicin and LXR agonists with and without knockdown of Pgp expression. To validate siRNA and drug efficacy *ABCB1* mRNA was measured before and after exposure to LXR ligand GW3965 with and without siRNA against Pgp (**Figure 3.4A**). GW3965 induced a 1.5-fold increase in *ABCB1* mRNA expression in siCON treated MDA-MB-468 cells (one-way ANOVA: $p < 0.0001$) and rescued cells from epirubicin mediated cell death (**Figure 3.4B** compare columns 3 and 4). Targeted siRNA reduced *ABCB1* mRNA expression by 10-fold (one-way ANOVA; $p < 0.0001$) and GW3965 failed to increase *ABCB1* mRNA expression under these conditions (one-way ANOVA: $p > 0.05$). In response to epirubicin treatment, cell viability fell by approximately 35% for both siCON+EPI and siPgp+EPI compared to their siCON and siPgp, respectively (one-way ANOVA: $p = 0.0001$ and $p = 0.0004$). GW3965 reversed epirubicin mediated cell death in siCON ($p = 0.0009$) but not in siPGP ($p > 0.05$) treated cells (**Figure 3.4B**). These data supported the hypothesis that GW3965 induced resistance to epirubicin required induction of Pgp.

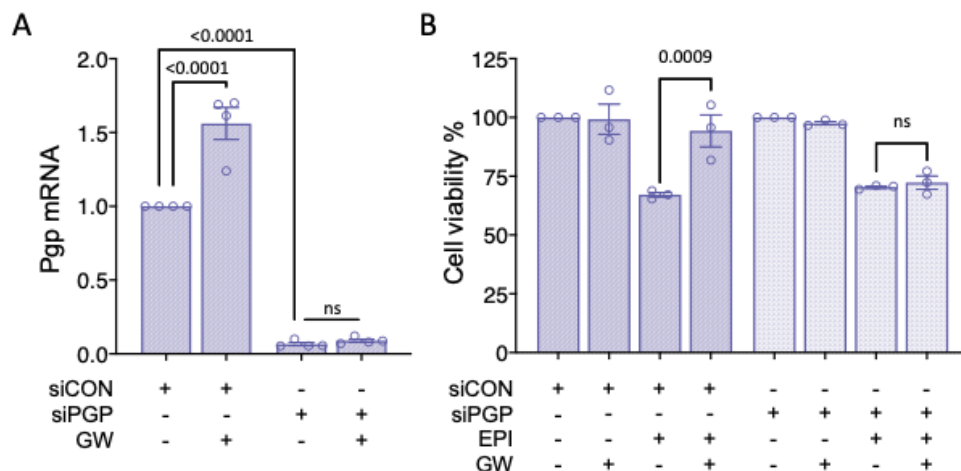


Figure 3.4 LXR confers chemoresistance to epirubicin exclusively through P-glycoprotein.

(A) Pgp expression following 16 h treatment with GW3965 in siCON and siPgp treated cells. (B) MTT in MDA-MB-468 cells after siPgp shows GW3965 no longer enhances protection to epirubicin (EPI) treatment without Pgp expression. Data presented are mean with SEM of 3 independent replicates of 6 technical replicates. P-values calculated using one-way ANOVA with multiple comparisons.

3.4.2 *CH25H* correlates with *ABCB1* at mRNA level in primary TNBC samples

Treatments of synthetic and natural LXR ligands induce Pgp expression and chemotherapy resistance in TNBC cell lines, however this does not represent the physiological environment of the tumour. *CH25H* is a known transcriptional target of LXR (Liu, Y. et al., 2018) and reciprocally its protein product catalyses the synthesis of 25OHC, an LXR ligand (Hutchinson et al., 2019b). To assess if LXR activity was correlated with expression of *ABCB1* in tumours, the mRNA levels of *NR1H3* (the gene that codes for LXR α), *CH25H* and two other oxysterol producing enzymes (*CYP46A1* and *CYP27A1*) were correlated with that of *ABCB1* in a cohort of primary TNBC samples (Koboldt et al., 2012). Assessment of TNBC tumours from the TCGA dataset showed that *NR1H3* and *CH25H*, both positively correlated with *ABCB1* (Figure 3.5; Spearman's rank *NR1H3*: $R^2=0.2$ $p<0.0001$; *CH25H*: $R^2=0.5$, $p<0.001$). Correlations between *CYP46A1* or *CYP27A1* with *ABCB1* were not significant ($p>0.05$). These data indicate that while LXR expression is correlated with its transcriptional targets, its activity, at least in TNBC is not linked to oxysterol products of *CYP46A1* or *CYP27A1*.

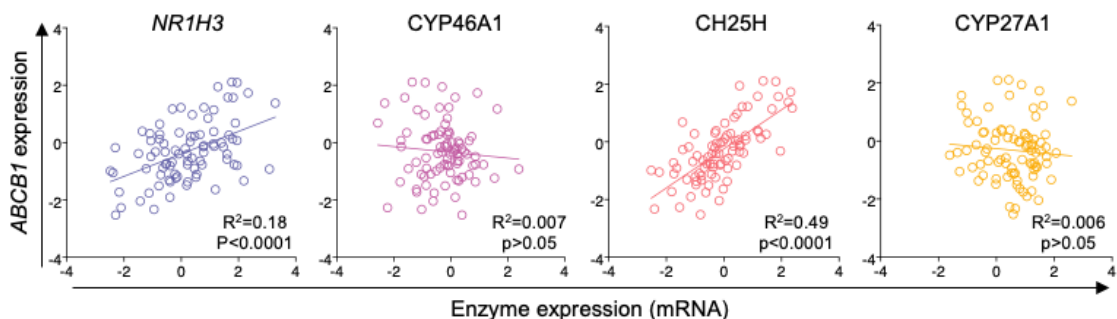


Figure 3.5 Pgp correlates with LXR α and *CH25H* at mRNA level in TNBC.

Correlation analysis of TNBC tumours obtained from TCGA (n=89) dataset accessed via cBioportal. *NR1H3*, *CYP46A1*, *CH25H* and *CYP27A1* are represented along the x-axes and *ABCB1* along the y-axes. Pearson's rank was performed to test for significance from TCGA dataset.

3.4.3 Oxysterol synthesising enzymes correlate with expression of Pgp in triple negative breast tumours at protein level

To confirm whether intratumour production of oxysterols associates with Pgp expression, cancer cell populations within TNBC tumours were assessed for their expression of oxysterol producing enzymes; CYP46A1, CH25H and CYP27A1 and correlated with Pgp expression. All antibodies against oxysterol synthesising enzymes used were validated for their accuracy against their targets (**Appendix Figure A1-3**) and a well-validated (Mechetner and Roninson, 1992) antibody against Pgp used frequently in breast cancer was selected (Thorne et al., 2018; Kim, B. et al., 2013). Optimisation steps for staining of all antibodies are shown in **Appendix Figure A.4-7**. A TMA of 146 pre-treatment TNBC tumours was stained for Pgp and the three oxysterol producing enzymes, all of which were quantified using weighted H-scores (see **Appendix Figure A.8A** for Pgp and **Figure 3.6A** for oxysterol producing enzyme representative images).

Epithelial Pgp was more highly expressed in patients that suffered relapse, metastasis or death (termed 'Event' group) than those that had not (termed 'No Event' group) (**Appendix Figure A.8B**). High epithelial cell expression of Pgp associated with reduced DFS (**Appendix Figure A.8C-D**; log-rank test: $p=0.002$), as has been shown in other general breast cancer cohorts (Gregorcyk et al., 1996; Tsukamoto et al., 1997). Expression of all three enzymes significantly positively correlated with that of Pgp (**Figure 3.6B**; Pearson's rank: CYP46A1: $R^2=0.3$, $p<0.0001$; CH25H: $R^2=0.57$, $p<0.0001$; CYP27A1: $R^2=0.07$, $p=0.0067$). These data suggest that protein expression of oxysterol producing enzymes within TNBC epithelial cells could be important for cancer cell expression of Pgp. Furthermore, these measurements validate previous correlations of mRNA expression (**section 3.4.2**) at the protein level.

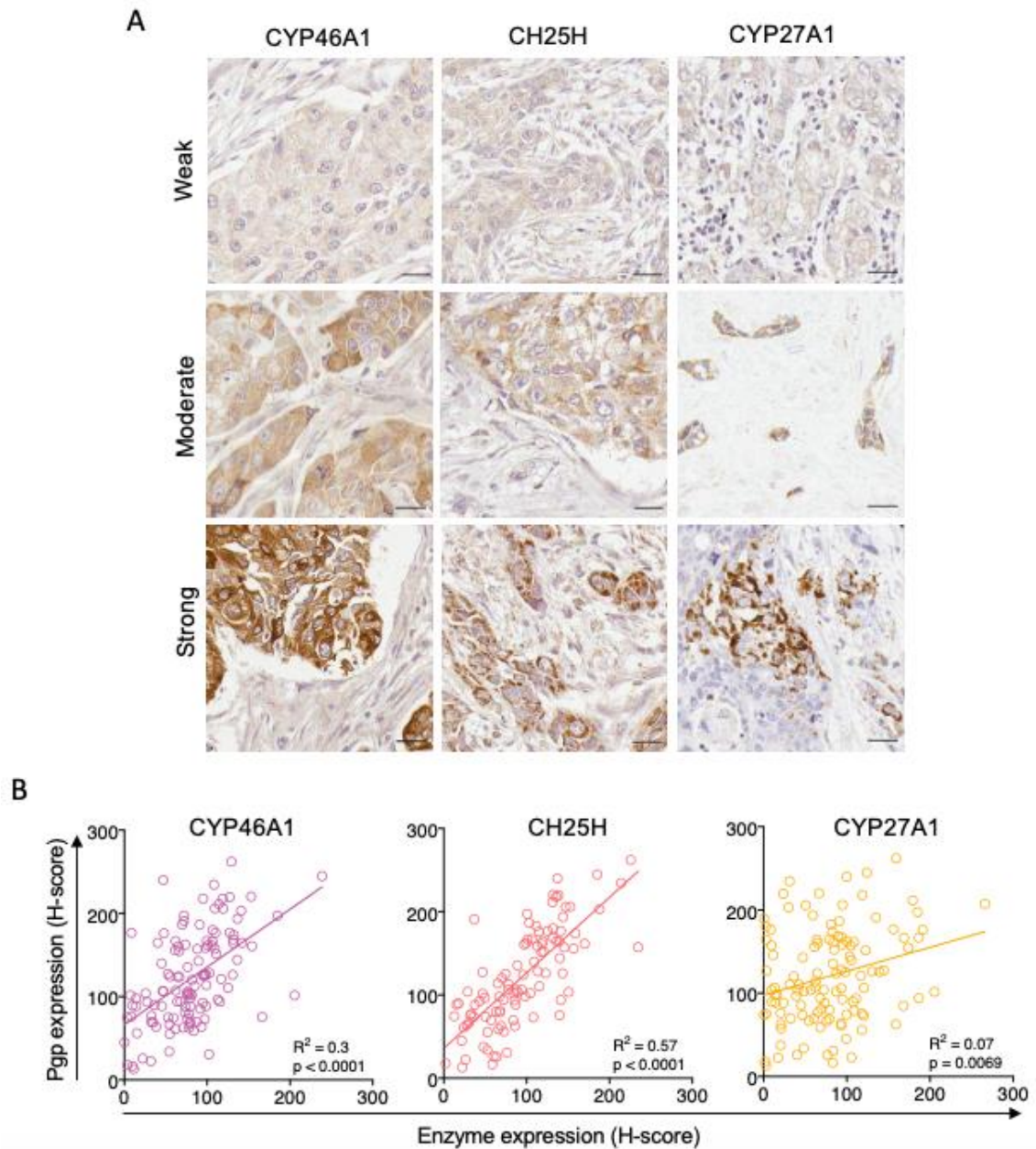


Figure 3.6 Protein expression of oxysterol producing enzymes, CYP46A1, CH25H and CYP27A1 in stroma correlate with Pgp expression in TNBC epithelial cells.

(A) Representative images of breast tumour stains containing cancer cells that are considered either; weakly stained, moderately stained or strongly stained for CYP27A1, CH25H and CYP46A1. Scale bars represent 25 μ m. (B) Correlation between the expression of both CYP27A1, CH25H and CYP46A1 to the expression of Pgp in matched tumours. Pearson's rank was performed to assess correlations.

3.4.4 The intratumour correlation between 24OHC and Pgp is decoupled in ER-negative, No Event patients

Further validation of the oxysterol-Pgp association was performed through the quantification of oxysterol concentration in tumours. The concentration of total 24OHC, 25OHC and 26OHC were measured through LC-MS/MS in triplicate slices from matched ER-negative tumours from the LBRTB cohort of 47 (31 TNBC and 16 HER2-enriched). These tumours had previously been assessed for expression of various mRNAs including *ABCB1*. To address known issues of high intratumour heterogeneity of OHC concentration (Solheim et al., 2019), the average oxysterol concentrations from three tissue slices per tumour was calculated. Average concentrations for each OHC were then correlated with *ABCB1* mRNA from matched tumours. High *ABCB1* mRNA expression within ER-negative tumours associated with reduced DFS (**Appendix Figure A.9A-D**; log-rank test: $p=0.014$), which has been demonstrated previously in breast cancer (Atalay et al., 2008). Of the oxysterols assessed in ER-negative tumours (**Figure 3.7**), 24OHC was associated with *ABCB1* mRNA expression (Pearson's rank: $p=0.011$); 25OHC and 26OHC were not. Furthermore, 24OHC was only correlated with Pgp in patients who had suffered a relapse or disease specific death (Event: $R^2=0.14$, $p=0.011$) but not in patients who had survived disease free (No event: $p>0.05$). These data suggested that 24OHC may be most likely responsible for driving LXR mediated Pgp expression *in vivo*. When stratified by clinical subtype (TNBC or HER2-enriched), only 24OHC in TNBC Event patients positively correlated with *ABCB1* mRNA expression (**Appendix Figure A.10**; $p=0.11$).

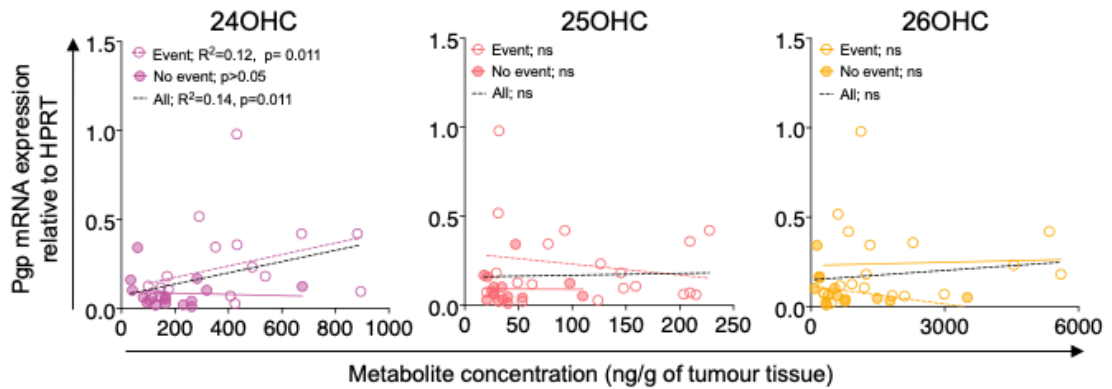


Figure 3.7 24OHC associates with *ABCB1* mRNA expression in patients that have suffered an event.

Correlation analysis between tumour concentration of 24OHC, 25OHC and 26OHC and *ABCB1* mRNA expression relative to HPRT. Cohort split between Event (dotted, coloured line and open circles), No Event (solid coloured line and closed circles) patients and All patients (black dotted line). Lines indicate linear regression, correlations calculated using Spearman's rank.

3.4.5 High expression of CYP46A1 and CH25H associate with reduced disease-free survival in triple-negative breast cancer

To establish whether oxysterol producing enzymes were predictive of DFS in TNBC, the expression of CYP46A1, CH25H and CYP27A1 was associated with patient information regarding whether they had suffered an event or not. First, the expression of CYP46A1, CH25H and CYP27A1 were compared between Event and No Event patients (**Appendix Figure A.11A**), finding that both CH25H and CYP46A1 were more highly expressed in Event patients (Student's t-test: CH25H: $p=0.007$ and CYP46A1: $p=0.0007$). ROC curves were used to determine expression cut off (**Appendix Figure A.11B**) for assessment of whether the enzymes were predictive of DFS. High expression of either CH25H and CYP46A1 associated with reduced DFS (**Figure 3.8**; log-rank test: $p=0.005$ and $p=0.002$ respectively).

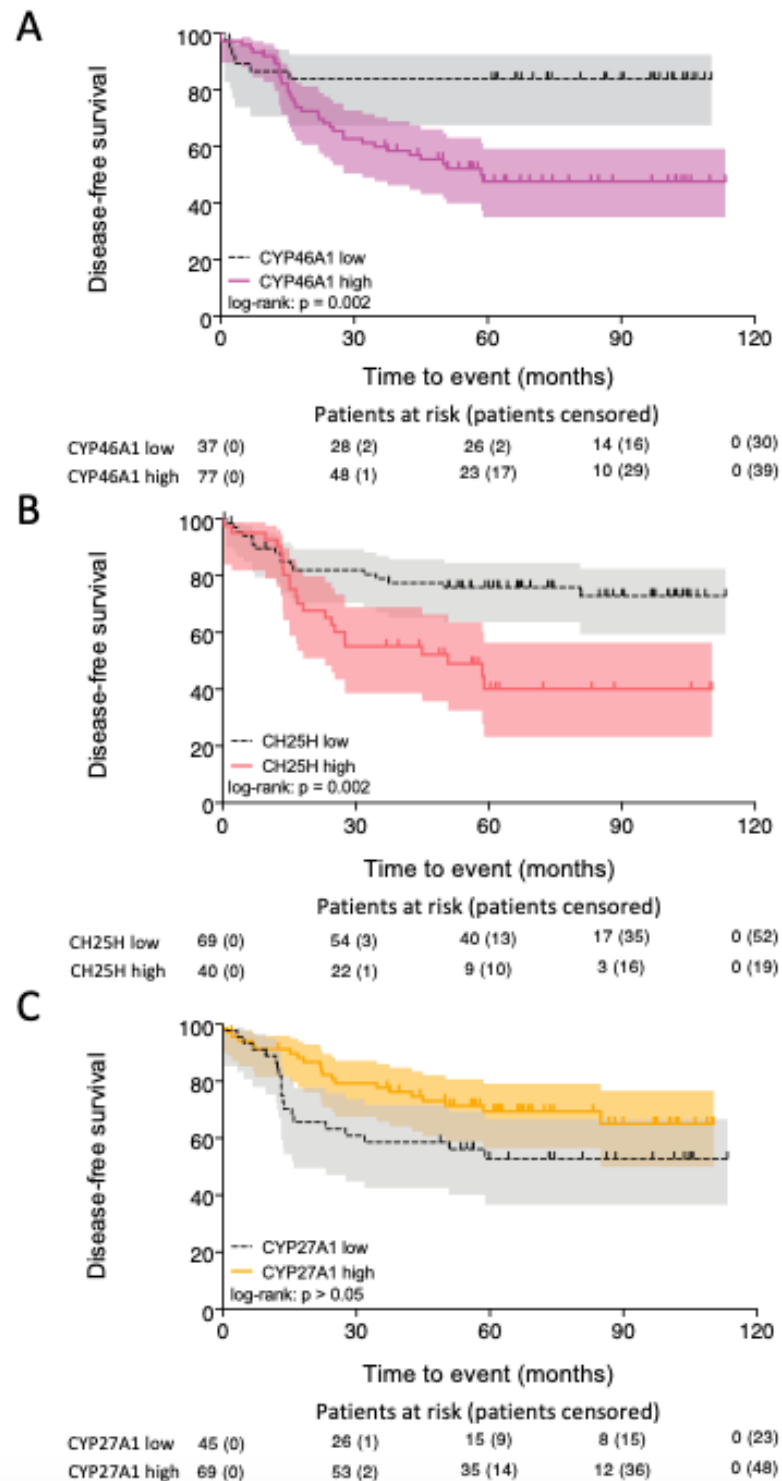


Figure 3.8 High expression of CYP46A1 and CH25H is predictive of reduced disease-free survival.

Kaplan-Meier analysis of (A) CYP46A1 (low H-score= <65, high H-score= >65), (B) CH25H (low H-score= <113.2, high H-score= >113.2) and (C) CYP27A1 (low H-score= <63.3, high H-score= >63.3). ROC curves were performed to dichotomise high and low expression. Log-rank test was performed to assess significance. Shaded areas represent 95% CI. Patients at risk of event are shown beneath each Kaplan-Meier curve.

3.4.6 High concentrations of 24OHC, 25OHC and 26OHC associate with reduced disease-free survival in ER-negative tumours

Oxysterol content was then compared between ER-negative Event and No Event patients. All oxysterols (**Appendix Figure A.12A**; Mann-Whitney test: 24OHC: $p=0.024$, 25OHC: $p=0.004$ and 26OHC: $p=0.005$) were significantly higher in concentration in tumours from Event compared to No Event patients. Patients were then dichotomised into high and low tumour concentration of the assessed oxysterols through receiver operating characteristic (ROC) curve analysis (**Appendix Figure A.12B**) and Kaplan-Meier curves generated using patient information regarding DFS. Survival curve analysis showed that all three oxysterols associated with reduced DFS when present in tumours at high concentrations (**Figure 3.9**; log-rank test: 24OHC: $p=0.02$, 25OHC: $p=0.01$ and 26OHC: $p=0.01$). When analysing the smaller cohort ($n=27$) containing just TNBC patients, only high concentrations of 26OHC ($p=0.04$) associated with shorter DFS (**Appendix Figure A.13A**). However, in HER2-enriched tumours ($n=12$) high concentrations of all three oxysterols remained associated with reduced DFS (**Appendix Figure A.13B**; log-rank test: 24OHC: $p=0.04$, 25OHC: $p=0.004$ and 26OHC: $p=0.03$).

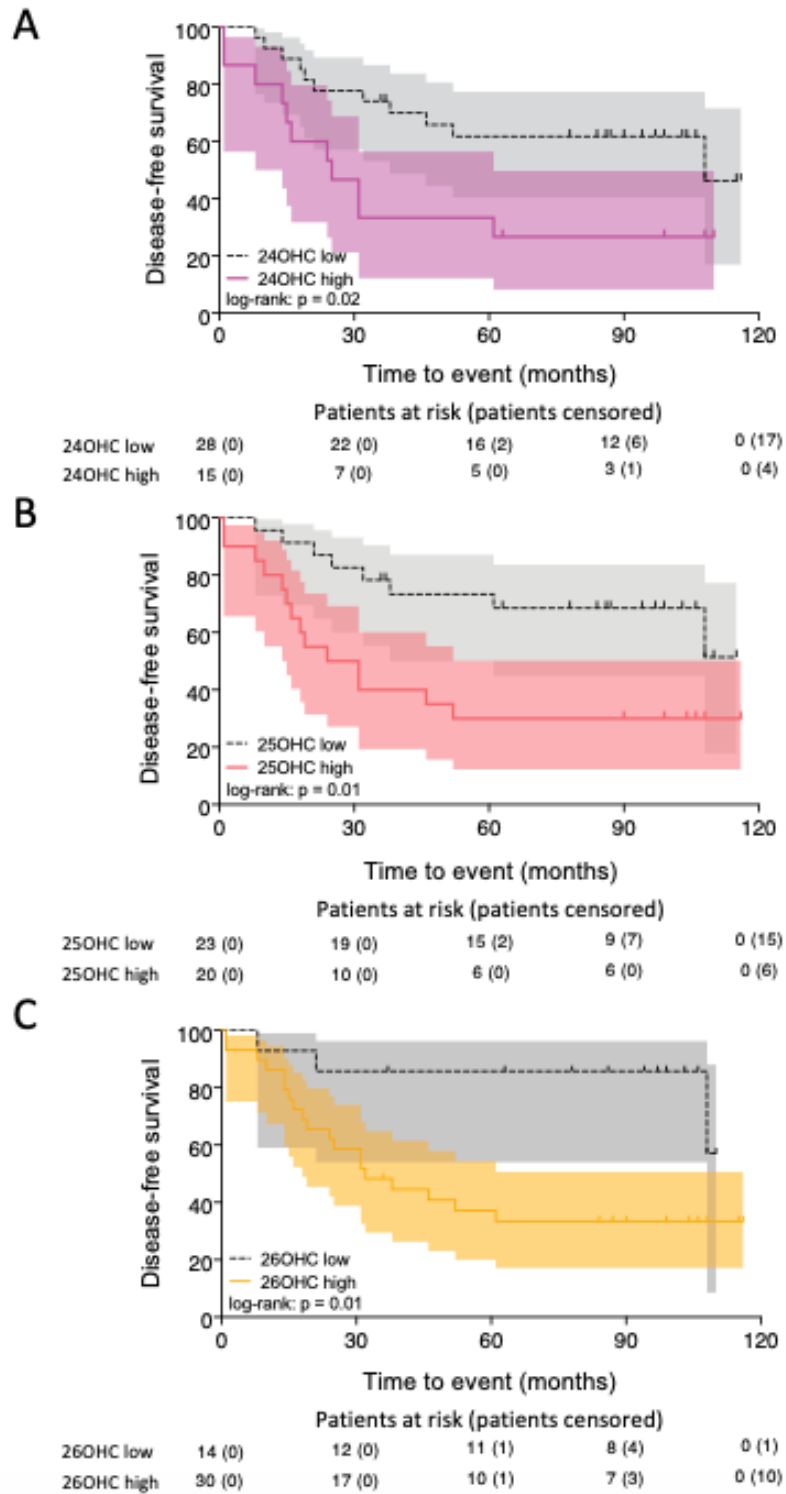


Figure 3.9 High concentrations of oxysterols are predictive of reduced disease-free survival. Kaplan-Meier analysis of (A) 24OHC (low ng/g = <286.5, high ng/g = >286.5), (B) 25OHC (low ng/g = <57.22, high ng/g = >57.22) and (C) 26OHC (low ng/g = <346.9, high ng/g = >346.9). Log-rank test was performed to assess significance. Shaded areas represent 95% CI and patients at risk of suffering an event are shown beneath each Kaplan-Meier curve.

3.5 Discussion

The overall aim of this chapter was to test the hypothesis that oxysterol-mediated resistance to epirubicin is mediated via Pgp upregulation and that the oxysterol/LXR axis is associated with reduced DFS. Our group previously established that transactivation of LXR by oxysterols is more potent in ER-negative than ER-positive breast cancer cell lines (Hutchinson et al., 2019b). This sensitivity to oxysterol signalling, coupled with a lack of targeted therapies for TNBC, were important parameters in the decision to further investigate the oxysterol-LXR axis in this disease subtype. Treatment of TNBC cells with LXR ligands (GW3965, 24OHC, 25OHC and 26OHC) was previously found to increase resistance to epirubicin and induce expression of Pgp (Hutchinson et al., 2021). Pgp is most commonly overexpressed in TNBC compared to other breast cancer subtypes (Millis et al., 2015) and confers resistance to epirubicin via its xenobiotic efflux functions (Chen, Y.N. et al., 1990). Pgp was therefore a likely mediating candidate of the chemoresistance induced by oxysterol-LXR pathway.

Although oxysterols were demonstrated to upregulate Pgp expression and induce chemotherapy resistance through LXR in TNBC cells, whether LXR-mediated chemoresistance was induced solely through Pgp was unclear. Therefore, the first aim of this chapter was to demonstrate that LXR-mediated resistance to chemotherapy acted through increased Pgp expression. Treatment of MDA-MB-468s with GW3965 increased *ABCB1* expression and was unable to induce expression in siPgp treated cells. A subsequent MTT assay mirroring this experiment showed that siPgp inhibited GW3965-mediated resistance to epirubicin, suggesting that LXR-induced chemotherapy resistance to epirubicin is driven by upregulation of Pgp.

To examine whether Pgp may be under the regulatory control of the oxysterol-LXR axis in patients, three experiments were undertaken. Pgp expression was measured in three independent cohorts and the pathway was measured at the levels of mRNA, protein and oxysterol concentrations. Contrasting with mRNA expression data harvested from TCGA, CYP46A1 protein showed a strong correlation with Pgp expression within the TMA.

Considering CYP46A1 produces 24OHC, one of the more proficient LXR activators (Lehmann, J.M. et al., 1997; Janowski et al., 1999; Hutchinson et al., 2019b), this is understandable. Furthermore, CYP46A1 has been implicated in catalysing the final step in an alternate shunt in the mevalonate pathway. This shunt leads to the production of another potent LXR ligand (Lehmann, J.M. et al., 1997; Janowski et al., 1999), 24,25EC (Griffiths et al., 2016b), potentially enhancing the correlation between CYP46A1 and Pgp. Additionally, 24OHC was found to positively correlate with *ABCB1* expression within TNBC and HER2+ tumours. This suggests that CYP46A1 production of 24,25EC is not driving the association between CYP46A1 and Pgp but may still complement it. Interestingly, when tumours were stratified on Event or No Event patients, the association between 24OHC and *ABCB1* remained only within the Event group. This finding could be due to a range of factors, such as enhanced expression of LXR co-repressors in No Event patients (Hutchinson et al., 2019b), leading to repression of LXR signalling. Alternatively, reduced expression of DBD lacking LXR isoforms in Event patients could result in less ligand binding competition for active LXR isoforms and increased transcription of LXR target genes (Lianto et al., 2021). Both CYP46A1 and 24OHC were predictive of reduced DFS and their presence in tumours were significantly higher in Event patients compared to No Event patients. These findings may be due to upregulation of Pgp through the LXR-oxysterol axis, however it is possible there are other mechanisms involved.

CH25H exerts the greatest influence over Pgp expression of the tested enzymes at protein level in the TMA cohort. This supports findings from mRNA data analysis, which found that only *CH25H* expression of the tested oxysterol producing enzymes has a positive relationship with *ABCB1* expression in the TCGA cohort. However, the LXR-ligand product of CH25H, 25OHC, is not a proficient LXR agonist (Lehmann, J.M. et al., 1997; Janowski et al., 1999) and was the poorest ligand tested for inducing chemotherapy resistance in MTT assays (Hutchinson et al., 2021), making these results somewhat surprising. Observed associations within patient cohorts thus, may in fact not be due to the efficacy of 25OHC, but rather the result of both CH25H and Pgp both being LXR targets. CH25H is upregulated in liver cancer cell line, HepG2, in response to

treatments with both natural (25OHC) and synthetic (T317) LXR ligands (Liu, Ying et al., 2018). This suggests that stimulation of LXR *in vivo* would induce both Pgp and CH25H expression, enhancing any association between CH25H and Pgp. Furthermore, concentration of 25OHC within TNBC and HER2+ tumours did not correlate with expression of *ABCB1*, supporting the suggestion that correlation between proteins may be a result of being gene targets of LXR. Additionally, tumour concentration of 25OHC may not directly reflect expression of CH25H, with enzymes involved in 25OHC metabolism varying in expression between tumours. Despite the lack of association between 25OHC and *ABCB1*, 25OHC and CH25H are still predictive of DFS, suggesting they may be involved in alternative mechanisms in cancer progression.

Compared to CYP46A1 and CH25H, the correlation between CYP27A1 and Pgp is considerably weaker. This may be due to the fact that CYP27A1 can further metabolise both 26OHC (Griffiths et al., 2019) and 24OHC (Abdel-Khalik, Jonas et al., 2018) into inert LXR agonists (Soroosh et al., 2014). Additionally, CYP27A1 has other off-pathway targets, such as vitamin D3 (Sawada et al., 2000), with these potentially saturating the enzyme and reducing its efficacy for 26OHC production. This is reflected in the lack of separation between patients whose tumours express high and low levels of CYP27A1 and no significant difference between CYP27A1 expression between Event and No Event patients. Furthermore, the respective products of CYP27A1 may induce alternate effects on patient prognosis. Treatment with 26OHC induces metastasis through LXR in an MMTV-PyMT cancer model and induced a significant reduction in animal survival (Nelson, E. R. et al., 2013). However, CYP27A1 also catalyses 25-hydroxylation of vitamin D3 (Sawada et al., 2000), an essential step enabling the conversion of vitamin D to its functionally active form. High levels of 25-hydroxyvitamin D has been demonstrated to associate with a reduced risk of TNBC cancer progression (Yao et al., 2011), suggesting that CYP27A1 hydroxylation of vitamin D3 may improve patient outcome. Contrastingly, high tumour concentration of CYP27A1 product, 26OHC, associates with DFS, however did not associate with *ABCB1* expression in our cohort. Subsequently, it is likely that the association between 26OHC and DFS is due to the previously established 26OHC-mediated induction of metastasis (Nelson, E. R. et al., 2013).

Treatments with GW3965 have been shown to induce chemotherapy resistance in 4T1 allograft models (Hutchinson et al., 2021). Expansion upon this experiment could be to graft 4T1 cells pre-treated with siRNA targeting CYP46A1. Prognostic data associating CYP46A1 expression and 24OHC concentration with Pgp expression and DFS suggests that knockdown of CYP46A1 in animal xenograft model would reduce tumour resistance to epirubicin treatment and lead to enhancing epirubicin mediated tumour destruction. Alternatively, overexpression plasmids could be utilised to enhance expression of CYP46A1 in the allografted cells, improving epirubicin resistance.

With both 24OHC and CYP46A1 showing an association with Pgp expression at mRNA and protein level, respectively and 24OHC inducing chemoresistance in breast cancer cells, a targetable mechanism to prevent chemotherapy resistance has emerged. Tissue concentration of 26OHC has been shown to be influenced by dietary intake of cholesterol in animal models (Sozen et al., 2018) and both 24OHC and 26OHC concentrations in serum correlate with that of their precursor, cholesterol (Stiles et al., 2014), suggesting that oxysterol content can be influenced by diet. Furthermore, statins reduce circulating levels of 25OHC (Dias et al., 2018) and 24OHC (Vega et al., 2003). Therefore, TNBC patients may benefit from a dietary intervention targeting cholesterol reduction or statin therapy to reduce circulating and intratumoural levels of 24OHC.

3.6 Conclusion

The development of chemotherapy resistance continues to be a major setback in the treatment of TNBC, leading to the development of new agents less susceptible to common resistance mechanisms. Moreover, there is a requirement to further understand the mechanisms that lead to chemotherapy resistance, which may identify targetable pathways to prevent the induction of chemotherapy resistance. In this chapter, oxysterols have been demonstrated to induce chemotherapy resistance through upregulation of Pgp. Furthermore, both oxysterols and the enzymes responsible for their production have been shown to associate with reduced DFS in high

concentrations. Oxysterols are derived from cholesterol and their concentration in serum correlates with cholesterol content (Stiles et al., 2014). Therefore, TNBC patients may benefit from either dietary or pharmacologic interventions targeting cholesterol to impair induction of chemotherapy resistance through the oxysterol:LXR:Pgp axis. To summarise, endogenous LXR ligands are prognostic biomarkers for TNBC patient survival and present a targetable mechanism to be explored in clinical trials to reduce incidence of chemotherapy resistance.

Chapter 4: Oxysterols from cancer-associated fibroblasts impact LXR signalling in triple negative breast cancer

4.1 Introduction

In the previous chapter, the intratumour oxysterol concentration and epithelial cell expression of enzymes responsible for oxysterol production were shown to associate with DFS. Combined with previous research from the laboratory, the hypothesis that the oxysterol-LXR axis could induce Pgp-mediated chemotherapy resistance was established. However, epithelial cells are not the only cell type within a tumour, with a rich network of non-cancer cells present for epithelial cells to interact with. These non-cancer cells form the TME and include the resident fibroblasts and adipocytes and the infiltrating immune cells. The tumour stroma refers to the non-cancer region of the TME, which primarily consist of fibroblasts and the extra-cellular matrix that they secrete. Stroma rich triple-negative tumours have shorter periods of relapse-free survival (de Kruijf et al., 2011; Moorman et al., 2012; Dekker et al., 2013) and overall survival (Moorman et al., 2012; Millar et al., 2020). Fibroblasts make up a large constituent of the cellular material in the tumour stroma and have been shown to associate with aggressive cancer phenotypes (Zhou et al., 2018).

Tumour residing fibroblasts will receive signals from cancer cells which induce their conversion from normal fibroblasts to cancer-associated fibroblasts. Cancer-associated fibroblasts are significantly different from normal fibroblasts in regards to their expression profiles (González et al., 2016) and their morphology (Olsen et al., 2010). CAFs can also be sourced from infiltrating mesenchymal stem cells (Weber et al., 2015) and adipocytes (Bochet et al., 2013). CAFs derived from different breast cancer subtypes exhibit specific gene expression profiles (Tchou et al., 2012). In fact, four different CAF subtypes (CAF-S1-S4) have been identified within human breast cancers through the expression of canonical CAF marker proteins: α SMA, caveolin-1, FAP, FSP-1, integrin β 1 and PDGFR β . Of these four subtypes, only two (CAF-S1 and CAF-S4) were found to be majorly present in TNBC and accumulate differentially between TNBC tumours (Costa, A. et al., 2018). CAF subtypes appear to have distinct roles on epithelial cells, with CAF-

S1 and CAF-S4 performing complementary roles in inducing metastasis. CAF-S1 cells appear to prime epithelial cells for metastasis by instigating epithelial to mesenchymal transition, whereas CAF-S4 cells initiate cancer invasion through Notch signalling (Pelon et al., 2020). These CAF subtypes may also act as prognostic indicators, with the presence of CAF-S4 in the lymph nodes associated with reduced overall survival (Pelon et al., 2020). CAFs can not only influence epithelial cells but can also alter other non-cancer cells of the tumour microenvironment. The CAF gene signature in TNBC tumours was found to negatively correlate with cytotoxic T-cells (Wu, S.Z. et al., 2020).

Fibroblasts have been shown to produce oxysterols (Kannenbergh et al., 2013; Lange et al., 2009; Saucier, S. E. et al., 1985); however, oxysterol production within CAFs has not yet been elucidated. Furthermore, if CAFs can produce oxysterols, whether oxysterols are secreted in sufficient quantity into the TME would heavily impact their influence on epithelial LXR transactivation. Mechanisms of cellular oxysterol export have been identified, with one such being the export through ABCG1 (Xu, M. et al., 2009). Oxysterols exported through ABCG1 were shown to be taken up by adjacent cells (Xu, M. et al., 2009), demonstrating oxysterol-mediated paracrine signalling. ABCA1 was unable to export 7KC (Xu, M. et al., 2009), however could export 25OHC (Tam et al., 2006). Additionally, small quantities of 7KC are also exported through HDL-bound ApoA-I (Gelissen et al., 1999). Oxysterols were found to be exported from cells in exosomes, however the concentration of oxysterols exported by exosomes was unrelated to intracellular oxysterol levels (Roberg-Larsen et al., 2017). There has been an accumulation of evidence stating the importance of exosomes in many cancer hallmarks (Giordano et al., 2020) and oxysterols may be an important component within exosomes for inducing pro-cancer pathways. Therefore, the association between high CAF cell number and tumour aggressiveness in TNBC (Zhou et al., 2018) may be related to oxysterols secreted by CAFs. Secreted oxysterols may be able to induce LXR α signalling in adjacent or distant epithelial cells and activate pro-cancer pathways, such as chemotherapy resistance through Pgp upregulation.

4.2 Hypothesis and aims

Oxysterols secreted by cancer-associated fibroblasts can induce chemotherapy resistance in adjacent epithelial cancer cells through LXR-mediated upregulation of Pgp.

The aims of this chapter were to:

- Identify TNBC-specific markers of cancer-associated fibroblasts and examine if their expression correlates with expression of LXR target genes in TNBC and Basal-like/Claudin-low tumours.
- Elucidate whether CAFs increase the ability of LXR to transactivate LXR-target genes in TNBC cells.
- Examine whether stromal expression of oxysterol producing enzymes associates with epithelial Pgp expression and DFS in TNBC tumours.

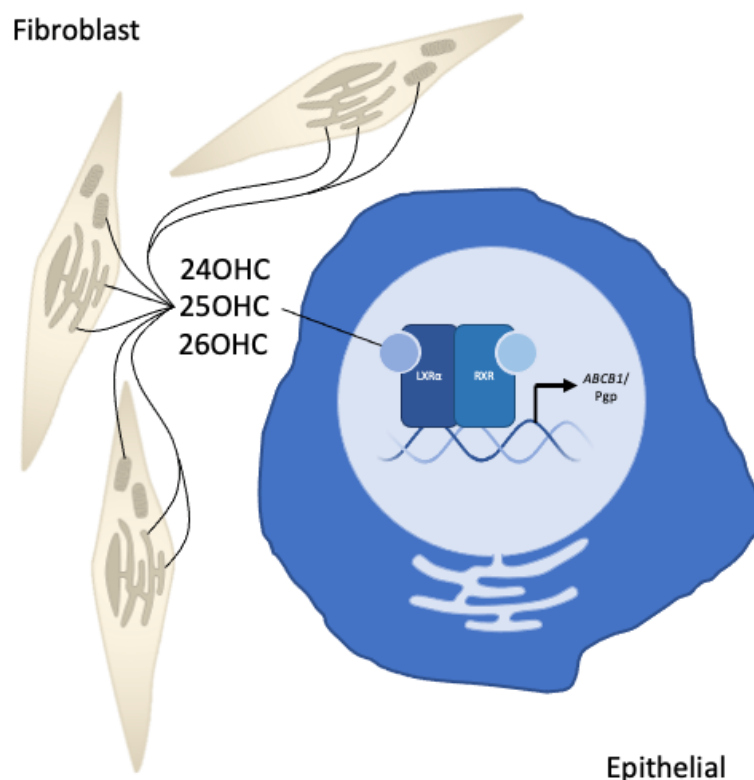


Figure 4.1 Graphical hypothesis: Cancer associated fibroblast transactive LXR signalling in triple negative breast cancer epithelial cells through secreted oxysterols.

24OHC, 25OHC and 26OHC are secreted by cancer-associated fibroblasts that are adjacent to epithelial cells within a TNBC tumour. Oxysterols are taken up by the epithelial cell and used to induce LXR signalling, leading to an increase in *ABCBI* mRNA expression and Pgp protein expression.

4.3 Materials and methods

4.3.1 Systematic review

4.3.1.1 Search strategy

Searches were carried out using the Pubmed and Scopus databases during August 2021. The search strategy used was published on the PROSPERO database (CRD42021272880), however the strategy identified markers for cancer-associated adipocytes and macrophages in addition to CAFs. For this chapter, only CAF markers are addressed. Search strategy: (((((TNBC[Title/Abstract]) OR (triple negative breast[Title/Abstract])) OR ("ER Negative" "PR Negative" "HER2 Negative"[Title/Abstract])) OR (BLBC[Title/Abstract])) OR (Basal* breast cancer[Title/Abstract])) AND (((((macrophage*[Title/Abstract]) OR (monocyte*[Title/Abstract])) OR (Fibroblast*[Title/Abstract])) OR (adipos*[Title/Abstract])) OR (adipocyte*[Title/Abstract])).

4.3.1.2 Study selection

Titles and abstracts that were identified from the search strategy were screened against the following inclusion criteria: 1) The article is in English. 2) The article describes an original (primary data) study. 3) The article investigates TNBC. 4) The article investigates adipocytes, fibroblasts or macrophages. 5) The article identifies potential marker genes/proteins in adipocytes, fibroblasts or macrophages. Publications from predatory journals listed on <https://beallslist.net/> were excluded from our review, as were case studies. Studies that assessed gene expression in fibroblasts or macrophages, however not in the context of TNBC-association were excluded from our review. Screening was performed by two independent assessors (either Shounak Barua, Wing Lee, Jing Zhang, Ruiming Zhang or Qinghui Zhu) and validated by a third (either Dr Giorgia Cioccoloni or Alex Websdale). Identification process for marker genes is summarised in **Figure 4.2**.

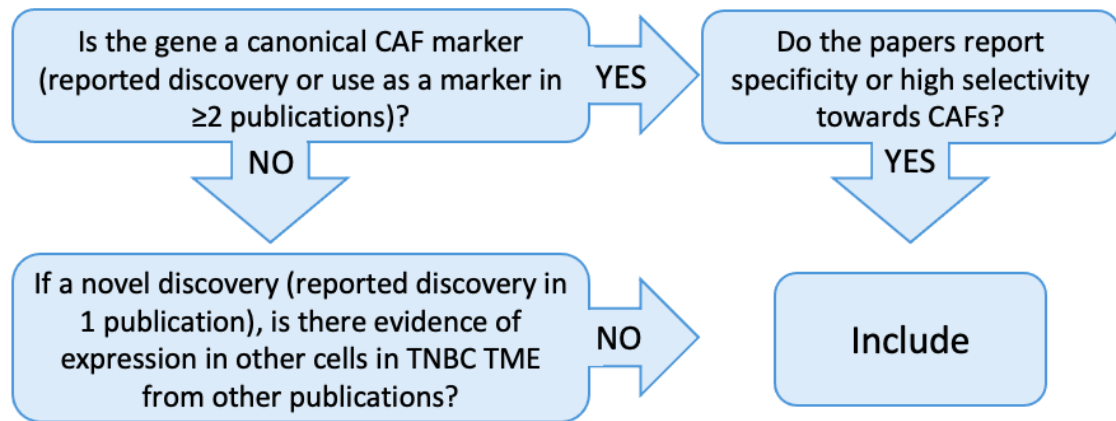


Figure 4.2 Decision tree for identifying TNBC-specific CAF marker genes.

Reported discovery of a CAF marker describes a gene that has upregulated expression in TNBC-CAFs following their conversion from normal fibroblasts.

4.3.2 TCGA and METABRIC dataset analysis

4.3.2.1 Data extraction and analysis

mRNA expression z-scores relative to diploid samples of our gene cohort in breast tumours were obtained from <http://cBioportal.org> (Cerami et al., 2012). Breast cancer gene expression databases provided by TCGA (Koboldt et al., 2012) and METABRIC (Curtis et al., 2012) were used. Expression data was assessed for both TNBC and Basal-like and claudin-low (BLCL). To generate TNBC cohorts, clinical information of the entire TCGA and METABRIC datasets were obtained and filtered for negativity of ER, PR and HER2 status. For BLCL tumours from TCGA, basal-like and claudin-low expression data was selected for from <http://cBioportal.org>. To generate METABRIC BLCL cohorts, basal-like and claudin-low tumours were chosen using the PAM50 classification reported in clinical information. mRNA expression z-scores relative to diploid samples were downloaded for all samples. Expression data for TNBC patients was obtained from TCGA (n=123) and METABRIC (n=299). Expression data for BLCL patients was obtained from TCGA (n=85) and METABRIC (n=398). Data was then imported into PRISM for analysis. Clinicopathological features of TNBC and BLCL cohorts are listed for METABRIC (**Table 4.1**) and TCGA (**Table 4.2**).

Table 4.1 Patient characteristics

Clinicopathological features of the METABRIC breast cancer cohort separated by TNBC subtype (n = 299) by receptor status or Basal and Claudin low subtype (n = 398) by PAM50 method. N/A=not available.

| Characteristic | Category | METABRIC TNBC No. of Patients = 299 (%) | METABRIC Basal + Claudin-Low No. of Patients = 398 (%) |
|-------------------|-------------|---|--|
| Tumour Stage | 0 | 0 (0) | 1 (0) |
| | 1 | 62 (21) | 91 (23) |
| | 2 | 130 (44) | 170 (43) |
| | 3 | 25 (8) | 34 (9) |
| | 4 | 0 (0) | 0 (0) |
| | N/A | 82 (27) | 102 (25) |
| Tumour size | < 35 mm | 230 (77) | 309 (78) |
| | ≥ 35 mm | 65 (22) | 82 (20) |
| | N/A | 4 (1) | 7 (2) |
| Survival Status | Alive | 139 (46) | 198 (50) |
| | Deceased | 160 (54) | 200 (50) |
| Recurrence Status | None | 177 (59) | 248 (62) |
| | Present | 122 (41) | 150 (38) |
| PAM50 Subtype | Basal | 151 (51) | 199 (50) |
| | Claudin-low | 106 (35) | 199 (50) |
| | HER2 | 30 (10) | 0 (0) |
| | Luminal A | 2 (1) | 0 (0) |
| | Luminal B | 0 (0) | 0 (0) |
| | Normal | 20 (3) | 0 (0) |

Table 4.2 Patient characteristics

Clinicopathological features of the TCGA breast cancer cohort separated by TNBC subtype (n = 123) by hormone receptor status or Basal and Claudin low subtype (n = 85) by PAM50 method. N/A=not available.

| Characteristic | Category | TCGA TNBC No. of Patients = 123 (%) | TCGA Basal + Claudin-Low No. of Patients = 85 (%) |
|-----------------|-------------|-------------------------------------|---|
| Tumour Stage | 0 | 0 (0) | 0 (0) |
| | 1 | 26 (21) | 21 (25) |
| | 2 | 82 (66) | 55 (65) |
| | 3 | 11 (9) | 7 (8) |
| | 4 | 2 (2) | 1 (1) |
| | N/A | 2 (2) | 1 (1) |
| Survival Status | Alive | 104 (85) | 75 (88) |
| | Deceased | 19 (15) | 10 (12) |
| PAM50 Subtype | Basal | 76 (62) | 81 (95) |
| | HER2 | 5 (4) | 0 (0) |
| | Luminal A | 4 (3) | 0 (0) |
| | Luminal B | 1 (1) | 0 (0) |
| | Normal | 2 (2) | 0 (0) |
| | Claudin-low | 0 (0) | 4 (5) |
| | N/A | 35 (28) | 0 (0) |

4.3.2.2 Generation of heatmaps

Statistical analysis of correlation data was conducted using R version 3.6.3, RStudio version 2021.09.0 Build 351 by Olivia Burton and Dr Elton Vasconcelos with thanks to LeedsOmics. Pearson's correlation was used to generate R values for correlations between TNBC-specific CAF marker genes and canonical LXR target genes and a False Discovery Rate of 1% was applied to the resulting p-value. Heatmaps were generated from R values using the heatmap.2 command (Liaw A, 2020) within the gplots package (Warnes GR, 2020) by Olivia Burton and Elton Vasconcelos with thanks to LeedsOmics. Genes were divided into different clusters through hierarchical clustering.

4.3.3 Cell culture assays

4.3.3.1 Cell lines

MDA-MB-468 cells were obtained from Dr Thomas A. Hughes and MDA-MB-453 cells were obtained from Dr Laura Mathews, originally from ATCC. An LXR α controlled luciferase reporter cell line has been developed from MDA-MB-468 cells (see **3.3.1 Cell culture**) via a published method (Hutchinson and Thorne, 2019). In brief, cells were transfected with Lentiviral particles containing a firefly luciferase reporter expressing luciferase under the control of LXR-binding elements and also encoding puromycin resistance. LXR α -inducible MDA-MB-468s were referred to as MDA-MB-468-LXR-Luc cells. CAF cells were from Dr Thomas A. Hughes. CAFs were generated by viral-mediated immortalisation through overexpression of hTERT in fibroblasts extracted from inside luminal A tumour masses (Broad et al., 2021). Cells were grown as reported in **3.3.1 Cell culture**.

4.3.3.2 Co-culture

CAFs and MDA-MB-468-LXR-Luc cells were seeded into opaque walled 96 well plates with flat and clear bottoms. LXR α -inducible MDA-MB-468s were always seeded at a density of 10,000 cells per well. CAF seeding density ranged from 0, 2.5×10^3 , 5×10^3 , 1×10^4 and 2×10^5 cells per well. Cells were co-cultured together for 16 h before being assessed for luciferase expression via luciferase assays (see **4.3.3.5 Luciferase assay**).

4.3.3.3 Conditioned media

CAF conditioned media (CM) was generated by adding 10 mL of DMEM containing 10% FBS into a confluent T75 and incubating for 44 h. MDA-MB-468 conditioned media was generated by seeding 4.5×10^5 cells per mL and conditioning DMEM containing 10% FBS for 24 h. All media was centrifuged upon collection for 5 minutes at 200 rcf and stored at -80°C until use. MDA-MB-468-LXR-Luc cells were treated with conditioned media for 24 h before being assessed for luciferase expression via luciferase assays (see **4.3.3.5 Luciferase assay**) or mRNA expression (see **3.3.4 Quantification of gene expression**).

4.3.3.4 DMEM acidity assessment

CAFs and MDA-MB-468s were seeded as per **4.3.3.3** and left to condition media. 600 μL of media was taken at time points: 16, 20, 24, 40 and 44 h. 200 μL of conditioned media from each time point was aliquoted into 96-well plates in triplicate. DMEM acidity of conditioned media was assessed by absorbance at 560 nm (Held, 2018) read using CLARIOstar Plus plate reader.

4.3.3.5 Luciferase assay

Luciferase expression in MDA-MB-468-LXR-Luc cells were measured using the Luciferase Assay system (E1500, Promega, UK). Cells were grown in opaque walled 96 well plates with flat and clear bottoms. For LXR α inducible cell lines, cells were treated with LXR ligand or a matched volume of vehicle control for 16 h. Cells were then carefully washed with 100 μL of PBS and lysed in 100 μL 1X Passive Lysis Buffer (PLB) (E1500, Promega, UK). Following addition of PLB, plates were frozen at -80°C for at least 2 h before thawing. Luciferase expression was measured through the addition of 150 μL of LAR II (E1500, Promega, UK) and luminescent signal measured using the CLARIOstar Plus microplate reader (BMG Labtech, UK).

4.3.3.6 siRNA knockdowns

For siRNA knockdown methods and reagents used, see **3.3.3.2 siRNA knockdowns**. For simultaneous knockdown of CYP46A1, CH25H and CYP27A1, 4 nM of each tri-silencer (SR307399A+C, SR305950B+C and SR301124A+B) were used following the incubation

times stated in **3.3.3.2 siRNA knockdowns**. siRNA duplexes used are listed in **Table 4.3**. Tri-silencers and scrambled RNA control were obtained from OriGene, USA.

Table 4.3 Table of siRNAs used

Gene names and product codes for siRNA tri-silencers used.

| Gene name | siRNA ID |
|---------------|----------|
| CYP46A1 | SR307399 |
| CH25H | SR305950 |
| CYP27A1 | SR301124 |
| Scrambled RNA | SR322981 |

4.3.4. Immunohistochemistry

4.3.4.1 Quantification of immunohistochemical staining

For immunohistochemical staining, manual histoscore, generation of TMAs and patient characteristics see **3.3.5 Immunohistochemistry**. Stromal proportions of tumour cores were measured using ImageScope version 12.4.3 (Aperio Technologies, US) by drawing around the perimeter of the core, excluding necrotic regions and drawing around cancer regions in the core. Cancer area was then subtracted from the total area to find the stromal area of the core. Stromal area was then divided by total area to find the stromal proportion of the tumour. Immunohistochemical staining within stromal regions was quantified using positive pixel count version 9 algorithm (Aperio Technologies, US) for ImageScope.

4.3.5 Quantification of gene expression

For extraction of RNA, conversion of RNA to cDNA and assessment of gene expression, see **3.3.4 Quantification of gene expression**. Taqman assays (4331182, Thermo Fisher, UK) used within this chapter are displayed in **Table 4.4**.

Table 4.4 Taqman assays.

Gene names and product codes for qPCR primers used.

| Gene Name | Taqman ID |
|------------------|------------------|
| HPRT1 | Hs02800695 |
| ABCA1 | Hs01059137 |
| ABCB1 | Hs00184500 |
| CYP46A1 | Hs01042347 |
| CH25H | Hs04187516 |
| CYP27A1 | Hs00168003 |

4.4 Results

4.4.1 Expression of multiple CAF marker genes associate with canonical LXR targets

4.4.1.1 Determining the TNBC-specific CAF marker gene panel

To determine if the presence of CAFs in TNBC was linked to activity of LXR, a list of genes that could identify the presence of CAFs within TNBC was required. Most genes are expressed in multiple cell types at different levels. Therefore, a key criterion was to identify genes that were strongly expressed in TNBC CAFs but were very low or absent in other cell types of the TME. To address this, a systematic review was performed to identify TNBC-specific and CAF-specific marker genes. Once identified, expression of these genes could be used as a semi-quantitative surrogate marker for the presence of CAFs in each tumour in the cohort. Such a list was then used to assess if the presence of CAFs associated with outcome metrics (survival, relapse) and with LXR activity (a similar list was developed for LXR target genes, see **4.4.1.2**).

Our search strategy returned 720 records from PubMed and 858 from Scopus. De-duplication generated 901 unique records to be screened against inclusion criteria. After abstract screening, 229 records that investigated gene expression in TNBC CAFs, CAMs or CAAs remained. Gene lists for CAMs and CAAs were also generated but were determined by other group members so are not included here. Subsequent full text screening identified 52 records reporting expression of 41 different genes in TNBC CAFs. Of these 41 genes, 33 were expressed in other TME cells including macrophages (n=3), adipocytes (n=2), or epithelial cells (n=28). In total 11 genes from 23 publications were found to be highly specific to TNBC-CAFs (see **Table 4.5**). The Prisma flow diagram of the screening process is shown in **Figure 4.3**. The most frequently used CAF marker in TNBC was *ACTA2*/ α SMA, used in 15 different studies. *FAP* was the next most common (n=9), followed by *CAV1*/caveolin-1 (n=7), *PDGFRB*/*PDGFR* β (n=6), *PDGFRA*/*PDGFR* α (n=4), *PDPN*/podoplanin (n=4) and *CXCL12*/*SFD1* (n=4). A further four markers were reported in just one study each, namely *C1S* (Tchou et al., 2012), *TMTC1* (Tchou et al., 2012), *COL1A1*/collagen type I alpha 1 chain (Wu, S.Z. et al., 2020) and *ITGA11*/integrin α 11 (Smeland et al., 2020). The roles of the 11 final TNBC CAF marker genes are summarised in **Table 4.5**. One notable absence from our final list of TNBC-specific CAF markers was

S100A4/*FSP1*, which has been used as a CAF marker multiple times previously (Camorani et al., 2017; Costa, A. et al., 2018; Gagliano et al., 2020; Lee, J.H. et al., 2018; Park, S.Y. et al., 2015; Kim, H.M. et al., 2015; Wu, S.Z. et al., 2020). *FSP1* was excluded here due to high expression in cancer cells (Abdel-Khalik, J. et al., 2018) meaning this marker is not CAF selective.



PRISMA 2009 Flow Diagram

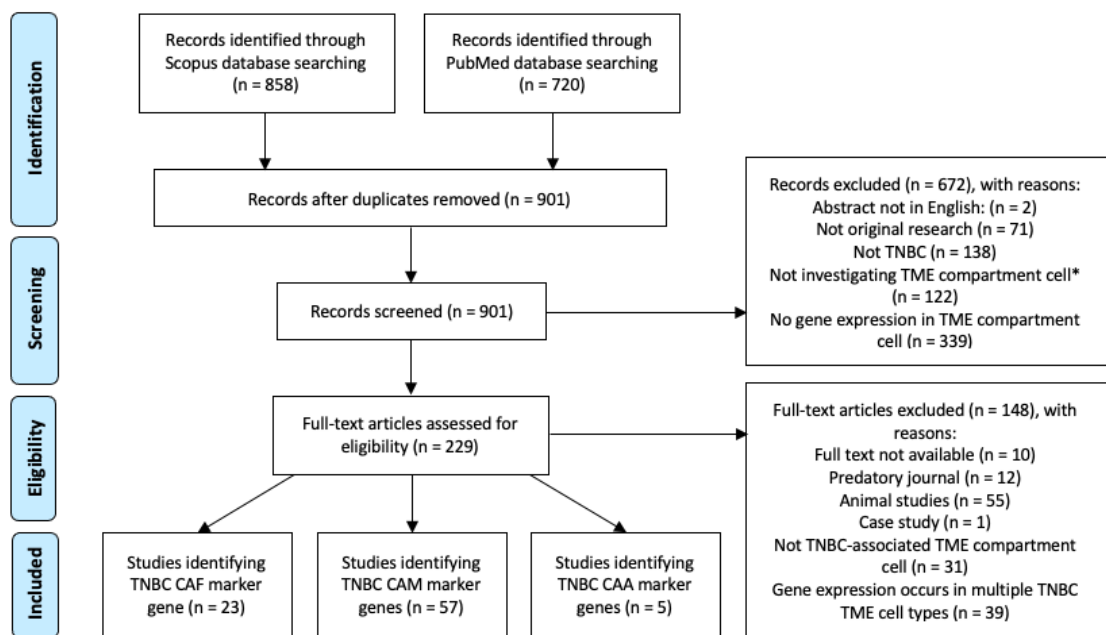


Figure 4.3 Study discovery and distribution.

PRISMA flow diagram showing searching, screening, eligibility and inclusion process. Four studies that had their full text assessed for eligibility measured gene/protein markers in both TNBC-associated macrophages and fibroblasts. *TME compartment cells refers to either adipocytes, fibroblasts or macrophages.

Table 4.5 TNBC-specific CAF marker genes

List of TNBC-specific CAF marker gene names, protein names and their abbreviations if appropriate and normal protein function.

| Gene List | Encoded Protein | Function |
|------------------|---|--|
| ACTA2 | Smooth Muscle α -2 actin (α -SMA) | One of six actin isoforms. Involved in the formation of actin microfilament bundles and enables formation of focal adhesions through these bundles (Hinz, Boris et al., 2003). Involved in the contraction apparatus of myofibroblasts (Shinde et al., 2017; Hinz, B. et al., 2001). |
| C1S | Complement component 1s (C1s) | Serine protease component of the complement component 1 (C1) complex. C1s serine protease function initiates the complement signalling cascade through cleavage of other C1 complex components (Reid, 1986). Also cleaves non-complement proteins such as MHC class 1 molecule (Eriksson and Nissen, 1990), insulin-like growth factor binding protein 5 (Busby et al., 2000) and Wnt receptor, lipoprotein receptor-related protein 6 (Naito et al., 2012). |
| CAV1 | Caveolin-1 | Scaffolding protein that is the main component of caveolae (Rothberg et al., 1992). Furthermore, can interact with many proteins outside of the exocytosis mechanism. For example, binds to TLR4 to suppress macrophage proinflammatory signalling (Wang, X.M. et al., 2009), β 1 integrin to initiate actin remodelling (Yang, B. et al., 2011) and Rho-GTPase to initiate cell migration (Arpaia et al., 2012). |
| COL1A1 | Collagen type 1 α 1 | Component of type 1 collagen, the dominant protein in connective tissue from tendon (Hanson and Bentley, 1983). Forms the heteromeric type pro-alpha 1 chain. Formation of a type 1 collagen molecule requires two type pro-alpha 1 chains and one pro-alpha2 chain (Gura et al., 1996). |
| CXCL12 | Stroma cell-derived factor 1 (SDF1) | Induces strong chemotaxis of lymphocytes (Bleul et al., 1996) mediated through chemokine receptor (CXCR) 4 binding (Schiraldi et al., 2012). Stimulates angiogenesis through CXCR7 activation (Zhang, M. et al., 2017). Important for embryogenesis, immune regulation and tissue regeneration (Cheng, J.W. et al., 2014). |
| FAP | Fibroblast activation protein (FAP) | Atypical serine protease with dual-specificity dipeptidyl-peptidase function that either resides on cell surface or in plasma in its truncated form. Cleavage function has demonstrated importance in blood clotting (Lee, K.N. et al., 2004), obesity (Dunshee et al., 2016) and is expressed highly during embryogenesis. |
| ITGA11 | Integrin α 11 | The alpha chain of heterodimeric integrin dimer with integrin beta 1 (Velling et al., 1999). Important for cell binding to type 1 collagen and oncogene phosphorylation (Erusappan et al., 2019). |
| PDGFRA | Platelet-derived growth factor receptor alpha (PDGFR α) | Cell-surface receptor tyrosine kinase that binds to and is activated by platelet derived growth factors (PDGF). Once bound to PDGF, the receptor heterodimerises and phosphorylates itself and other proteins to initiate a signalling cascade. Important during embryogenesis (Schatteman et al., 1992) and angiogenesis (Zhu, K. et al., 2013). |
| PDGFRB | Platelet-derived growth factor receptor beta (PDGFR β) | Cell-surface receptor tyrosine kinase that binds to and is activated by PDGF. Once bound to PDGF, the receptor heterodimerises and phosphorylates itself and other proteins to initiate a signalling cascade. Phosphorylation creates binding site for PI3K (Kazlauskas and Cooper, 1990), which stimulates PI3K/Akt signalling pathway (Wang, H. et al., 2012) |

| | | |
|---------------------|---|---|
| <i>PDPN</i> | Podoplanin | Mucin-type transmembrane glycoprotein. Essential for organ and lymphatic tissue in embryonic development. Important for development of organs such as lungs (Ramirez et al., 2003) and the lymphatic system (Schacht et al., 2003). Only known agonist to myeloid origin protein, CLEC2, who's activation induces immunosuppression (Rayes et al., 2017). |
| <i>TMTC1</i> | Transmembrane O-Mannosyltransferase Targeting Cadherins 1 (TMTC1) | Endoplasmic reticulum (ER) integral membrane protein involved in ER calcium homeostasis (Sunryd et al., 2014). |

Prior studies have identified that CAF marker genes strongly correlate with each other within whole-tissue mRNA-Seq databases (Qiu et al., 2021; Kelley et al., 2018). Therefore, to verify whether the selected TNBC-specific CAF marker genes identified during the literature review stage were accurate indicators that CAFs were present within tumours, the marker genes were correlated against one another. Correlations (Spearman's rank, FDR 1%) were performed in an exploratory cohort (**Figure 4.4A**; TCGA, n=123) and a validation cohort (**Figure 4.4B**; METABRIC, n=299) for TNBC. For heatmap generation, hierarchical clustering of genes was performed. Within both the exploratory and validation cohorts, two clusters of TNBC-specific marker genes formed. These clusters appear to be influenced by positive correlations or absence of correlation between marker genes. Within both cohorts, TMTC1 rarely correlates with other marker genes and is the only occupant in the "absence of correlation" cluster in the validation cohort. C1S joins TMTC1 in the "absence of correlation cluster" in the validation cohort. Every other TNBC-specific CAF marker gene exhibited strong correlations. These findings were replicated in BLCL tumours from the same databases (TCGA, n=85; METABRIC, n=398; **Appendix Figure B.1A-B**; Venn diagram showing overlap in patients between TNBC and BLCL cancers in the two cohorts shown in **Appendix Figure B.2**). The strong correlations between all CAF-markers suggested there were not multiple CAF-subtypes.

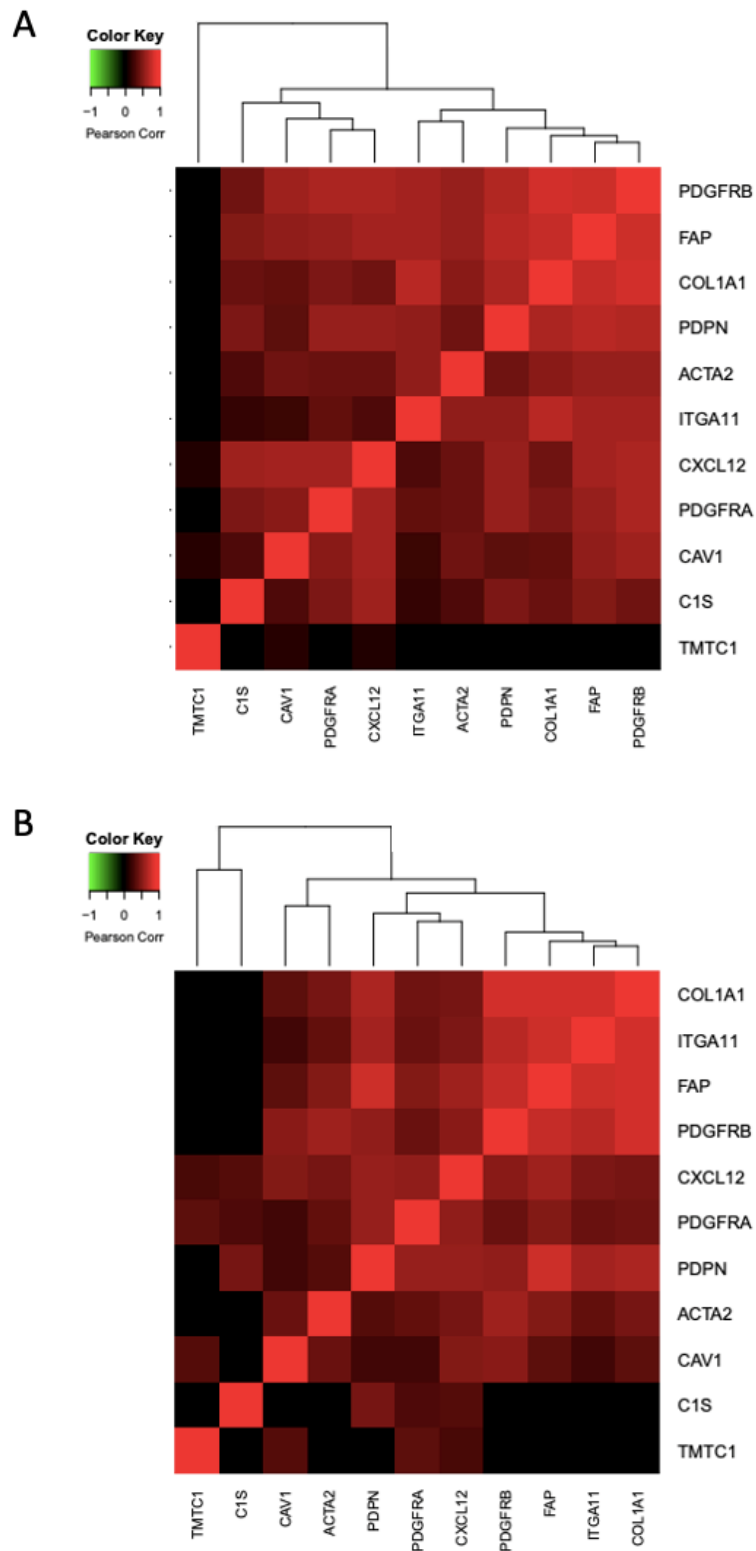


Figure 4.4 Correlations between triple negative breast cancer-associated fibroblast markers.

Correlations between TNBC-CAF markers. Dendrograms represent subgrouping of genes within the heatmap. (A) Validation cohort of mRNA-Seq data from 123 TNBC tumours from TCGA. (B) Experimental cohort of mRNA-Seq data from 299 TNBC tumours from METABRIC. Analysis performed and heat-maps generated by Olivia Burton, Elton Vasconcelos and LeedsOmics.

4.4.1.2 Expression of CAF-marker genes correlates with expression of a subset of LXR target genes in TNBC and BLCL tumours

Following the generation of a panel of TNBC-specific CAF marker genes, the next step was to understand whether CAFs potentially induce LXR signalling in whole TNBC tumours. To elucidate this, TNBC-specific CAF markers were associated with a panel of canonical LXR target genes. LXR target genes were selected based on evidence of an LXR binding site present in their promoter region and increased mRNA expression in response to natural or synthetic LXR agonist treatment (**Table 4.6**). TNBC-specific CAF markers were also correlated against negative control genes, to highlight the association between CAFs and LXR-target genes (*NR1H2*, *CYP7A1* and *MLXIPL*).

Table 4.6 Table of LXR target genes

| Gene name | LXR promoter binding in human cells/tissue | Change in gene expression in response to LXR ligands in human cells/tissue |
|----------------------|--|--|
| <i>ABCA1</i> | (Laffitte et al., 2001a) | (Ulven et al., 2004; Ignatova et al., 2013b; Menke et al., 2002; Mak et al., 2002; Beyea et al., 2007) |
| <i>ABCB1</i> | (Hutchinson et al., 2021) | (Hutchinson et al., 2021; ElAli, A. and Hermann, D. M., 2012; Saint-Pol et al., 2013) |
| <i>ABCG1</i> | (Laffitte et al., 2001a) | (Ignatova et al., 2013a; Menke et al., 2002; Edwards et al., 2002; Beyea et al., 2007) |
| <i>ABCG5</i> | (Back et al., 2013) | (Dianat-Moghadam et al., 2021) |
| <i>ABCG8</i> | (Back et al., 2013) | (Dianat-Moghadam et al., 2021) |
| <i>APOE</i> | (Laffitte et al., 2001b) | (Suon et al., 2010; Hutchinson et al., 2019b) |
| <i>CETP</i> | (Luo, Y. and Tall, 2000) | (Honzumi et al., 2010; Lakomy et al., 2009) |
| <i>CH25H</i> | (Liu, Y. et al., 2018) | (Liu, Y. et al., 2018) |
| <i>LPL</i> | (Zhang, Y. et al., 2001) | (Zhang, Y. et al., 2001) |
| <i>NR1H3</i> | (Laffitte et al., 2001a) | (Laffitte et al., 2001a) |
| <i>SREBF1</i> | (Fernández-Alvarez et al., 2011) | (Menke et al., 2002; Beyea et al., 2007) |

Correlations (Spearman's rank, FDR 1%) were performed in an exploratory cohort (**Figure 4.5A**; TCGA, n=123) and a validation cohort (**Figure 4.5B**; METABRIC, n=299) for TNBC tumours. In the exploratory cohort *ABCA1*, *ABCB1*, *CETP* and *CH25H* positively correlated with six or more TNBC-CAF marker genes. However, in the validation cohort, *ABCA1*, *ABCB1*, *ABCG1*, *CETP*, *CH25H* and *LPL* positively correlated with six or more TNBC-specific CAF marker genes. These correlations were also performed with BLCL expression data (TCGA, n=85; METABRIC, n=398), with similar correlation patterns found, albeit stronger (**Appendix Figure B.3A-B**). *ITGA11* and *ACTA2* show little to no association in LXR target genes. In both dendrograms, four LXR target genes; *ABCA1*,

ABCB1, *CH25H* and *CETP* are clustered together. However, in the exploratory cohort *APOE* is included in this cluster, whereas *ABCG1* and *LPL* are integrated within the cluster in the METABRIC validation cohort. From the exploratory cohort, *PDGFRB* and *CAV1* are lost from a cluster of CAF marker genes that strongly correlate with LXR target genes. TNBC CAF-specific marker genes that correlate with LXR targets consistently across the TNBC and BLCL validation cohorts are *C1S*, *CAV1*, *CXCL12*, *PDGFRA*, *PDGFRB* and *PDPN*. This suggested that the presence of CAFs in primary TNBC was correlated with LXR activity. Previous reports have indicated that CAFs are able to synthesise and secrete oxysterols (Kannenberget al., 2013; Lange et al., 2009; Saucier, S. E. et al., 1985) so the next section evaluated if CAFs could activate LXR activity when co-cultured in vitro.

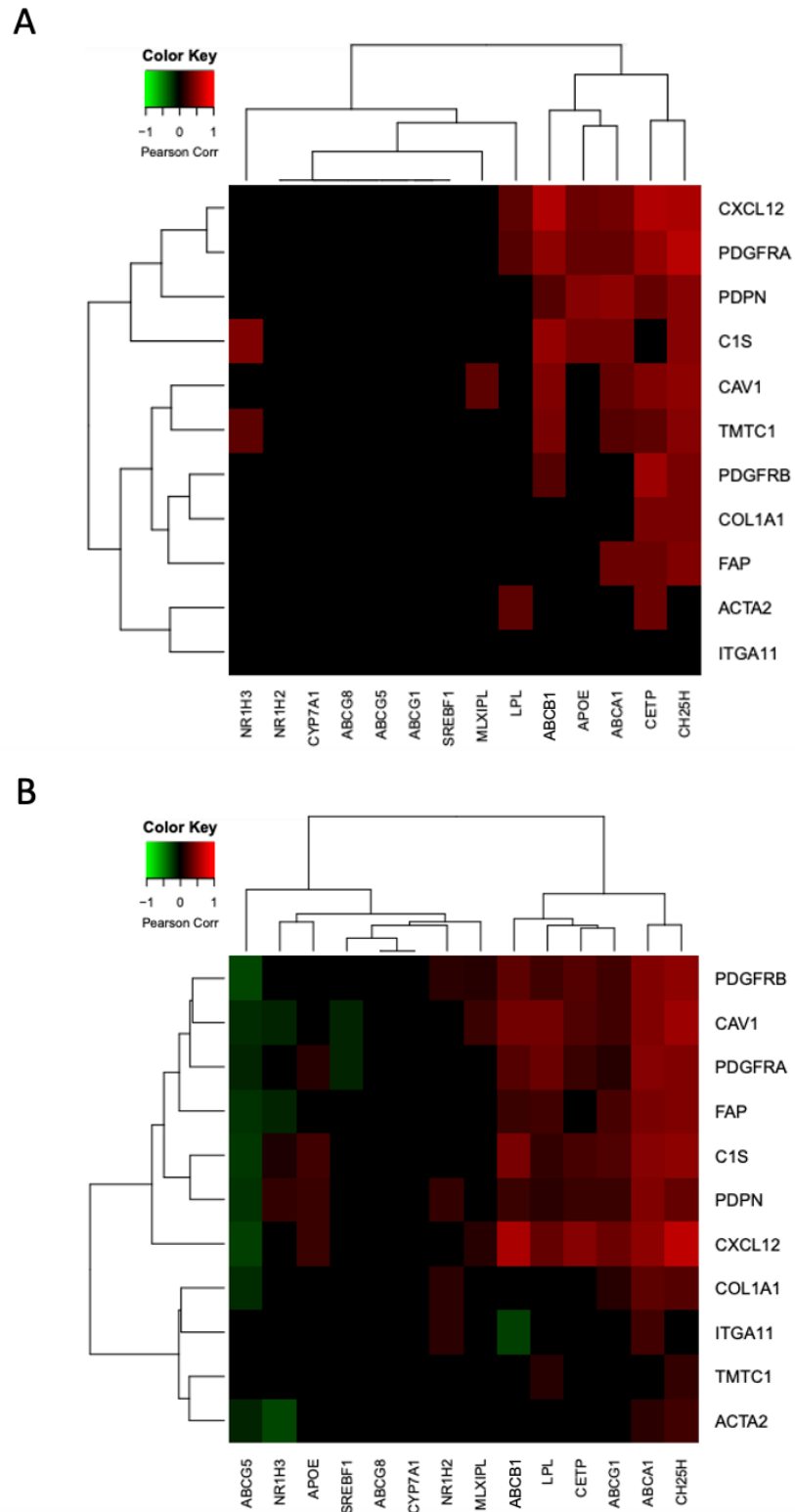


Figure 4.5 Triple negative breast cancer-specific cancer associated fibroblast marker genes correlate with canonical LXR marker genes in triple negative breast tumours.

Correlations between TNBC-CAF markers, LXR target genes and control genes. Dendrograms represent subgrouping of genes within the heatmap. (A) Validation cohort of mRNA-Seq data from 123 tumours from TCGA. (B) Experimental cohort of mRNA-Seq data from 299 tumours from METABRIC. Analysis performed and heat-maps generated by Olivia Bunton, Elton Vasconcelos and LeedsOmics.

4.4.2 Oxysterols secreted by CAFs activate LXR in epithelial cells

Correlations between TNBC-specific CAF marker genes and a subset of canonical LXR target genes suggest that CAFs can induce LXR signalling in the TME. I hypothesised that this pathway was mediated by oxysterols secreted by the CAFs. To establish if CAFs activated LXR signalling in adjacent TNBC epithelial cells, the capacity of CAFs to produce OHCs was determined and then whether co-culture of CAFs with TNBC cells led to LXR activation was determined and if this was dependent on OHC production.

4.4.2.1 Comparison of oxysterol producing enzyme expression and oxysterol concentration in cancer cells and CAFs

To assess the potential contribution of oxysterols to the TME from CAFs, their expression of oxysterol producing enzymes; CYP46A1, CH25H and CYP27A1 was determined. The CAFs I used were cancer-associated fibroblasts derived from a luminal A breast tumour (Verghese et al., 2011). CAF cells expressed a significantly higher level of both CYP46A1 and CYP27A1 than MDA-MB-468 cells (**Figure 4.6**; two-tailed t-test: $p < 0.0001$ for both), however there was no significant difference in CH25H expression between the two cell lines. CAF cells were also compared to another TNBC cell line, MDA-MB-453. CAFs expressed higher levels of CH25H and CYP27A1 (**Appendix Figure B.4A**; $p < 0.0001$ for both) than MDA-MB-453s but lower CYP46A1 ($p < 0.0001$)

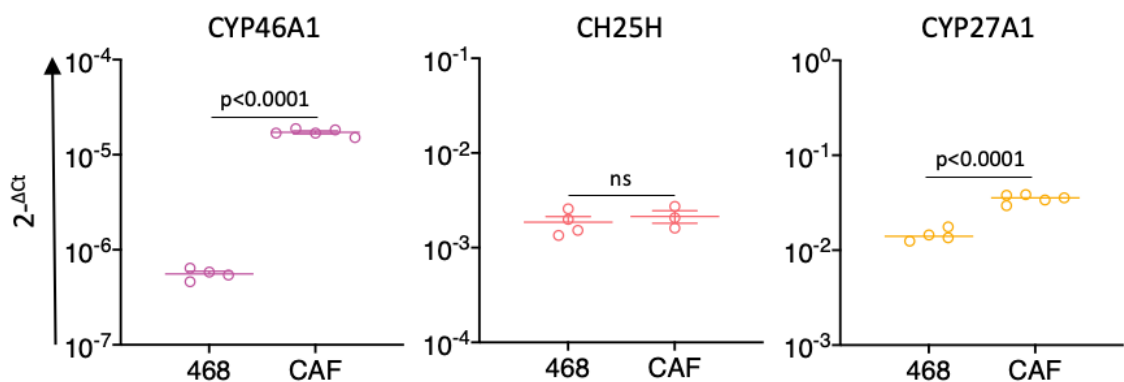


Figure 4.6 CAFs and epithelial cells have differential expression of oxysterol producing enzymes.

Epithelial cells (MDA-MB-468) and cancer-associated fibroblasts (CAF) were cultured individually and assessed for expression of CYP46A1, CH25H and CYP27A1 and compared using $\Delta\Delta Ct$ method normalised to HPRT expression. Data presented are the mean and SEM from three to five biological replicates of two technical replicates. P-values generated using two-tailed t-tests.

Furthermore, to identify whether CAFs of breast tumours have high intracellular oxysterol content relative to cancer cells, oxysterols were measured in CAFs and MDA-MB-468s by LC-MS/MS (cells pelleted by Dr Sam Hutchinson and measured by Dr Hanne Roberg-Larsen). CAFs contained significantly higher levels of 24OHC (CAF to MDA-MB-468: 104 to 8 pmol/100,000 cells; $p=0.007$), 25OHC (CAF to MDA-MB-468: 108 to 5 pmol/100,000 cells; $p=0.03$) and 26OHC (CAF to MDA-MB-468: 556 to 58 pmol/100,000 cells $p=0.05$) than MDA-MB-468s (**Figure 4.7**). CAFs contain significantly higher intracellular levels of all three oxysterols compared to MDA-MB-453 cells (**Appendix Figure B.4B**; 24OHC: $p=0.02$, 25OHC: $p=0.03$, 26OHC: $p=0.04$).

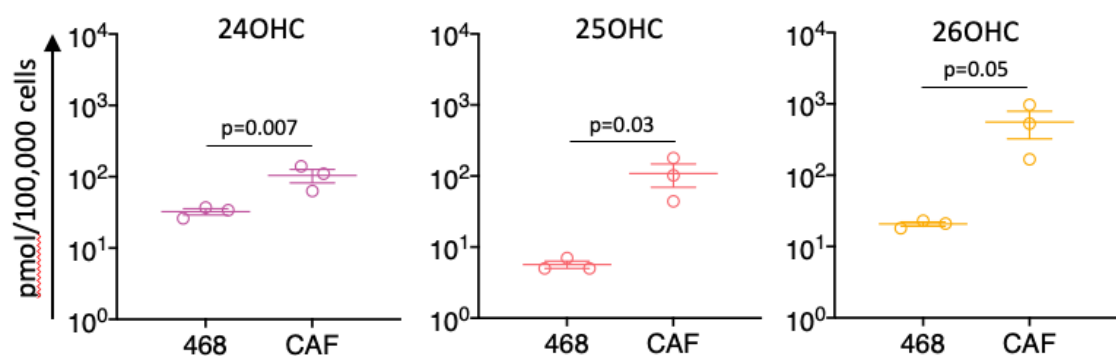


Figure 4.7 CAFs contain higher intracellular concentrations of oxysterols than MDA-MB-468s. Intracellular concentrations of oxysterols within CAF and MDA-MB-468 cells measured using LC-MS/MS. P-values generated using one-tailed t-tests.

To assess the potential for CAFs and cancer cells to secrete oxysterols into their surroundings, CAF and MDA-MB-468 conditioned media were assessed for oxysterol content. Cells conditioned media until the media began to acidify (**Appendix Figure B.5**) (Held, 2018), with oxysterols measured from this point by LC-MS/MS (measured by Dr Hanne Roberg-Larsen). CAF conditioned media contained higher levels of 24OHC (884 to 285 pmol/L) and 25OHC (676 to 413 pmol/L) than MDA-MB-468s (**Figure 4.8**; two-tailed t-test: 24OHC: $p=0.02$, 25OHC: $p=0.05$), although there was no difference in 26OHC concentration in media conditioned by the two cell lines. CAF conditioned media contains significantly higher levels of 26OHC (**Appendix Figure B.4C**; $p<0.0001$) than MDA-MB-453 CM, however had lower levels of 24OHC ($p=0.04$) and no significant difference in 25OHC.

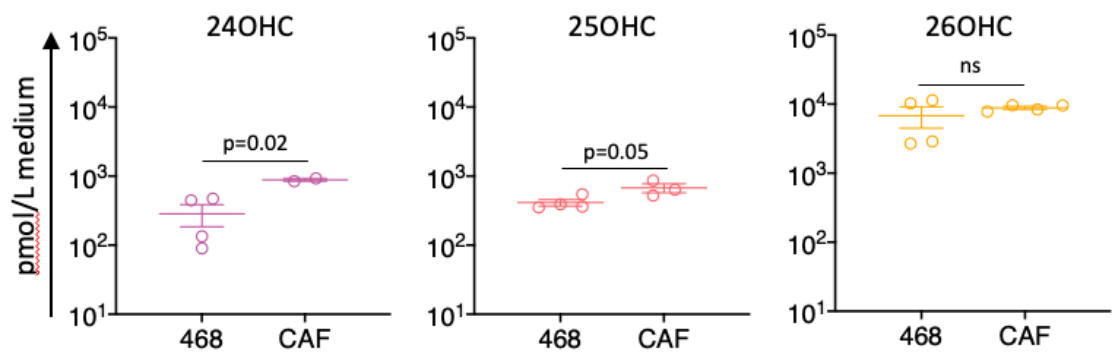


Figure 4.8 CAFs secrete higher concentrations of 24OHC and 25OHC than MDA-MB-468s. Oxysterol concentrations in media conditioned by CAFs and MDA-MB-468s measured using LC-MS/MS. P-values generated using two-tailed t-tests.

4.4.2.2 CAFs require oxysterol synthesising enzymes to activate LXR in adjacent TNBC cells

As shown in 4.4.2.1, CAFs express oxysterol producing enzymes and can both produce and secrete oxysterols. To test if the production of oxysterols by CAFs was sufficient to drive LXR activity in adjacent TNBC cells, co-culture assays were performed. LXR transactivation in adjacent TNBC cells was quantified using MDA-MB-468-LXR-Luc cells. The expression of luciferase protein in these cancer cells provides a quantifiable signal of LXR-dependent transactivation. Cells were cultured together at four different ratios (all shown as MDA-MB-468:CAF): 1:0.25, 1:0.5, 1:1 and 1:2, with CAFs tested at four different seeding densities and MDA-MB-468 cell number unchanged. After 16 h of incubation, luciferase signal was assessed, finding that there was a significant increase in luciferase transactivation in ratios; 1:0.25, 1:0.5 and 1:1 (Figure 4.9; one-way ANOVA: $p=0.05$, $p=0.001$ and $p=0.001$, respectively).

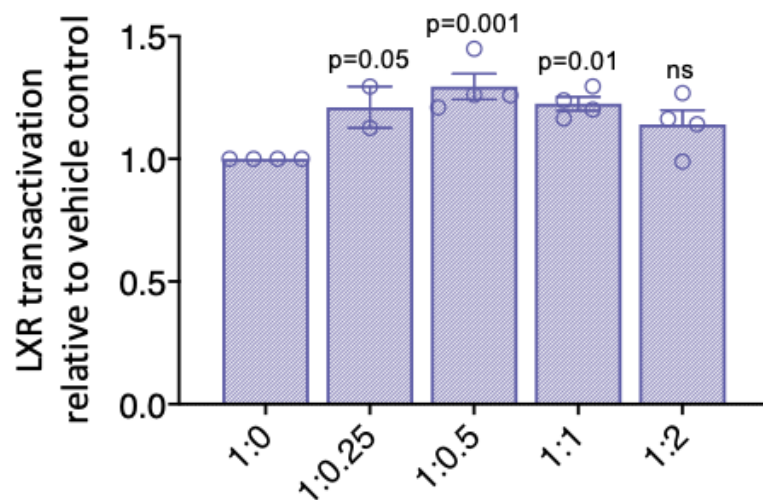


Figure 4.9 CAF secretions induce LXR signalling in MDA-MB-468s.

LXR inducible luciferase reporter MDA-MB-468 cells were co-cultured with CAF cells for 16 h at 5 different cellular ratios; 1:0, 1:0.25, 1:0.5, 1:1 and 1:2, with MDA-MB-468 cells representing the left value and CAF cells representing the right value. One-way ANOVA with multiple comparisons was performed.

To assess whether luciferase induction in cancer cells is driven through oxysterol secretions from co-cultured CAFs, a triple knockdown of three major oxysterol producing enzymes (CYP46A1, CH25H and CYP27A1) was performed (**Figure 4.10A**; one-way ANOVA: all three $p < 0.0001$). When these triple KD CAFs were co-cultured with MDA-MB-468-LXR-Luc reporter cells, their ability to induce LXR-dependent activation was significantly reduced compared to mock (siCON) transfected cells (**Figure 4.10B**) by around 10-15%. (1:0.25 ratio $p = 0.0001$, 1:0.5 ratio $p = 0.01$). These results support the hypothesis that oxysterols are the mediating signal that cause CAFs to increase the activity of LXR in adjacent cancer cells. However, assessment of LXR transactivation in MDA-MB-468 monoculture as an additional control would have provided further evidence on whether CYP46A1, CH25H and CYP27A1 were driving the CAF-mediated LXR transactivation.

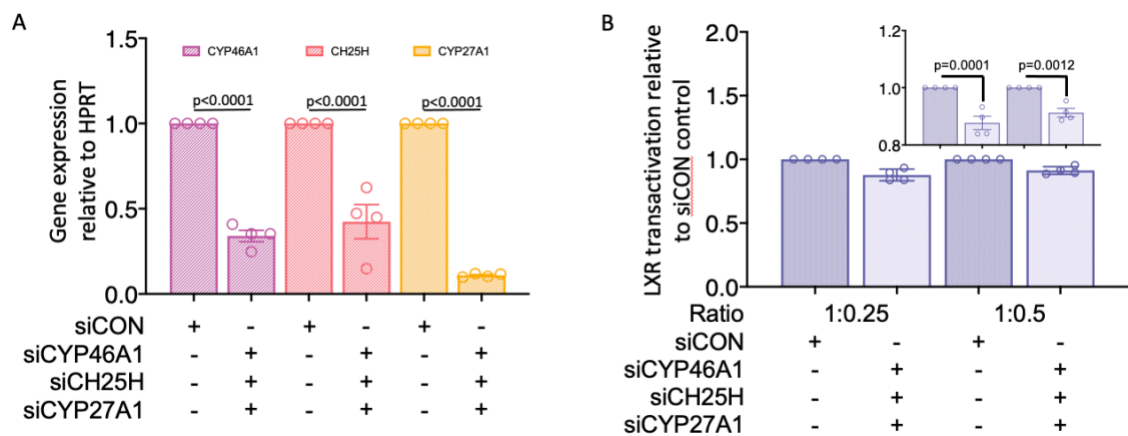


Figure 4.10 Knockdown of oxysterol producing enzymes in CAFs may impair ability to induce LXR.

(A) Gene expression analysis of CAF cells that were simultaneously transfected with either siRNA targeting CYP27A1, CH25H and CYP46A1, or siCON for 72 h. Changes in expression of CYP27A1, CH25H and CYP46A1 were assessed. Gene expression was normalised against samples treated with siCON. (B) LXR inducible luciferase reporter MDA-MB-468 cells were co-cultured with CAF cells with siCYP27A1, siCH25H and siCYP46A1 knockdown for 16 h. Co-cultures were performed at two cellular ratios; 1:0.25 and 1:0.5, with MDA-MB-468 cells representing the left value and CAF cells representing the right value. Data are presented on a continuous axis and on a reduced axis insert to aid clarity. Data presented as four biological replicates of six technical replicates. One-way ANOVA with multiple comparisons was performed.

4.4.2.3 CAF conditioned media activates LXR in TNBC cells

To establish whether the factors derived from CAFs that activated LXR were secreted, media collected from CAFs was added to MDA-MB-468-LXR-Luc cells. If the factors were secreted (as expected for oxysterols) then LXR should still be activated. If LXR was not activated by CM, then either cell-cell contact or a bi-directional communication is required. CAF-CM significantly increased LXR reporter gene activity (**Figure 4.11A**; 16 h: $p=0.037$); 24 h $p=0.028$) and endogenous LXR target gene expression (**Figure 4.11B**; *ABCA1*: 48 h $p=0.002$; **Figure 4.11C**; *ABCB1*: 24 h $p=0.0017$). These data demonstrate the ability of the CAF secretome to activate LXR and upregulate expression of canonical LXR marker genes, *ABCA1* and *ABCB1*.

The evidence provided suggests that CAFs induce LXR signalling in adjacent epithelial cells through oxysterol secretions. CAF secretion of oxysterols can occur irrespective of contact or communication with epithelial cells. Oxysterols secreted by CAFs may be inducing expression of canonical LXR targets, *ABCA1* and *ABCB1*, through transactivating LXR.

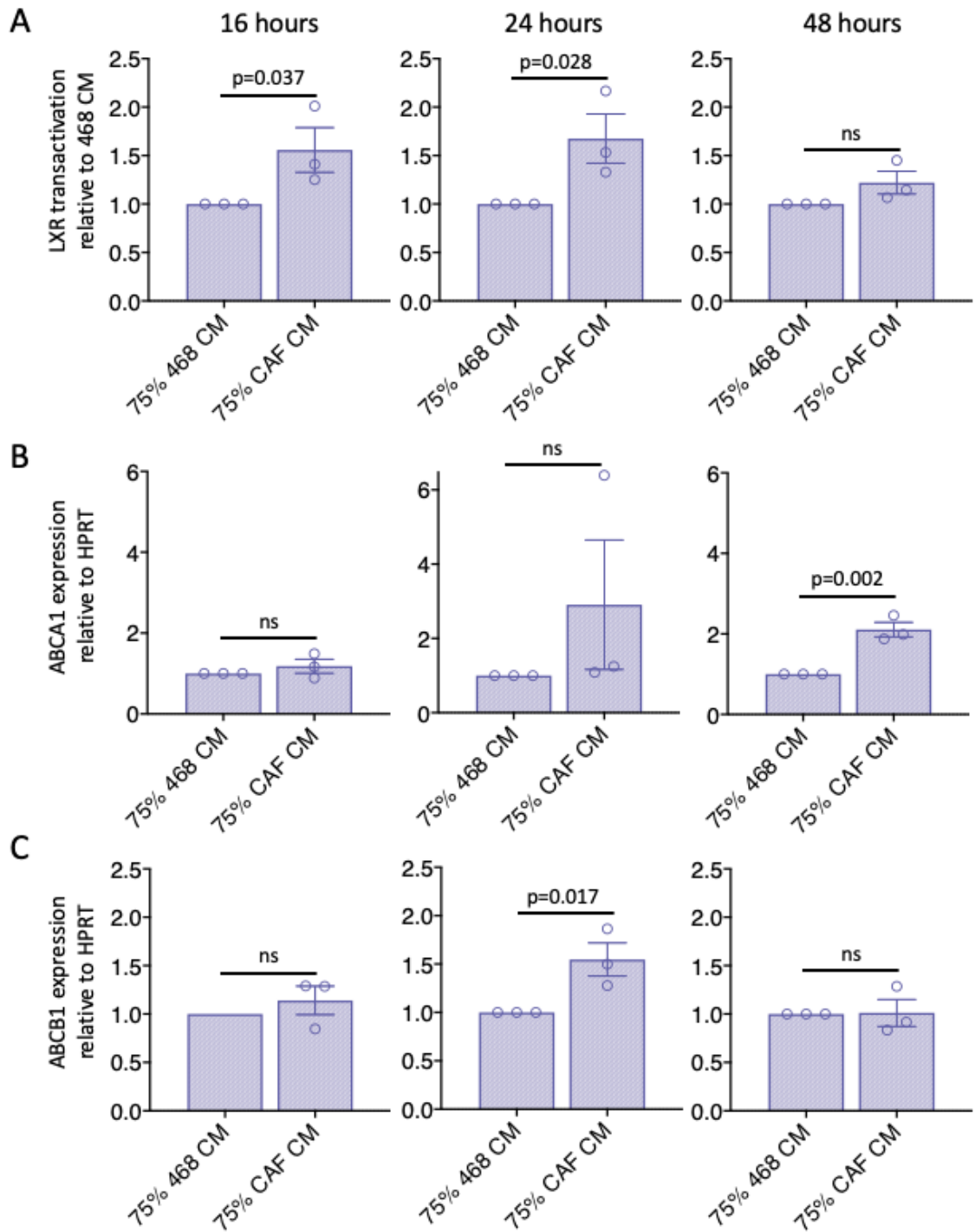


Figure 4.11 CAF conditioned media induces expression of *ABCA1* and *ABCB1*.

LXR inducible luciferase reporter MDA-MB-468 cells were treated with either 75% CAF or 75% MDA-MB-468 CM for 16, 24 or 48 h. (A) Comparison of luciferase expression, (B) *ABCA1* mRNA expression and (C) *ABCB1* mRNA expression in MDA-MB-468 cells treated with either MDA-MB-468 CM or CAF CM. Data presented as three biological replicates, with one-tailed student's t-test performed.

4.4.3 Stromal oxysterol synthesising enzymes associate with epithelial Pgp expression

4.4.3.1 Stromal expression of oxysterol producing enzymes associates with DFS and epithelial Pgp expression

CAFs are the most abundant non-cancer cell type within breast tumour stroma. Consequently, stromal proportion provides a rough estimate as to how rich in CAFs tumours are. Furthermore, section 4.4.2.2 highlighted the importance of the expression of oxysterol producing enzymes in CAFs for LXR transactivation. Therefore, to determine whether expression of oxysterol producing enzymes in CAFs *in vivo* influence epithelial Pgp expression and DFS, the stromal expression of oxysterol producing enzymes, CYP46A1, CH25H and CYP27A1 were quantified in the TMA cohort. All antibodies used were validated for target specificity and optimised in **Appendices Figure A.1-7**. Weighted histoscores were calculated for total stroma of the three enzymes (respective images in **Figure 4.12A**). CYP46A1 and CH25H were expressed more highly in tumour stroma from patients that had suffered an event against those that had not (**Appendix Figure B.6A**; Welch's t-test: CYP46A1, $p=0.034$; CH25H, $p=0.037$). The expression was measured to assess if it was predictive of DFS, with cut off points determined using ROC curves (**Appendix Figure B.6B**). High expression of all three enzymes associated with reduced DFS (**Figure 4.12B**; log-rank test: CYP46A1, $p=0.008$; CH25H, $p=0.002$; CYP27A1, $p=0.018$). Additionally, stromal expression of all three enzymes also positively associated epithelial expression of Pgp (**Figure 4.12C**; Pearson's rank: CYP46A1, $R^2=0.22$, $p<0.0001$; CH25H, $R^2=0.34$, $p<0.0001$; CYP27A1, $R^2=0.07$, $p=0.014$). Furthermore, *stromal* expression of all three enzymes also positively correlated with *epithelial* CH25H expression (**Appendix Figure B.7**; Spearman's rank: CYP46A1, $R^2=0.28$, $p<0.0001$; CH25H, $R^2=0.51$, $p<0.0001$; CYP27A1, $R^2=0.04$, $p=0.04$).

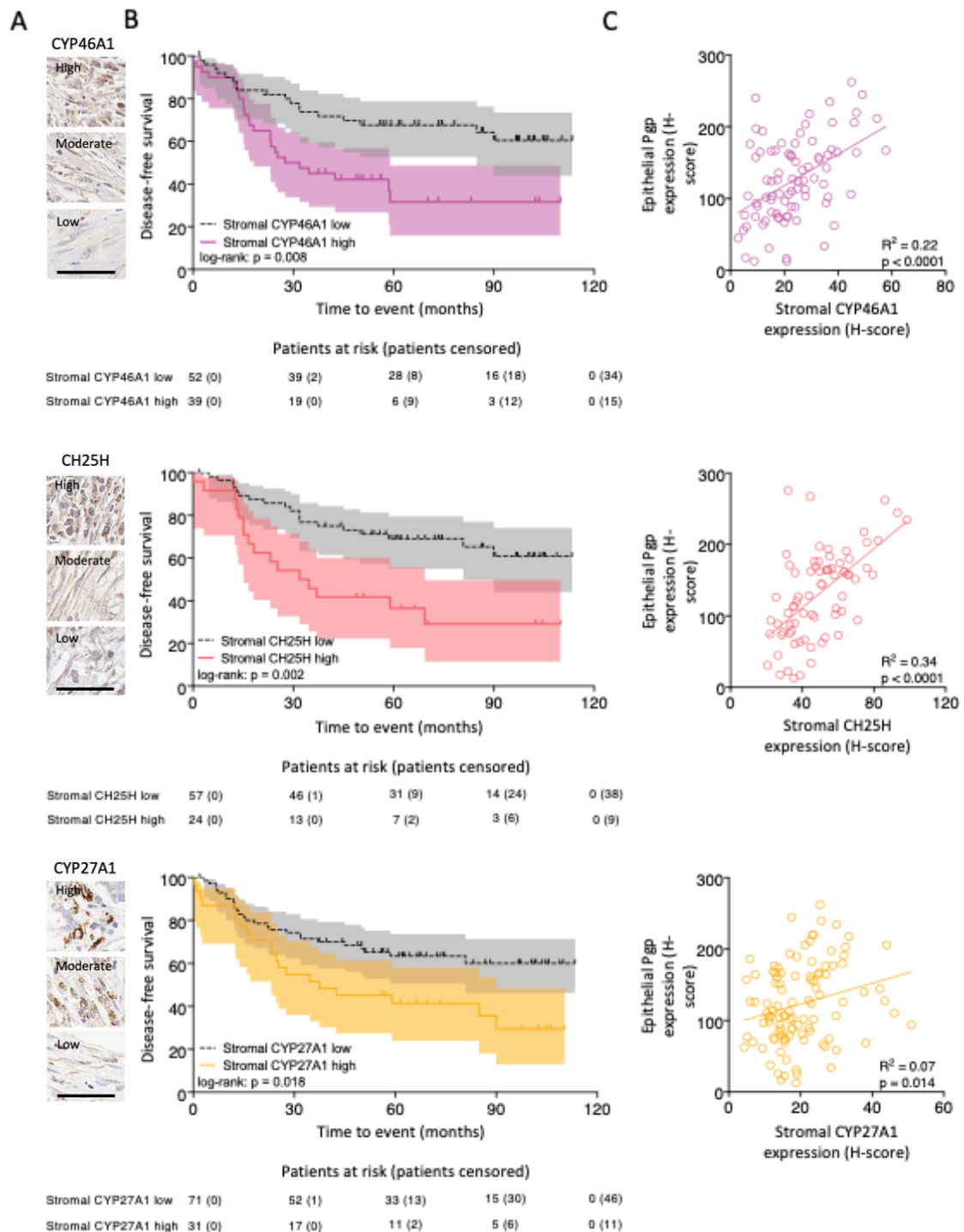


Figure 4.12 High expression of oxysterol producing enzymes in stroma are predictive of reduced disease-free survival and associate with epithelial Pgp expression.

(A) Representative images of low, moderate and high stromal stains for CYP46A1, CH25H and CYP27A1. Kaplan-Meier analysis of (B) CYP46A1 (low H-score= <24.7, high H-score= >24.7), CH25H (low H-score= <58.7, high H-score= >58.7) and CYP27A1 (low H-score= <23.2, high H-score= >23.2). Log-rank test was performed to assess significance. Shaded areas represent 95% CI and patients at risk of suffering an event are shown beneath each Kaplan-Meier curve. (C) Correlation between stromal CYP46A1, CH25H and CYP27A1 expression and epithelial Pgp expression. Pearson's rank used to test association.

4.4.3.2 Combining stromal expression of oxysterol producing enzymes and stromal proportion strengthens the association with epithelial Pgp expression

Within the TMA, stroma accounted for 9-98% (median: 68%, SD: 22%) of the total tumour (**Appendix Figure B.8**). This high variation in stromal proportion may influence the association between stromal oxysterol producing enzyme expression and both epithelial Pgp expression and DFS. Therefore, the contribution of the stromal proportion was assessed to epithelial Pgp expression and DFS. A representative image of epithelial and stromal proportions within a tumour is shown in **Figure 4.13A**. First, the stromal proportion was compared against patients that had suffered an event and those that had not, finding no significant difference in stromal proportion (**Appendix Figure B.9A**). A ROC curve was generated (**Appendix Figure B.9B**) to dichotomise the data for assessment of stromal proportion as a prognostic indicator, finding that high stromal proportions within TNBC tumours associated with reduced DFS (**Figure 4.13B**; log-rank test: $p=0.017$). Furthermore, stromal proportions also positively correlated with epithelial Pgp expression (**Figure 4.13C**; Spearman's rank: $R^2=0.09$, $p=0.003$). Additionally, stromal proportions positively correlated with epithelial CH25H expression (**Appendix Figure B.10**; Spearman's rank: $R^2=0.04$, $p=0.05$), another LXR target gene (Liu, Y. et al., 2018).

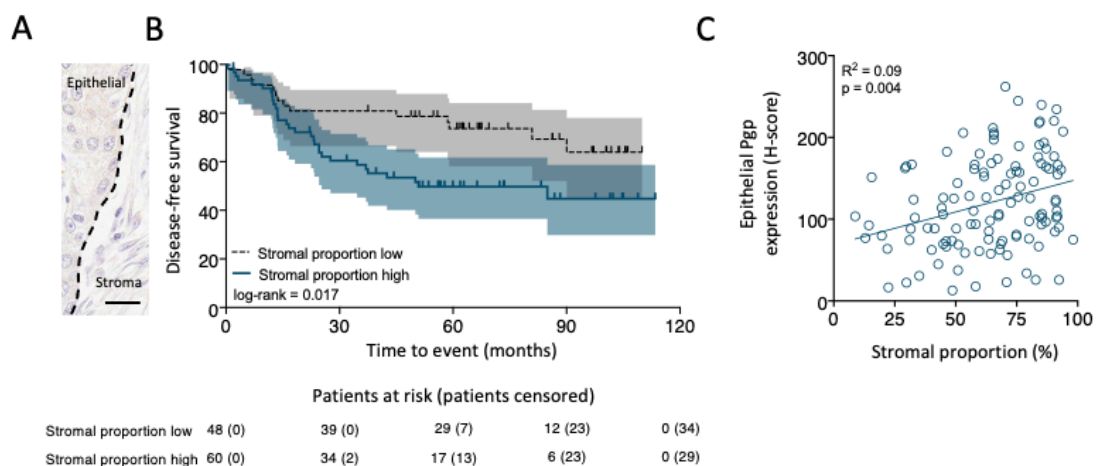


Figure 4.13 Increased tumour stroma associates with likelihood of event and Pgp expression. (A) Representative image of epithelial and stromal proportions within a tumour core. Scale bar represents 25 μm . (B) Kaplan-Meier analysis with 95% confidence intervals of stromal proportions (low stromal proportion = $<62.2\%$, high stromal proportion = $>62.2\%$). Log-rank test was performed to assess significance. Patients at risk of suffering an event are shown beneath each Kaplan-Meier curve. (C) Correlation of stromal proportions with Pgp H-score in epithelial cells. Spearman's rank was used to assess correlation.

The stromal proportion and stromal expression of oxysterol producing enzymes were then multiplied together, thereby creating an assessment of overall amount of stromal oxysterol producing enzymes in the tissue, and assessments were made as to whether this improved associations with epithelial Pgp expression. CYP46A1, CH25H and CYP27A1 all remained significant (**Figure 4.14A-C**; all $p < 0.0001$) and all R^2 values increased significantly from those seen with expression level within the stromal compartment alone (**Figure 4.14D**; paired t-test: $p = 0.035$). These data suggest that stromal proportions and stromal expression of oxysterol producing enzymes are complement each other in the induction of epithelial Pgp expression.

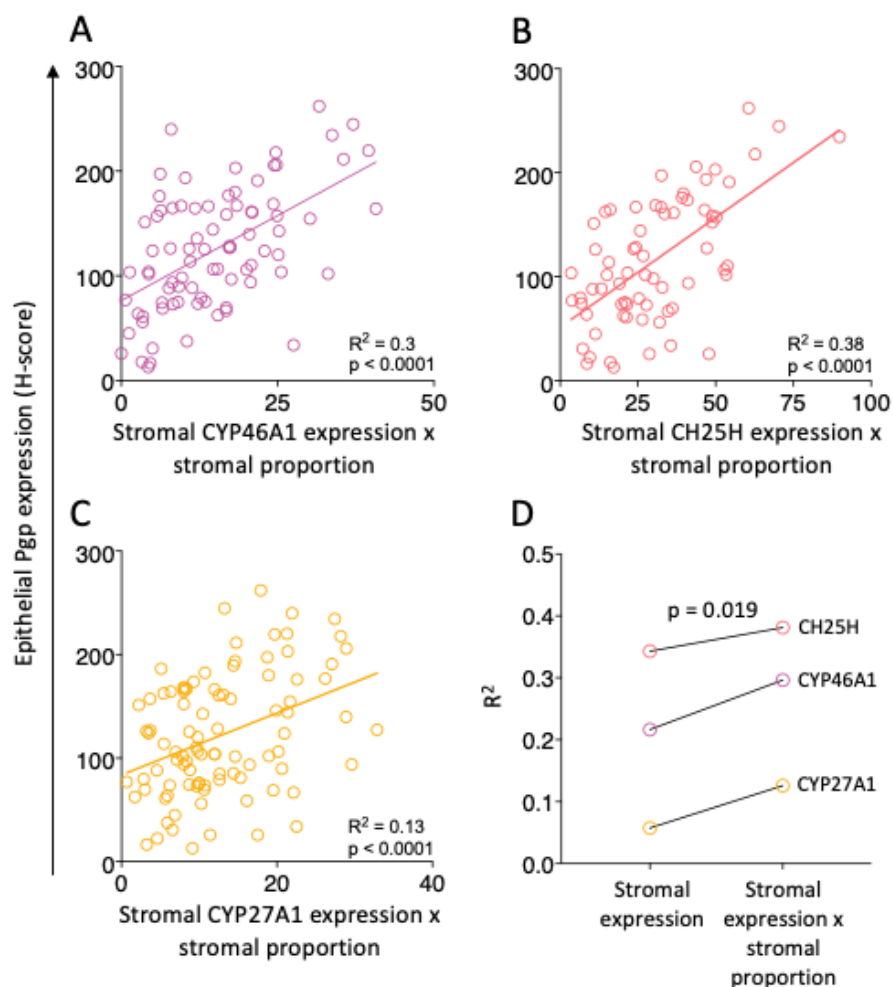


Figure 4.14 Stromal expression of oxysterol producing enzymes works synergistically with stromal proportion to improve association with epithelial Pgp expression.

(A-C) Stromal expression of CYP46A1, CH25H and CYP27A1 were multiplied by the stromal proportion as correlated with epithelial Pgp expression. (D) Change in R^2 before and after stromal expression was multiplied by stromal proportion. Pearson's rank was used to test association.

4.5 Discussion

This work suggests that there is a contribution of CAFs to epithelial LXR signalling and Pgp expression. 24OHC and 26OHC and their synthesising enzymes CYP46A1 and CYP27A1 were higher in CAFs than 468 cells. Surprisingly, despite an approximate 10-fold difference in intracellular 25OHC content and increased secretion of 25OHC in CAFs compared to MDA-MB-468s, there is no significant difference in CH25H between the two cell lines. The production of 25OHC by CYP27A1 (Li, X. et al., 2007) and CYP46A1 (Lund, E.G et al., 1999) may be driving increased 25OHC production in CAFs, although the enzymes' rates of 25OHC production are much lower than CH25H. Therefore, this is more likely to be the result of reduced 25OHC metabolising enzymes in CAFs compared to MDA-MB-468s, such as CYP7B1 (Griffiths et al., 2016a).

CAF express oxysterol producing enzymes to a higher degree than TNBC cells and have higher intracellular oxysterol content than MDA-MB-468s. However, intracellular content of oxysterols may not associate with oxysterol concentration secreted in exosomes. TNBC cell line, MDA-MB-231, shows that despite considerably higher intracellular content of 26OHC than its luminal A-derived counterpart, MCF7, the oxysterol is secreted in exosomes to a 10-fold lesser extent (Roberg-Larsen et al., 2017). Evidently, this also seems apparent in CAFs and MDA-MB-468s. Despite high expression of CYP27A1 and intracellular concentration of 26OHC in CAFs compared to MDA-MB-468s, there is no significant difference in the concentration of 26OHC secreted into the media between the two cell lines. This may be due to differences in efflux mechanism for oxysterols, for example 7KC can be exported from the cell by ABCG1 but not ABCA1 (Xu, M. et al., 2009). However, 24OHC and 25OHC are secreted at significantly higher levels by CAFs than MDA-MB-468s, which match the intracellular concentrations of the oxysterols in their respective cells.

The CAF cells used within these experiments are derived from a luminal A tumour (Verghese et al., 2011). Luminal A cancers exhibit a muted response to LXR signalling (Hutchinson et al., 2019b). Therefore, this may result in CAFs that are relatively weaker producers or secreters of oxysterols compared to TNBC-derived CAFs, due to reduced requirement for LXR signalling in luminal A tumours. Moreover, there is differential

expression of CAF marker genes between CAFs derived from tumours of different breast cancer subtypes (Costa, A. et al., 2018), suggesting that differential capabilities to produce and secrete oxysterols between differently derived CAFs may not be unrealistic. Consequently, a greater rate of oxysterol secretion may be obtained from CAFs derived from TNBC tumours. However, there is crossover between CAF subtypes present in luminal A tumours and TNBC tumours. In particular, CAF-S4s are present in a high number of luminal A and TNBC patients (Costa, A. et al., 2018). To identify whether our CAF cell line belongs to CAF subtypes found within TNBC, the expression of CAF markers used in Costa et al. could be assessed within the CAF cell line (Costa, A. et al., 2018).

Irrespective of their CAF subtype, luminal-derived CAF cells elicited an increase in LXR transactivation in MDA-MB-468s in co-culture experiments. However, compared to treatments of the same MDA-MB-468 cells with natural and synthetic ligands, the LXR transactivation is considerably weaker (Hutchinson et al., 2019b). Nevertheless, these experiments using natural ligands were performed at doses 10,000-fold higher than oxysterol concentrations found within conditioned media. Therefore, these changes found following CAF co-culture are more biologically relevant and represent a long-term increased induction of LXR activation over the course of months or years within a tumour. Interestingly, co-culture of MDA-MB-468s and CAFs at a ratio of 1:2 did not find a significant change, although this may be indicative of limitations of cell growth on plates. CAF CM also increased in LXR transactivation relative to MDA-MB-468 CM, suggesting that CAF oxysterol secretions alone are enough to transactivate epithelial LXR irrespective of cell-to-cell contact. Additionally, CAFs were shown to induce expression of canonical LXR target *ABCA1* and *ABCB1*, a chemotherapy resistance protein that is regulated through LXR (Hutchinson et al., 2021). Typically, oxysterol treatments on MDA-MB-468s induce an upregulation of *ABCA1* that is 60-fold larger than to *ABCB1* (Hutchinson et al., 2019b; Hutchinson et al., 2021). Concerningly, *ABCB1* mRNA expression was upregulated here to a greater degree than *ABCA1*, suggesting that some *ABCB1* mRNA upregulation may be the result of other factors secreted by CAFs. For example, in an *in vivo* model of non-small cell lung carcinoma, targeting the CAF proportion within these xenografts with a low dose of 5-fluorouracil lead to the downregulation of epithelial Pgp expression (Ma et al., 2017). Interestingly, primary

culture of CAFs and non-small cell lung carcinoma cells induced Pgp-mediated chemotherapy resistance in epithelial cells through CAF secretion of IGF2, which induced *ABCB1* expression through AKT signalling (Zhang, Q. et al., 2018). IGF2 was secreted in primary breast tumour CAFs more highly than by normal fibroblasts (Gui et al., 2019). Furthermore, following co-culture with MDA-MB-436 cells, secretion of IGF2 increased compared to mono-culture (Gui et al., 2019).

Due to the time constraints of my PhD, I was unable to verify whether epithelial *ABCB1* expression was modulated by CAF oxysterol secretions rather than other components within CAF CM. This could be confirmed through simultaneous knockdown of LXR α and LXR β in MDA-MB-468s before treatment with CAF CM. If epithelial *ABCB1* expression is dependent on oxysterols derived from CAF CM, double knockdown of both LXR α and LXR β will prevent induction of LXR signalling and impair upregulation of *ABCB1* mRNA expression. Similarly, a simultaneous, triple-knockdown of *CYP46A1*, *CH25H* and *CYP27A1* could be performed in the CAF cells to impair their production of 24OHC, 25OHC and 26OHC, respectively. However, whether this would alter the rate of oxysterol secretion would first have to be investigated. Furthermore, there is currently a lack of evidence demonstrating that the increased *ABCB1* induced by CAF CM leads to chemotherapy resistance in epithelial cells. In theory, cell viability assays could show the change in epithelial cell resistance to chemotherapy agent, epirubicin, following treatment with CAF conditioned media. As previously performed in Hutchinson et al., colony forming assays, MTTs and chemotherapy agent efflux assays would demonstrate that CAF CM-mediated upregulation of *ABCB1*/Pgp is driving chemotherapy resistance (Hutchinson et al., 2021). Again, this can be validated through pre-treatment of epithelial cells with siRNA targeting LXR α and LXR β before CAF CM treatment.

Correlations between TNBC-specific CAF marker genes and canonical LXR targets within our METABRIC cohort identified a subgroup of CAF marker genes that strongly correlate with LXR target genes. This subgroup included *C1S*, *CAV1*, *CXCL12*, *PDGFRA*, *PDGFRB* and *PDPN*. Interestingly, very few of these genes have any association with LXR activation *in vitro*, either through increased oxysterol production or upregulation of related genes. In the colon, stromal cells positive for *PDPN* and negative for *CD34* were shown to exhibit

enhanced expression of *CH25H* over infiltrating immune cells and epithelial cells. 25OHC metabolising enzyme, *CYP7B1* was also found to be overexpressed, however to a lesser degree than *CH25H* (Emgård et al., 2018). Interestingly, these colonic fibroblasts resemble CAFs in their marker gene expression. For example, *CD34* negativity is characteristic of CAFs in breast cancer (Gui et al., 2019). Furthermore, overexpression of *CAV1* in aortic endothelial cells coincided with upregulation of canonical LXR target gene, *ABCA1* (Lin et al., 2007). Contrastingly, caveolin-1 has been shown to facilitate the degradation of *ABCA1* (Lu, R. et al., 2016). Additionally, *CXCL12*, which exhibited a remarkably strong association with LXR target genes, has been shown to downregulate *ABCA1* expression *in vitro* (Gao, J.H. et al., 2019). There is no evidence of any interaction between *C1S*, *PDGFR α* and *PDGFR β* with LXR signalling in the current literature. Therefore, marker gene correlations with LXR targets may be driven through their representation of the oxysterol secreting-CAF proportion of tumours, rather than the genes driving LXR signalling themselves.

Our systematic approach to identifying TNBC-specific CAF marker genes was designed to capture as many genes as possible but were definitively able to demark the presence of CAFs in TNBC. However, this method may have led to the inclusion of non-specific genes if they had not been researched in TNBC previously. For example, there is limited information regarding *C1S* and *TMTC1* in TNBC and none relating their expression to any other cell type outside of the studies identified from the systematic review. Monocytes (Bensa et al., 1983), macrophages (Loos et al., 1981) and dendritic cells (Li, K. et al., 2011) have all been shown to produce *C1S* under normal conditions, however their production within a cancer setting, particularly TNBC, is unexplored. In clear-cell renal cell carcinoma, *C1S* was found to be produced by the epithelial cells and not expressed in infiltrating macrophages (Roumenina et al., 2019). Elevated mRNA expression of *C1S* was also found in cutaneous squamous cell carcinoma cells compared to normal skin cells (Riihilä et al., 2020). There has not been any investigation into cellular expression of *TMTC1*. In particular, the inclusion of *TMTC1* a TNBC-specific CAF marker seems questionable as it rarely correlated with other CAF marker genes, suggesting that the presence of *TMTC1* in tumours does not indicate the presence of CAFs (Qiu et al., 2021; Kelley et al., 2018). Another limitation of the selection method was the decision to

choose CAF markers that were highly selective or specific rather than just specific. This choice was due to the high crossover in expression of CAF markers with epithelial cells (Abdel-Khalik, J. et al., 2018). Therefore, expression of marker genes that also appear in epithelial cells would have interfered with LXR target gene correlations if they had been included, potentially impairing hierarchical clustering of CAF subgroups.

Despite the limitations of the systematic approach and *in silico* analysis, the association between the stromal proportion in TNBC tumours and expression of canonical LXR target, Pgp, mirrored findings from the CAF marker-LXR target gene correlations. This suggested that the stromal proportion may induce LXR target gene expression independently from epithelial cells. Furthermore, stroma rich tumours associated with reduced DFS, replicating findings from previous studies (de Kruijf et al., 2011; Moorman et al., 2012; Dekker et al., 2013). Additionally, the expression of oxysterol producing enzymes were measured in the stroma and were also found to positively associate with epithelial Pgp expression. Moreover, combining the stromal proportion with stromal expression of oxysterol producing enzymes enhances the positive association with epithelial Pgp expression and DFS. However, the use of stromal proportions introduces the caveat that stroma is not exclusively composed of CAFs but also adipocytes and infiltrating immune cells. Therefore, these cells may be driving expression of LXR target genes in epithelial cells. This could be resolved through multiplex staining of the TMA, co-staining the oxysterol producing enzymes against macrophage and T-cell markers would enable quantification of CYP46A1, CH25H and CYP27A1 within specific cell types.

4.6 Conclusion

Understanding the role of the tumour microenvironment in tumour progression is of growing importance. Despite evidence of their value as prognostic indicators in TNBC, there has been little investigation into how non-cancer cells can influence cancer hallmarks. Here, we demonstrate how the presence of CAFs associated with the activation of LXR target genes, in particular *ABCB1*/Pgp, in both our *in-silico* analysis using a panel of TNBC-specific CAF marker genes and in human TNBC tumour tissue. Furthermore, we demonstrated how CAFs can transactivate LXR in TNBC epithelial cells through oxysterol secretions and induce *ABCB1* expression. Further research is necessary to verify whether changes in *ABCB1* expression in epithelial cells is mediated through oxysterol secretions and whether this *ABCB1* upregulation improves epithelial cell response to chemotherapy drugs. Nevertheless, this chapter provides the groundwork towards further elucidating the contribution of the TME to cancer progression.

Chapter 5: Pharmacologic and genetic inhibition of cholesterol esterification impairs cancer progression – a systematic review and meta-analysis of preclinical models

5.1 Introduction

Esterification is an integral component of cholesterol homeostasis, enabling cholesterol storage within lipid droplets. Intra-cellular storage of cholesterol as esters generates an accessible supply for rapidly proliferating cells to utilise and meet the high requirement for plasma membrane synthesis. Several diseases are linked with imbalances in cholesterol esterification, such as neurological conditions (Vanier et al., 1988), liver disorders (Min et al., 2012) and cancers (de Gonzalo-Calvo et al., 2015). Cholesterol esterification can be carried out by SOAT1 and SOAT2, which conjugate an acyl chain via an ester bond to the third carbon of the cholesterol molecule. Despite high structural homogeneity between the two enzymes, they exhibit different preferences for fatty acid substrate during ester generation. For example, SOAT1 preferentially utilises the 18 carbon oleoyl CoA to produce cholesteryl oleate (**Figure 5.1A**), whereas SOAT2 utilizes 16 carbon palmitoyl CoA to produce cholesteryl palmitate (**Figure 5.1B**) (Cases et al., 1998). Additionally, LCAT can produce cholesteryl esters (CEs) by utilising phosphatidylcholine (lecithin) (**Figure 5.1C**) (Rousset et al., 2009). SOAT1 is ubiquitously expressed in tissues, whereas SOAT2 is restricted to the liver (Chang, T.-Y. et al., 2001). LCAT is produced in the liver and secreted into the circulation, conjugated to the membranes of lipid complexes (Szedlacsek et al., 1995).

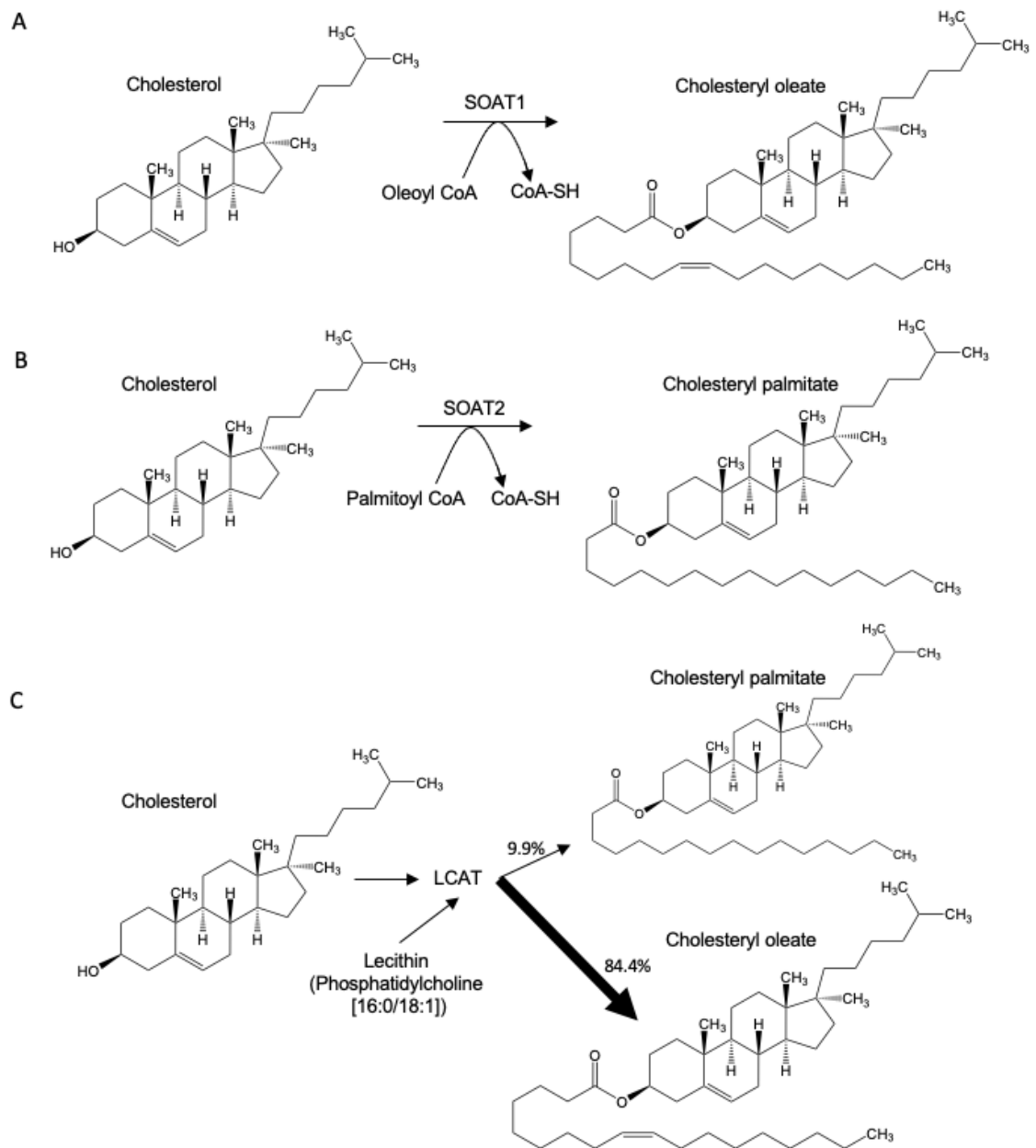


Figure 5.1 Mechanisms of cholesterol esterification.

(A) The preferred substrates and products of SOAT1. (B) The preferred substrates and products of SOAT2. (C) The preferred substrates and products of LCAT. Reaction specificities of SOAT1 and SOAT2 were determined in SOAT1 or SOAT2 expressing H5 cells (Cases et al., 1998). Reaction specificities for LCAT were determined using LCAT isolated from human serum (Szedlacsek et al., 1995).

Cholesterol esterification is beneficial for cancer growth and as such, the expression of SOAT1, SOAT2 and LCAT have prognostic value. High SOAT1 has been shown to be a marker for poor prognosis in adrenocortical (Lacombe et al., 2020), glioma (Chi et al., 2019), liver (Jiang, Y. et al., 2019) and pancreatic (Li, J. et al., 2016) cancers and has been

associated to higher grades of both breast (Huang, Y. et al., 2017) and renal cancer (Matsumoto et al., 2008). Lipid droplet formation is indicative of cholesterol esterification and high lipid droplet content in glioblastoma associates with reduced overall survival (Geng et al., 2016) and high tumour grade in prostate cancer (Yue et al., 2014). Furthermore, cholesteryl oleate has been identified as a potential biomarker for prostate cancer (Li, Jia et al., 2016). Conversely, LCAT is associated with improved prognosis for liver cancer patients (Long et al., 2019) and is often found reduced in liver cancer tissue compared to normal liver in liver cancer patients (Ouyang et al., 2020) and rat models (Pattanayak et al., 2014; Thirunavukkarasu et al., 2003; Veena et al., 2006).

Many small molecule inhibitors of SOAT-mediated cholesterol esterification have been developed and evaluated in clinical trials against non-cancer diseases. These studies provide additional information regarding secondary outcome measures such as drug tolerability, toxicity and side effects. One such drug, avasimibe, was developed in 1996 as a dual inhibitor of SOAT1 and SOAT2 and has been demonstrated as safe at 750 mg daily for 24 months (Tardif et al., 2004). Nevertheless, avasimibe therapy was not found to significantly alleviate symptoms of either atherosclerosis (Tardif et al., 2004) or homozygous familial hypercholesterolemia (Raal et al., 2003). Low solubility and poor bioavailability in circulation and tissues of avasimibe has led to the development of a lipid encapsulated form, known as avasimin (Lee, S.S.-Y. et al., 2015). K604, a SOAT1 specific inhibitor which does not affect systemic cholesterol metabolism (Ikenoya et al., 2007), was used in a clinical trial against atherosclerosis, however no results have currently been published. ATR-101, otherwise known as nevanimibe, is the only SOAT inhibitor currently tested against cancer (adrenocortical carcinoma) however, tumour did not respond to the treatment (Smith, David C et al., 2020b). Pactimibe, a non-selective SOAT inhibitor, has been tested in clinical trials against three different disorders. However, only one study has reported their findings and was terminated early due to increased incidence of major cardiovascular events (NCT00151788). Pactimibe is currently untested in pre-clinical models of cancer, likely due to its severe side effects. Drugs targeting cholesterol esterification that have been tested in clinical trials are summarised in **Table 5.1**. There are many other small molecule inhibitors shown to inhibit either SOAT1 or SOAT2 activity that are currently untested in human studies. For

example, both pyripyropene A (Ohshiro et al., 2011) and Sandoz 58-305 (Williams et al., 1989) reduce serum levels of CEs in mice through SOAT inhibition.

Table 5.1 SOAT inhibitors assessed in clinical trials.

National clinical trial number is abbreviated to NCT.

| Drug/Target | NCT | Reference | Condition or disease | Phase | Outcomes |
|-----------------------------------|-------------|---------------------------------|--|-----------|--|
| Avasimibe (CI-1011)/SOAT | NA | (Insull Jr et al., 2001) | Short-term safety | Phase 1 | Avasimibe was tolerated at 500 mg daily for 8 weeks. Avasimibe induced reductions in triglycerides and VLDL cholesterol. |
| | NA | (Tardif et al., 2004) | Atherosclerosis | NA | Avasimibe was tolerated at maximum dosage of 750 mg daily for 24 months. Avasimibe caused a moderate increase in LDL cholesterol and did not alter coronary atherosclerosis. |
| | NA | (Raal et al., 2003) | Homozygous familial hypercholesterolemia | NA | Avasimibe monotherapy was tolerated at 750 mg for 6-weeks. Avasimibe did not induce any significant lipid changes. |
| K-604/SOAT1 | NCT00851500 | Completed, no results published | Atherosclerosis | Phase 2 | NA |
| Nevanimibe (ATR-101)/SOAT1 | NCT01898715 | (Smith, David C. et al., 2020) | Adrenocortical carcinoma | Phase 1 | Nevanimibe was tolerated at up to 158.5 mg for 5 weeks. No tumour response to treatment at any dosages. |
| | NCT02804178 | (El-Maouche et al., 2020) | Congenital adrenal hyperplasia | Phase 2 | Nevanimibe was tolerated at 1000 mg twice daily for 2 weeks. Nevanimibe reduced 17-hydroxyprogesterone levels. |
| | NCT03669549 | Terminated | Congenital adrenal hyperplasia | Phase 2 | NA |
| | NCT03053271 | Terminated | Endogenous Cushing's syndrome | Phase 2 | NA |
| Pactimibe (CS-505)/SOAT | NCT00151788 | (Meuwese et al., 2009) | Familial hypercholesterolemia | Phase 2/3 | Pactimibe at a dosage of 100 mg increased low-density lipoprotein cholesterol. Pactimibe increased incidence of major cardiovascular events. |
| | NCT00185042 | Completed, no results | Coronary artery disease | Phase 2 | NA |
| | NCT00185146 | Completed, no results published | Atherosclerosis | Phase 2 | NA |

There are a vast number of SOAT inhibitors currently untested against cancer in clinical trials, however many have been tested in pre-clinical models of cancer. These studies provide insights into the pro-cancer mechanisms that SOAT-mediated cholesterol esterification influences and highlight pharmacological inhibitors of SOAT fit for repurposing as anticancer therapies. This systematic review and meta-analysis summarises the current evidence regarding the role of cholesterol esterification enzymes as therapeutic targets in cancer and identify the mechanisms through which they may enable cancer progression.

5.2 Hypothesis and aims

Inhibition of SOAT1 and/or SOAT2 increases the intratumour content of free cholesterol and oxysterols, leading to reduced tumour volume through a variety of mechanisms.

The aims of this chapter were to:

- Compare cholesteryl ester concentration in tumour and non-tumour tissue in preclinical models of cancer
- Examine whether inhibition of cholesterol esterification in pre-clinical models of cancer leads to reduced tumour volume
- Elucidate the mechanisms involved in cholesteryl ester-mediated tumour progression

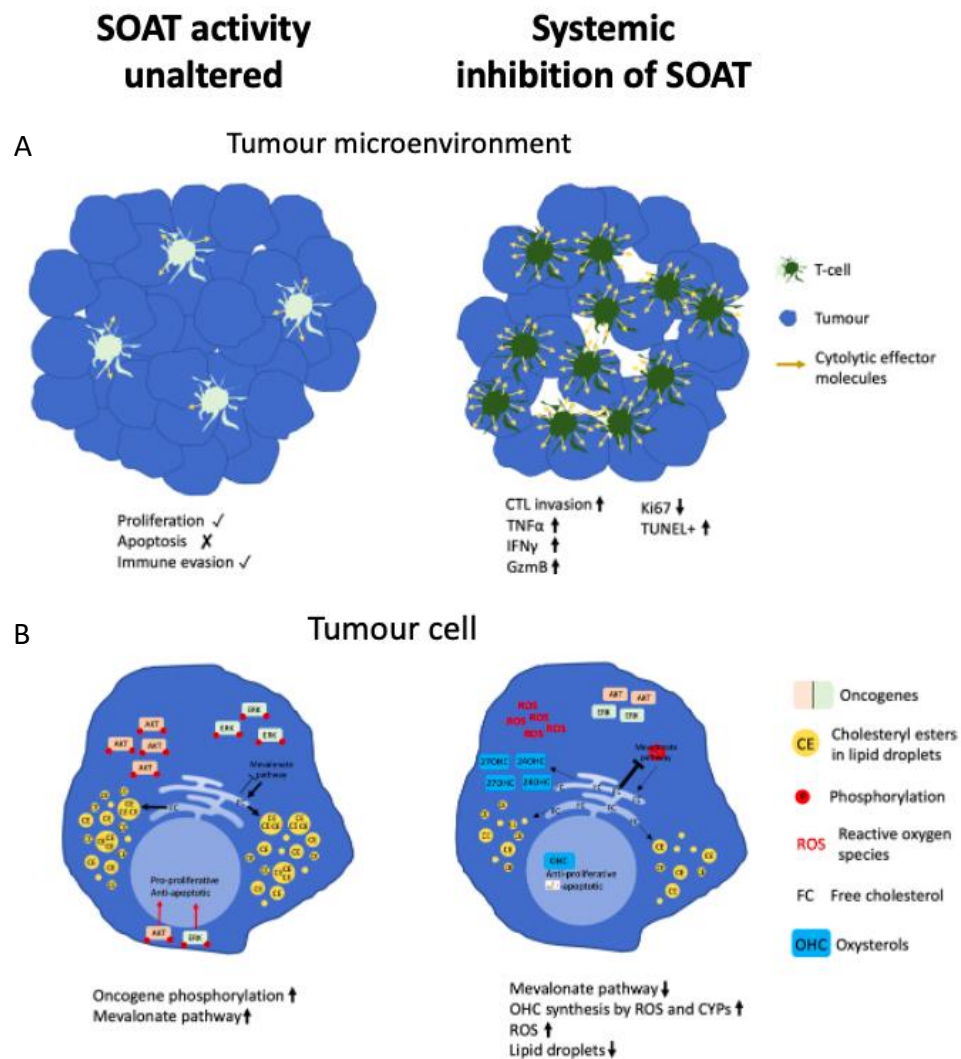


Figure 5.2 Graphical abstract: How does SOAT inhibition impair cancer progression?

(A) SOAT inhibition increases the cytotoxic capabilities of tumour-infiltrating T-cells. (B) SOAT inhibition impacts oncogene signalling, oxysterol production and ROS formation.

5.3 Materials and methods

5.3.1 Search strategy

We systematically searched four databases: Pubmed, Scopus, Web of Science and Cochrane Library. The last search took place in April 2021. Search strategy used for this search was registered on the PROSPERO database (CRD42020202409), however we did not include studies investigating cholesterol sulphation due to lack of data. Search strategy: (Cholesterol est* [Title/Abstract] OR Cholesteryl est* [Title/Abstract] OR Oxysterol est* [Title/Abstract] OR hydroxycholesterol est* [Title/Abstract] OR Cholesterol sulf* [Title/Abstract] OR Cholesterol sulph* [Title/Abstract] OR oxysterol sulf* [Title/Abstract] OR oxysterol sulph* [Title/Abstract] OR hydroxycholesterol sulf* [Title/Abstract] OR hydroxycholesterol sulph* [Title/Abstract] OR ketocholesterol est* [Title/Abstract] OR ketocholesterol sulph* [Title/Abstract] OR ketocholesterol sulf* [Title/Abstract] OR LCAT [Title/Abstract] OR Cholesterol Acyltransferase [Title/Abstract] OR ACAT* [Title/Abstract] OR SOAT* [Title/Abstract] OR AACT* [Title/Abstract] OR ARGP2 [Title/Abstract] OR Sterol O-Acyltransferase [Title/Abstract] OR SULT2B1b [Title/Abstract] OR HSST2 [Title/Abstract] OR Hydroxysteroid sulfotransferase [Title/Abstract] OR Cytosolic sulfotransferase 2B1b [Title/Abstract] OR Sulfotransferase Family 2B Member 1 [Title/Abstract] OR Sulfotransferase 2 B1 [Title/Abstract]) AND (Cancer [Title/Abstract] OR neoplasm [Title/Abstract] OR tumour [Title/Abstract] OR tumor [Title/Abstract] OR carcinoma [Title/Abstract] OR Oncolog* [Title/Abstract] OR Malignan* [Title/Abstract])

5.3.2 Study selection

The inclusion criteria for which titles and abstracts were screened against were: 1) the article describes an original (primary data) study. 2) The article investigates cancer 3) The article investigates an *in-vivo* pre-clinical animal model. 4) The article investigates modulation of cholesterol esterification. Publications from predatory journals were excluded from our meta-analysis. Screening was performed by two independent assessors (either Xinyu Chen, Rufaro Mwarzi or Ruoying Wu) and discrepancies were solved by a third assessor (Alex Websdale). All studies that satisfied each of these criteria were included in the meta-analysis.

5.3.3 Data extraction

Publications that reported suitable data for quantitative assessment were included in our meta-analysis. All data were extracted in duplicate by independent assessors, with disagreements solved by discussion with the research team. Only data from *in vivo* animal models assessing CE concentrations, or SOAT/LCAT modulation were included, with any comparisons reporting other enzymes or combination therapies excluded. Where data was only presented in figures, Webplot Digitizer (v4.2) was used to extract data. Data regarding to animals, study design, SOAT modulation, cancer type and outcomes were assessed.

5.3.4 Statistical analysis

Review manager version 5.4 (The Nordic Cochrane Centre, Denmark, 2014) was used for meta-analysis. Where multiple treatment doses were used in comparison to control, the largest was reported in meta-analysis. Where studies reported data as a fold change, fold changes were normalised to tumour size at the initiation of the experiment by us to standardise the data. Tumour volumes and diameters were standardised to cm across studies. Mean differences were used when available, but when measurements were not shared within an outcome, standardised mean difference (SMD) was used. SMD describes the effect size of the intervention group relative to the variability observed within the study. Random effects model was used due to the high heterogeneity anticipated between studies brought on by variation in SOAT modulation therapies, cancers assessed and animal models used. Heterogeneity was assessed using I^2 , with an I^2 value of >75 deemed a marker of high heterogeneity between studies. Evidence of high or low heterogeneity within studies was discussed.

5.3.5 Publication bias

Evidence of publication bias was assessed using funnel plots. Where funnel plots suggested publication bias, a corrected overall effect was generated by Duval and Tweedie's trim and fill method using Comprehensive Meta Analyst version 3 (Biostat inc. USA, 2014).

5.3.6 Risk of bias

Risk of Bias (ROB) was adapted from Cioccoloni et al., which summarises guidelines published by the British Journal of Pharmacology and SYRCLE (Cioccoloni et al., 2020). ROB was performed by two independent assessors and used to assess experimental design, animal experiments and both immunoblotting and immunohistochemistry.

5.4 Study characteristics

5.4.1 Records returned

Our search strategy identified 3026 records from PubMed (n=847), Scopus (n=970), Web of Science (n=1189) and Cochrane Library (n=20). A further four were identified during background reading. After removing duplicates there were a total of 1543 unique records available for abstract screening. Abstract screening returned 84 records that either measured changes in tumour size following SOAT1, SOAT2 or LCAT modulation (n=43) or compared inter/intra-animal CE content in tumour and normal tissue (n=41). Full text screening identified 24 publications assessing pharmacological or genetic inhibition of cholesterol esterification enzymes that were suitable for both quantitative and qualitative analysis. A further 13 studies assessing CE concentrations were suitable for qualitative analysis, ten of which were included in quantitative analysis. This process is summarised with a PRISMA flow diagram (**Figure 5.3A**).

5.4.2 Cancer sites

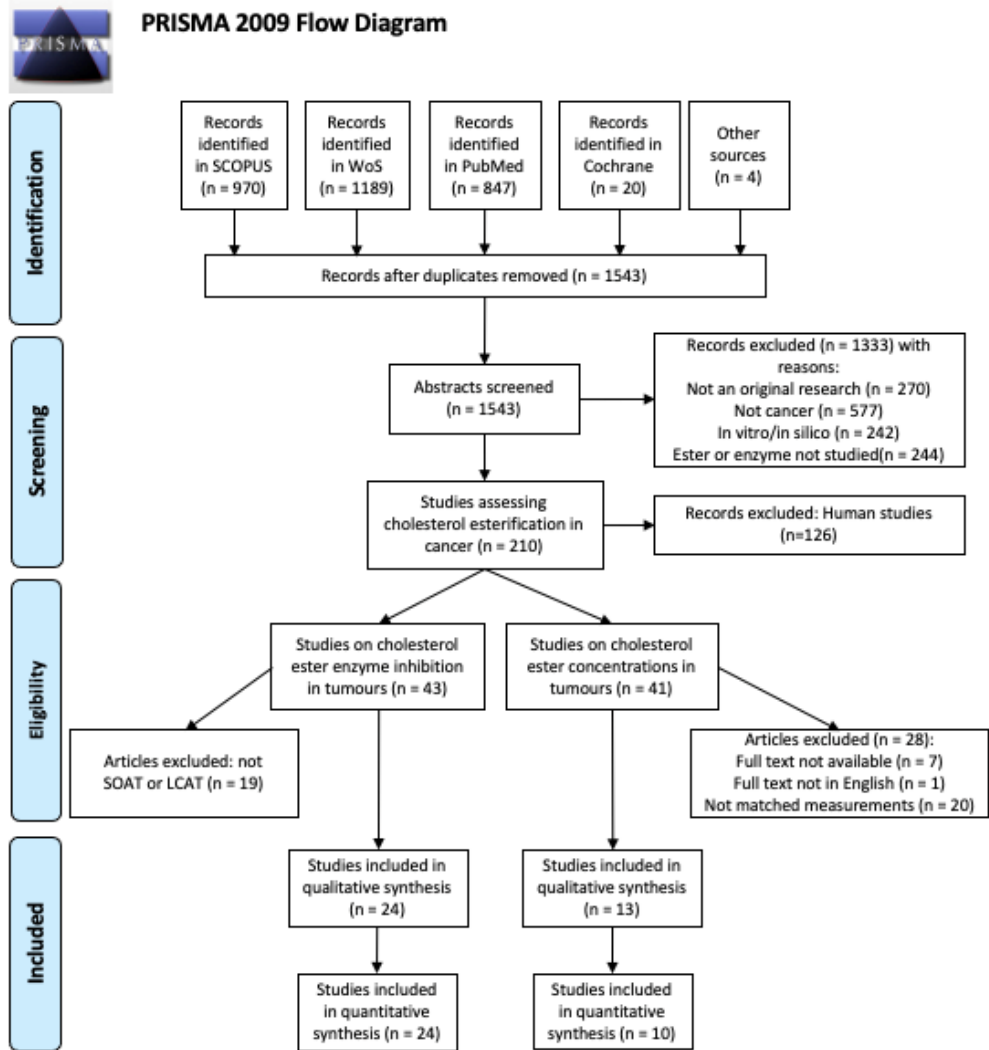
All 46 comparisons from 24 studies included in qualitative analysis of cholesterol esterification were either xenograft or allograft models assessing SOAT1 and/or SOAT2 inhibition. Of the 46 comparisons, 12 assessed liver cancer, eight skin cancer, seven prostate cancer, six pancreatic, six brain cancer, two on lung, two on colorectal and breast, bone and leukaemia were only studied once. No records investigating LCAT modulation appeared from our search. Of the 13 qualitative studies assessing CE concentration in tumours, nine assessed liver, two evaluated testicular and pancreatic or renal cancers were examined once (**Figure 5.3B**). Seven pre-clinical models were either xenografts or allografts, whilst one was a radiation induced model.

5.4.3 Interventions and dosing

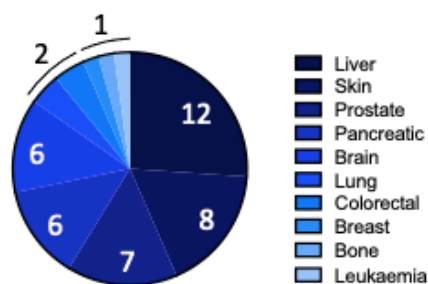
A total of five different pharmacological inhibitors were used across the 46 comparisons, in addition to RNA interference and genetic knockout (**Figure 5.3C**). Avasimibe was the most common SOAT inhibition therapy assessed, featuring in 26 of the 46 qualitative comparisons. Avasimibe was primarily used at 15 mg/kg (17/26 studies), with lower concentrations of 7.5 mg/kg (3 comparisons) and 2 mg/kg (5 comparisons) also tested.

Two further comparisons also assessed 30 mg/kg. Pre-treatment of cancer cells with either shRNA or siRNA targeting SOAT1/2 before grafting was the second most common approach, after avasimibe therapy. Lipid encapsulated avasimibe (avasimin) was used four times at 75 mg/kg, containing a total of 7.5 mg/kg avasimibe. RNA interference occurred in five comparisons in cancer cells and twice in CAR-T cells. Genetic knockouts were performed in four comparisons, once using CRISPR/Cas9 pre-treatment before grafting and three times using transgenic mice with a SOAT1 knockout specific to the T-cells. K-604 was used twice to specifically inhibit SOAT1, whereas SOAT2 was inhibited twice using Pyripyropene A. Both ATR-101 and Sandoz 58-035 were used in one comparison each. Drugs were administered by six different routes. The most common method of administration was intraperitoneal injection (IP) (n=10) followed by intravenous injection (IV) (n=3), per oral (PO) (n=3), intragastric administration (IG) (n=2) and both intratumoural (IT) and subcutaneous injection were used once. Despite being bioavailable when orally administered, avasimibe was only assessed twice following PO administration. This administrative route was only found to be effective at 30 mg/kg on the U2OS bone cancer xenograft model, with PC3 prostate cancer xenograft resistant to a 15 mg/kg dose (Lee, S.S.-Y. et al., 2015).

A



B



C

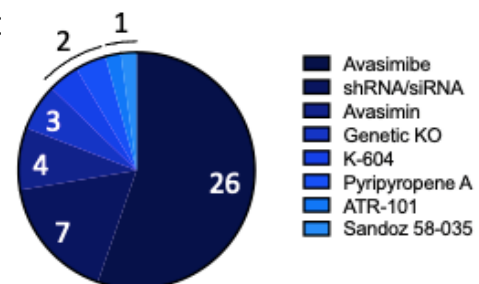


Figure 5.3 Study discovery and distribution.

(A) PRISMA flow diagram showing searching, screening, eligibility and inclusion process. (B) Number of papers assessing different cancer types in SOAT inhibition studies. (C) Number of papers assessing different SOAT inhibiting treatments in SOAT inhibition studies.

5.5 Results

5.5.1 Cholesteryl esters are concentrated in tumour tissue

To understand whether CEs were a cancer selective target for anti-cancer therapy, the CE content was compared between tumour and non-tumour tissue. Eight studies compared CE content in tumour and normal tissue in the same animal. Six of these comparisons were performed in liver cancer models (Barnard et al., 1986; Erickson et al., 1988; Ruggieri, Salvatore et al., 1976; Ruggieri, S and Fallani, 1979; Thirunavukkarasu et al., 2003; Wood et al., 1978), with testicular (Konishi et al., 1991) and renal (Talley et al., 1983) cancers assessed once. Overall, there was an increase in CE concentration in tumour tissue compared to normal tissue from the same animal (SMD = 1.29; 95% CI: 0.68 to 1.90; $I^2 = 31\%$; $p < 0.0001$; **Figure 5.4A**). Harry et al., found that CE content was increased in three different hepatocarcinoma xenografts (**Appendix Table C.1**) (Harry et al., 1971). However, microsomal fractions from tumour and non-tumour tissue exhibited no difference in CE concentration (van Heushen et al., 1983). Surprisingly, comparisons between tumour tissue and normal tissue from non-tumour bearing animals found no significant differences in CE concentration (**Figure 5.4B**).

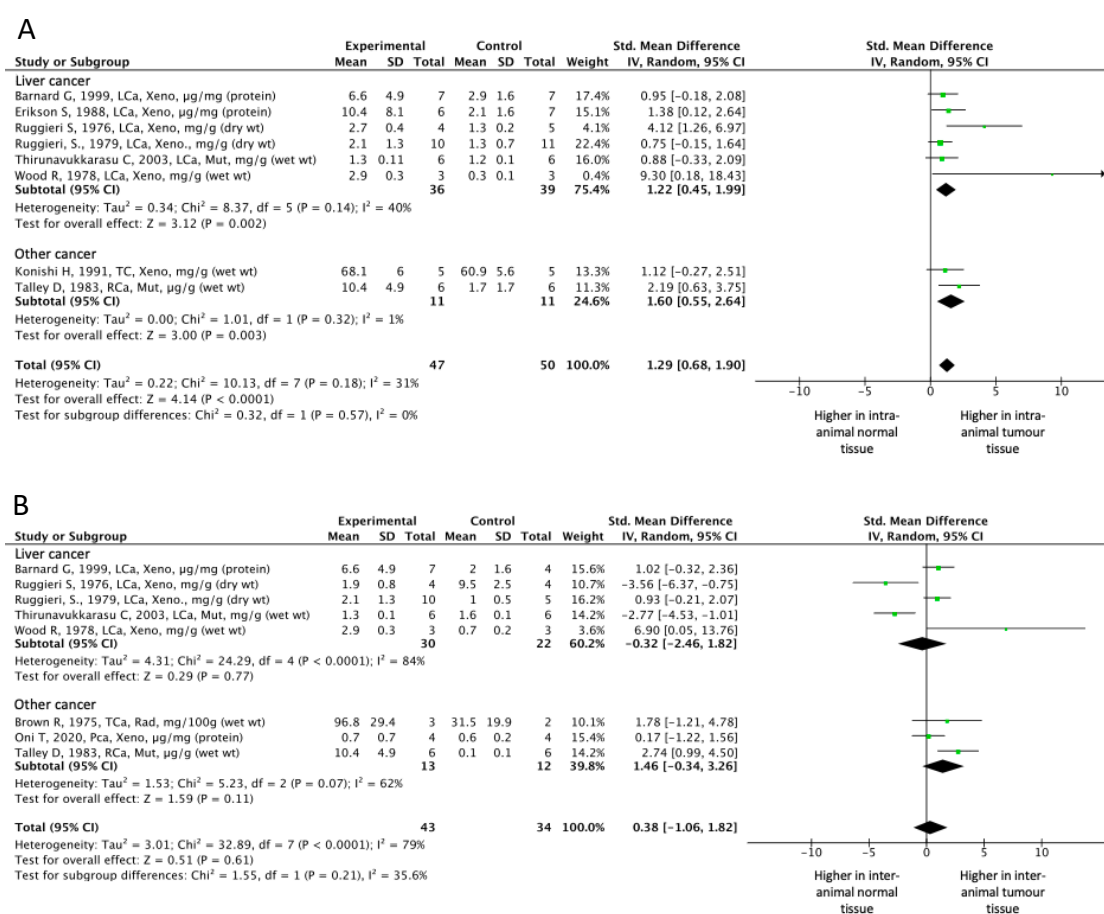


Figure 5.4 Cholesteryl ester concentration in tumour tissue and matched-normal tissue from control littermates.

(A) Cholesteryl ester concentration in tumour tissue and matched-normal tissue from the same mouse. (B) Cholesteryl ester concentration in tumour tissue and matched-normal tissue from non-tumour bearing littermates. Differences in cholesteryl ester concentration between tissues is represented as a standardised mean difference.

5.5.2 SOAT promotes tumour growth

To establish whether inhibiting cholesterol esterification can impair tumour growth, previous studies investigating this in animal models were collated and the change in tumour size was assessed in overall cancer and individual cancers. Across 24 studies, there were 40 comparisons reporting changes in tumour size in response to pharmacologic or genetic inhibition of SOAT, compared to control mice. Of these 40 comparisons, 27 reported a significant reduction in tumour size following SOAT inhibition as measured by either volume (cm³), diameter (cm²) or radiance (units of photons/seconds/cm²/units of solid angle or steradian, abbreviated to p/s). Across all 40 comparisons and 555 mice assessed, SOAT inhibition associated with reduced

tumour size (SMD = -2.1; 95% CI: -2.56 to -1.64; $I^2 = 75\%$; $p < 0.00001$; **Appendix Figure C.1**). Furthermore, enough studies assessed specific cancer types (≥ 3) to enable individual meta-analyses on brain cancer, liver cancer, pancreatic cancer, prostate cancer and skin cancer. Cancers that were not studied in sufficient numbers for subgroup analyses were subsequently grouped together as “other cancers”.

5.5.2.1 Brain cancer

Subgrouping for brain cancers included four models of glioblastoma (Geng et al., 2016; Liu, J.Y. et al., 2021; Luo, Yidan et al., 2020) and just one of adrenocortical carcinoma (Cheng, Y. et al., 2016). All comparisons found significant reductions in tumour size following SOAT inhibition as reported by either volume or radiance measurements (SMD = -3.26; 95% CI: -4.53 to -1.99; $I^2 = 52\%$; $p < 0.00001$; **Figure 5.5**). Cheng et al., was the only study assessing adrenocortical carcinoma, demonstrating that PO administration of ATR-101 is sufficient to reduce H295R xenograft volume (Cheng, Y. et al., 2016). The U87 glioblastoma model was tested against both avasimibe at 15 and 30 mg/kg (Liu, J.Y. et al., 2021) in addition to pre-treatment of cells with shRNA against SOAT1 (Geng et al., 2016); all treatments reduced tumour burden. There was no significant difference between the two avasimibe doses for size or weight (**Appendix Table C.2**). In addition to U87 cells, Geng et al., also treated GBM30 cells with SOAT1 shRNA pre-graft, finding that the GBM30 xenograft model was sensitive to SOAT1 inhibition (Geng et al., 2016). The largest reduction in tumour size was attributed to a 7.5 mg/kg treatment of avasimibe on the LN229 xenograft model, with the authors associating this to the loss of long non-coding RNA linc00339 (**Appendix Table C.2**); overexpression of linc00339 impaired avasimibe mediated growth inhibition (Luo, Yidan et al., 2020).

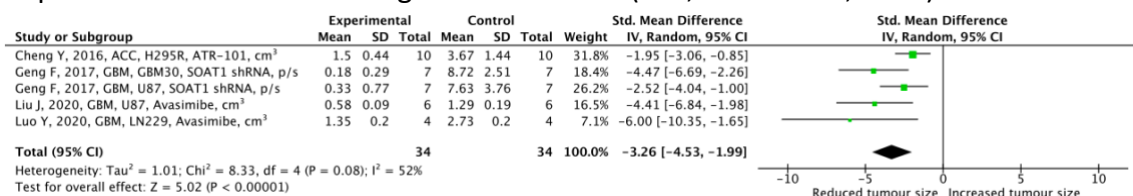


Figure 5.5 Change in tumour size following disruption of SOAT in brain cancer. Standardised mean difference in brain tumour size.

5.5.2.2 Liver cancer

Nine comparisons assessing changes in liver cancer volume following SOAT or SOAT1 specific inhibition were identified from our search strategy (Jiang, Y. et al., 2019; Lu, Ming et al., 2013), with SOAT disruption inducing a significant reduction in tumour volume in only three comparisons. Nevertheless, the subgrouping exhibited a significant reduction in tumour volume across the nine comparisons (MD = -0.28; 95% CI: -0.47 to -0.1; $I^2 = 84\%$; $p = 0.002$; **Figure 5.6**). SOAT1 expression was measured across six patient derived xenografts (PDX) and interestingly, tumours that expressed high levels of SOAT1 were more susceptible to avasimibe treatment. No PDXs expressing low levels SOAT1 protein were significantly reduced in volume following avasimibe treatment (Jiang, Y. et al., 2019). Huh7 and HepG2 xenografts found that inhibition of SOAT2 by the specific SOAT2 inhibitor, Pyripyropene A, or gene ablation using RNAi induced a significant reduction in tumour volume, whereas inhibition of SOAT1 induced no significant change (**Appendix Table C.2**) (Lu, Ming et al., 2013). This may be attributed to enhanced expression of SOAT2 over SOAT1 within HepG2 cells as reported by The Protein Atlas (Huh7 not reported) (Uhlen et al., 2017b; Uhlen et al., 2017a) and SOAT2 is upregulated frequently in hepatocellular carcinomas (Song et al., 2006).

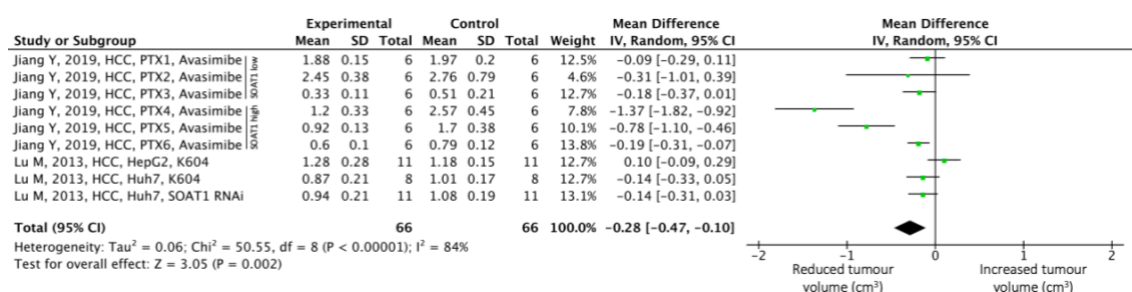


Figure 5.6 Change in tumour size following disruption of SOAT in liver cancer.
 Mean difference (cm³) in liver cancer volume.

5.5.2.3 Pancreatic cancer

We identified six studies that explored SOAT inhibition in pancreatic cancer, of which all assessed changes in tumour volume (Li, J. et al., 2016; Li, J. et al., 2018; Oni, T. E. et al., 2020; Zhao et al., 2020). Our meta-analyses showed that tumour volume was significantly reduced in these SOAT inhibited tumours (MD = -0.56; 95% CI: -0.79 to -0.33; $I^2 = 85\%$; $p < 0.0001$; **Figure 5.7**). One study found that pre-treatment of T8 pancreatic cancer organoid cells with shSOAT1 led to complete tumour ablation at 58 days after grafting. The same study also performed CRISPR knockout of SOAT1 in M3L pancreatic cancer organoid cells, inducing a reduction in tumour volume by 4cm³, compared to wild type cells (Oni, T. E. et al., 2020). shSOAT1 was also assessed in MIA-PaCa pancreatic cancer cells, however tumour remained, albeit significantly smaller than with control shRNA (Li, J. et al., 2018). Two studies assessed avasimibe treatment on MIA-PaCa xenografts. Surprisingly, 7.5 mg/kg daily for 33 days induced a larger reduction in tumour volume (Li, J. et al., 2018) than double the dose for 28 days (Li, J. et al., 2016). Furthermore, siRNA-mediated knockdown of SOAT1 was restricted to CAR-T cells introduced into immunodeficient, NSG mice. Genetic ablation of SOAT1 in CAR-T cells appeared to be sufficient to induce a significant reduction in tumour volume compared to siCON treated CAR-T cells (Zhao et al., 2020).

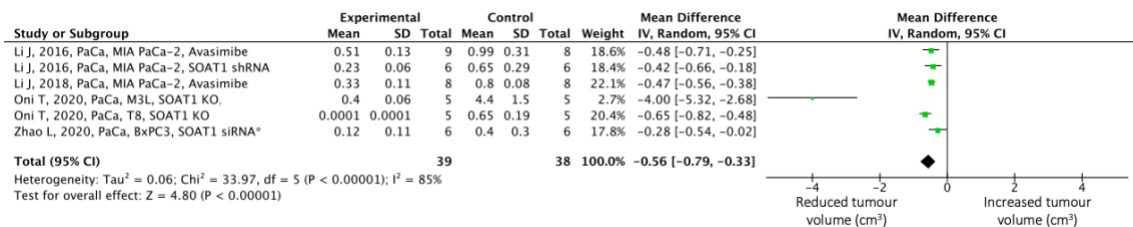


Figure 5.7 Change in tumour size following disruption of SOAT in pancreatic cancer.

Mean difference (cm³) in pancreatic cancer volume. * denotes modifications localized to CAR T-cells.

5.5.2.4 Prostate cancer

Our systematic review identified four studies assessing prostate cancer (Lee, H.J. et al., 2018; Lee, S.S.-Y. et al., 2015; Liu, Y. et al., 2021; Yue et al., 2014). Across the seven comparisons from these studies, there was a reduction in tumour size as measured by either volume or radiance following SOAT inhibition (SMD = -1.78; 95% CI: -2.83 to -0.73; $I^2 = 76%$; $p = 0.0008$; **Figure 5.8**). Only one study assessed PO administration of avasimibe, demonstrating that this was a considerably weaker method to administer the drug than IP (Lee, S.S.-Y. et al., 2015). Matched doses of avasimibe and Sandoz 58-035 showed avasimibe reduces tumour volume by a greater amount suggesting avasimibe was a more potent inhibitor (Yue et al., 2014). However, studies assessing SOAT inhibition *in vitro* by either avasimibe (Terasaka et al., 2007; Ikenoya et al., 2007) or Sandoz 58-035 (Tabas et al., 1990) suggest that Sandoz requires a smaller dose to inhibit SOAT. This implies that the increased efficacy of avasimibe *in vivo* over Sandoz 58-035 may be an issue of bioavailability. Furthermore, lipid soluble version of avasimibe was also tested. Interestingly, Lee et al., used 7.5 mg/kg lipid encapsulated avasimibe (avasimin), with this inducing less fold change in tumour volume compared to 15 mg/kg avasimibe treatment. However, dosing schedules were drastically different between these two studies, with avasimibe treated daily, whereas avasimin treatment was daily for the first five days, followed by treatment every subsequent four days (Lee, S.S.-Y. et al., 2015). However, daily treatment of avasimin could not induce significant reduction in tumour volume or radiance in mice injected with PC3M cells and PC3 cells, respectively (Lee, H.J. et al., 2018).

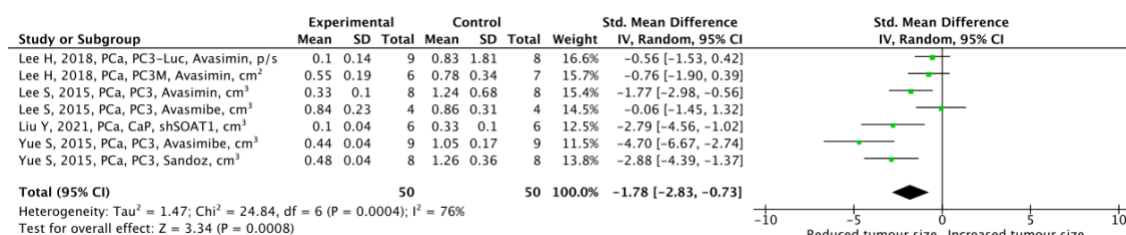


Figure 5.8 Change in tumour size following disruption of SOAT in prostate cancer.
 Standardised mean difference in prostate cancer size.

5.5.2.5 Skin cancer

Growth of skin cancer models was significantly reduced across six comparisons from four studies (Chen, X. et al., 2017; Hao et al., 2020; Li, M. et al., 2018; Yang, W. et al., 2016) (SMD = -3.61; 95% CI: -4.55 to -2.67; $I^2 = 25\%$; $p < 0.00001$; **Figure 5.9**). Hao et al., compared the co-treatment of avasimibe with T-cell therapy against T-cell therapy alone, finding a significant reduction in tumour size. Furthermore, avasimibe therapy alone was sufficient to significantly reduce tumour burden in immunodeficient mice (Hao et al., 2020). Moreover, Yang et al., investigated the effects of CRISPR knockout of SOAT1 restricted to T-cells, finding that SOAT1 deficiency in the T-cells alone was sufficient to reduce tumour volume (Yang, W. et al., 2016). These experiments suggests that SOAT may be driving tumour progression through multiple mechanisms, one of which being the immune response. Only one study did not assess the B16F10 allograft model, instead investigating the squamous skin carcinoma cell line, SCC7, finding that SCC7 allografts responded to avasimibe in a similar manner to B16F10 (Chen, X. et al., 2017). Interestingly, Hao et al., not only used the lowest avasimibe dosage but also only performed two administrations, compared to 15 mg/kg doses every two days (Hao et al., 2020). This may explain the relatively small change in volume in comparison to other studies, with the remarkably low standard deviation accounting for the larger SMD fold change.

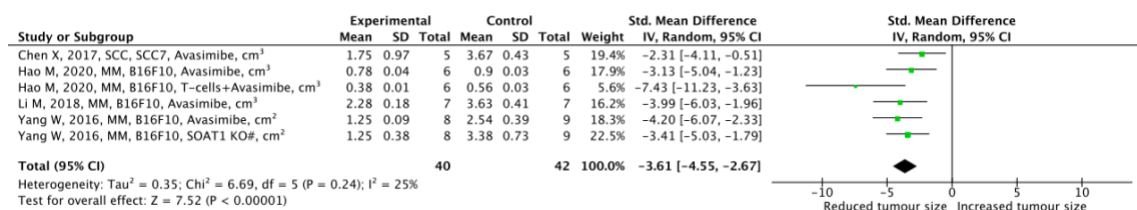


Figure 5.9 Change in tumour size following disruption of SOAT in skin cancer.

Standardised mean difference in skin cancer size. # denotes modifications localized to T-cells.

5.5.2.6 Other cancers

The other cancer subgrouping contained two colorectal cancer xenografts (Lee, H.J. et al., 2018; Xu, H. et al., 2021), two lung cancer xenografts (Bi et al., 2019; Pan, J. et al., 2019) and one breast (Lei et al., 2020), bone (Wang, L. et al., 2019) and leukaemia (Bandyopadhyay et al., 2017) xenograft models. All models within the subgroup were treated with either avasimibe or avasimin, inducing a significant reduction in tumour volume across the seven studies (MD = -0.31; 95% CI: -0.48 to -0.15; $I^2 = 89\%$; $p < 0.00001$; **Figure 5.10**). The only xenograft insensitive to SOAT inhibition was the K562R, chronic myelogenous leukaemia (CML) model. This is possibly driven through the BCR-ABL translocation, commonly found in CML (Sawyers, 1999). The BCR-ABL fusion increases activation of multiple oncogenes including MAPK, AKT and MYC (Cilloni and Saglio, 2012). Avasimibe has only been found to decrease signalling of the MAPK pathway (Bandyopadhyay et al., 2017).

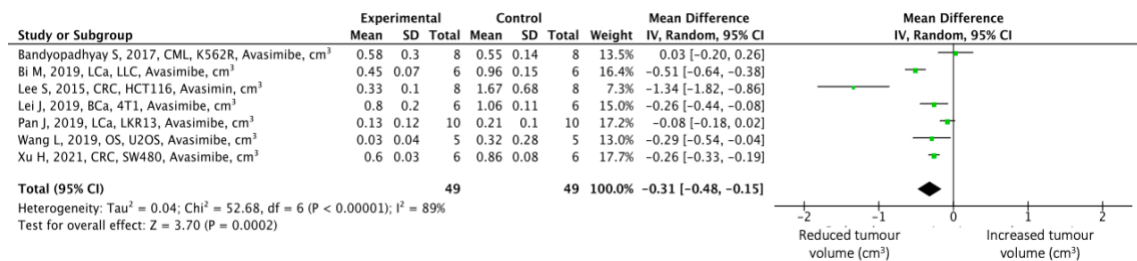


Figure 5.10 Change in tumour size following disruption of SOAT.
 Mean difference (cm³) in other cancer volume.

5.5.3 SOAT expression is associated with enhancement of cancer hallmarks

5.5.3.1 SOAT inhibition prolongs survival

Preclinical studies are bound by ethical considerations to prevent prolonged animal suffering, which increases with tumour burden. Different ethical governing boards present different requirements on the terminal tumour volume or animal weight loss, that when reached, the animal in question must be sacrificed. From these data, a hazard ratio function has been generated that describes the risk of early euthanasia based on tumour burden or significant weight loss. Thirteen comparisons from seven studies were included for this analysis (Chen, X. et al., 2017; Geng et al., 2016; Hao et al., 2020; Lee, S.S.-Y. et al., 2015; Lei et al., 2020; Oni, T. E. et al., 2020; Yang, W. et al., 2016; Li, J. et al., 2018), finding that animals in the intervention group exhibited an 85% reduction in risk of being euthanised early (HR = 0.15; 95% CI: 0.08 to 0.28; $I^2 = 63\%$; $p < 0.00001$; **Figure 5.11**). Furthermore, the effects of SOAT inhibition on survival within models of metastasis has also been assessed. Both systemic avasimibe treatment and T-cell specific SOAT1 knockdown induced a significant reduction in hazard ratio for intravenously injected Lewis lung carcinoma (LLC) and B16F10 cells (Yang, W. et al., 2016). The importance of the immune system in SOAT inhibition-mediated risk of euthanasia was demonstrated in another B16F10 metastasis model, showing that treatment with 2 mg/kg avasimibe was not enough to induce a significant reduction in risk of euthanasia, whereas co-therapy of avasimibe at the same dose with T-cells reduced risk of euthanasia by 43% (Hao et al., 2020).

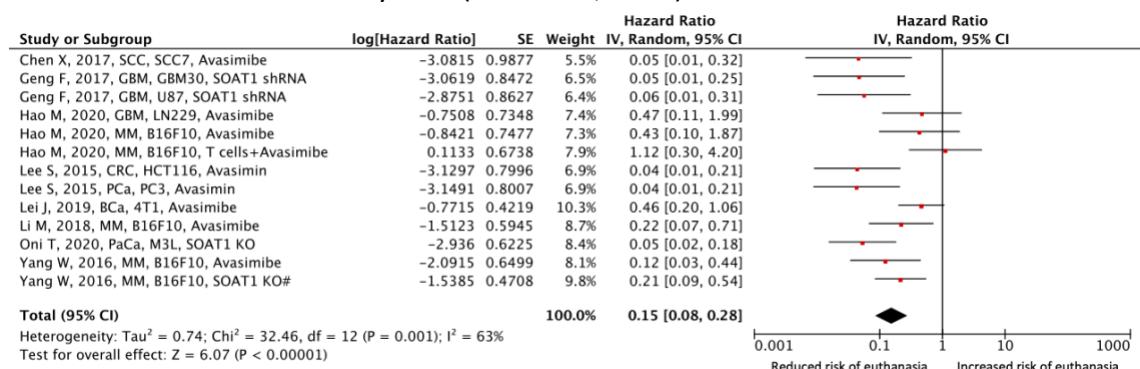


Figure 5.11 Forest plot showing changes in risk of arrival at maximal tumour volume following disruption of SOAT.

Differences shown as hazard ratios as calculated by Mantel-Haenszel between SOAT disruption test groups and control test groups. # denotes modifications localized to T-cells.

5.5.3.2 Sustained proliferative signalling

The impact of inhibiting cholesterol esterification on tumour growth was demonstrated through a reduction in tumour volume, however the mechanisms driving this were unclear. First, assessment of proliferative potential was assessed through the number of Ki67-positive cancer cells. SOAT inhibition was associated with a significant reduction in proliferative potential, as shown by a reduced number of Ki67-positive cancer cells (Hao et al., 2020; Lee, H.J. et al., 2018; Pan, J. et al., 2019; Yue et al., 2014) (MD = 14.43; 95% CI: -22.32 to 6.55; $I^2 = 98\%$; $p = 0.0003$; **Figure 5.12**). Within Hao et al., treatment with avasimibe concurred with other studies, finding a significant reduction in Ki67 expression, albeit to a considerably weaker degree. This is likely due to the low dose and infrequent administration of avasimibe compared to other studies. Surprisingly, co-treatment of avasimibe with T-cells conducted within the same study resulted in an increase in Ki67 positive cancer cells compared to those treated with just T-cells. Despite this, T-cell and avasimibe co-treatment still induced significant tumour destruction, indicating that mechanisms may be involved independent of Ki67-mediated proliferation (Pan, J. et al., 2019). Similarly, Pan et al. assessed the impact of the SOAT deficient immune system on epithelial Ki67 expression. By using a synergistic LKR13 allograft model, the authors were able retain an active immune response within the tumour model, finding that systemic avasimibe treatment reduced Ki67 positive epithelial cell number (Pan, J. et al., 2019). Contrastingly, treatment of H295R xenografts with ATR-101 did not induce a significant reduction in either Ki67 or Brdu, suggesting an alternate mechanism may be behind ATR-101 mediated tumour destruction (**Appendix Table C.2**) (Cheng, Y. et al., 2016). The oncogene YAP does not appear to be involved with SOAT-mediated proliferation, with SOAT inhibition upregulating YAP expression, despite reducing tumour size (**Appendix Table C.2**) (Xu, H. et al., 2021). Reduced proliferation in SOAT1-ablated CaP xenografts was attributed to a reduced production of monounsaturated fatty acids derived from SCD1 downregulation (**Appendix Table C.2**) (Liu, Y. et al., 2021).

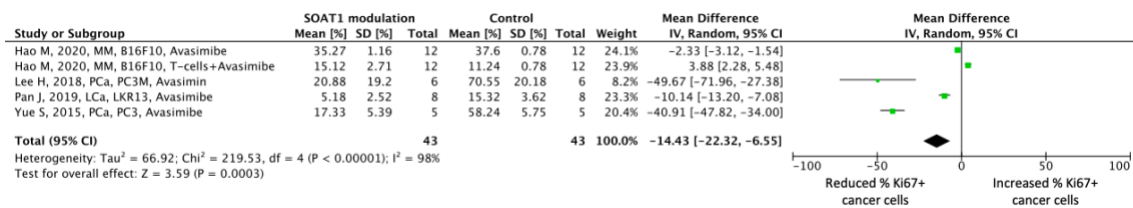


Figure 5.12 Forest plots showing changes in proliferation.

Mean difference (percentage Ki67 +cells) between experimental and control groups in tumour expression of Ki67.

5.5.3.3 Resisting cell death

Furthermore, whether apoptosis was driving SOAT-inhibition mediated reduced tumour volume was investigated. Typically, apoptosis is assessed through apoptosis assays such as the TUNEL+ assay, quantification of apoptosis related proteins and measuring the mitochondrial membrane potential. Our meta-analysis returned four comparisons from three studies (Lee, S.S.-Y. et al., 2015; Lee, H.J. et al., 2018; Yue et al., 2014) assessing change in cancer cells undergoing apoptosis using the TUNEL+ stain following SOAT inhibition with either avasimin or avasimibe. Studies either quantified the percentage positively stained with TUNEL+ cancer cells or the number of positively stained TUNEL+ cells per area. Across the four experiments, SOAT inhibition significantly increased epithelial apoptosis (Yue et al., 2014; Lee, H.J. et al., 2018; Lee, S.S.-Y. et al., 2015) (SMD = 5.64; 95% CI: 1.57 to 9.71; I² = 83%; p = 0.007; **Figure 5.13**). Increased apoptosis was also discovered within H295R xenografts treated with ATR-101 (**Appendix Table C.2**) (Cheng, Y. et al., 2016), suggesting that increased apoptosis rather than reduced proliferation was driving the reduced volume of these tumours.

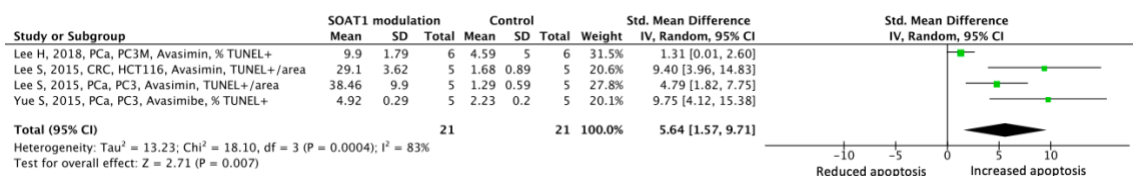


Figure 5.13 Forest plots showing changes in apoptosis.

Standardised mean difference between experimental and control groups in apoptotic cells in the tumour as measured by TUNEL +stain assay.

5.5.3.4 Evasion of immune detection

The anti-cancer immune response can be initiated upon reception of tumour antigens by CD8+ T-cells. High immune cell infiltration within tumours has been identified as a marker for good prognosis in breast (Menegaz et al., 2008), colorectal (Galon et al., 2006), lung (Kawai et al., 2008), prostate (Richardsen et al., 2008) and skin cancer (Clemente et al., 1996). However, the impact of SOAT inhibition on T-cell function was unclear. Our meta-analysis demonstrated that SOAT inhibition was sufficient to increase tumour infiltration of CD3+ CD8+ or CD8+ T-cells (Lei et al., 2020; Pan, J. et al., 2019; Yang, W. et al., 2016) (SMD = 1.12; 95% CI: 0.46 to 1.77; $I^2 = 0\%$; $p = 0.0009$; **Figure 5.14A**). Avasimibe also impaired efficiency of the immunosuppressive environment through a decrease in CD4+ Treg cells in lung cancer models (Pan, J. et al., 2019). CD4+ Treg cells have been shown to reduce CD8 proliferation, potentially explaining the increase in CD8 infiltration. However, CD4+ Treg infiltration was unaltered by T-cell specific knockout of SOAT1 in B16F10 xenograft (Yang, W. et al., 2016). T-cell specific knockout of SOAT1 also significantly increased CD8+ cell infiltration (Yang, W. et al., 2016), suggesting that SOAT1 disruption in CD8+ T-cells was sufficient to induce increased infiltration, irrespective of the CD4+ Treg population and systemic SOAT inhibition.

Despite the increased tumour invasion of CD8+ cells, immune-mediated destruction of cancer is typically hampered by the high number of resident immune cells exhibiting anergy, meaning these cells are unable to mount a sufficient cytotoxic response. Our subsequent meta-analysis of a range of cytotoxic effector cytokines, found that cytokines were consistently upregulated in SOAT inhibited xenografts: TNF α (MD = 11.54; 95% CI: 5.08 to 18.01; $I^2 = 94\%$; $p = 0.0005$; **Figure 5.14B**), IFN γ (MD = 8.10; 95% CI: 3.14 to 13.05; $I^2 = 84\%$; $p = 0.001$; **Figure 5.14C**) and cytotoxic effector molecule, GzmB (MD = 3.67; 95% CI: 0.02 to 7.37; $I^2 = 97\%$; $p = 0.05$; **Figure 5.14D**). These findings suggest that SOAT disruption not only increased the infiltrative capabilities of the T-cells but enhanced their cytotoxic, anti-cancer properties.

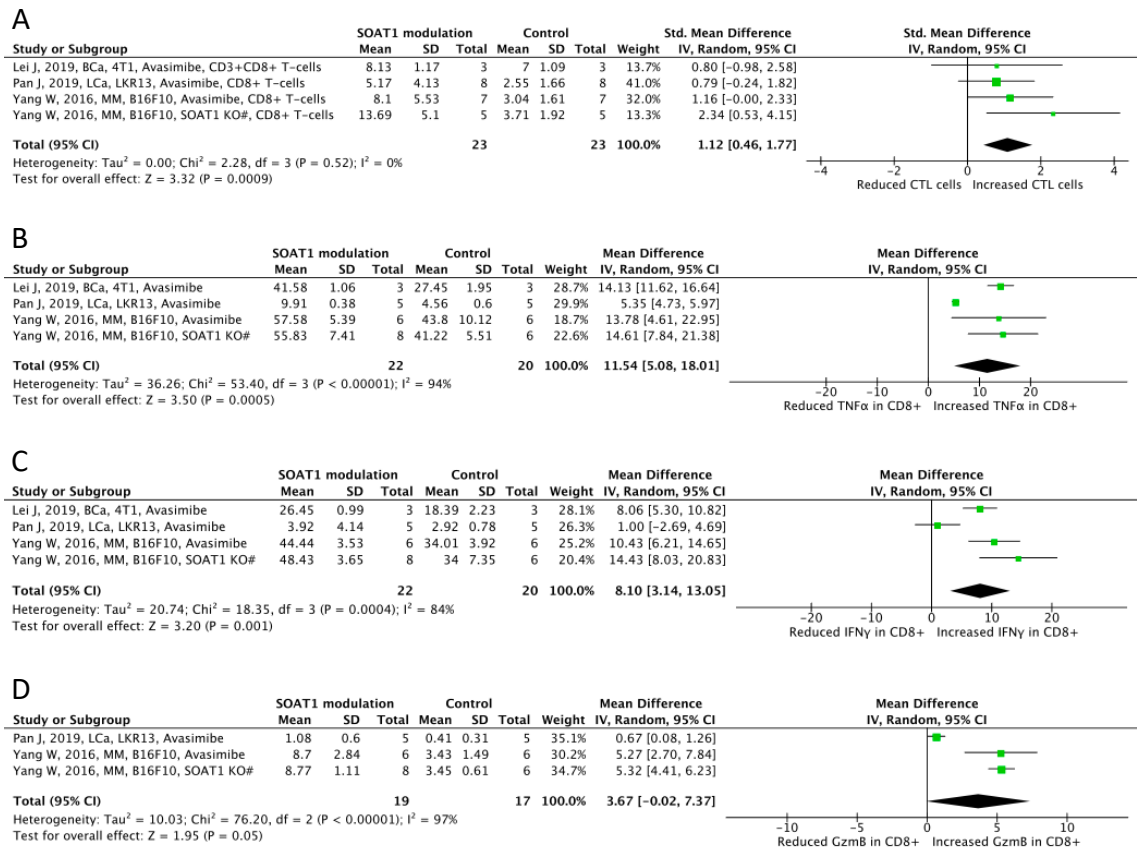


Figure 5.14 Forest plots of change in immune responses following disruption of SOAT.

(A) Standardised mean difference between experimental and control in tumour infiltration of CD8 +cells. (B) Mean difference (percentage CD8 +cells) between experimental and control in TNF α expression in CD8 +cells. (C) Mean difference (percentage CD8 +cells) between experimental and control in IFN γ expression in CD8 +cells. (D) Mean difference (percentage CD8 +cells) between experimental and control in GzmB expression in CD8 +cells. # denotes modifications localized to T-cells.

5.5.3.5 Activating invasion and metastasis

Larger tumours are associated with an increased likelihood of lymph node positivity (Andea et al., 2004) and metastasis (Munajat et al., 2008; Jia, B. et al., 2020). Therefore, the impact of inhibiting cholesterol esterification was assessed on metastasis. There was a significant reduction in metastases to either lymph, lung, pulmonary or whole mouse, with this measured by tumour node number on the respective organ, organ weight or radiance from luciferase expressing cells (Lee, H.J. et al., 2018; Lei et al., 2020; Li, J. et al., 2016; Li, M. et al., 2018) (SMD = 2.21; 95% CI: 3.17 to 1.26; $I^2 = 57%$; $p < 0.00001$; **Figure 5.15**). Only Lee et al. reported xenograft metastasis to all organs within the mouse by using PC3 cells constitutively expressing luciferase, showing tumour burden across all organs was reduced following avasimin treatment (Lee, H.J. et al., 2018). Treatments of either avasimibe or avasimin reduced metastasis frequency in breast (Lei et al., 2020), pancreatic (Li, J. et al., 2016) and prostate cancer (Lee, H.J. et al., 2018). Additionally, pre-treatment of pancreatic cancer cell line MIA PaCa-2 with shRNA against SOAT1 also induced a significant reduction in tumour metastasis to the lymph nodes (Li, J. et al., 2016). Li et al., recorded metastasis to two organs, finding concordance between reduced metastases to lymph nodes and liver following SOAT inhibition (Li, J. et al., 2016). Furthermore, avasimibe was shown to impair lung colonisation of intravenously injected LLC cell, suggesting avasimibe therapy impaired their metastatic potential (Yang, W. et al., 2016). Moreover, SOAT1 genetic knockdown restricted to mouse T-cells was also found to significantly reduce tumour multiplicity of the lungs in both LLC and B16F10 metastasis models (**Appendix Table C.2**) (Yang, W. et al., 2016). Contrastingly, Hao et al., found no significant change in lung colonisation of intravenously administered B16F10 cells after avasimibe therapy. Co-treatment of avasimibe and T-cells could also not significantly alter tumour burden in the lungs (**Appendix Table C.2**) (Hao et al., 2020) however, this may have been due to low avasimibe dose.

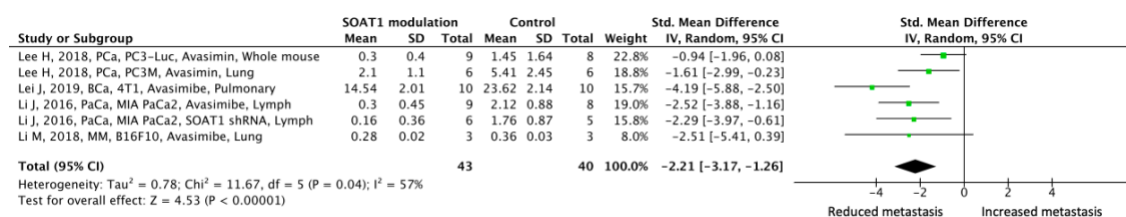


Figure 5.15 Forest plot showing changes in metastasis.

Standardised mean difference between experimental and control number of metastases.

5.6 Risk of bias

5.6.1 Study criteria

Risk of bias analyses highlight the likelihood that aspects of study design may generate misleading results. As a meta-analysis summarises the work of many studies, there is an increased importance to highlight where bias may have been introduced. Therefore, the risk of bias introduced to the meta-analysis through the quality of reported data was assessed; issues regarding study design, ethical considerations and reproducibility were discussed. Under 50% of studies reported SOAT modification as effective, either through demonstrating reduced CE concentration within tumour tissue or showing reduced expression of SOATs following genetic knockdown/knockout. Most studies accounting for poor reporting of SOAT modulation validation used avasimibe, which is already well characterised. Furthermore, most studies assessed avasimibe at 15 mg/kg (66%), perhaps explaining the lack of reporting on dosing rationale. There was also limited reporting on selection bias within studies assessing SOAT modulation, with only 54% of studies reporting randomisation. Of those 54%, none reported the method of randomisation. Additionally, only one study reported blinding of investigators to animal groups (**Appendix Figure C.2**). Studies investigating SOAT modulation against tumour size performed considerably better on the ROB survey than studies assessing CE content within pre-clinical tumours (**Appendix Figure C.3**). However, studies from the latter cohort were considerably older (average publication date: 1986) than the former (average publication date: 2018). Outside of these notable findings, risk of bias was adequate and thus, risk of bias for study design was deemed low. However, there are greater chances of bias being introduced through immunoblotting and immunohistochemical approaches, with clarity lacking on reporting of the antibody used, controls, blinding, statistical analysis and antibody validation (**Appendix Figure C.4**).

5.6.2 Heterogeneity

As anticipated, there was high heterogeneity within analysis of tumour size between subgroups ($I^2 = 82\%$) indicating that despite the assessed cancers exhibiting reduced volume in response to SOAT inhibition, the magnitude of reduction appears to vary. This can likely be attributed to variable expression of SOATs within the cell lines assessed. For example, Jiang et al., assessed the expression of SOAT1 within PDXs, separating these models into high and low SOAT1 expression (Jiang, Y. et al., 2019). PDX models were then treated with avasimibe, finding that SOAT1 expression is crucial for the efficacy of the therapy. Furthermore, Lu et al., assessed HepG2 cells, who exhibit enhanced SOAT2 expression over SOAT1 and found that these xenografts were significantly more susceptible to SOAT2 specific inhibition over SOAT1 (Lu, Ming et al., 2013). Unsurprisingly, other cancers exhibit the highest heterogeneity of the subgroups ($I^2 = 89\%$), likely since five of the seven comparisons are investigating different cancers. Skin cancer exhibited low heterogeneity ($I^2 = 25$), likely driven by the recurrence of B16F10 allografts across five of the six comparisons. Prostate cancer studies exhibited high heterogeneity ($I^2 = 76\%$), despite all studies being performed from the same research group and all but one comparison assessing PC3 cells. Notably, comparisons derived from Hao et al., frequently disrupt heterogeneity analyses, likely through their low avasimibe dose and administration frequency compared to other studies (Hao et al., 2020).

5.6.3 Publication bias

Bias can be introduced through the selective publication of significant over non-significant or unfavourable results. Therefore, funnel plots were inspected for evidence of potential publication bias for analyses of tumour size and risk of early euthanasia. Both analyses exhibited funnel plot asymmetry, indicating publication bias. This was likely driven through the assessment of different cancers and study design; however, as all individual cancer assessments were lowly powered, trim and fill analysis was used to estimate the overestimation induced by publication bias in tumour size and risk of early euthanasia across all cancers. Trim and fill analyses predicted that SOAT inhibition-mediated reduction in tumour size was overestimated by 33% (**Figure 5.16A**) as was the change in hazard ratio by 18% (**Figure 5.16B**).

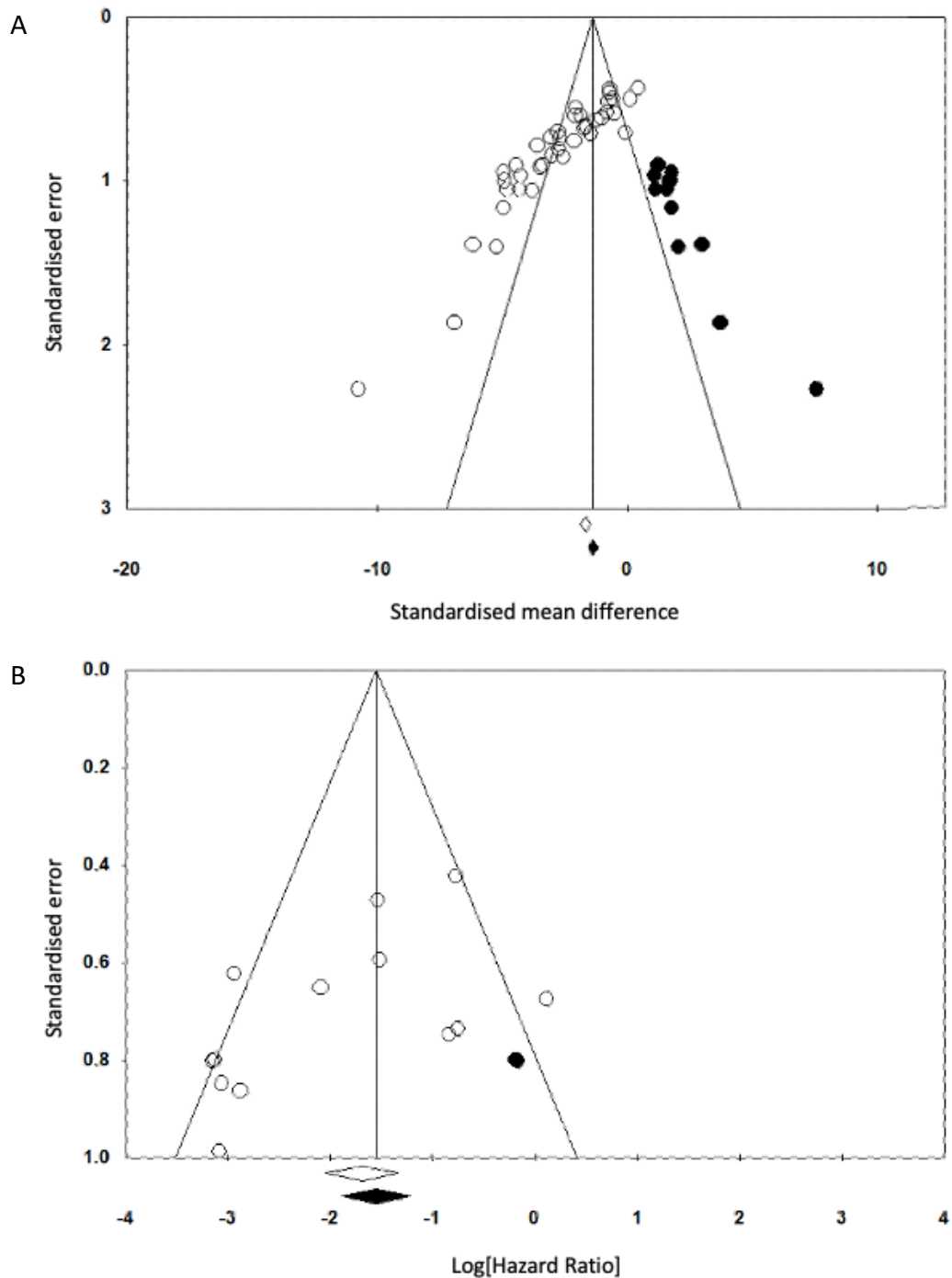


Figure 5.16 Risk of publication bias.

(A) Funnel plot to detect publication bias within SOAT tumour metrics dataset with trim and fill method applied to assess overestimation of SMD. (B) Funnel plot to detect publication bias within survival dataset with overestimation of hazard ratio determined through trim and fill analysis. Open dots indicate observed studies and closed dots indicate missing studies. Open diamond indicates observed change and the closed diamond indicates change after missing studies are factored in.

5.7 Discussion

This meta-analysis shows that across 37 different studies there is a consistent increase in CE content within tumour tissue compared to normal tissue. Furthermore, SOAT-mediated cholesterol esterification presents a targetable mechanism to reduce tumour volume. The use of SOAT inhibitors was shown to target multiple cancer hallmarks to reduce tumour size, including proliferation, apoptosis and immune cell mediated tumour destruction. These findings were highly significant and occurred irrespective of the cancer type assessed.

Increased cholesterol loading to the membrane facilitates enhanced T-cell receptor clustering through increased membrane fluidity, leading to increased CD8⁺ T-cell activation and cytotoxicity. SOAT depletion within T-cells leads to reduced cholesterol esterification and increased membrane cholesterol to allow for increased T-cell activity (Yang, W. et al., 2016; Hao et al., 2020). Lei et al., suggested that enhanced cytotoxic response of CD8⁺ cells is the driving factor behind avasimibe-mediated tumour destruction, showing little change in intratumour T-cell infiltration of 4T1 grafted BALB/c mice (Lei et al., 2020). Furthermore, SOAT1 deficient CAR-T cells did not exhibit enhanced tumour infiltration *in vivo* (Zhao et al., 2020) and avasimibe loading of T-cells resulted in no change in response to chemoattractant, MCP-1, *in vitro* (Hao et al., 2020). However, there is contrasting evidence provided by other studies. Both T-cell specific knockout and IP avasimibe treatment in C57BL/6 mice with B16F10 allografts found a significant increase in CD8⁺ cell tumour infiltration (Yang, W. et al., 2016). Similarly, IP avasimibe treatment of sv129 bearing the LKR13 allograft found increased infiltration of CD8⁺ cells into tumours (Pan, J. et al., 2019). Reduced efficacy on T-cells derived from BALB/c mice compared to C57B1/6 and sv129 mice may be driving variable stimulation of tumour infiltration. BALB/c and C57B1/6 mice exhibit differences between the immune systems with regards to cytokine production (Trunova et al., 2011) and a larger population of Treg cells in BALB/c mice (Chen, X. et al., 2005), which may cause different susceptibilities to SOAT inhibition with regards to T-cell infiltration.

Many studies report enhanced cytotoxicity in response to SOAT inhibition *in vivo* and *in vitro* and is perhaps a combination of increased infiltration and enhanced cytotoxicity that increases tumour destruction. SOAT1 knockdown in CAR-T cells increases IFN γ expression (Zhao et al., 2020). *In vitro*, T-cells treated with avasimibe demonstrated significantly higher cytotoxicity than control T-cells. Interestingly, the same treatment also enhanced antibody production in native B-cells (Chen, X. et al., 2017). This does not appear to be true for all cancers, with avasimibe treated T-cells exhibiting enhanced cytotoxicity against B16F10 melanoma cells, but not C26 colon cancer cells (Li, M. et al., 2018). Furthermore, treatment of T-cells with K604 increased expression of cytokines and cytotoxicity (Yang, W. et al., 2016).

CD8⁺ T-cells isolated from B16F10 grafted mice treated with both avasimibe and paclitaxel or paclitaxel monotherapy were reintroduced into new B16F10 allograft bearing mice. T-cells from co-treated mice induced significantly more tumour destruction compared to T-cells from mice treated with only paclitaxel. However, neither CD8⁺ T-cells from paclitaxel treated mice or those co-treated with avasimibe induced a significant change in serum cytokine content, leading the authors to suggest that tumour destruction was due to the antigen specific immune response (Li, M. et al., 2018). Interestingly, avasimibe treatment has been shown to increase the efficacy of the specific immune response. B-cells harvested from the spleens of avasimibe treated mice secreted significantly more antibodies than those from control spleens. Alternatively, as these T-cells were derived from C57B1/6 mice, increased tumour destruction could be due to increased invasion of T-cells into the tumour in response to avasimibe, as reported in Yang et al. (Yang, W. et al., 2016).

Furthermore, tetrazine (Tre) groups were inserted into the T-cell membranes through lipid insertion and liposomal avasimibe containing bicyclononyne (BCN), which bind to Tre groups and enable liposomal avasimibe (BCN-Lipo-Ava) retention to the cell surface. This enhanced avasimibe retention to T-cells during circulation and extravasation. *In vitro*, treatment of BCN-Lipo-Ava on Tre containing T-cells performed similarly to normal T-cells treated with avasimibe regarding TCR clustering and subsequent increase in cytokine expression (IFN γ , TNF α , IL-2). However, when tested *in vivo*, the importance of

avasimibe restriction to the T-cells was highlighted, with significant increases in IFN γ , GzmB and TNF α reported between Tre T-cell+BCN-Lipo-Ava cells and T-cells pre-treated with avasimibe. There was also a significant decrease in tumour volume, Ki67 status, hazard ratio and lung metastasis between these conditions (Hao et al., 2020). This study demonstrates how lipid encapsulation of avasimibe can be utilised to selectively target certain cell types. Nevertheless, lipid encapsulated avasimibe administered either intravenously has shown to have increased blood and tumour bioavailability over avasimibe (Lee, S.S.-Y. et al., 2015).

Increased immune mediated tumour destruction is likely not the only anti-cancer mechanism involved following SOAT modulation. Many studies investigated xenograft models, which require the use of immunodeficient or lymphodepleted mice to prevent graft rejection. As such, a direct effect of SOAT inhibition on cancer cells is likely. For example, oncogenic signalling appears to be influenced by CEs. Reduced phosphorylation of AKT (Li, J. et al., 2018; Yue et al., 2014; Liu, Y. et al., 2021) and ERK (Wang, L. et al., 2019; Oni, T. E. et al., 2020; Liu, Y. et al., 2021) were frequently reported throughout studies identified within our systematic review. It is understood that high CE content within tumours upregulates SREBP-1, leading to an increased uptake of essential fatty acids and subsequent phosphorylation of AKT (Yue et al., 2014). Reduced SREBP-1 caused by SOAT inhibition has been reported in both glioblastoma cells (Geng et al., 2016) and pancreatic cancer cells. Additionally, AKT, mTOR and p-70S6K phosphorylation increased significantly following cholesteryl oleate treatment, which was reversed with the addition of avasimibe (Wei et al., 2021). Furthermore, reduction of ERK phosphorylation was again driven through an increase in free cholesterol. However, downregulation of ERK phosphorylation instead acts through inhibition of the mevalonate pathway through a free cholesterol-mediated negative feedback loop. In non-SOAT inhibited tumours, ERK signalling can be induced by side products of an upregulated mevalonate pathway (Oni, T. E. et al., 2020). Furthermore, avasimibe has also been shown to reduce expression of ARK1C, through downregulation of FOXM1 in both osteosarcoma (Wang, L. et al., 2019) and cholangiocarcinoma (Gao, Y. et al., 2021) cells. In addition to upregulation of oncogenic activity, SOAT has also been implicated in the downregulation of tumour suppressor genes, such as E2F-1 (Xiong, K. et al., 2021).

It is understood that the increase in cellular free cholesterol upregulates E2F-1 expression, which then exerts its repression of tumour growth through increased activation of apoptosis.

Esterification is not the only cholesterol modification; many other enzymes can convert cholesterol into oxysterols by adding hydroxyl, keto or epoxy groups. It was demonstrated that treatments of Huh7 and HepG2 xenografts with SOAT2 specific inhibitor, PPPA, resulted in a significant increase in 24OHC and 26OHC intratumour concentration *in vivo* and intracellular content *in vitro*. Interestingly, the use of a SOAT1 specific inhibitor, K604, did not induce a significant change in oxysterol content either *in vivo* or *in vitro*. Both PPPA and siSOAT2 treatments of HepG2 and Huh7 xenografts were able to significantly reduce tumour volume, whereas K604 and siSOAT1 could not. This led the authors to attribute the anti-tumour effects of SOAT2 inhibition on the increase in intratumour concentrations of antiproliferative oxysterols (Lu, M. et al., 2013). Consequently, this suggests that cancers store cholesterol as CEs to limit the production of oxysterols, which reduce their proliferation. Furthermore, reactive oxygen species can also generate oxysterols. Treatments of PC3 and DU145 prostate cancer cells with avasimibe (Xiong, K. et al., 2021) and H295R adrenocortical carcinoma cells with ATR-101 (Cheng, Y. et al., 2016) significantly increased intracellular ROS content, providing an alternate mechanism for OHC production in SOAT inhibited tumours. Interestingly, the addition of synthetic LXR ligand, T0901317, inhibits AKT phosphorylation (Pommier et al., 2010), suggesting that SREBP-1 may not be the only SOAT-dependent mechanism that affects AKT phosphorylation.

Cholesterol is not the sole substrate for SOAT1, with oxysterols also confirmed targets of recombinant enzyme *in vitro* (Cases et al., 1998) and in *in vivo* animal models of cancer (Lu, M. et al., 2013). Oxysterols can modulate cell signalling through their action on LXR, with esterification by SOAT1 potentially altering their efficacy as LXR ligands. Consequently, altered efficacy of esterified oxysterols as LXR ligands may be another mechanism behind altered gene expression in cancer and immune cells following SOAT1 disruption.

The effects of esterification on oxysterol:LXR signalling could be tested through siRNA knockdowns of both SOAT1 and SOAT2 in LXR-inducible luciferase reporter cells before treating with oxysterols. Changes in luciferase expression following knockdown of SOAT1/2 will determine whether esterified oxysterols are more or less potent as LXR ligands. Oxysterol free and esterified content in these siSOAT1/SOAT2 cells can also be measured to see the influence these enzymes have on the esterification of individual oxysterols. Furthermore, SOAT2 was presented in liver cancer cells as the primary mediator of oxysterol esterification, however there may be compensation between these two enzymes. Investigation should be made into the compensatory increase in expression of one gene when the other is knocked down.

Since the completion of the systematic search, two non-graft pre-clinical models have been published showing how modulating CEs can impair tumour generation in autonomous or carcinogen-induced cancer models. One such study, supplemented MMTV-PyMT mice with a high cholesterol diet. Firstly, time until initial tumour formation decreased and tumour weight increased with cholesterol ester supplementation. Furthermore, there was a dose dependent response between the percentage of Ki67 positive cells and CE supplementation to the diet (Wei et al., 2021). Diets were also supplemented with cholesterol, showing a significant increase in serum CE levels. This again resulted in increased tumour weight and Ki67 positivity (Wei et al., 2021). Supplementing hepatocellular carcinoma mouse models with a high fat diet increased SOAT1 expression in liver cancer tissues, possibly to store increased cholesterol obtained from diet. Treatment of mice with avasimibe completely abrogated the increased rate of tumour growth induced by high fat diet (Ren, M. et al., 2021). Surprisingly, avasimibe did not induce a significant reduction in HepG2 xenografts in the absence of high fat diets compared to controls (Ren, M. et al., 2021). HepG2s have demonstrated that SOAT2 exhibits the greatest control over cholesterol esterification and tumour volume rather than SOAT1. Assessment of avasimibe selectivity towards SOAT1 and SOAT2 has been mixed, and perhaps this study is evidence it is more selective to SOAT1.

Our risk of bias analysis highlighted a significant risk of publication bias amongst our meta-analyses. However, results from trim and fill method may have been skewed due to the moderate and high heterogeneity of the studies assessed ($I^2=71\%$ and 41% , respectively), with tests for publication bias lacking power in cases of higher heterogeneity (Lau et al., 2006). Subsequently, funnel plot asymmetry may be a result of inter-study differences rather than an under-reporting of non-significant studies or studies with unexpected results. However, with a high number of significant studies from both analyses (60% and 92% respectively) from relatively small average group sizes (7.08 and 9.66 , respectively), the evidence of publication bias is high. Moreover, the consistent lack of reporting on animal randomisation and assessor blinding increases the risk of bias introduced through study design. With these seemingly a common occurrence amongst pre-clinical models (Henderson et al., 2015; Augustine et al., 2017; Jue et al., 2018), improvements are required to scientific reporting on studies of this kind to improve their relevance in the decision to test a drug in a clinical setting.

5.8 Conclusion

The data we have summarised shows that imbalanced cholesterol homeostasis can influence strong changes to tumour signalling pathways that alter proliferation and the anti-tumour response of the immune system. The summary we provide here highlights a targetable mechanism that can be used to target the hallmarks of cancer. Many small molecule inhibitors affecting cholesterol esterification have already been identified as safe for use in humans and present themselves as ideal candidates for repurposing as anti-cancer therapies.

Chapter 6: Discussion

6.1 Cholesterol metabolism pathways are linked

The aims of this study were to highlight the mechanisms through which cholesterol derivatives can lead to cancer progression, be it through cholesterol hydroxylation or esterification. It is apparent that these mechanisms are intrinsically linked, with cholesterol esterification reducing the pool of free cholesterol to be converted into oxysterols (Lu, Ming et al., 2013). Furthermore, 25OHC has been shown to increase SOAT-mediated cholesterol esterification in insect cells and rat intestinal microsomes, suggesting oxysterols can modulate cholesterol storage (Cheng, D. et al., 1995; Field and Mathur, 1983). In terms of proliferation, these two pathways are conflicting. Cholesteryl esters promote cancer growth through cellular restriction of free cholesterol, resulting in activation of oncogenes AKT (Liu, Y. et al., 2021; Li, J. et al., 2018; Yue et al., 2014) and ERK (Wang, L. et al., 2019; Oni, T. E. et al., 2020; Liu, Y. et al., 2021). Conversely, oxysterols are anti-proliferative through their induction of LXR signalling (Fukuchi et al., 2004).

Despite their anti-proliferative effects on tumour growth, oxysterols and oxysterol producing enzymes are often associated with poor prognosis in breast cancers (Nelson, Erik R et al., 2013; Wu, Q. et al., 2013) and I have contributed to this research by demonstrating that 24OHC, 25OHC and 26OHC all associate with reduced DFS in ER-negative patients. Furthermore, I have produced strong evidence showing that the association between 24OHC and reduced DFS is mediated through LXR-dependent upregulation of chemotherapy efflux pump, Pgp. Therefore, findings from these chapters suggest that if SOAT-mediated esterification was targeted in ER-negative cancers, these tumours may exhibit impaired proliferation and increased apoptosis but may also develop resistance to Pgp-targeting chemotherapy agents. Furthermore, activity of CYP3A4, an enzyme involved in the metabolism of many chemotherapy agents (Harmsen et al., 2007), is increased in hepatocytes treated with the SOAT inhibitor avasimibe (Sahi et al., 2003). Alleviating some of these concerns were *in vivo* animal studies performing combination therapies with chemotherapy agents and SOAT inhibition (Li, M. et al., 2018; Li, J. et al., 2018; Bandyopadhyay et al., 2017; Pan, J. et al.,

2019; Bi et al., 2019). Overexpression of Pgp in the chronic myelogenous leukaemia cell line K562 provided resistance to imatinib treatment (Peng et al., 2012). However, avasimibe treatment in combination with imatinib therapy on imatinib resistant K562 cells reduced tumour volume by 60% compared to imatinib monotherapy (Bandyopadhyay et al., 2017). Furthermore, doxorubicin is both a target of Pgp mediated efflux (Gottesman et al., 2002) and CYP3A4-mediated metabolism (Goldstein et al., 2013). However, doxorubicin treatment on 4T1 allograft models was more potent when administered alongside avasimibe (Lei et al., 2020). This suggests that neither avasimibe stimulation of CYP3A4 or Pgp upregulation through SOAT inhibition-mediated increased intratumour oxysterol content was reducing the efficacy of doxorubicin treatment. Additionally, concerns over increased oxysterol content in response to SOAT inhibition are not exclusive to ER-negative cancers.

Oxysterols are also esterified, however there is limited investigation into whether oxysterol esters have altered efficacy as LXR agonists. Inhibition of SOAT2 in Huh7 cells treated with LDL-sized particles were found to have reduced concentrations of esterified 24OHC and 26OHC compared to the control. Interestingly, the addition of SOAT1 inhibitor, K604, did not alter concentrations of either esterified oxysterols or cholesterol (Lu, Ming et al., 2013). Furthermore, SOAT2 produces cholesteryl esters and 26OHC esters at a higher rate than SOAT1 (Cases et al., 1998). Studies have shown that treatments with excess 7KC can induce apoptosis through LXR signalling (Levy et al., 2019). However, treatments of excess 7KC alongside SOAT inhibition with Sandoz 58-035 in macrophages suppressed apoptosis (Freeman et al., 2005), suggesting that esterification may prevent 7KC-mediated apoptosis.

6.2 Cholesterol metabolism determines the TME composition

CAFs can produce oxysterols and secrete them into the TME, which can transactivate LXR in surrounding epithelial cells. However, there is also the contribution of the other non-cancer cells of the tumour microenvironment to consider. Macrophages (Lavrnja et al., 2017; Kimura et al., 2016; Hansson et al., 2003; Rowe et al., 2003), adipocytes (Li, Jiehan et al., 2014; Franck et al., 2011), T-cells (Reome et al., 2004; Lu et al., 2014),

dendritic cells (Liu et al., 2011a), NK cells (Liu et al., 2011a; Nong et al., 2020; Kopcow et al., 2010) and B cells (Liu et al., 2011a) are all proven producers of oxysterols under normal conditions. Additionally, CAMs can also produce 26OHC at high levels (Shi et al., 2019). Co-culture and conditioned media experiments could be replicated to using these other cell types in the place of fibroblasts to assess their potential to induce LXR signalling in epithelial cells. Furthermore, the assessment of stromal expression of CYP46A1, CH25H and CYP27A1 will have accounted for the contribution of non-cancer cells other than the CAFs.

Additionally, inhibition of SOAT may also have implications on the infiltration and oxysterol production of TME cells. Increased intratumour oxysterol content through SOAT2 inhibition (Lu, Ming et al., 2013) may increase chemoattractant signals for immune cells. $7\alpha,25\text{OHC}$, which is produced by CYP7B1-mediated hydroxylation of 25OHC, directs migration of monocytes (Preuss et al., 2014), B-cells and T-cells (Liu et al., 2011a). Therefore, by enhancing intratumour $7\alpha,25\text{OHC}$ content through SOAT inhibition, the CAM population may increase. Furthermore, macrophages treated with SOAT inhibitor, oleic acid anilide, induced expression of CYP27A1, enhancing the potential for 26OHC production (An et al., 2008).

The implications of SOAT inhibition on adipocyte oxysterol production are unclear. However, adipocytes promote cancer progression through the release of free fatty acids stored in lipid droplets. Fatty acids are then absorbed by cancer cells and prevent the initiation of the programmed cell death following cell detachment from the ECM and promote tumour growth (Wang, Y.Y. et al., 2017). Knockdown of either SOAT1 or SOAT2 in adipocytes *in vitro* reduces lipid content by approximately 40% (Zhu, Y. et al., 2018), possibly suggesting there is less availability of free fatty acid secretions for cancer cells to absorb.

Infiltrating T-cells have already been widely reported to exhibit increased activity following inhibition of SOAT. This increased activity has primarily been attributed to increased membrane cholesterol content enabling rapid clustering of TCR complexes to the immunological synapse (Yang, W. et al., 2016; Hao et al., 2020). However, systemic

inhibition of SOAT may lead to increased intratumour concentration of 26OHC as shown *in vivo* (Lu, Ming et al., 2013) and demonstrated in cells through upregulation of CYP27A1 (An et al., 2008). Increased intratumour 26OHC would lead to an increased tumour infiltration of $\gamma\delta$ -T cells (Baek, Amy E. et al., 2017). $\gamma\delta$ -T cells are known to suppress CD8 cell cytotoxicity through induction of granulocyte expansion and have been shown to induce metastasis in E0771 and Met1 metastatic *in vivo* models. There is currently no evidence on increased infiltration of $\gamma\delta$ -T cells following SOAT inhibition. Nevertheless, there are alternate options for SOAT targeted therapy through CAR-T cell specific inhibition of SOAT, which should alleviate any issues of enhanced systemic oxysterol content. *In vivo* models have demonstrated that SOAT deficient CAR-T cells alone are enough to significantly impair tumour growth in pancreatic tumours (Zhao et al., 2020).

6.3 Future prospects

Specific inhibitors to oxysterol producing enzymes have been identified. For example, GW273297X has been frequently used as an inhibitor of CYP27A1 in animal models of cancer (Baek, Amy E. et al., 2017; Nelson, Erik R et al., 2013), however this has not been validated as safe in humans. Furthermore, CYP46A1 inhibitors have also been assessed *in vivo* (Fourgeux et al., 2014; Popiolek et al., 2020) but not in the context of cancer. Furthermore, the efficacy of cholesterol esterification inhibiting drugs has been frequently tested in animal models of cancer with consistent success (Websdale et al., 2021). However, when tested in clinical trials against cholesterol linked conditions (Insull Jr et al., 2001; Tardif et al., 2004; Raal et al., 2003), SOAT inhibitors did not induce the desired effect. Currently, only ATR-101 has been assessed as a SOAT-inhibitor in cancer clinical trials, although this did not induce a significant tumour response (Smith, David C. et al., 2020). Therefore, targeting upstream of both oxysterol and cholesteryl ester production may benefit patients. As such, dietary interventions aimed at cholesterol rather than drug therapies targeting oxysterols may be important routes of investigation.

Cholesterol lowering diets have already been investigated in breast cancer, finding they can reduce the risk of relapse in ER-negative breast cancers (Chlebowski et al., 2006). Additionally, patients with low LDL-C compared to high LDL-C associated with increased DFS and overall survival (Dos Santos et al., 2014). Not only do cholesterol concentrations in serum positively correlate with serum oxysterols (Stiles et al., 2014) but LDL can also transport 24OHC, 25OHC and 26OHC (Babiker and Diczfalusy, 1998), demonstrating the link between LDL-C and oxysterol signalling. In addition to dietary interventions, cholesterol lowering drugs such as statins could be employed to similar effect. A meta-analysis summarising studies assessing statin therapy in breast cancer found statins significantly reduced the chance of recurrence and BCSD (Manthravadi et al., 2016). When separating breast cancer patients using statins by subtype, TNBC was considerably more sensitive to statin therapy than non-TNBC subtypes for BCSD (Nowakowska et al., 2021).

Additionally, phytosterols have been long proven to reduce cholesterol levels in both organisms and cells. However, these phytochemicals appear to interact with a greater network of mechanisms, one of which being LXR signalling. Structural similarities between phytosterols and oxysterols have been highlighted, leading to the discovery of many phytosterols acting as weak agonists for LXR (Plat et al., 2005). The weak agonist activity of phytosterols has also been demonstrated in breast cancer cells. However, when cells are treated with phytosterols in conjunction with oxysterols, oxysterol mediated LXR activation is impaired (Hutchinson et al., 2019a). These experiments suggest competitive binding of the LBD of LXR between phytosterols and oxysterols, impairing oxysterol ability to induce LXR. Therefore, via the introduction of naturally occurring phytosterols to the diet, the output of the oxysterol-LXR axis can be dampened. Phytosterols have not been tested against cancer in a clinical setting, however a case controlled study demonstrated that phytosterols inversely associated with risk of developing breast cancer (Ronco et al., 1999). Furthermore, a meta-analysis assessing phytosterol treatments as anti-cancer therapies in *in vivo* animal models showed that phytosterols can reduce breast cancer graft volume (MD = -827.17 mm^3 ; 95% CI: -1297.26 to -357.07 ; $I^2 = 100\%$; $p < 0.001$). Analysis of the mechanisms involved in reduced tumour volume found that phytosterols likely reduced tumour volume

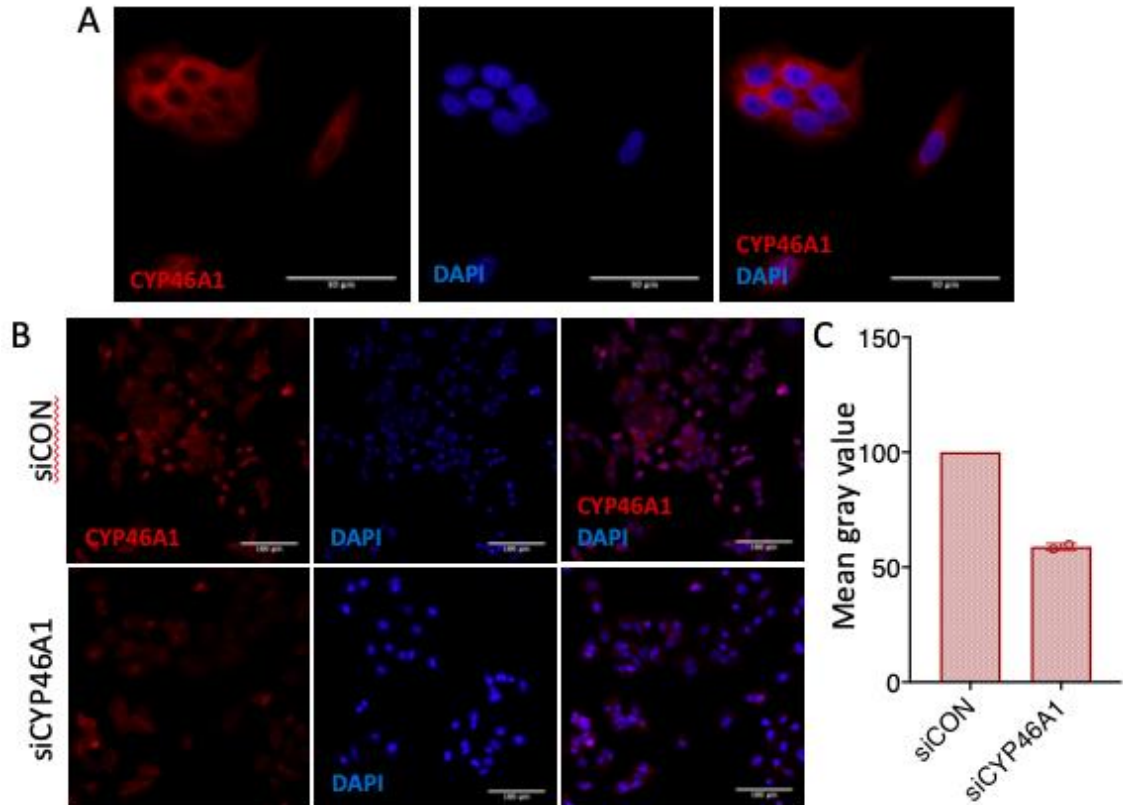
through increased apoptosis and reduced proliferation (Cioccoloni et al., 2020). These findings suggest that phytosterols may impair breast cancer progression by reducing the pool of free cholesterol for esterification and by impairing LXR signalling.

6.4 Conclusion

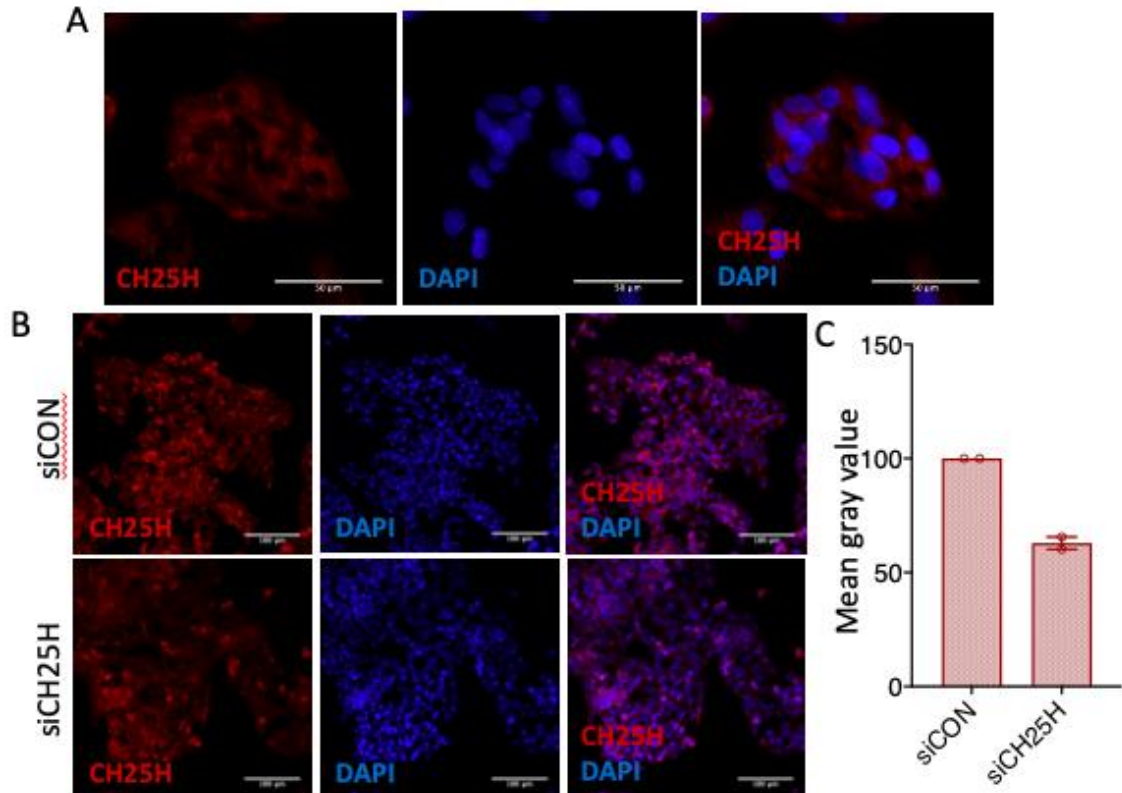
Oxysterols have been demonstrated to induce chemotherapy resistance in TNBC through LXR signalling. Chemoresistance was shown to be instigated through Pgp upregulation, a now verified LXR target in breast cancer cells. Furthermore, the expression of oxysterol producing enzymes associated with Pgp expression and DFS in human tumours. Additionally, only Event patients exhibited a positive association between intratumour 24OHC concentration and *ABCB1* mRNA expression. Investigations into the role of the TME in transactivating epithelial LXR identified that CAFs may be contributing a large proportion of oxysterols to the total tumour oxysterol content. However, further work is required to verify whether *ABCB1* upregulation is driven solely through LXR signalling. Furthermore, this research opens questions as to whether other cells of the TME can also drive chemoresistance through LXR transactivation. The fact that other non-cancer cells of the TME are capable of oxysterol production suggests so, however whether there is redundancy in oxysterol production between these cells is also an area of interest. Additionally, cholesteryl esters drive cancer progression through other mechanisms. Inhibition of cholesteryl esterification appears to enhance the immune anti-cancer response, demonstrating further involvement of the TME. These two mechanisms of cancer progression are linked by cholesterol, suggesting that cholesterol lowering methods would be a suitable as an adjuvant to chemotherapy.

Appendices

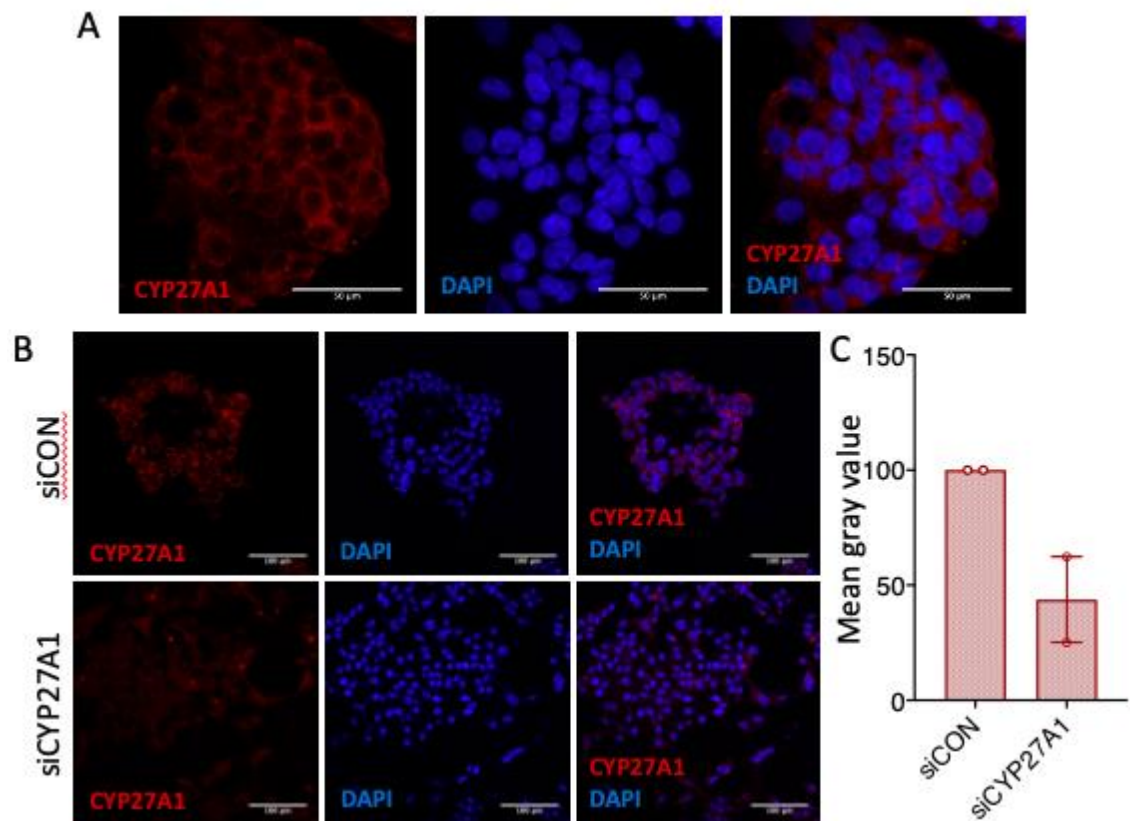
Appendix A Supplementary Data for Chapter 3



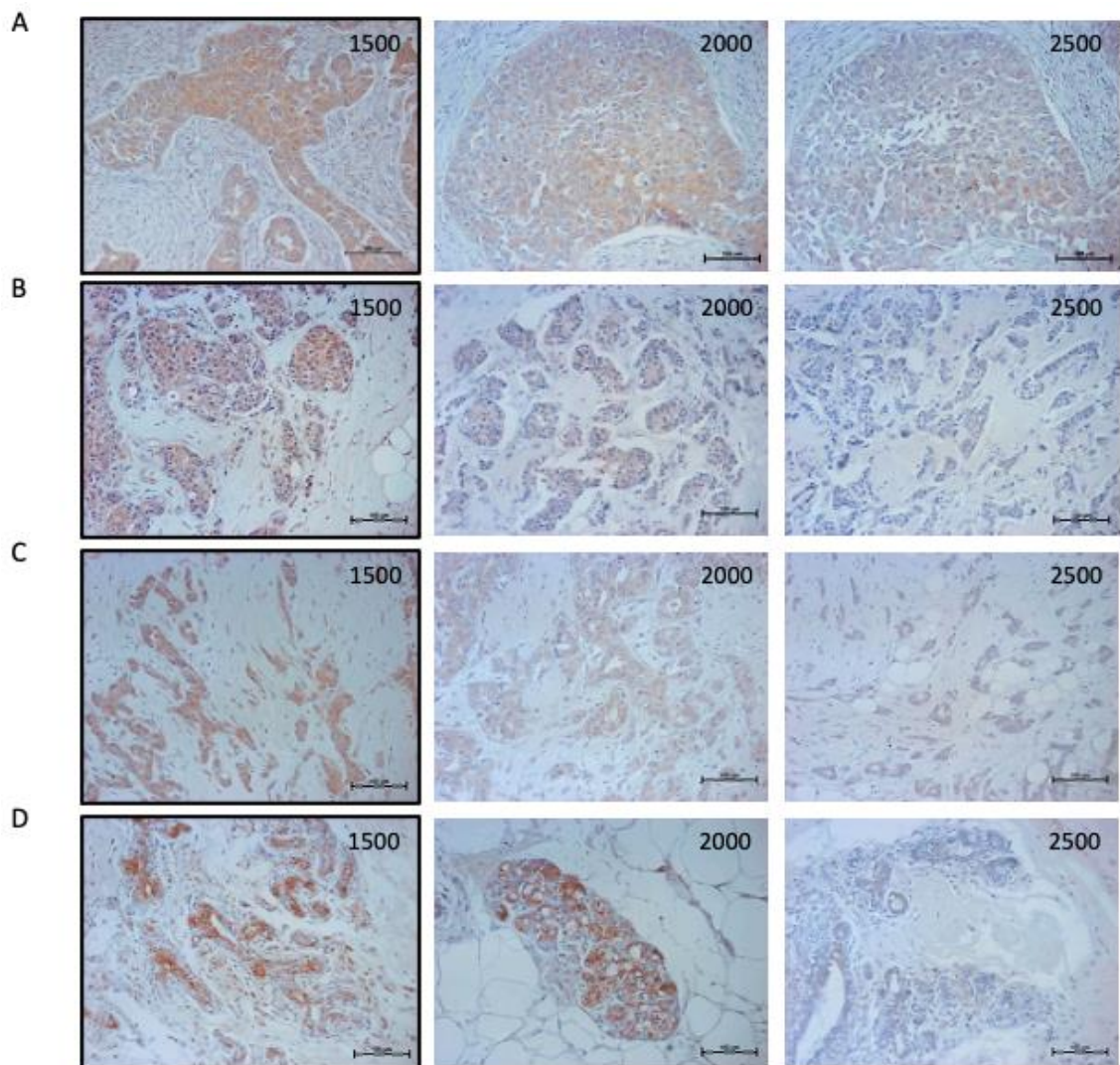
Appendix Figure A.1 Validation of CYP46A1 antibody accuracy. MCF7 cells were transfected with siCYP46A1 and CYP46A1 protein visualized using a CYP46A1 antibody. Immunofluorescence was normalized against control MCF7 cells transfected with scrambled siRNA and stained for CYP46A1. Panel A shows representative stain of untreated MCF7 cells with CYP46A1 at x63 magnification. Scale bars show 50 μ M. Panel B shows SCYP46A1 expression in scrambled and siRNA knockdowns respectively in magenta and blue fluorescence visualizing nuclei. Panel is split between CYP46A1 expression, DAPI stain and merge of the two. Scale bars show 100 μ M. Images taken at x20 magnification. Panel C shows quantification of siCYP46A1 knockdown mean gray value following stain, normalized to the scrambled. Error bars represent SEM of 2 independent repeats.



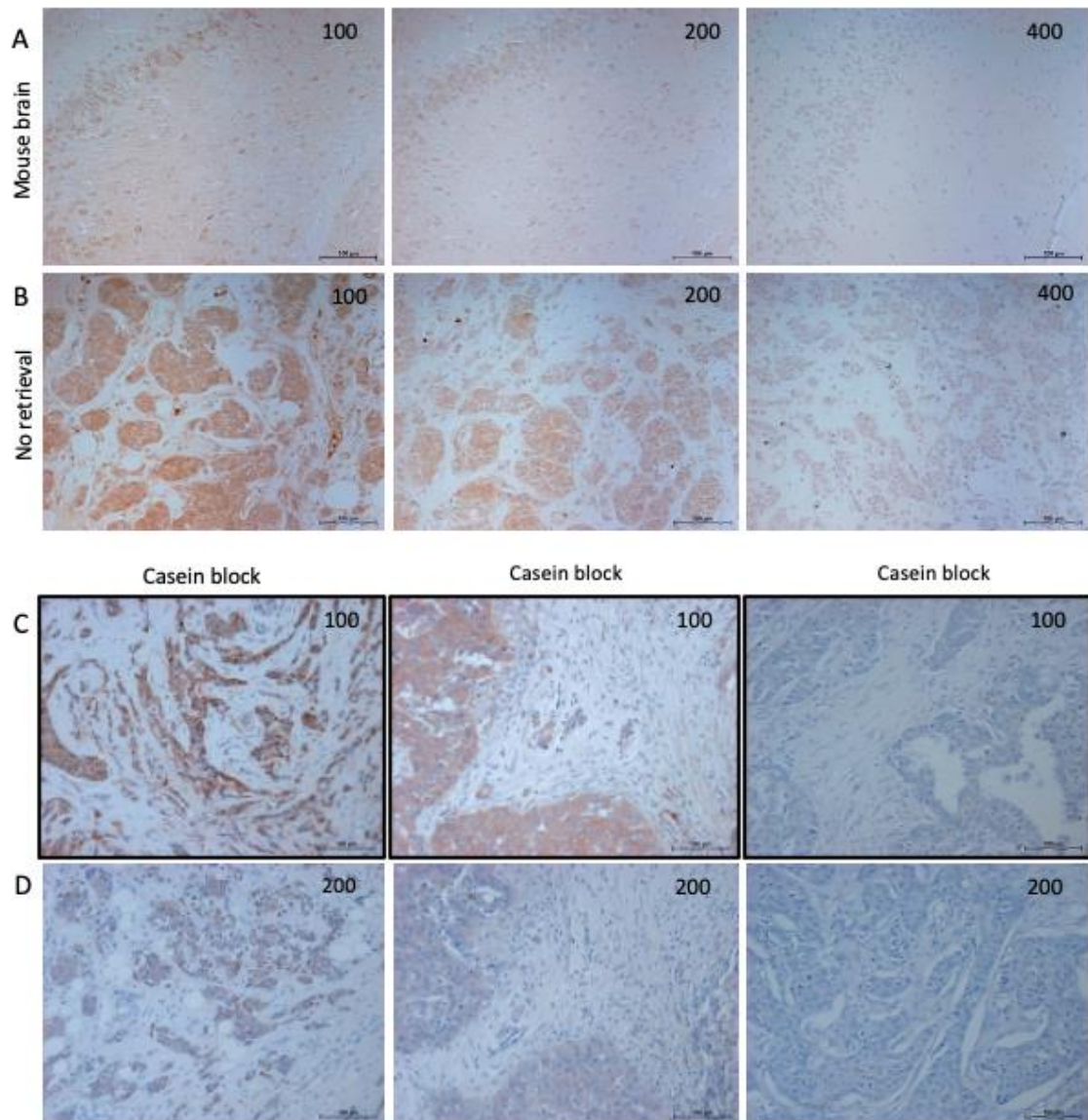
Appendix Figure A.2 Validation of CH25H antibody accuracy. HepG2 cells were transfected with siCH25H and CH25H protein visualized using a CH25H antibody. Immunofluorescence was normalized against control HepG2 cells transfected with scrambled siCON and siCH25H. Panel A shows representative stain of untreated HepG2 cells with CH25H at x63 magnification. Scale bars show 50 μ M. Panel B shows CH25H expression in siCON and siCH25H knockdowns respectively in red and blue fluorescence visualizing nuclei. Panel is split between CH25H expression, DAPI stain and merge of the two. Scale bars show 100 μ M. Images taken at x20 magnification. Panel C shows quantification of siCH25H knockdown mean gray value following stain, normalized to the scrambled. Error bars represent SEM of 2 independent repeats.



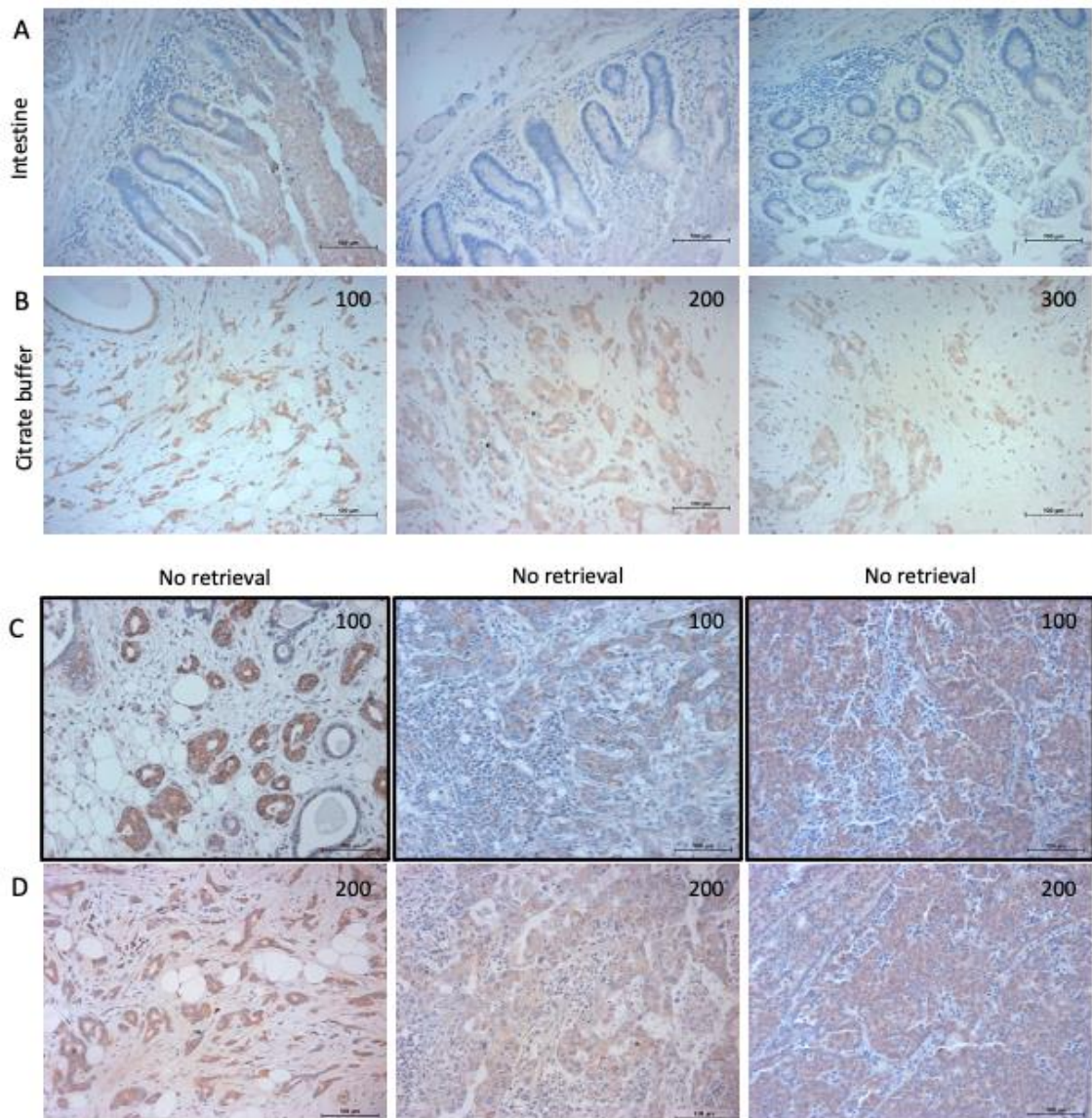
Appendix Figure A.3 Validation of CYP27A1 antibody accuracy. HepG2 cells were transfected with siCYP27A1 and CYP27A1 protein visualized using a CYP27A1 antibody. Immunofluorescence was normalized against control HepG2 cells transfected with siCON and stained for CYP27A1. Panel A shows representative stain of untreated HepG2 cells with CYP27A1 at x63 magnification. Scale bars show 50 μ M. Panel B shows CYP27A1 expression in siCON and siCYP27A1 knockdowns respectively in orange and blue fluorescence visualizing nuclei. Panel is split between CYP27A1 expression, DAPI stain and merge of the two. Scale bars show 100 μ M. Images taken at x20 magnification. Panel C shows quantification of siCYP27A1 knockdown mean gray value following stain, normalized to the scrambled. Error bars represent SEM of 2 independent repeats.



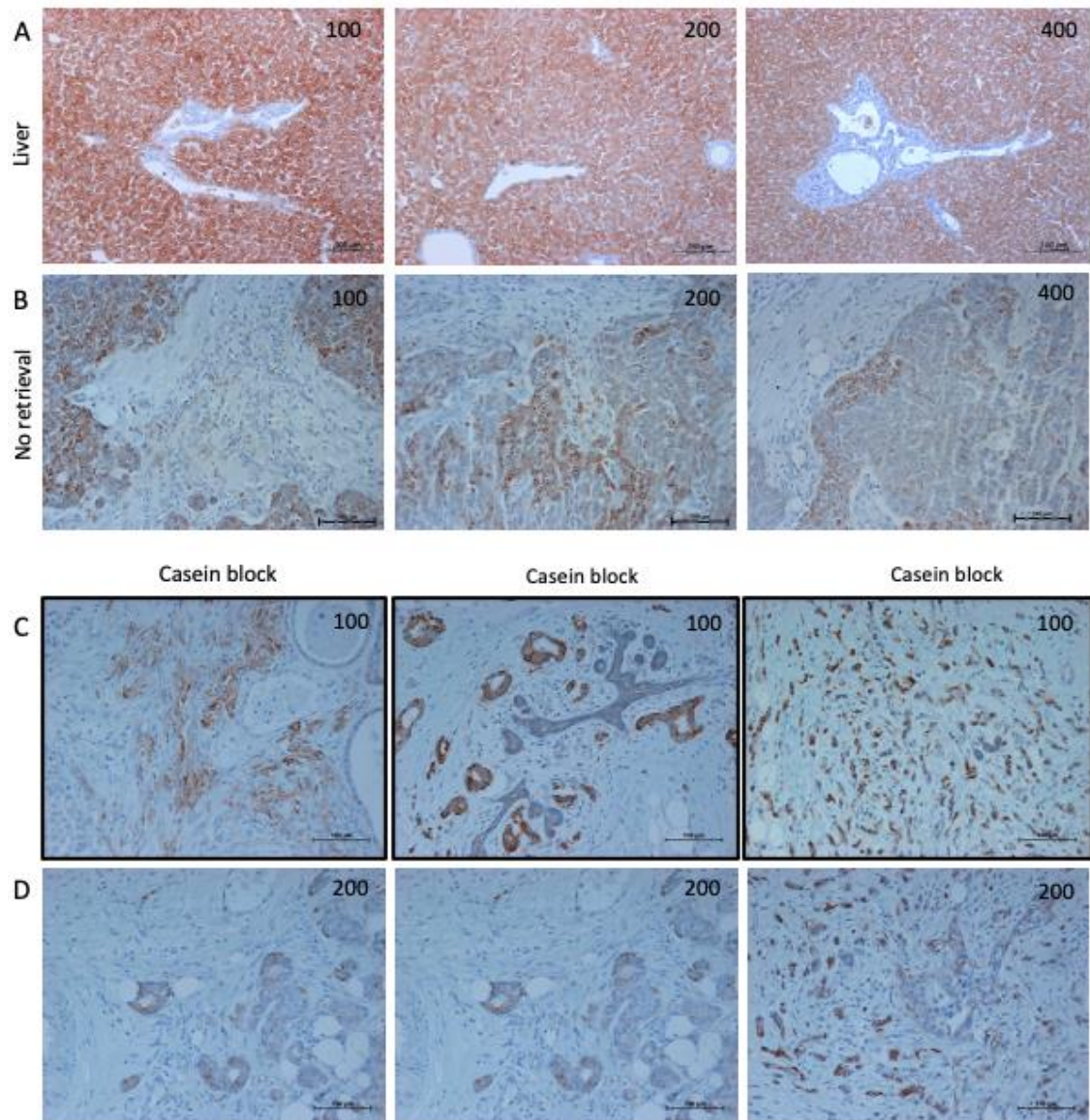
Appendix Figure A.4 Optimisation of P-glycoprotein antibody. Sections of four different breast tumours (BT1, 3, 5 and 6) were stained to visualize expression of Pgp using IHC with three different concentrations of antibody (1:1500, 1:2000 & 1:2500). Rows A-D represent the four different tumours, while greater antibody concentrations shown from left to right. Scale bar represents 100µm.



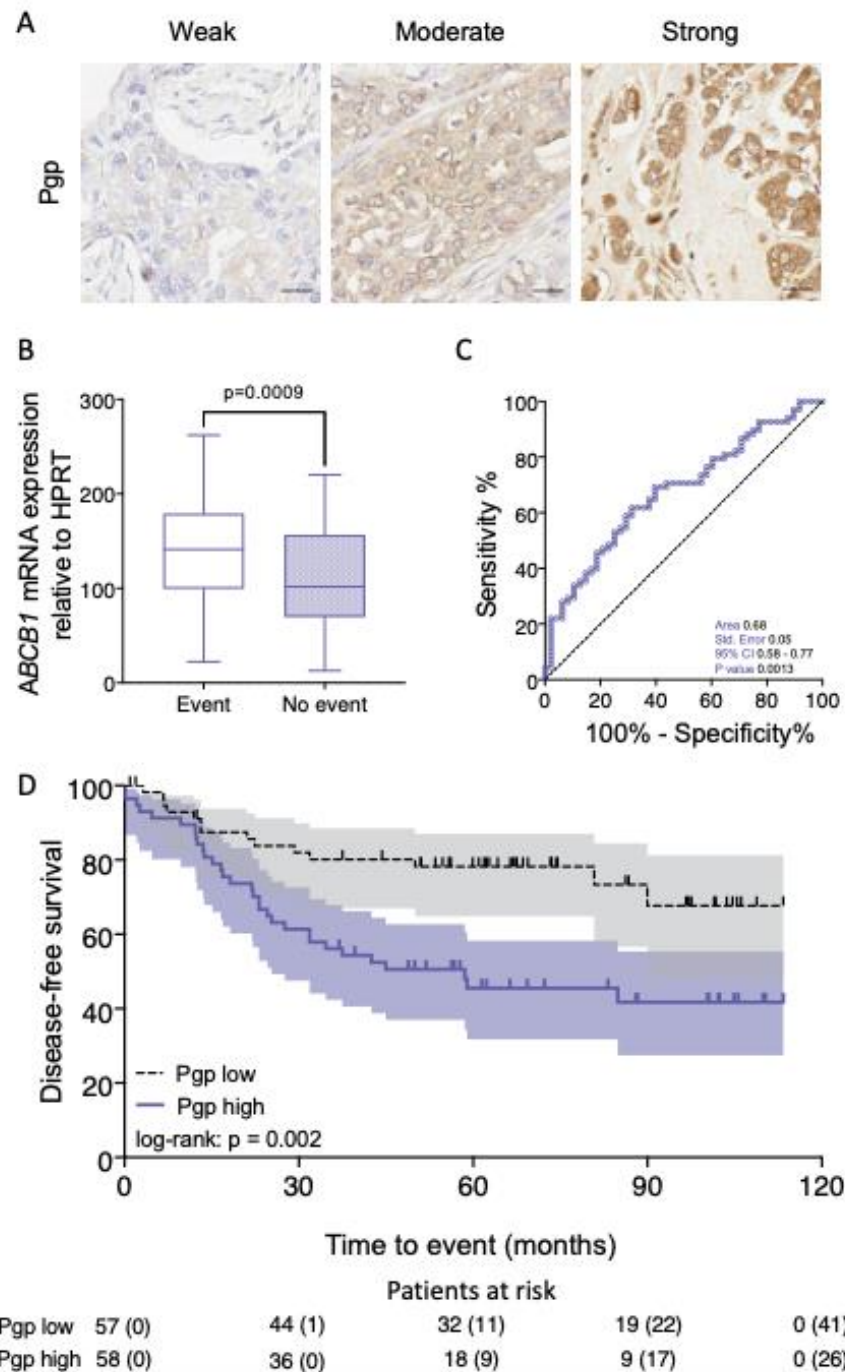
Appendix Figure A.5 Antibody optimization of CYP46A1. Mouse brain sections were stained to visualize expression of CYP46A1 with no retrieval. Breast tumour (BT8) was then stained with different antibody concentrations (1:100, 1:200 and 1:400) with no retrieval. A further three breast tumours (BT11, 10 and 1) were then stained with different antibody concentrations (1:100 and 1:200) with a casein block. Row A represents the liver, Row B shows BT1 and C-D shows tumours BT11, 10 and 1 from left to right with greater antibody concentrations shown descending. Scale bar represents 100 μ m.



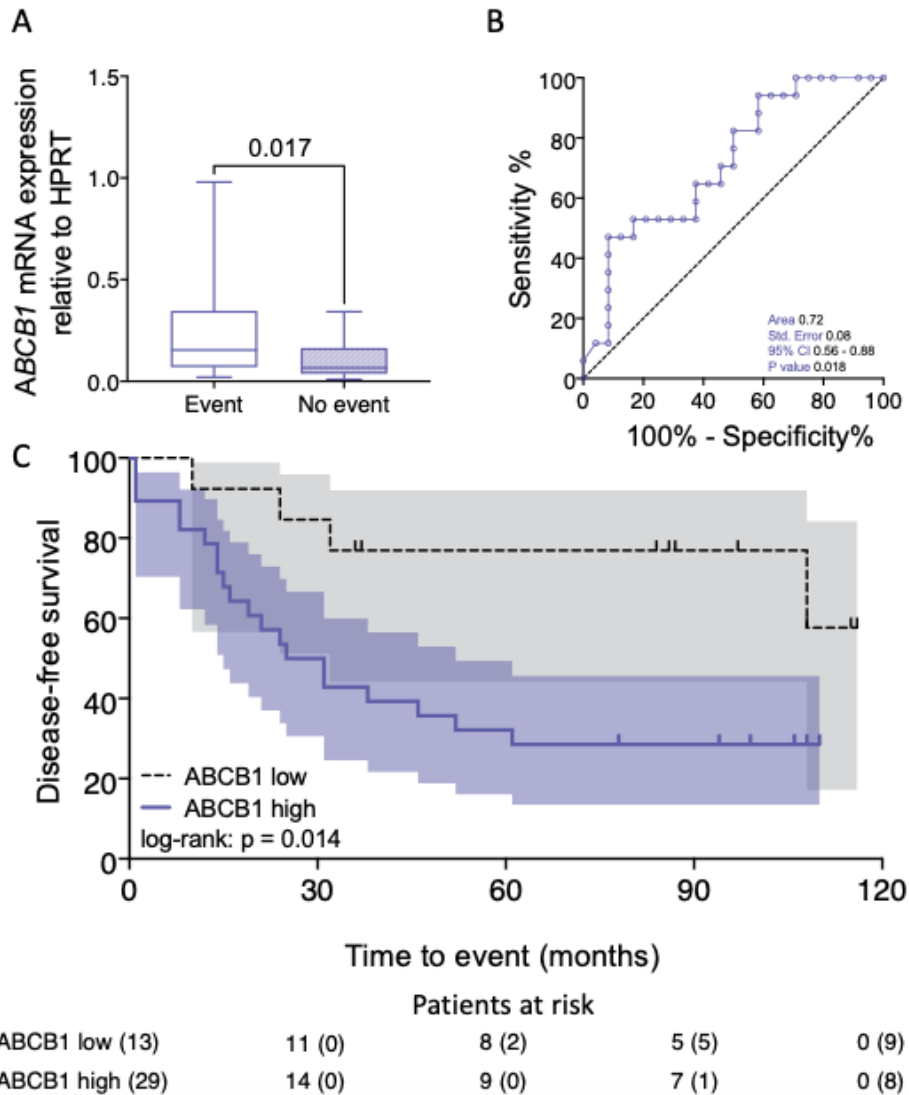
Appendix Figure A.6 Antibody optimization of CH25H. Intestine sections were stained to visualize expression of CH25H with citrate buffer retrieval. Breast tumour (BT5) was then stained with different antibody concentrations (1:100, 1:200 and 1:300) with citrate buffer. Row C and D show BT5 repeat stain with no antigen retrieval alongside a further two breast tumours (BT7 and BT10) at different antibody concentrations (1:100 and 1:200) with a casein block. Scale bar represents 100µm.



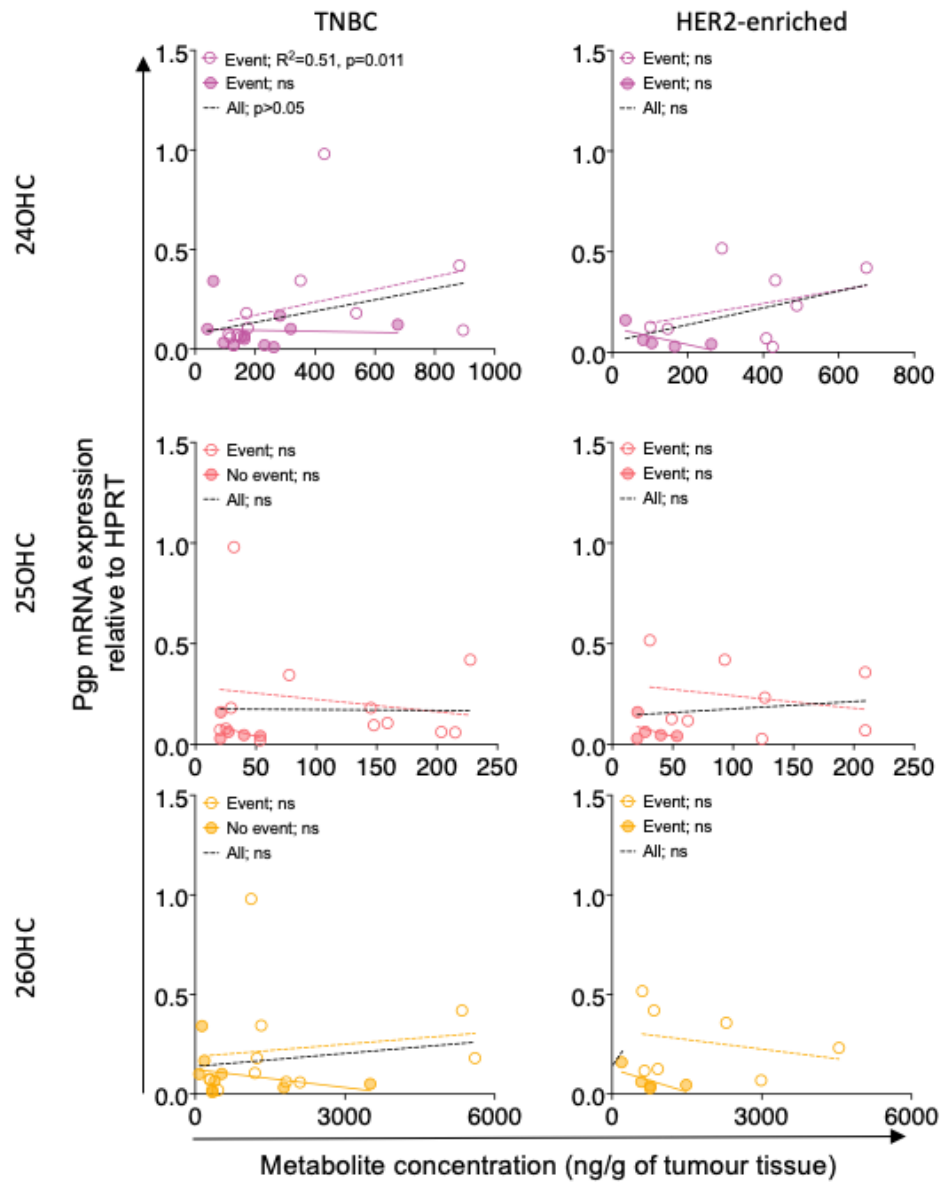
Appendix Figure A.7 Antibody optimization of CYP27A1. Liver sections were stained to visualize expression of CYP27A1 with either citrate buffer retrieval or no retrieval tested. Breast tumour (BT1) was then stained with different antibody concentrations (1:100, 1:200 and 1:400) with citrate buffer retrieval. A further three breast tumours (BT2-4) were then stained with different antibody concentrations (1:100 and 1:200) with a casein block. Row A represents the liver, Row B shows BT1 and C-D shows tumours BT2-4 from left to right with greater antibody concentrations shown descending. Scale bar represents 100 μ m.



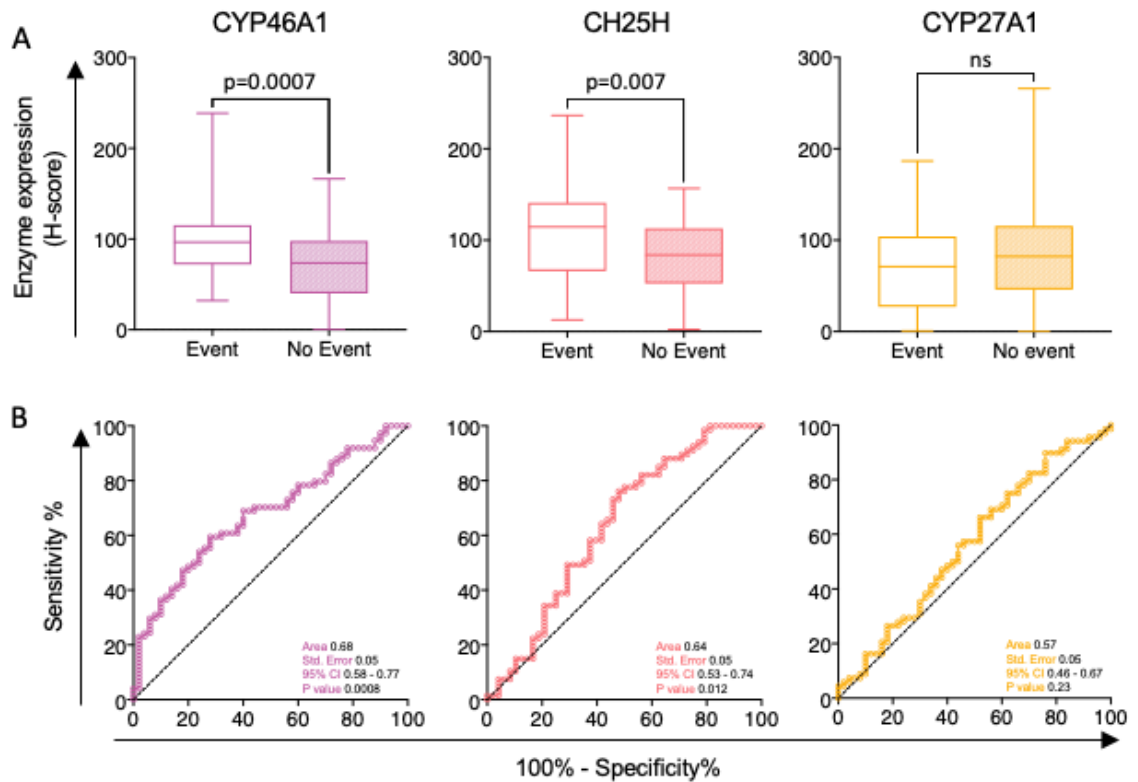
Appendix Figure A.8 Increased expression of Pgp in triple negative tumours associates with early event. RNA was isolated from 41 ER-negative tumours (28 TNBC and 13 HER2+). Gene expression of *ABCB1* was quantified with qPCR. (A) Representative images of breast tumour stains containing cancer cells that are considered either; not stained, weakly stained, moderately stained, or strongly stained. Scale bars represent 25 μ m. (B) Expression of Pgp assessed between Event and No Event patients. Mann-Whitney test performed to assess significance. (C) ROC curve used to determine cut offs used in Kaplan-Meier analysis. (D) Kaplan-Meier analysis of Pgp low (H-score <110.3)/ Pgp high (H-score >110.3). Log-rank test was performed to test for significance. Shaded areas represent 95% CI and patients at risk of suffering an event are shown beneath each Kaplan-Meier curve.



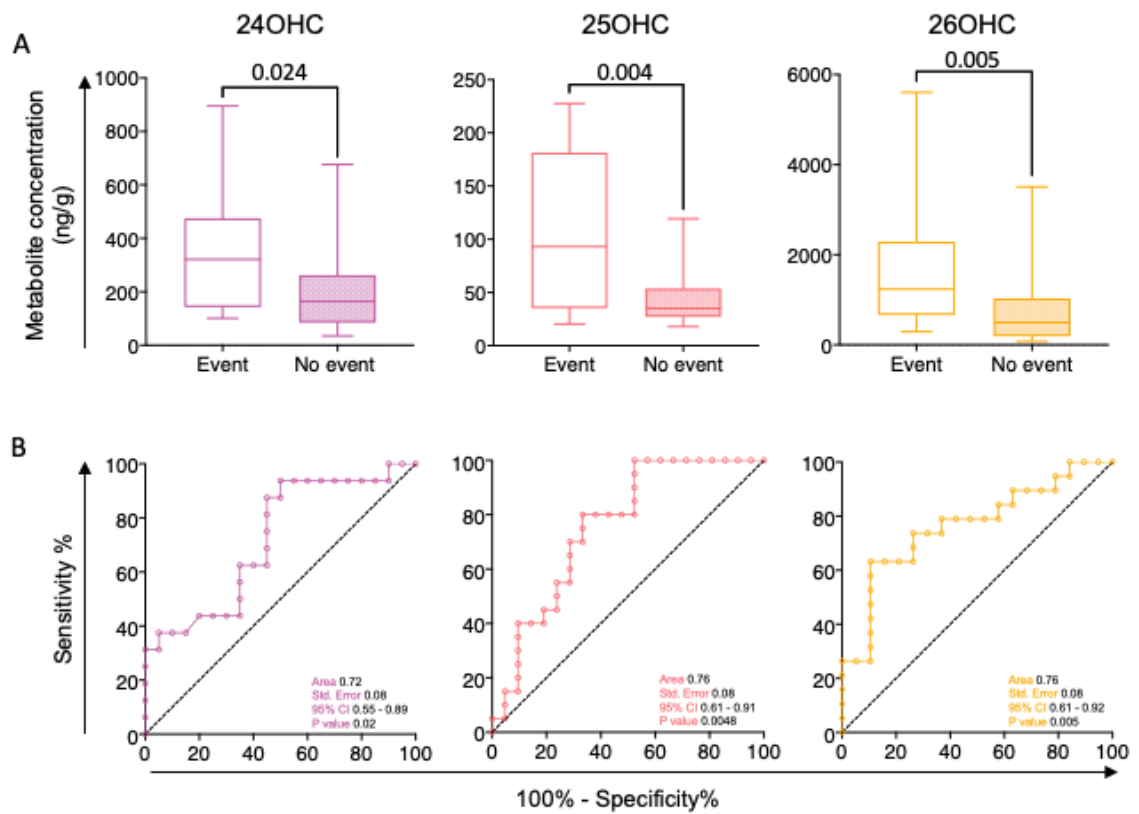
Appendix Figure A.9 *ABCB1* expression in ER-negative tumours associates with reduced disease-free survival. RNA was isolated from 41 ER-negative tumours (28 TNBC and 13 HER2+). Gene expression of *ABCB1* was quantified with qPCR. (A) Expression of *ABCB1* assessed between patients that suffered an event and patients that did not. Mann-Whitney test performed to assess significance. (B) ROC curve used to determine cut offs used in Kaplan-Meier analysis. (C) Kaplan-Meier analysis of *ABCB1* low ($\Delta\Delta CT < 0.067$)/*ABCB1* high ($\Delta\Delta CT > 0.067$). Log-rank test was performed to test for significance. Shaded areas represent 95% CI and patients at risk of suffering an event are shown beneath each Kaplan-Meier curve. RNA isolation and mRNA quantification performed by Samantha A. Hutchinson.



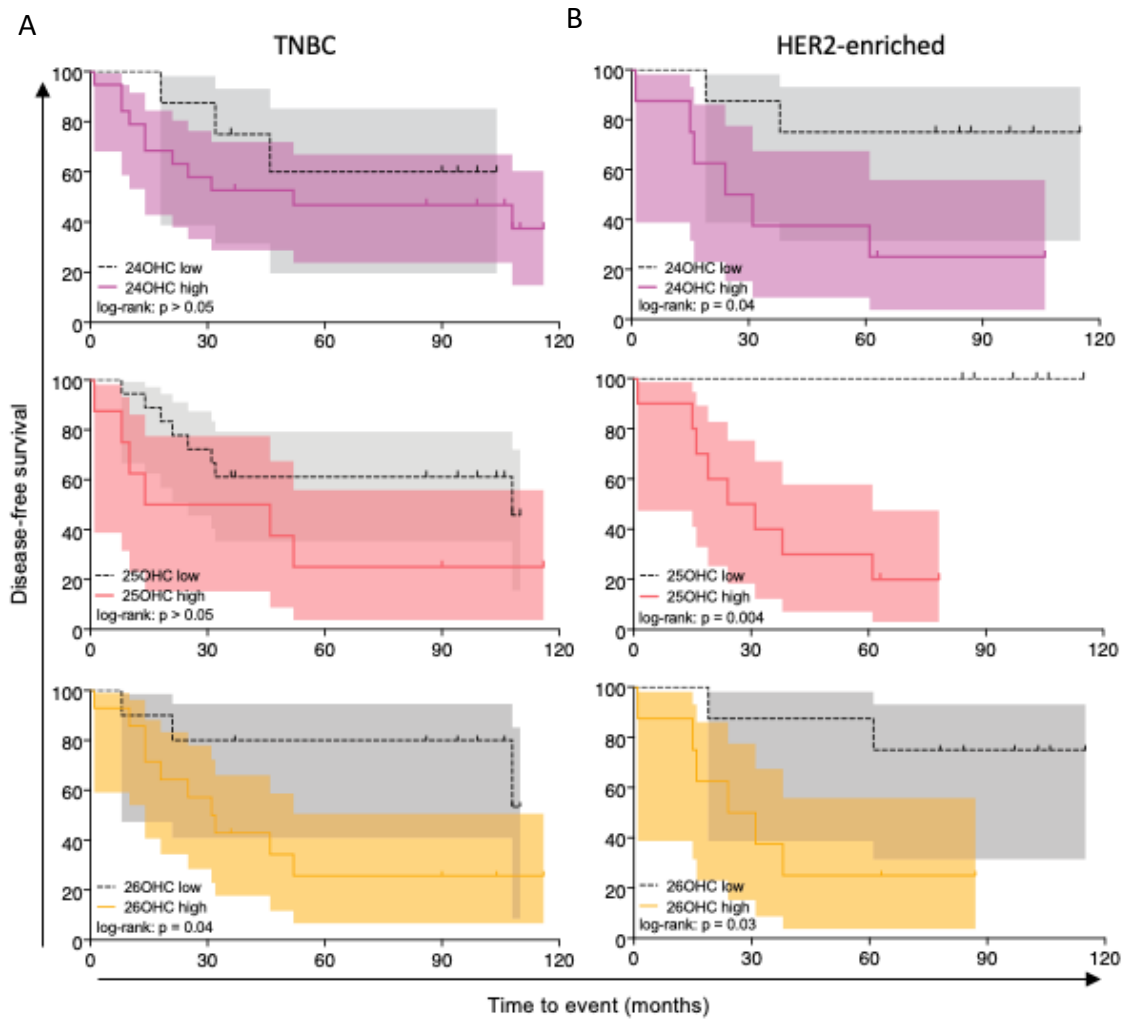
Appendix Figure A.10 TNBC and HER2+ oxysterol content correlations with *ABCB1* mRNA. Correlation analysis between tumour concentration of 24OHC, 25OHC and 26OHC and *ABCB1* mRNA expression relative to HPRT. Cohort split between patients that have or have not suffered an event in TNBC and HER2+ tumours. Lines indicate linear regression, correlations calculated using Spearman's rank.



Appendix Figure A.11 Determination of Kaplan-Meier curve cut offs for immunohistochemical quantification. (A) variance of CYP46A1, CH25H and CYP27A1 between Event and No Event patients, n=118. Welch's t-test was performed to test for significance. (B) ROC curve used to determine cut offs for Kaplan-Meier analysis.

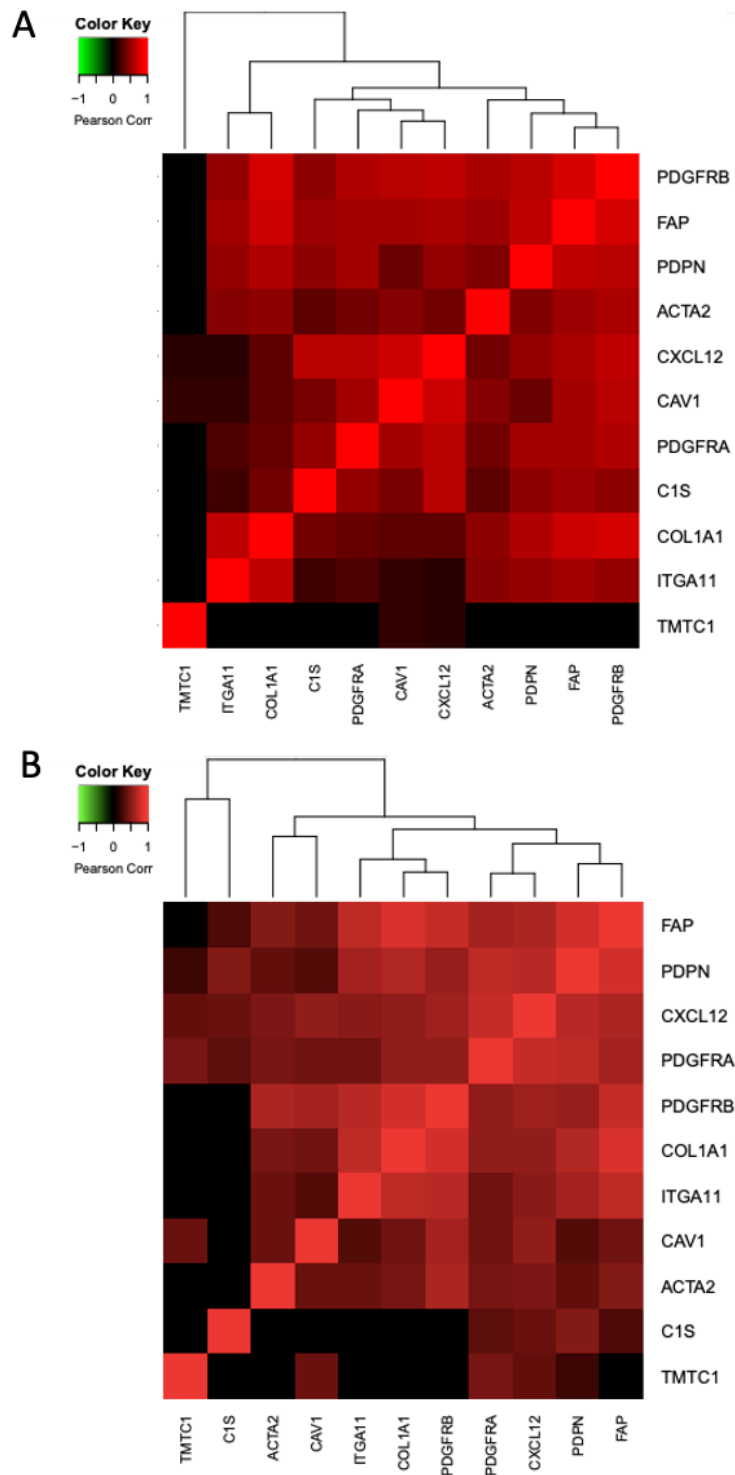


Appendix Figure A.12 Determination of Kaplan-Meier curve cut offs for LC-MS quantification. (A) variance of both CYP27A1 and CYP46A1 between patients that suffered an event and patients that did not, n=43. Mann-Whitney test was performed to test for significance. (B) ROC curves used to determine cut offs for Kaplan-Meier analysis.



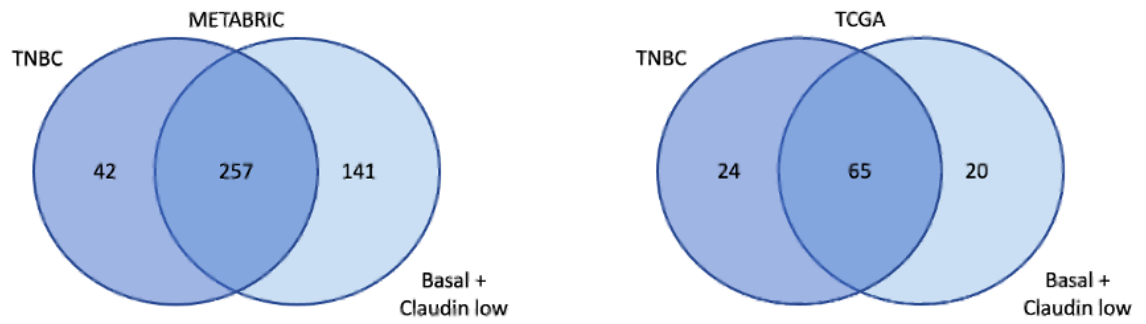
Appendix Figure A.13 TNBC and HER2+ patient survival in incidence of high and low oxysterols. Kaplan-Meier analysis of 24OHC (TNBC: low ng/g = <103.5, high ng/g = >103.5; HER2+: low ng/g = <276.3, high ng/g = >121.6), 25OHC (TNBC: low ng/g = <121.6, high ng/g = >121.6, HER2+: low ng/g = <44.6, high ng/g = >44.6) and 26OHC (TNBC: low ng/g = <625.4, high ng/g = >625.4; HER2+: low ng/g = <803.4, high ng/g = >803.4) for (A) TNBC and (B) HER2+ patients. Log-rank test was performed to assess significance. Patients at risk of suffering an event are shown for 30-month intervals beneath each Kaplan-Meier curve. Shaded areas represent 95% C

Appendix B Supplementary Data for Chapter 4

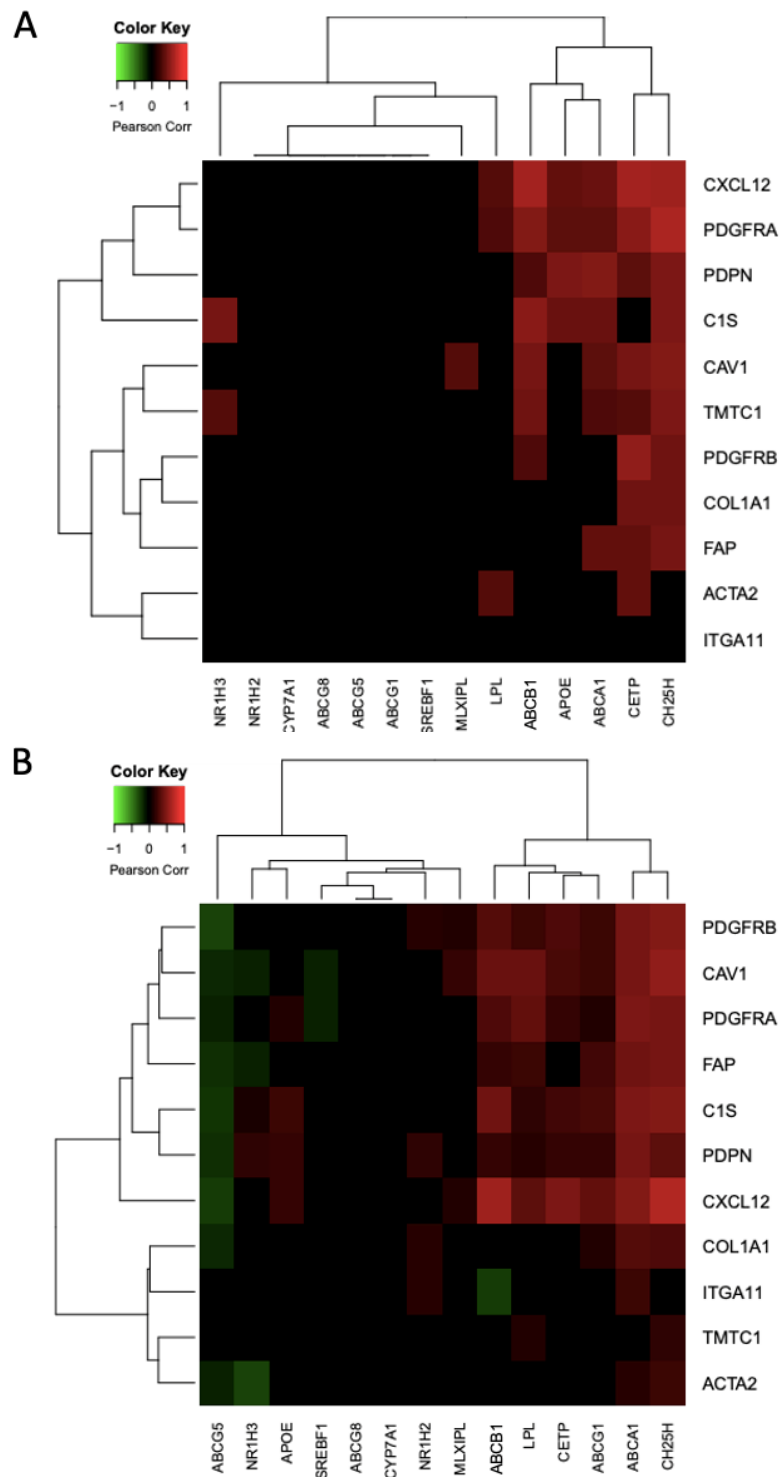


Appendix Figure B.1 Correlation expression patterns of TNBC cancer-specific cancer associated fibroblast marker in BLCL tumours. Correlations between TNBC-CAF markers. Dendrograms represent subgrouping of genes within the heatmap. (A) Validation cohort of mRNA-Seq data from 123 tumours from TCGA. (B) Experimental cohort of mRNA-Seq

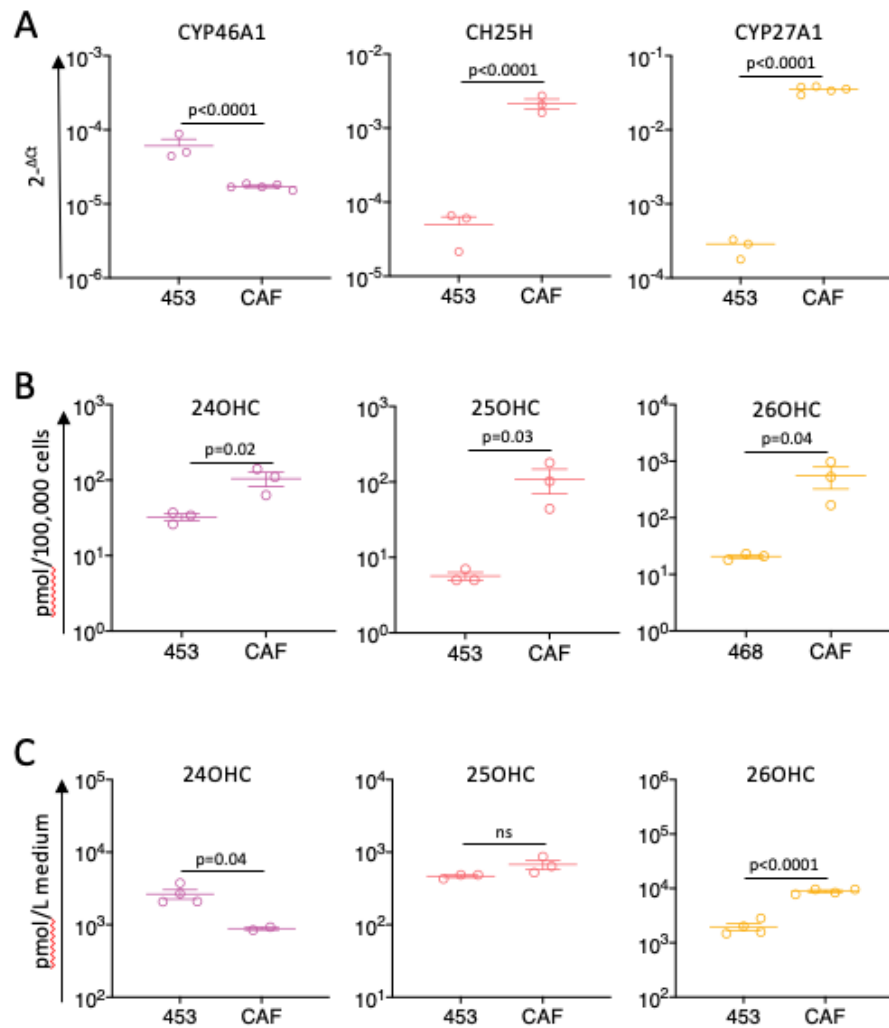
data from 299 tumours from METABRIC. Analysis performed and heat-maps generated by Olivia Bunton, Elton Vasconcelos and LeedsOmics.



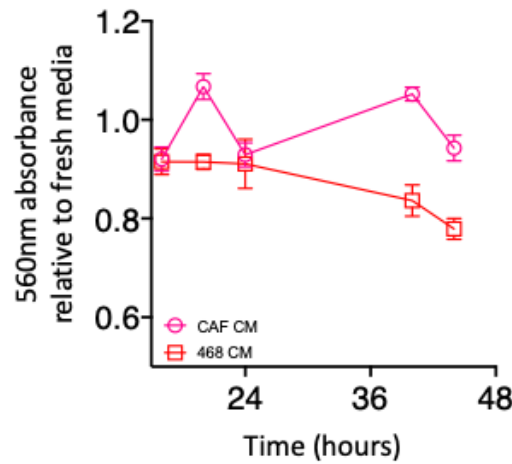
Appendix Figure B.2 Overlap of patients between TNBC and BLCL subgroups.



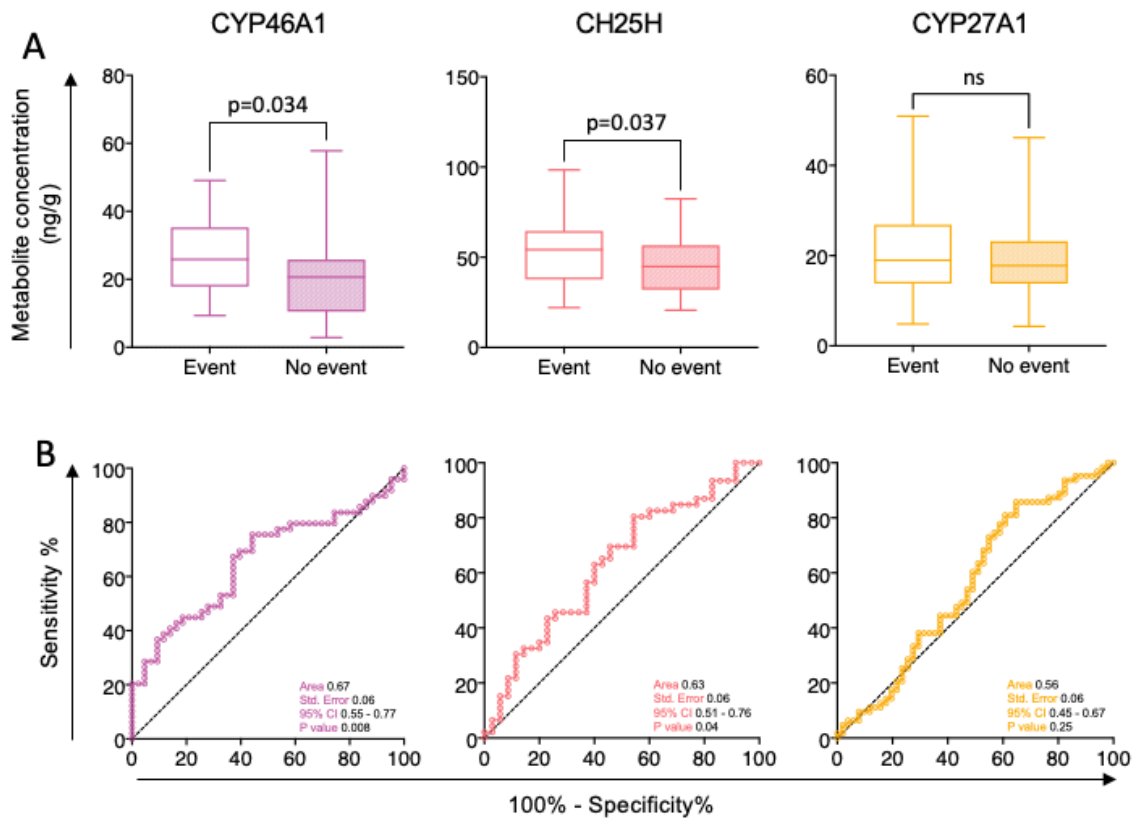
Appendix Figure B.3 TNBC-associated fibroblast marker genes correlate with canonical LXR marker genes in BLCL tumours. Correlations between TNBC-CAF markers, LXR target genes and control genes. Dendrograms represent subgrouping of genes within the heatmap. (A) Validation cohort of mRNA-Seq data from 123 tumours from TCGA. (B) Experimental cohort of mRNA-Seq data from 299 tumours from METABRIC. Analysis performed and heat-maps generated by Olivia Bunton, Elton Vasconcelos and LeedsOmics.



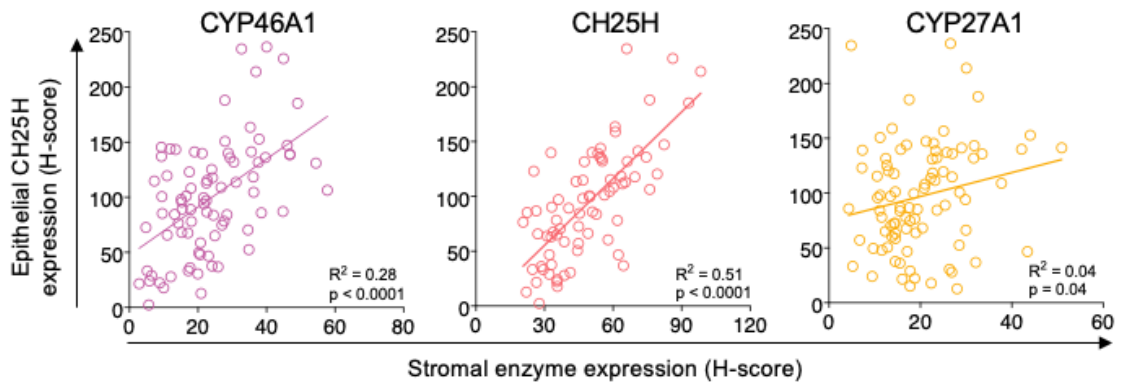
Appendix Figure B.4 Comparison of oxysterol production in CAF and MDA-MB-453 cells. MDA-MB-453 and CAF cells were cultured individually and assessed for expression of CYP46A1, CH25H and CYP27A1 and compared using $\Delta\Delta C_t$ method normalised to HPRT expression. Data presented are the mean and SEM from three to five biological replicates of two technical replicates. P-values generated using two-tailed t-tests. (B) Intracellular concentrations of oxysterols within CAF and MDA-MB-453 cells measured using LC-MS/MS. P-values generated using one-tailed t-tests. (C) Oxysterol concentrations in media conditioned by CAFs and MDA-MB-453s measured using LC-MS/MS. P-values generated using two-tailed t-tests.



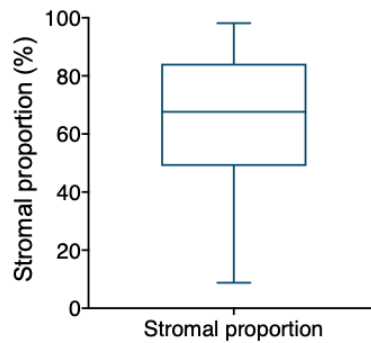
Appendix Figure B.5 Change in absorbance at 560 nm for CAF and MDA-MB-468 conditioned media over time.



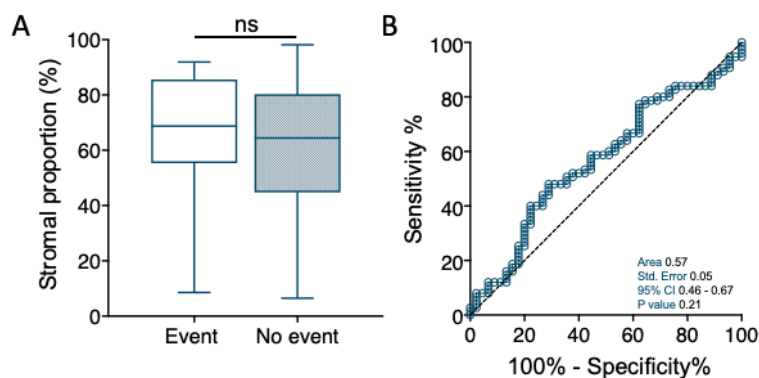
Appendix Figure B.6 Determination of Kaplan-Meier curve cut offs for stromal immunohistochemical quantification. (A) Expression of CYP46A1, CH25H and CYP27A1 in patients that suffered an event and patients that did not. Mann-Whitney test performed to assess significance. (B) ROC curve used to determine cut offs used in Kaplan-Meier analysis



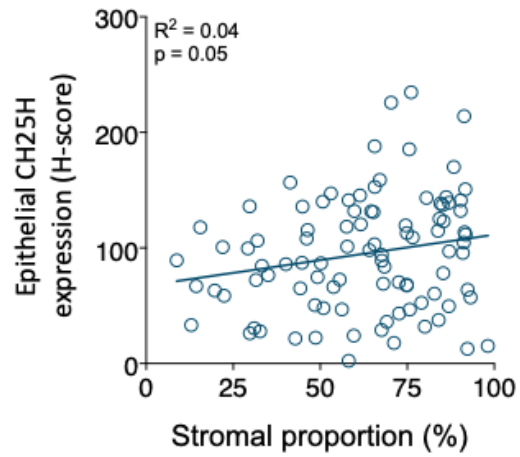
Appendix Figure B.7 Expression of oxysterol producing enzymes, CYP46A1, CH25H and CYP27A1 in the stroma correlate with epithelial CH25H expression in TNBC. Correlation between the stromal expression of CYP27A1, CH25H and CYP46A1 and the expression of canonical LXR target gene, CH25H, in epithelial cells. Pearson's rank was performed to assess correlations.



Appendix Figure B.8 Range of stromal proportions in TNBC tumours. Stromal proportions assessed between in TNBC patients presented as a percentage of total tumour.



Appendix Figure B.9 Determination of Kaplan-Meier curve cut offs for stromal proportions. (A) Stromal proportions assessed between patients that suffered an event and patients that did not. Mann-Whitney test performed to assess significance. (B) ROC curve used to determine cut offs used in Kaplan-Meier analysis.



Appendix Figure B.10 Stromal proportion correlates with epithelial CH25H expression in TNBC. Correlation between the stromal proportion and the expression of canonical LXR target gene, CH25H, in epithelial cells. Pearson's rank was performed to assess correlation.

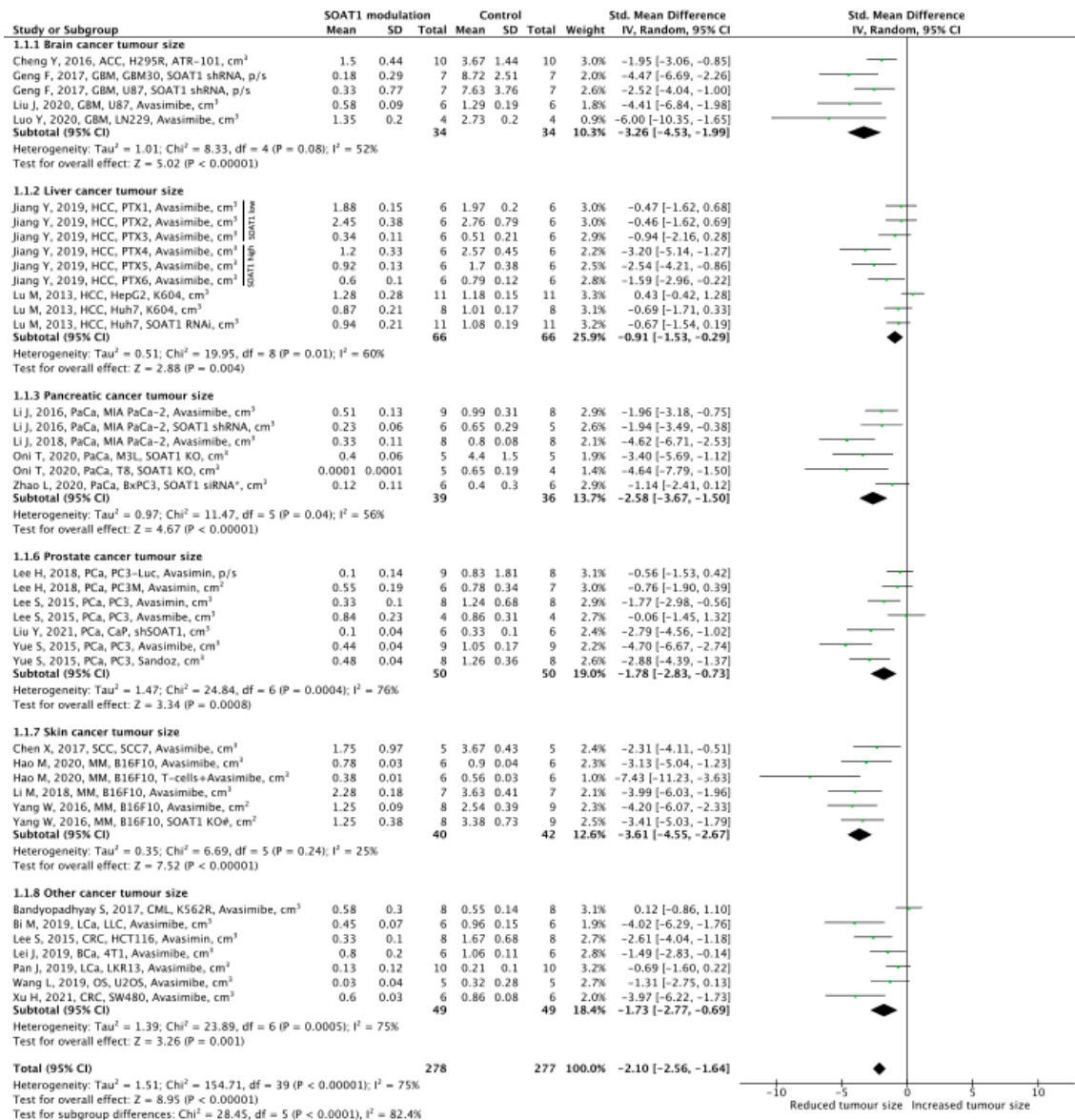
Appendix C Supplementary Data for Chapter 5

Appendix Table C.1 Summary of extracted data from cholesteryl ester measurement studies. *Italic entries were not included in meta-analysis to avoid double counting of controls.* Abbreviations: DEN = Diethylnitrosamine, T organoids = Xenografted tumour cells from KrasLSL-G12D/+; Trp53LSL-R172H/+; Pdx1-Cre mouse tumour. NR = not recorded.

| Article | Cancer | Model; Mouse strain; Sample size | Units: | Sample type | Units | Cholesteryl Ester Concentration | | | | | |
|-------------------------|------------|---|---------------|---|-----------------------------|---------------------------------|-----------------|--------------------------|------------|------------------------------|-----------|
| | | | | | | Tumour mouse | | Control (tumour bearing) | | Control (non-tumour bearing) | |
| | | | | | | N | Mean ± SD | N | Mean ± SD | N | Mean ± SD |
| (Barnard et al., 1986) | Liver | Xenograft: HTC 7288C; Buffalo and Sprague Dawley rat; 3-7/group | 10 weeks | Intramuscular hepatoma, matched and non-matched liver | µg/mg protein | 7 | 6.6 ± 4.9 (ns) | 7 | 2.9 ± 1.6 | 4 | 2.0 ± 1.6 |
| | | | | Subcutaneous hepatoma, matched and non-matched liver | | 3 | 2.2 ± 1.7 (ns) | | | | |
| (Brown et al., 1975) | Leukaemia | Radiation: Gamma ray; C57BL/6J mice; 2-6/group | 3 days | Irradiated thymus and non-matched thymus | mg/100g tissue (wet weight) | 2 | 1.7 ± 0.5 (ns) | | | 6 | 0.8 ± 0.6 |
| | | | 5 months | Irradiated thymus and non-matched thymus | | 3 | 1.0 ± 0.3 (ns) | | | 2 | 0.4 ± 0.1 |
| (Erickson et al., 1988) | Liver | Xenograft: Morris Hepatoma 9108; ACI rat; 6-7/group | µg/mg protein | Tumour and matched liver | 3-5 weeks | 6 | 10.4 ± 8.1 | 7 | 2.1 ± 1.6 | | |
| (Harry et al., 1971) | Liver | Xenograft: Morris Hepatoma 7787; Buffalo rat; 1/group | 7 days | Tumour and matched liver | µmol/g tissue (wet weight) | 1 | 3.8 (ns) | 1 | 0.8 | | |
| | | | 14 days | | | 1 | 5.7 (ns) | 1 | 1.5 | | |
| | | | 21 days | | | 1 | 4.2 (ns) | 1 | 0.8 | | |
| | | | 7 days | | | 1 | 1.1 (ns) | 1 | 3.4 | | |
| | | | 14 days | | | 1 | 2.1 (ns) | 1 | 3.4 | | |
| | | | 21 das | | | 1 | 2.7 (ns) | 1 | 0.8 | | |
| | | | 3 days | | | 1 | 2.4 (ns) | 1 | 0.7 | | |
| | | | 7 days | | | 1 | 4.0 (ns) | 1 | 0.8 | | |
| | | | 14 days | | | 1 | 9.3 (ns) | 1 | 1.4 | | |
| | | | 21 days | | | 1 | 9.4 (ns) | 1 | 2.0 | | |
| (Konishi et al., 1991) | Testicular | Xenograft: Leydig Cell; Fischer 344/ DuCrj rat; 5/group | 18 months | Tumour and matched testis | mg/g tissue (wet weight) | 5 | 32.8 ± 1.1 (ns) | 5 | 3.7 ± 0.4 | | |
| | | | 21 months | | | 4 | 27.1 ± 1.2 (ns) | 4 | 17.5 ± 1.0 | | |
| | | | 23 months | | | 5 | 68.1 ± 6.0 (ns) | 5 | 60.9 ± 5.6 | | |

| | | | | | | | | | | | |
|------------------------------------|------------|--|-----------|--|--|----|---|----|----------------|---------------|---------------|
| (Olsson et al., 1991) | Liver | Mutagen: 2-acetylaminofluorene; Wistar rat; 8/group | 29 weeks | Microsomal subfraction of liver nodule and non-matched liver | $\mu\text{g}/\text{mg}$ protein | 8 | 2.0 ± 0.6 | | 8 | 1.4 ± 0.4 | |
| | | | 29 weeks | Mitochondrial subfraction of liver nodule and non-matched liver | | 8 | 0.5 ± 0.2 (ns) | | 8 | 0.3 ± 0.1 | |
| | | | 29 weeks | lysosomal subfraction of liver nodule and non-matched liver | | 8 | 7.4 ± 2.2 | | 8 | 3.3 ± 0.8 | |
| (Oni, Tobiloba E et al., 2020) | Pancreatic | Xenograft: T organoids*; C57BL/6J mice; 4/group | NR | Tumour and non-matched pancreas | $\mu\text{g}/\text{mg}$ protein | 4 | 0.7 ± 0.7 (ns) | | 4 | 0.6 ± 0.2 | |
| (van Heushen et al., 1983) | Liver | Xenograft: Morris Hepatoma 7777; Buffalo rat; 2-3/group | NR | Microsomal fraction of tumour, matched liver & non-matched liver | $\mu\text{g}/\text{mg}$ protein | 3 | 3.5 ± 2.3 (ns) | 2 | 0.6 ± 0.4 | 4 | 2.1 ± 1.2 |
| | | Xenograft: Morris Hepatoma 5123D; Buffalo rat; 2-3/group | NR | | | 3 | 3.6 ± 1.8 (ns) | 2 | 3.5 ± 1.0 | | |
| | | Xenograft: Morris Hepatoma 7787; Buffalo rat; 3-4/group | NR | | | 4 | 1.2 ± 1.7 (ns) | 3 | 0.9 ± 0.4 | | |
| (Ruggieri, S and Fallani, 1979) | Liver | Xenograft: Yoshida ascites hepatoma AH 130; Wistar rats; 10-11/group | 7-10 days | Tumour, matched liver and non-matched liver | mg/g tissue (dry weight) | 10 | 2.1 ± 1.3 (ns) | 11 | 1.3 ± 0.7 | 5 | 1.0 ± 0.5 |
| (Ruggieri, Salvatore et al., 1976) | Liver | Xenograft: Yoshida ascites hepatoma AH 130; Wistar rats; 4-5/group | 5 weeks | Tumour, matched liver and non-matched liver | mg/g tissue (dry weight) | 4 | 2.7 ± 0.4 (ns against tumour bearing) | 5 | 1.3 ± 0.2 | 4 | 2.5 ± 0.9 |
| (Talley et al., 1983) | Kidney | Mutagen: oestrogen; Golden Syrian hamsters; 6/group | NR | Tumour, matched and non-matched kidney | $\mu\text{g}/\text{g}$ tissue (wet weight) | 6 | 10.4 ± 4.9 | 6 | 1.7 ± 1.7 | 6 | 0.1 ± 0.1 |
| | | Xenograft: primary, oestrogen induced tumour; Golden Syrian hamsters; 6/group | NR | | | 6 | 3.4 ± 0.9 | 6 | 0.4 ± 0.2 | | |
| | | Xenograft: secondary, oestrogen induced tumour; Golden Syrian hamsters; 6/group | NR | | | 6 | 0.9 ± 0.2 | 6 | 0.3 ± 0.2 | | |
| | | Xenograft: primary, diethylstilbestrol-induced tumour; Golden Syrian hamsters; 6/group | NR | | | 6 | 0.9 ± 0.4 | 6 | 0.4 ± 0.40 | | |
| (Thirunavukkarasu et al., 2003) | Liver | Mutagen: DEN; Wistar albino rats; 6/group | 14 weeks | Tumour, matched and non-matched liver | mg/g tissue (wet weight) | 6 | 1.3 ± 0.1 (ns against tumour bearing) | 6 | 1.2 ± 0.1 | 6 | 1.6 ± 0.1 |
| (Wood et al., 1978) | Liver | Xenograft: Hepatoma 7288CTC; Buffalo rat; 3/group | 4 weeks | Tumour, matched and non-matched liver | mg/g tissue (wet weight) | 3 | 2.9 ± 0.3 | 3 | 0.3 ± 0.1 | 3 | 0.7 ± 0.2 |

(ns against
non-tumour
bearing)



Appendix Figure C.1 Change in tumour size following disruption of SOAT in overall cancer. Standardised mean difference in skin cancer size. # denotes modifications localized to T-cells. * denotes modifications localized to CAR T-cells.

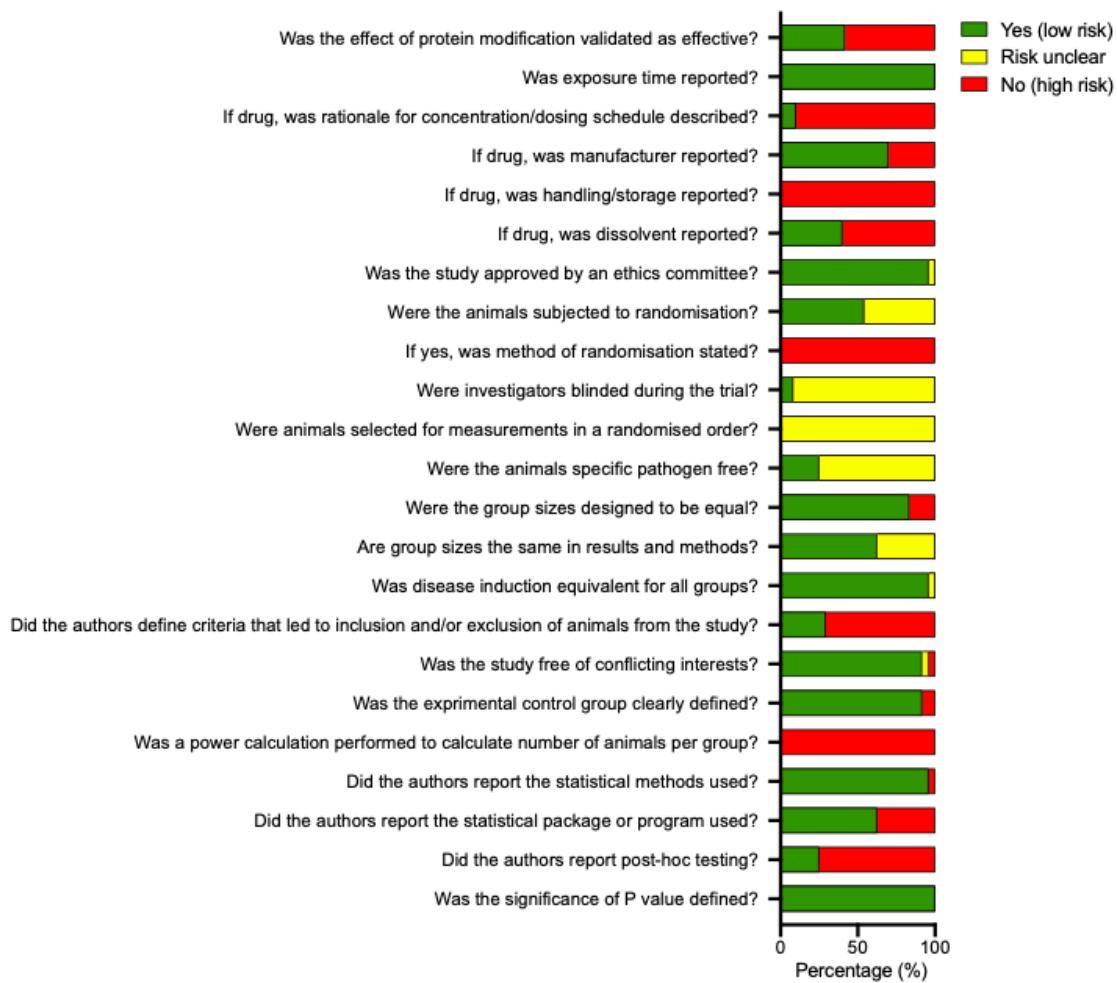
Appendix Table C.2 Summary of extracted data from SOAT1/2 inhibition studies. *Italic entries were not included in meta-analysis.* Abbreviations: CAR-T = chimeric antigen receptor T, con. = control, CTL = cytotoxic T lymphocyte, exp. = experimental, GzmB = granzyme b, IFN γ = interferon gamma, IG = intragastric administration, IP = intraperitoneally, IV = intravenously, IT = intratumourally, NR = not recorded, ns = not significant, TNF α = tumour necrosis factor

| Article | Cancer | Model: Mouse strain: Sample size: | Treatment | Tumour metric measurement: Raw values (con. - exp.): | Additional outcomes |
|------------------------------|-----------|--|--|---|--|
| (Bandyopadhyay et al., 2017) | Leukaemia | Xenograft: K562R; Athymic nude mice; 8/group | Avasimibe, 7.5 mg/kg, IP, daily, 11 days | Volume (mm ³): 547.63 - 575.61 (ns) | NR |
| (Bi et al., 2019) | Lung | Allograft: LLC; C57BL/6; 6/group | Avasimibe, 15 mg/kg, IP, every two days, 35 days | Volume (mm ³): 963.09 - 445.06 | NR |
| (Chen, X. et al., 2017) | Skin | Allograft: SCC7; C3H mice; 5/group | Avasimibe 15 mg/kg, IP, every 2 days, 33 days | Volume (mm ³): 3076.41 - 1745.53 | Immune response: CTL cytotoxicity (%): 6.71 - 12.05, Survival: Hazard ratio (Mantel-Haenszel reciprocal): 0.05 |
| (Cheng, Y. et al., 2016) | Brain | Xenograft: H295R; CB17-SCID mice; 8/group | ATR-101 0.7 mg/kg, PO, daily, 33 days | Volume (mm ³): 3670.04 - 1496.43, Weight (g): 2.64 - 1.43 | Apoptosis: TUNEL+ (% positive cells): 2.3 - 11.03, Proliferation: Ki67 (% positive cells): 26.92 - 24.77 (ns), Brdu (% positive cells): 18.42 - 15.75 (ns) |
| (Geng et al., 2016) | Brain | Xenograft: GBM30; Athymic nude mice; 7/group | SOAT1 shRNA cells, 15 days | Luminescence (p/sec/cm ² /sr): 8.72 - 0.18 | Survival: Hazard ratio (Mantel-Haenszel reciprocal): 0.05 |
| | | Xenograft: U87; Athymic nude mice; 7/group | SOAT1 shRNA cells, 15 days | Luminescence (p/sec/cm ² /sr): 7.63 - 0.33 | Survival: Hazard ratio (Mantel-Haenszel reciprocal): 0.06 |
| (Hao et al., 2020) | Skin | Allograft: B16F10; | Avasimibe 2 mg/kg, IV, 20 days, day 8 and 14 | Volume (mm ³): 895.31 - 783.39 | Proliferation: Ki67 (% positive cells), Survival: Hazard ratio (Mantel-Haenszel reciprocal): 0.41 |
| | | Allograft: B16F10; | T-cells and Avasimibe 2mg/kg, IV, 20 days, day 18 and 14 | Volume (mm ³): 555.96-379.06 | Proliferation: Ki67 (% positive cells), Survival: Hazard ratio (Mantel-Haenszel reciprocal): 1.18 |
| | | Metastasis: B16F10-luc: | Avasimibe 2 mg/kg, 30 days, IV, day 8 and 14 | NR | Metastasis: Tumour area as a percentage of total lung area: 37.6 - 35.27, Survival: Hazard ratio (Mantel-Haenszel reciprocal): 0.98 |
| | | Metastasis: B16F10-luc: | T-cells and Avasimibe 2mg/kg, IV, 30 days, day 8 and 14 | NR | Metastasis: Tumour area as a percentage of total lung area: 11.24 - 15.12, Survival: Hazard ratio (Mantel-Haenszel reciprocal): 0.57 |
| | Brain | Xenograft: LN229; | Avasimibe 2 mg/kg, 30 days, IV, day 8 and 14 | NR | Survival: Hazard ratio (Mantel-Haenszel reciprocal): 0.47 |
| (Jiang, Y. et al., 2019) | Liver | Xenograft: Patient derived hepatocellular carcinoma (SOAT1 ^{low}); NOD/SCID; 6/group (1) | Avasimibe 15 mg/kg, IP, daily, 28 days | Volume (mm ³): 1969.59 - 1878.38 (ns) | NR |

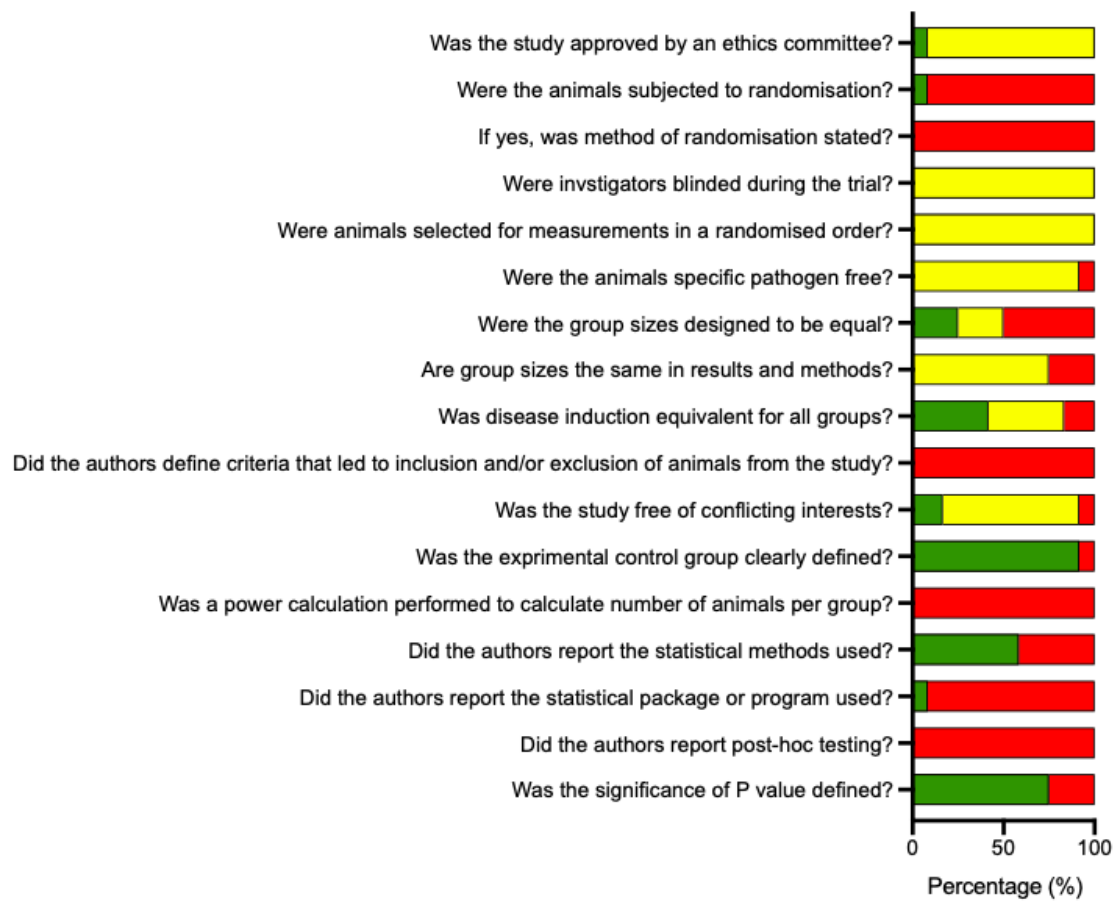
| | | | | | |
|-----------------------------|----------|--|---|--|--|
| | | Xenograft: Patient derived hepatocellular carcinoma (SOAT1 ^{low}); NOD/SCID; 6/group (2) | Avasimibe 15 mg/kg, IP, daily, 28 days | Volume (mm ³): 2755.1 - 2448.98 (ns) | NR |
| | | Xenograft: Patient derived hepatocellular carcinoma (SOAT1 ^{low}); NOD/SCID; 6/group (3) | Avasimibe 15 mg/kg, IP, daily, 28 days | Volume (mm ³): 507.07 - 333.33 (ns) | NR |
| | | Xenograft: Patient derived hepatocellular carcinoma (SOAT1 ^{high}); NOD/SCID; 6/group (4) | Avasimibe 15 mg/kg, IP, daily, 28 days | Volume (mm ³): 2572.82 - 1203.89 | NR |
| | | Xenograft: Patient derived hepatocellular carcinoma (SOAT1 ^{high}); NOD/SCID mice; 6/group (5) | Avasimibe 15 mg/kg, IP, daily, 28 days | Volume (mm ³): 1696.43 - 916.67 | NR |
| | | Xenograft: Patient derived hepatocellular carcinoma (SOAT1 ^{high}); NOD/SCID mice; 6/group (6) | Avasimibe 15 mg/kg, IP, daily, 28 days | Volume (mm ³): 791.22 - 602.51 | NR |
| (Lee, H.J. et al., 2018) | Prostate | Xenograft: PC3M; NSG mice; 6/group | Avasimin 75 mg/kg, IP, daily, 25 days | Diameter (cm ²): 0.78 - 0.55 | Apoptosis: TUNEL+ (% positive cells): 4.59 - 9.9, Metastasis: Lung metastasis (average metastases per lung section): 5.41 - 2.1, Proliferation: Ki67 (% positive cells): 70.55 - 20.88 |
| | | Xenograft: PC3-Luciferase; NSG mice; 8-9/group | Avasimin 75 mg/kg, IP, daily, 35 days | Luminescence (p/sec/cm ² /sr): 0.83 - 0.1 | Metastasis: Luminescence (p/sec/cm ² /sr): 1.45 - 0.3 |
| (Lee, S.S.-Y. et al., 2015) | Colon | Xenograft: HCT116; Athymic nude mice; 8/group | Avasimin 75 mg/kg, IV, daily for 5 days and once every 4 days subsequently, 39 days | Volume (mm ³): 1670.23 - 491.96 | Apoptosis: TUNEL+ (cells per area): 1.68 - 29.1, Survival: Hazard ratio (Mantel-Haenszel reciprocal): 0.04 |
| | Prostate | Xenograft: PC3; Athymic nude mice; 4-8/group | Avasimin 75 mg/kg, IV, daily for 5 days and once every 4 days subsequently, 39 days | Volume (mm ³): 1235.77 - 333.05 | Apoptosis: TUNEL+ (cells per area): 1.29 - 38.56, Survival: Hazard ratio (Mantel-Haenszel reciprocal): 0.04 |
| | | | Avasimibe, 15 mg/kg, PO, daily, 45 days | Volume (mm ³): 860 - 840 | NR |
| (Lei et al., 2020) | Breast | Allograft: 4T1; BALB/c nude mice; 6-13/group | Avasimibe 15 mg/kg, IG, once every 3 days, 32 days | Volume (mm ³): 1062.14 - 802.57 | Immune response: CTL in tumour (% of infiltrative t cells): 6.98 - 8.13 (ns), IFN γ in CD8 (%): 18.39 - 26.45, TNF α in CD8 (%): 27.45 - 41.58, Metastasis: Pulmonary metastasis (number of metastatic nodules): 23.62 - 14.54, Survival: Hazard ratio (Mantel-Haenszel reciprocal): 0.35 |

| | | | | | |
|---------------------------|------------|---|---|--|---|
| (Li, J. et al., 2016) | Pancreatic | Xenograft: MIA PaCa-2; NSG mice; 5-9/group | Avasimibe 15 mg/kg, IP, daily, 28 days | Volume x0.51 (mm ³): 993.65 - 510.67, Weight (mg): 792.47 - 587.55 | Metastasis: Lymph metastasis (number of metastatic lesions): 15.07 - 4.46, Liver metastasis (number of metastatic lesions): 2.12 - 0.3 |
| | | | SOAT1 shRNA cells, 35 days | Volume (mm ³): 651.05 - 226.45, Weight (mg): 644.39 - 312.92 | Metastasis: Lymph metastasis (number of metastatic lesions): 9.42 - 1.5, Liver metastasis (number of metastatic lesions): 1.76 - 0.16 |
| (Li, J. et al., 2018) | Pancreatic | Xenograft: MIA PaCa-2; Athymic nude mice; 8/group | Avasimibe 7.5 mg/kg, IP, daily, 33 days | Volume (mm ³): 799.15 - 327.43 | NR |
| (Li, M. et al., 2018) | Skin | Allograft: B16F10; C57BL/6; 3-7/group | Avasimibe 15 mg/kg, IV, 2 full doses followed by an interval of 2 days, 19 days | Volume (mm ³): 3631.76 - 2282.33 | Metastasis: Lung metastasis (g): 0.36 - 0.28, Survival: Hazard ratio (Mantel-Haenszel reciprocal): 0.22 |
| (Liu, J.Y. et al., 2021) | Brain | Xenograft: U87; BALB/c-nu nude mice; 6/group | Avasimibe 30 mg/kg, IP, daily, 32 days | Volume (mm ³): 1294.61 - 578.66, Weight (g): 0.92 - 0.51 | NR |
| | | | Avasimibe 15 mg/kg, IP, daily, 32 days | Volume (mm ³): 1294.61 - 750, Weight (g): 0.92 - 0.54 | NR |
| (Liu, Y. et al., 2021) | Prostate | Xenograft: CaP; Athymic nude mice; 6/group | shSOAT1, 29 days | Volume (mm ³): 329.37 - 95.24 | Proliferation: SCD-1: 1.21 - 0.31 |
| (Lu, Ming et al., 2013) | Liver | Xenograft: Huh7; BALB/c nude mice; 8-11/group | K-604 30ug ¹ .cm ³ tumour, IT, 4 times in 10 days | Volume (mm ³): 1014.2 - 869.32 (ns), Weight (g): 0.76 - 0.55 (ns) | NR |
| | | | Pyripyropene A 60ug ¹ .cm ³ tumour, IT, 4 times in 10 days | Volume (mm ³): 1014.2 - 605.14, Weight (g): 0.76 - 0.34 | NR |
| | | | SOAT1 RNAi cells, 23 days | Volume (mm ³): 1083.68 - 939.72 (ns), Weight (g): 1.01 - 0.89 | NR |
| | | | SOAT2 RNAi cells, 23 days | Volume (relative to start point): 10.84 - 4.83, Weight (g): 1.01 - 0.37 | NR |
| | | Xenograft: HepG2; BALB/c nude mice; 11/group | K-604 30ug ¹ .cm ³ tumour, IT, every 3-4 days, 20 days | Volume (mm ³): 1183.91 - 1275.86, (ns), Weight (g): 0.48 - 0.45 (ns) | NR |
| | | | Pyripyropene A 60ug ¹ .cm ³ tumour, IT, every 3-4 days, 20 days | Volume (mm ³): 1183.91 - 632.18, Weight (g): 0.48 - 0.21 | NR |
| (Luo, Yidan et al., 2020) | Brain | Xenograft: LN229; Nude mice; 4/group | Avasimibe 7.5 mg/kg, subcutaneously, every 2 days, 28 days | Volume (mm ³): 2732.67 - 1346.53, Weight (g): 3.12 - 1.18 | Proliferation: linc00339 (relative expression): 1 - 0.49 |

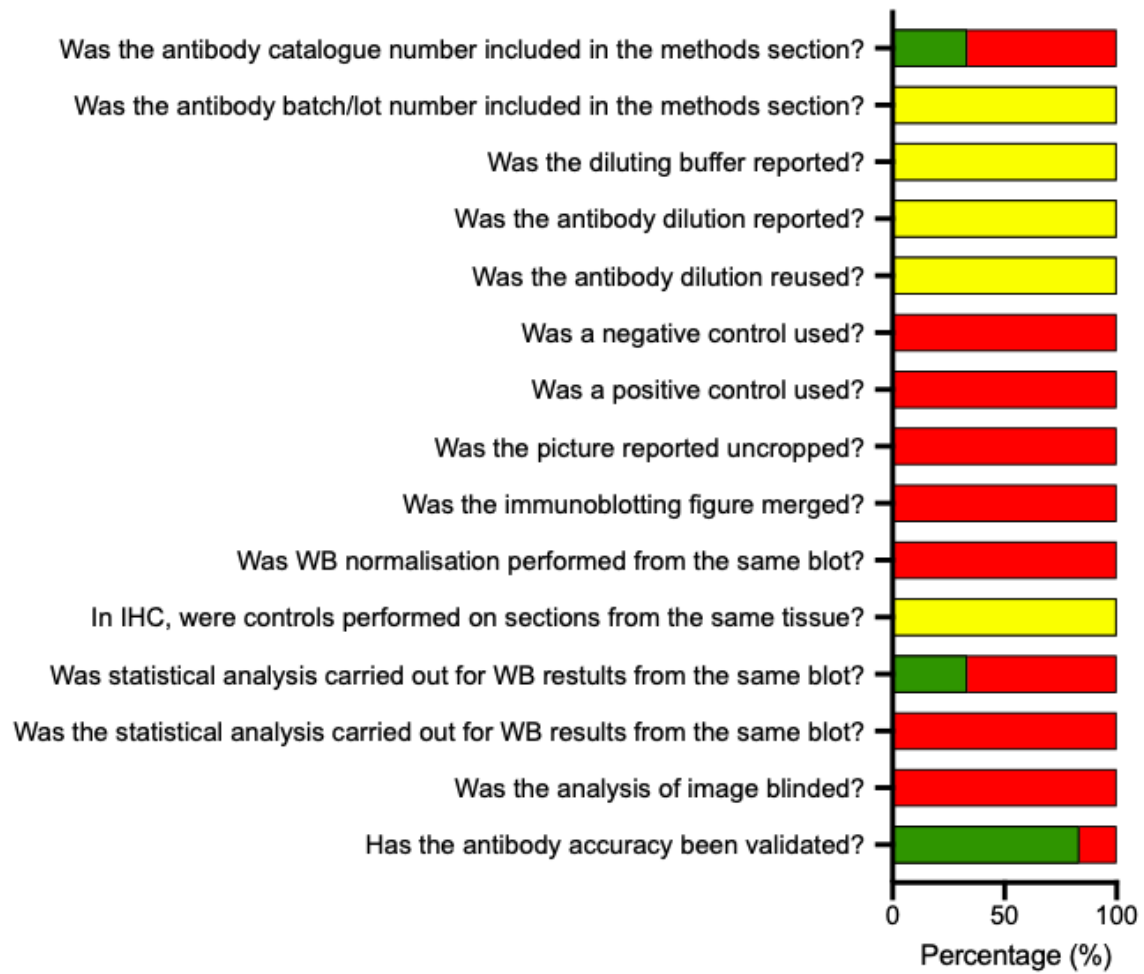
| | | | | | |
|---------------------------|------------|---|--|--|---|
| (Oni, T. E. et al., 2020) | Pancreatic | Xenograft: M3L; nu/nu mice; 5/group | CRISPR knockout, 48 days | Volume (mm ³): 4400 - 400 | Survival: Hazard ratio (Mantel-Haenszel reciprocal): 0.05 |
| | | Xenograft: T8; M3L; NOD scid gamma mice; 4-5/group | SOAT1 shRNA, 58 days | Volume (mm ³): 646.71 - 0 | NR |
| (Pan, J. et al., 2019) | Lung | Allograft: LKR13; Kras ^{LA1} -sv129 mice; 5-10/group | Avasimibe 15 mg/kg, IG, every 2 days, 28 days | Volume (mm ³): 212.71 - 129.43 | Immune response: CD3 of CD8+ (%): 19.52 - 45.33, CD4 of Tregs (%): 50.2 - 30.14, IFN γ in CD8 (%): 2.92 - 3.92, TNF α in CD8 (%): 4.56 - 9.91, GzmB in CD8 (%): 0.4 - 1.08 (ns), CD8 in tumour (%): 2.55 - 5.16, Proliferation: Ki67 (% positive cells): 15.32 - 5.17 |
| (Wang, L. et al., 2019) | Bone | Xenograft: U2OS; BALB/c nude mice; 10/group | Avasimibe 30 mg/kg, PO, daily, 21 days | Volume (mm ³): 317.24 - 33.1, Weight (g): 1.46 - 0.68 | NR |
| (Xu, H. et al., 2021) | Colon | Xenograft: SW480; BALB/c nude mice; 6/group | Avasimibe 15 mg/kg, IP, daily, 28 days | Volume (mm ³) 861.54 - 595.42, Weight (g): 0.78 - 0.47 | Proliferation: YAP: 6.38 - 8.51 |
| (Yang, W. et al., 2016) | Lung | Metastasis: LLC; C57BL/6 mice; 5-7/group | Avasimibe 15 mg/kg, IP, every 2 days, 35 days | NR | Metastasis: Lung multiplicity: 55.22 - 22.18, Survival: Hazard ratio (Mantel-Haenszel reciprocal): 0.2 |
| | | | SOAT1 genetic knockout in mouse T-cells, 20 days | NR | Metastasis: Lung multiplicity: 36.06 - 10.67, Survival: Hazard ratio (Mantel-Haenszel reciprocal): 0.23 |
| | Skin | Allograft: B16F10; C57BL/6 mice; 8-15/group | Avasimibe 15 mg/kg, IP, every 2 days, 18 days | Diameter (mm ²): 338.18 - 125.11 | Immune response: GzmB in CD8 (%): 3.43 - 8.7, IFN γ in CD8 (%): 34.01 - 44.44, TNF α in CD8 (%): 43.8 - 57.58, CD8 infiltration (x10 ⁴ cells): 3.04 - 8.1, CD8/CD4 ratio: 0.91 - 1.94, Survival: Hazard ratio (Mantel-Haenszel reciprocal): 0.12 |
| | | | SOAT1 genetic knockout in mouse T-cells, 18 days | Diameter (mm ²): 254.98 - 124.94 | Immune response: GzmB in CD8 (%): 3.45 - 8.77, IFN γ in CD8 (%): 34 - 48.43, TNF α in CD8 (%): 41.22 - 55.83, CD8 infiltration (x10 ⁴ cells): 3.71 - 13.69, CD8/CD4 ratio: x1.84, Survival: Hazard ratio (Mantel-Haenszel reciprocal): 0.22 |
| | | Metastasis: B16F10; C57BL/6 mice; 6-9/group | SOAT1 genetic out in mouse T-cells, 20 days | NR | Metastasis: Lung multiplicity: 48.89 - 10.37, Survival: Hazard ratio (Mantel-Haenszel reciprocal): 0.21 |
| (Yue et al., 2014) | Prostate | Xenograft: PC3; Athymic nude mice; 6/group | Avasimibe 15 mg/kg, IP, daily, 30 days | Volume x0.42 (mm ³): 10.49 - 4.44, Weight (g): 1.21 - 0.76 | Apoptosis: TUNEL+ (% positive cells): 2.23 - 4.92, Proliferation: Ki67 (% positive cells): 58.24 - 17.33 |
| | | | Sandoz 15 mg/kg, IP, daily, 23 days | Volume (mm ³): 12.56 - 4.81, Weight (g): 1.1 - 0.73 | NR |
| (Zhao et al., 2020) | Pancreatic | Xenograft: BxPC3; NSG mice; 10/group | SOAT1 siRNA in CAR-T cells (1847), 33 days | Volume (mm ³): 401.81 - 98.66 | NR |
| | | | SOAT1 siRNA in CAR-T cells (1848), 33 days | Volume (mm ³): 401.81 - 119.44 | NR |



Appendix Figure C.2 Risk of experimental bias. Adherence scores for animal research in studies assessing SOAT inhibition.



Appendix Figure C.3 Risk of experimental bias. Adherence scores for animal research in studies measuring cholesterol ester content in tissue.



Appendix Figure C.4 Risk of experimental bias. Adherence scores for immunoblotting in studies assessing SOAT inhibition.

References

- Abdel-Khalik, J., Crick, P.J., Yutuc, E., DeBarber, A.E., Duell, P.B., Steiner, R.D., Laina, I., Wang, Y. and Griffiths, W.J. 2018. Identification of $7\alpha,24$ -dihydroxy-3-oxocholest-4-en-26-oic and $7\alpha,25$ -dihydroxy-3-oxocholest-4-en-26-oic acids in human cerebrospinal fluid and plasma. *Biochimie*. **153**, pp.86-98.
- Abdel-Khalik, J., Crick, P.J., Yutuc, E., DeBarber, A.E., Duell, P.B., Steiner, R.D., Laina, I., Wang, Y. and Griffiths, W.J. 2018. Identification of $7\alpha, 24$ -dihydroxy-3-oxocholest-4-en-26-oic and $7\alpha, 25$ -dihydroxy-3-oxocholest-4-en-26-oic acids in human cerebrospinal fluid and plasma. *Biochimie*. **153**, pp.86-98.
- Acheampong, T., Kehm, R.D., Terry, M.B., Argov, E.L. and Tehranifar, P. 2020. Incidence Trends of Breast Cancer Molecular Subtypes by Age and Race/Ethnicity in the US From 2010 to 2016. *JAMA Network Open*. **3**(8), pp.e2013226-e2013226.
- Albertsson, P.A., Basse, P.H., Hokland, M., Goldfarb, R.H., Nagelkerke, J.F., Nannmark, U. and Kuppen, P.J.J.T.i.i. 2003. NK cells and the tumour microenvironment: implications for NK-cell function and anti-tumour activity. **24**(11), pp.603-609.
- Albini, A. and Sporn, M.B. 2007. The tumour microenvironment as a target for chemoprevention. *Nature Reviews Cancer*. **7**(2), pp.139-147.
- Ali, H., Provenzano, E., Dawson, S.-J., Blows, F., Liu, B., Shah, M., Earl, H., Poole, C., Hiller, L. and Dunn, J. 2014. Association between CD8+ T-cell infiltration and breast cancer survival in 12 439 patients. *Annals of oncology*. **25**(8), pp.1536-1543.
- Almand, B., Resser, J.R., Lindman, B., Nadaf, S., Clark, J.I., Kwon, E.D., Carbone, D.P. and Gabrilovich, D.I. 2000. Clinical significance of defective dendritic cell differentiation in cancer. *Clinical Cancer Research*. **6**(5), pp.1755-1766.
- An, S., Jang, Y.-S., Park, J.-S., Kwon, B.-M., Paik, Y.-K. and Jeong, T.-S. 2008. Inhibition of acyl-coenzyme A:cholesterol acyltransferase stimulates cholesterol efflux from macrophages and stimulates farnesoid X receptor in hepatocytes. *Experimental & Molecular Medicine*. **40**(4), pp.407-417.
- Andea, A.A., Bouwman, D., Wallis, T. and Visscher, D.W. 2004. Correlation of tumor volume and surface area with lymph node status in patients with multifocal/multicentric breast carcinoma. *Cancer*. **100**(1), pp.20-27.
- Andersson, S., Davis, D., Dahlbäck, H., Jörnvall, H., Russell and DW. 1989. Cloning, structure, and expression of the mitochondrial cytochrome P-450 sterol 26-hydroxylase, a bile acid biosynthetic enzyme. *Journal of Biological Chemistry*. **264**(14), pp.8222-8229.
- Annalora, A.J., Marcus, C.B. and Iversen, P.L. 2020. Alternative Splicing in the Nuclear Receptor Superfamily Expands Gene Function to Refine Endo-Xenobiotic Metabolism. *Drug Metabolism and Disposition*. **48**(4), pp.272-287.
- Antalis, C.J., Arnold, T., Rasool, T., Lee, B., Buhman, K.K. and Siddiqui, R. 2008. Acyl-CoA:cholesterol acyl transferase (ACAT1) is highly expressed in human breast cancer cell lines and ACAT inhibition reduces proliferation. *Faseb Journal*. **22**.
- Antalis, C.J. and Buhman, K.K. 2010. LDL and free fatty acids increase proliferation and migration of estrogen receptor negative (ER-) MDA-MB-231 breast cancer cells: involvement of ACAT1 and MAPK signaling. *Faseb Journal*. **24**.
- Antalis, C.J., Uchida, A., Buhman, K.K. and Siddiqui, R.A. 2011. Migration of MDA-MB-231 breast cancer cells depends on the availability of exogenous lipids and cholesterol esterification. *Clinical & Experimental Metastasis*. **28**(8), pp.733-741.

Antoniou, A., Pharoah, P.D., Narod, S., Risch, H.A., Eyfjord, J.E., Hopper, J.L., Loman, N., Olsson, H., Johannsson, O. and Borg, Å. 2003. Average risks of breast and ovarian cancer associated with BRCA1 or BRCA2 mutations detected in case series unselected for family history: a combined analysis of 22 studies. *The American Journal of Human Genetics*. **72**(5), pp.1117-1130.

Apfel, R., Benbrook, D., Lernhardt, E., Ortiz, M.A., Salbert, G. and Pfahl, M. 1994. A novel orphan receptor specific for a subset of thyroid hormone-responsive elements and its interaction with the retinoid/thyroid hormone receptor subfamily. *Molecular and cellular biology*. **14**(10), pp.7025-7035.

Arpaia, E., Blaser, H., Quintela-Fandino, M., Duncan, G., Leong, H.S., Ablack, A., Nambiar, S.C., Lind, E.F., Silvester, J., Fleming, C.K., Rufini, A., Tusche, M.W., Brüstle, A., Ohashi, P.S., Lewis, J.D. and Mak, T.W. 2012. The interaction between caveolin-1 and Rho-GTPases promotes metastasis by controlling the expression of alpha5-integrin and the activation of Src, Ras and Erk. *Oncogene*. **31**(7), pp.884-896.

Atalay, C., Demirkazik, A. and Gunduz, U. 2008. Role of ABCB1 and ABCC1 gene induction on survival in locally advanced breast cancer. *J Chemother*. **20**(6), pp.734-739.

Auboeuf, D., Rieusset, J., Fajas, L., Vallier, P., Frering, V., Riou, J.P., Staels, B., Auwerx, J., Laville, M. and Vidal, H. 1997. Tissue distribution and quantification of the expression of mRNAs of peroxisome proliferator-activated receptors and liver X receptor- α in humans: no alteration in adipose tissue of obese and NIDDM patients. *Diabetes*. **46**(8), pp.1319-1327.

Augustine, S., Avey, M.T., Harrison, B., Locke, T., Ghannad, M., Moher, D. and Thébaud, B. 2017. Mesenchymal stromal cell therapy in bronchopulmonary dysplasia: systematic review and meta-analysis of preclinical studies. *Stem cells translational medicine*. **6**(12), pp.2079-2093.

Babiker, A., Andersson, O., Lund, E., Xiu, R.-J., Deeb, S., Reshef, A., Leitersdorf, E., Diczfalusy, U. and Björkhem, I. 1997. Elimination of cholesterol in macrophages and endothelial cells by the sterol 27-hydroxylase mechanism: comparison with high density lipoprotein-mediated reverse cholesterol transport. *Journal of Biological Chemistry*. **272**(42), pp.26253-26261.

Babiker, A. and Diczfalusy, U. 1998. Transport of side-chain oxidized oxysterols in the human circulation. *Biochimica et Biophysica Acta (BBA) - Lipids and Lipid Metabolism*. **1392**(2), pp.333-339.

Back, S.S., Kim, J., Choi, D., Lee, E.S., Choi, S.Y. and Han, K. 2013. Cooperative transcriptional activation of ATP-binding cassette sterol transporters ABCG5 and ABCG8 genes by nuclear receptors including Liver-X-Receptor. *BMB Rep*. **46**(6), pp.322-327.

Baek, A.E., Yen-Rei, A.Y., He, S., Wardell, S.E., Chang, C.-Y., Kwon, S., Pillai, R.V., McDowell, H.B., Thompson, J.W. and Dubois, L.G. 2017. The cholesterol metabolite 27 hydroxycholesterol facilitates breast cancer metastasis through its actions on immune cells. *Nature communications*. **8**(1), pp.1-11.

Baek, A.E., Yu, Y.-R.A., He, S., Wardell, S.E., Chang, C.-Y., Kwon, S., Pillai, R.V., McDowell, H.B., Thompson, J.W., Dubois, L.G., Sullivan, P.M., Kemper, J.K., Gunn, M.D., McDonnell, D.P. and Nelson, E.R. 2017. The cholesterol metabolite 27 hydroxycholesterol facilitates breast cancer metastasis through its actions on immune cells. *Nature Communications*. **8**(1), p864.

Bai, T., Zhu, B.B., Du, Z.Y., Shi, J.L., Shao, D.Y. and Kong, J. 2020. Amphiphilic star copolymers-mediated co-delivery of doxorubicin and avasimibe for effective combination chemotherapy. *Journal of Materials Science*. **55**(22), pp.9525-9537.

Balko, J.M., Giltneane, J.M., Wang, K., Schwarz, L.J., Young, C.D., Cook, R.S., Owens, P., Sanders, M.E., Kuba, M.G. and Sánchez, V. 2014. Molecular profiling of the residual disease

of triple-negative breast cancers after neoadjuvant chemotherapy identifies actionable therapeutic targets. *Cancer discovery*. **4**(2), pp.232-245.

Bandyopadhyay, S., Li, J., Traer, E., Tyner, J.W., Zhou, A., Oh, S.T. and Cheng, J.-X. 2017. Cholesterol esterification inhibition and imatinib treatment synergistically inhibit growth of BCR-ABL mutation-independent resistant chronic myelogenous leukemia. *PLoS one*. **12**(7), pe0179558.

Barnard, G.F., Erickson, S.K. and Cooper, A.D. 1986. Regulation of lipoprotein receptors on rat hepatomas in vivo. *Biochimica et Biophysica Acta (BBA)-Lipids and Lipid Metabolism*. **879**(3), pp.301-312.

Barry, W.T., Kernagis, D.N., Dressman, H.K., Griffis, R.J., Hunter, J.V.D., Olson, J.A., Marks, J.R., Ginsburg, G.S., Marcom, P.K. and Nevins, J.R. 2010. Intratumor heterogeneity and precision of microarray-based predictors of breast cancer biology and clinical outcome. *Journal of clinical oncology*. **28**(13), p2198.

Basse, P., Goldfarb, R., Herberman, R. and Hokland, M.J.I.v. 1994. Accumulation of adoptively transferred A-NK cells in murine metastases: kinetics and role of interleukin-2. **8**(1), pp.17-24.

Bayraktar, S., Gutierrez-Barrera, A.M., Liu, D., Tasbas, T., Akar, U., Litton, J.K., Lin, E., Albarracin, C.T., Meric-Bernstam, F., Gonzalez-Angulo, A.M., Hortobagyi, G.N. and Arun, B.K. 2011. Outcome of triple-negative breast cancer in patients with or without deleterious BRCA mutations. *Breast Cancer Res Treat*. **130**(1), pp.145-153.

Bell, D., Chomarat, P., Broyles, D., Netto, G., Harb, G.M., Lebecque, S., Valladeau, J., Davoust, J., Palucka, K.A. and Banchereau, J.J.J.o.E.M. 1999. In breast carcinoma tissue, immature dendritic cells reside within the tumor, whereas mature dendritic cells are located in peritumoral areas. **190**(10), pp.1417-1426.

Bennett, D.J., Carswell, E.L., Cooke, A.J., Edwards, A.S. and Nimz, O. 2008. Design, structure activity relationships and X-Ray co-crystallography of non-steroidal LXR agonists. *Curr Med Chem*. **15**(2), pp.195-209.

Bensa, J.C., Reboul, A. and Colomb, M.G. 1983. Biosynthesis in vitro of complement subcomponents C1q, C1s and C1 inhibitor by resting and stimulated human monocytes. *The Biochemical journal*. **216**(2), pp.385-392.

Berrodin, T.J., Shen, Q., Quinet, E.M., Yudt, M.R., Freedman, L.P. and Nagpal, S. 2010. Identification of 5 α , 6 α -epoxycholesterol as a novel modulator of liver X receptor activity. *Molecular pharmacology*. **78**(6), pp.1046-1058.

Beyea, M.M., Heslop, C.L., Sawyez, C.G., Edwards, J.Y., Markle, J.G., Hegele, R.A. and Huff, M.W. 2007. Selective up-regulation of LXR-regulated genes ABCA1, ABCG1, and APOE in macrophages through increased endogenous synthesis of 24(S),25-epoxycholesterol. *J Biol Chem*. **282**(8), pp.5207-5216.

Bi, M., Qiao, X., Zhang, H., Wu, H., Gao, Z., Zhou, H., Shi, M., Wang, Y., Yang, J., Hu, J., Liang, W., Liu, Y., Qiao, X., Zhang, S. and Zhao, Z. 2019. Effect of inhibiting ACAT-1 expression on the growth and metastasis of Lewis lung carcinoma. *Oncol Lett*. **18**(2), pp.1548-1556.

Björkström, N.K., Lindgren, T., Stoltz, M., Fauriat, C., Braun, M., Evander, M., Michaëlsson, J., Malmberg, K.-J., Klingström, J. and Ahlm, C. 2011. Rapid expansion and long-term persistence of elevated NK cell numbers in humans infected with hantavirus. *Journal of Experimental Medicine*. **208**(1), pp.13-21.

Bleul, C.C., Fuhlbrigge, R.C., Casasnovas, J.M., Aiuti, A. and Springer, T.A. 1996. A highly efficacious lymphocyte chemoattractant, stromal cell-derived factor 1 (SDF-1). *The Journal of experimental medicine*. **184**(3), pp.1101-1109.

Bochet, L., Lehuédé, C., Dauvillier, S., Wang, Y.Y., Dirat, B., Laurent, V., Dray, C., Guiet, R., Maridonneau-Parini, I. and Le Gonidec, S. 2013. Adipocyte-derived fibroblasts promote tumor progression and contribute to the desmoplastic reaction in breast cancer. *Cancer research*. **73**(18), pp.5657-5668.

Bodin, K., Andersson, U., Rystedt, E., Ellis, E., Norlin, M., Pikuleva, I., Eggertsen, G., Björkhem, I. and Diczfalusy, U. 2002. Metabolism of 4 beta -hydroxycholesterol in humans. *J Biol Chem*. **277**(35), pp.31534-31540.

Bodin, K., Bretillon, L., Aden, Y., Bertilsson, L., Broomé, U., Einarsson, C. and Diczfalusy, U. 2001. Antiepileptic drugs increase plasma levels of 4beta-hydroxycholesterol in humans: evidence for involvement of cytochrome p450 3A4. *J Biol Chem*. **276**(42), pp.38685-38689.

Borgquist, S., Broberg, P., Tojjar, J. and Olsson, H. 2019. Statin use and breast cancer survival—a Swedish nationwide study. *BMC cancer*. **19**(1), p54.

Bougaret, L., Delort, L., Billard, H., Le Huede, C., Boby, C., De la Foye, A., Rossary, A., Mojallal, A., Damour, O. and Auxenfans, C. 2018. Adipocyte/breast cancer cell crosstalk in obesity interferes with the anti-proliferative efficacy of tamoxifen. *PloS one*. **13**(2), pe0191571.

Brandt, J., Garne, J.P., Tengrup, I. and Manjer, J. 2015. Age at diagnosis in relation to survival following breast cancer: a cohort study. *World Journal of Surgical Oncology*. **13**(1), p33.

Broad, R.V., Jones, S.J., Teske, M.C., Wastall, L.M., Hanby, A.M., Thorne, J.L. and Hughes, T.A. 2021. Inhibition of interferon-signalling halts cancer-associated fibroblast-dependent protection of breast cancer cells from chemotherapy. *British Journal of Cancer*. **124**(6), pp.1110-1120.

Brown, R.C., Blank, M.L., Kostyu, J.A., Osburn, P., Kilgore, A. and Snyder, F. 1975. Analysis of tumor-associated alkyldiacylglycerols and other lipids during radiation-induced thymic leukemogenesis. *Proceedings of the Society for Experimental Biology and Medicine*. **149**(3), pp.808-813.

Busby, W.H., Nam, T.-J., Morales, A., Smith, C., Jennings, M. and Clemmons, D.R. 2000. The complement component C1s is the protease that accounts for cleavage of insulin-like growth factor-binding protein-5 in fibroblast medium. *Journal of Biological Chemistry*. **275**(48), pp.37638-37644.

Camorani, S., Hill, B.S., Fontanella, R., Greco, A., Gramanzini, M., Auletta, L., Gargiulo, S., Albanese, S., Lucarelli, E., Cerchia, L. and Zannetti, A. 2017. Inhibition of Bone Marrow-Derived Mesenchymal Stem Cells Homing Towards Triple-Negative Breast Cancer Microenvironment Using an Anti-PDGFR β Aptamer. *Theranostics*. **7**(14), pp.3595-3607.

Camp, J.T., Elloumi, F., Roman-Perez, E., Rein, J., Stewart, D.A., Harrell, J.C., Perou, C.M. and Troester, M.A. 2011. Interactions with fibroblasts are distinct in Basal-like and luminal breast cancers. *Molecular cancer research : MCR*. **9**(1), pp.3-13.

Carter, C.L., Allen, C. and Henson, D.E. 1989. Relation of tumor size, lymph node status, and survival in 24,740 breast cancer cases. *Cancer*. **63**(1), pp.181-187.

Cases, S., Novak, S., Zheng, Y.-W., Myers, H.M., Lear, S.R., Sande, E., Welch, C.B., Lusic, A.J., Spencer, T.A. and Krause, B.R. 1998. ACAT-2, a second mammalian acyl-CoA: cholesterol acyltransferase its cloning, expression, and characterization. *Journal of Biological Chemistry*. **273**(41), pp.26755-26764.

Casper, E.S., Guidera, C.A., Bosl, G.J., Hakes, T.B., Kaufman, R.J., Shurgot, B. and Kinne, D.W. 1987. Combined modality treatment of locally advanced breast cancer: Adjuvant combination chemotherapy with and without doxorubicin. *Breast Cancer Research and Treatment*. **9**(1), pp.39-44.

Cerami, E., Gao, J., Dogrusoz, U., Gross, B.E., Sumer, S.O., Aksoy, B.A., Jacobsen, A., Byrne, C.J., Heuer, M.L. and Larsson, E. 2012. *The cBio cancer genomics portal: an open platform for exploring multidimensional cancer genomics data*. *AACR*. 2. pp.401-404.

Chae, B.J., Bae, J.S., Lee, A., Park, W.C., Seo, Y.J., Song, B.J., Kim, J.S. and Jung, S.S. 2009. p53 as a specific prognostic factor in triple-negative breast cancer. *Japanese Journal of Clinical Oncology*. **39**(4), pp.217-224.

Chang, C., Dong, R., Miyazaki, A., Sakashita, N., Zhang, Y., Liu, J., Guo, M., Li, B.-L. and Chang, T.-Y. 2006. Human acyl-CoA: cholesterol acyltransferase (ACAT) and its potential as a target for pharmaceutical intervention against atherosclerosis. *Acta biochimica et biophysica Sinica*. **38**(3), pp.151-156.

Chang, T.-Y., Chang, C.C., Lin, S., Yu, C., Li, B.-L. and Miyazaki, A. 2001. Roles of acyl-coenzyme A: cholesterol acyltransferase-1 and-2. *Current opinion in lipidology*. **12**(3), pp.289-296.

Cheang, M.C., Chia, S.K., Voduc, D., Gao, D., Leung, S., Snider, J., Watson, M., Davies, S., Bernard, P.S. and Parker, J.S. 2009. Ki67 index, HER2 status, and prognosis of patients with luminal B breast cancer. *JNCI: Journal of the National Cancer Institute*. **101**(10), pp.736-750.

Chen, W., Chen, G., Head, D.L., Mangelsdorf, D.J. and Russell, D.W. 2007. Enzymatic reduction of oxysterols impairs LXR signaling in cultured cells and the livers of mice. *Cell metabolism*. **5**(1), pp.73-79.

Chen, X., Oppenheim, J.J. and Howard, O.Z. 2005. BALB/c mice have more CD4+ CD25+ T regulatory cells and show greater susceptibility to suppression of their CD4+ CD25- responder T cells than C57BL/6 mice. *Journal of leukocyte biology*. **78**(1), pp.114-121.

Chen, X., Song, Q., Xia, L. and Xu, X. 2017. Synergy of Dendritic Cell Vaccines and Avasimibe in Treatment of Head and Neck Cancer in Mice. *Medical science monitor : international medical journal of experimental and clinical research*. **23**, pp.4471-4476.

Chen, Y.N., Mickley, L.A., Schwartz, A.M., Acton, E.M., Hwang, J.L. and Fojo, A.T. 1990. Characterization of adriamycin-resistant human breast cancer cells which display overexpression of a novel resistance-related membrane protein. *Journal of Biological Chemistry*. **265**(17), pp.10073-10080.

Cheng, D., Chang, C.C., Qu, X.-m. and Chang, T.-Y. 1995. Activation of Acyl-Coenzyme A: Cholesterol Acyltransferase by Cholesterol or by Oxysterol in a Cell-free System (*). *Journal of Biological Chemistry*. **270**(2), pp.685-695.

Cheng, J.W., Sadeghi, Z., Levine, A.D., Penn, M.S., von Recum, H.A., Caplan, A.I. and Hijaz, A. 2014. The role of CXCL12 and CCL7 chemokines in immune regulation, embryonic development, and tissue regeneration. *Cytokine*. **69**(2), pp.277-283.

Cheng, Y., Kerppola, R.E. and Kerppola, T.K. 2016. ATR-101 disrupts mitochondrial functions in adrenocortical carcinoma cells and in vivo. *Endocr Relat Cancer*. **23**(4), pp.1-19.

Chi, K.-C., Tsai, W.-C., Wu, C.-L., Lin, T.-Y. and Hueng, D.-Y. 2019. An adult drosophila glioma model for studying pathometabolic pathways of gliomagenesis. *Molecular neurobiology*. **56**(6), pp.4589-4599.

Chlebowski, R.T., Blackburn, G.L., Thomson, C.A., Nixon, D.W., Shapiro, A., Hoy, M.K., Goodman, M.T., Giuliano, A.E., Karanja, N., McAndrew, P., Hudis, C., Butler, J., Merkel, D., Kristal, A., Caan, B., Michaelson, R., Vinciguerra, V., Del Prete, S., Winkler, M., Hall, R., Simon, M., Winters, B.L. and Elashoff, R.M. 2006. Dietary Fat Reduction and Breast Cancer Outcome: Interim Efficacy Results From the Women's Intervention Nutrition Study. *JNCI: Journal of the National Cancer Institute*. **98**(24), pp.1767-1776.

- Cho, J.A., Park, H., Lim, E.H. and Lee, K.W. 2012. Exosomes from breast cancer cells can convert adipose tissue-derived mesenchymal stem cells into myofibroblast-like cells. *International journal of oncology*. **40**(1), pp.130-138.
- Chu, F., Shi, M., Zheng, C., Shen, D., Zhu, J., Zheng, X. and Cui, L. 2018. The roles of macrophages and microglia in multiple sclerosis and experimental autoimmune encephalomyelitis. *Journal of neuroimmunology*. **318**, pp.1-7.
- Cilloni, D. and Saglio, G. 2012. Molecular pathways: Bcr-abl. *Clinical Cancer Research*. **18**(4), pp.930-937.
- Cioccoloni, G., Soteriou, C., Websdale, A., Wallis, L., Zulyniak, M.A. and Thorne, J.L. 2020. Phytosterols and phytostanols and the hallmarks of cancer in model organisms: A systematic review and meta-analysis. *Critical Reviews in Food Science and Nutrition*. pp.1-21.
- Clemente, C.G., Mihm Jr, M.C., Bufalino, R., Zurrida, S., Collini, P. and Cascinelli, N. 1996. Prognostic value of tumor infiltrating lymphocytes in the vertical growth phase of primary cutaneous melanoma. *Cancer: Interdisciplinary International Journal of the American Cancer Society*. **77**(7), pp.1303-1310.
- Cleveland, R.J., Eng, S.M., Abrahamson, P.E., Britton, J.A., Teitelbaum, S.L., Neugut, A.I. and Gammon, M.D. 2007. Weight gain prior to diagnosis and survival from breast cancer. *Cancer Epidemiology and Prevention Biomarkers*. **16**(9), pp.1803-1811.
- Colleoni, M., Gelber, S., Goldhirsch, A., Aebi, S., Castiglione-Gertsch, M., Price, K.N., Coates, A.S. and Gelber, R.D. 2006. Tamoxifen after adjuvant chemotherapy for premenopausal women with lymph node-positive breast cancer: International Breast Cancer Study Group Trial 13-93. *Journal of clinical oncology: official journal of the American Society of Clinical Oncology*. **24**(9), pp.1332-1341.
- Cook, I.T., Duniec-Dmuchowski, Z., Kocarek, T.A., Runge-Morris, M. and Falany, C.N. 2009. 24-hydroxycholesterol sulfation by human cytosolic sulfotransferases: formation of monosulfates and disulfates, molecular modeling, sulfatase sensitivity, and inhibition of liver x receptor activation. *Drug metabolism and disposition: the biological fate of chemicals*. **37**(10), pp.2069-2078.
- Cosentino, G., Romero-Cordoba, S., Plantamura, I., Cataldo, A. and Iorio, M.V. 2020. miR-9-Mediated Inhibition of EFEMP1 Contributes to the Acquisition of Pro-Tumoral Properties in Normal Fibroblasts. *Cells*. **9**(9), p2143.
- Costa, A., Kieffer, Y., Scholer-Dahirel, A., Pelon, F., Bourachot, B., Cardon, M., Sirven, P., Magagna, I., Fuhrmann, L. and Bernard, C. 2018. Fibroblast heterogeneity and immunosuppressive environment in human breast cancer. *Cancer cell*. **33**(3), pp.463-479. e410.
- Costa, A.R., Fontes, F., Pereira, S., Gonçalves, M., Azevedo, A. and Lunet, N. 2014. Impact of breast cancer treatments on sleep disturbances—A systematic review. *The Breast*. **23**(6), pp.697-709.
- Curtis, C., Shah, S.P., Chin, S.-F., Turashvili, G., Rueda, O.M., Dunning, M.J., Speed, D., Lynch, A.G., Samarajiwa, S. and Yuan, Y. 2012. The genomic and transcriptomic architecture of 2,000 breast tumours reveals novel subgroups. *Nature*. **486**(7403), pp.346-352.
- de Gonzalo-Calvo, D., López-Vilaró, L., Nasarre, L., Perez-Olabarria, M., Vázquez, T., Escuin, D., Badimon, L., Barnadas, A., Lerma, E. and Llorente-Cortés, V. 2015. Intratumor cholesteryl ester accumulation is associated with human breast cancer proliferation and aggressive potential: a molecular and clinicopathological study. *BMC cancer*. **15**, pp.460-460.

de Kruijf, E.M., van Nes, J.G.H., van de Velde, C.J.H., Putter, H., Smit, V.T.H.B.M., Liefers, G.J., Kuppen, P.J.K., Tollenaar, R.A.E.M. and Mesker, W.E. 2011. Tumor–stroma ratio in the primary tumor is a prognostic factor in early breast cancer patients, especially in triple-negative carcinoma patients. *Breast Cancer Research and Treatment*. **125**(3), pp.687-696.

de Medina, P., Payré, B.L., Bernad, J., Bosser, I., Pipy, B., Silvente-Poirot, S., Favre, G., Faye, J.-C. and Poirot, M. 2004. Tamoxifen is a potent inhibitor of cholesterol esterification and prevents the formation of foam cells. *Journal of Pharmacology and Experimental Therapeutics*. **308**(3), pp.1165-1173.

De Talhouet, S., Peron, J., Vuilleumier, A., Friedlaender, A., Viassolo, V., Ayme, A., Bodmer, A., Treilleux, I., Lang, N., Tille, J.-C., Chappuis, P.O., Buisson, A., Giraud, S., Lasset, C., Bonadona, V., Trédan, O. and Labidi-Galy, S.I. 2020. Clinical outcome of breast cancer in carriers of BRCA1 and BRCA2 mutations according to molecular subtypes. *Scientific Reports*. **10**(1), p7073.

Dekker, T.J.A., van de Velde, C.J.H., van Pelt, G.W., Kroep, J.R., Julien, J.P., Smit, V.T.H.B.M., Tollenaar, R.A.E.M. and Mesker, W.E. 2013. Prognostic significance of the tumor-stroma ratio: validation study in node-negative premenopausal breast cancer patients from the EORTC perioperative chemotherapy (POP) trial (10854). *Breast Cancer Research and Treatment*. **139**(2), pp.371-379.

DeNardo, D.G., Brennan, D.J., Rexhepaj, E., Ruffell, B., Shiao, S.L., Madden, S.F., Gallagher, W.M., Wadhvani, N., Keil, S.D. and Junaid, S.A. 2011. Leukocyte complexity predicts breast cancer survival and functionally regulates response to chemotherapy. *Cancer discovery*. **1**(1), pp.54-67.

Dent, R., Trudeau, M., Pritchard, K.I., Hanna, W.M., Kahn, H.K., Sawka, C.A., Lickley, L.A., Rawlinson, E., Sun, P. and Narod, S.A. 2007. Triple-negative breast cancer: clinical features and patterns of recurrence. *Clinical cancer research*. **13**(15), pp.4429-4434.

DeSantis, C.E., Ma, J., Gaudet, M.M., Newman, L.A., Miller, K.D., Goding Sauer, A., Jemal, A. and Siegel, R.L. 2019. Breast cancer statistics, 2019. *CA: a cancer journal for clinicians*. **69**(6), pp.438-451.

Dianat-Moghadam, H., Khalili, M., Keshavarz, M., Azizi, M., Hamishehkar, H., Rahbarghazi, R. and Nouri, M. 2021. Modulation of LXR signaling altered the dynamic activity of human colon adenocarcinoma cancer stem cells in vitro. *Cancer Cell International*. **21**(1), p100.

Dias, I.H., Milic, I., Lip, G.Y., Devitt, A., Polidori, M.C. and Griffiths, H.R. 2018. Simvastatin reduces circulating oxysterol levels in men with hypercholesterolaemia. *Redox biology*. **16**, pp.139-145.

Diczfalusy, U., Nylén, H., Elander, P. and Bertilsson, L. 2011. 4 β -Hydroxycholesterol, an endogenous marker of CYP3A4/5 activity in humans. *Br J Clin Pharmacol*. **71**(2), pp.183-189.

Dieci, M., Prat, A., Tagliafico, E., Paré, L., Ficarra, G., Bisagni, G., Piacentini, F., Generali, D., Conte, P. and Guarneri, V. 2016. Integrated evaluation of PAM50 subtypes and immune modulation of pCR in HER2-positive breast cancer patients treated with chemotherapy and HER2-targeted agents in the CherLOB trial. *Annals of Oncology*. **27**(10), pp.1867-1873.

Dirat, B., Bochet, L., Dabek, M., Daviaud, D., Dauvillier, S., Majed, B., Wang, Y.Y., Meulle, A., Salles, B. and Le Gonidec, S. 2011. Cancer-associated adipocytes exhibit an activated phenotype and contribute to breast cancer invasion. *Cancer research*. **71**(7), pp.2455-2465.

Dos Santos, C.R., Fonseca, I., Dias, S. and De Almeida, J.M. 2014. Plasma level of LDL-cholesterol at diagnosis is a predictor factor of breast tumor progression. *BMC cancer*. **14**(1), pp.1-10.

Dowsett, M., Smith, I.E., Ebbs, S.R., Dixon, J.M., Skene, A., Griffith, C., Boeddinghaus, I., Salter, J., Detre, S., Hills, M., Ashley, S., Francis, S., Walsh, G. and A'Hern, R. 2006. Proliferation and apoptosis as markers of benefit in neoadjuvant endocrine therapy of breast cancer. *Clin Cancer Res.* **12**(3 Pt 2), pp.1024s-1030s.

Du, J.-X., Liu, Y.-L., Zhu, G.-Q., Luo, Y.-H., Chen, C., Cai, C.-Z., Zhang, S.-J., Wang, B., Cai, J.-L. and Zhou, J. 2021. Profiles of alternative splicing landscape in breast cancer and their clinical significance: an integrative analysis based on large-sequencing data. *Annals of Translational Medicine.* **9**(1).

Dunshee, D.R., Bainbridge, T.W., Kljavin, N.M., Zavala-Solorio, J., Schroeder, A.C., Chan, R., Corpuz, R., Wong, M., Zhou, W. and Deshmukh, G. 2016. Fibroblast activation protein cleaves and inactivates fibroblast growth factor 21. *Journal of Biological Chemistry.* **291**(11), pp.5986-5996.

DuSell, C.D., Umetani, M., Shaul, P.W., Mangelsdorf, D.J. and McDonnell, D.P. 2008. 27-hydroxycholesterol is an endogenous selective estrogen receptor modulator. *Molecular endocrinology (Baltimore, Md.).* **22**(1), pp.65-77.

Edwards, P.A., Kennedy, M.A. and Mak, P.A. 2002. LXRs;: Oxysterol-activated nuclear receptors that regulate genes controlling lipid homeostasis. *Vascular pharmacology.* **38**(4), pp.249-256.

El-Maouche, D., Merke, D.P., Vogiatzi, M.G., Chang, A.Y., Turcu, A.F., Joyal, E.G., Lin, V.H., Weintraub, L., Plaunt, M.R., Mohideen, P. and Auchus, R.J. 2020. A Phase 2, Multicenter Study of Nevanimibe for the Treatment of Congenital Adrenal Hyperplasia. *The Journal of Clinical Endocrinology & Metabolism.* **105**(8), pp.2771-2778.

ElAli, A. and Hermann, D.M. 2012. Liver X receptor activation enhances blood-brain barrier integrity in the ischemic brain and increases the abundance of ATP-binding cassette transporters ABCB1 and ABCC1 on brain capillary cells. *Brain Pathol.* **22**(2), pp.175-187.

ElAli, A. and Hermann, D.M. 2012. Liver X Receptor Activation Enhances Blood–Brain Barrier Integrity in the Ischemic Brain and Increases the Abundance of ATP-Binding Cassette Transporters ABCB1 and ABCC1 on Brain Capillary Cells. *Brain Pathology.* **22**(2), pp.175-187.

Elston, C. 1984. The assessment of histological differentiation in breast cancer. *Australian and New Zealand Journal of Surgery.* **54**(1), pp.11-15.

Emgård, J., Kammoun, H., García-Cassani, B., Chesné, J., Parigi, S.M., Jacob, J.-M., Cheng, H.-W., Evren, E., Das, S., Czarnewski, P., Sleiers, N., Melo-Gonzalez, F., Kvedaraite, E., Svensson, M., Scandella, E., Hepworth, M.R., Huber, S., Ludewig, B., Peduto, L., Villablanca, E.J., Veiga-Fernandes, H., Pereira, J.P., Flavell, R.A. and Willinger, T. 2018. Oxysterol Sensing through the Receptor GPR183 Promotes the Lymphoid-Tissue-Inducing Function of Innate Lymphoid Cells and Colonic Inflammation. *Immunity.* **48**(1), pp.120-132.e128.

Erickson, S.K., Cooper, A.D., Barnard, G.F., Havel, C.M., Watson, J.A., Feingold, K.R., Moser, A.H., Hughes-Fulford, M. and Siperstein, M.D. 1988. Regulation of cholesterol metabolism in a slow-growing hepatoma in vivo. *Biochimica et Biophysica Acta (BBA)-Lipids and Lipid Metabolism.* **960**(2), pp.131-138.

Eriksson, H. and Nissen, M.H. 1990. Proteolysis of the heavy chain of major histocompatibility complex class I antigens by complement component C1s. *Biochimica et Biophysica Acta (BBA)-Protein Structure and Molecular Enzymology.* **1037**(2), pp.209-215.

Erusappan, P., Alam, J., Lu, N., Zeltz, C. and Gullberg, D. 2019. Integrin α 11 cytoplasmic tail is required for FAK activation to initiate 3D cell invasion and ERK-mediated cell proliferation. *Sci Rep.* **9**(1), p15283.

Farmer, P., Bonnefoi, H., Anderle, P., Cameron, D., Wirapati, P., Becette, V., André, S., Piccart, M., Campone, M. and Brain, E. 2009. A stroma-related gene signature predicts resistance to neoadjuvant chemotherapy in breast cancer. *Nature medicine*. **15**(1), p68.

Fernández-Alvarez, A., Alvarez, M.S., Gonzalez, R., Cucarella, C., Muntané, J. and Casado, M. 2011. Human SREBP1c expression in liver is directly regulated by peroxisome proliferator-activated receptor alpha (PPARalpha). *J Biol Chem*. **286**(24), pp.21466-21477.

Field, F.J. and Mathur, S.N. 1983. Regulation of acyl CoA: cholesterol acyltransferase by 25-hydroxycholesterol in rabbit intestinal microsomes and absorptive cells. *Journal of lipid research*. **24**(8), pp.1049-1059.

Fisher, B., Costantino, J., Redmond, C., Poisson, R., Bowman, D., Couture, J., Dimitrov, N.V., Wolmark, N., Wickerham, D.L., Fisher, E.R. and et al. 1989. A randomized clinical trial evaluating tamoxifen in the treatment of patients with node-negative breast cancer who have estrogen-receptor-positive tumors. *N Engl J Med*. **320**(8), pp.479-484.

Fisher, B., Dignam, J., Bryant, J., DeCillis, A., Wickerham, D.L., Wolmark, N., Costantino, J., Redmond, C., Fisher, E.R., Bowman, D.M., Deschênes, L., Dimitrov, N.V., Margolese, R.G., Robidoux, A., Shibata, H., Terz, J., Paterson, A.H., Feldman, M.I., Farrar, W., Evans, J. and Lickley, H.L. 1996. Five versus more than five years of tamoxifen therapy for breast cancer patients with negative lymph nodes and estrogen receptor-positive tumors. *J Natl Cancer Inst*. **88**(21), pp.1529-1542.

Fougner, C., Bergholtz, H., Norum, J.H. and Sørli, T. 2020. Re-definition of claudin-low as a breast cancer phenotype. *Nature Communications*. **11**(1), p1787.

Fourgeux, C., Martine, L., Acar, N., Bron, A.M., Creuzot-Garcher, C.P. and Bretilon, L. 2014. In vivo consequences of cholesterol-24S-hydroxylase (CYP46A1) inhibition by voriconazole on cholesterol homeostasis and function in the rat retina. *Biochemical and Biophysical Research Communications*. **446**(3), pp.775-781.

Franck, N., Gummesson, A., Jernås, M., Glad, C., Svensson, P.-A., Guillot, G., Rudemo, M., Nyström, F.H., Carlsson, L.M. and Olsson, B. 2011. Identification of adipocyte genes regulated by caloric intake. *The Journal of Clinical Endocrinology & Metabolism*. **96**(2), pp.E413-E418.

Freeman, N.E., Rusinol, A.E., Linton, M., Hachey, D.L., Fazio, S., Sinensky, M.S. and Thewke, D. 2005. Acyl-coenzyme A:cholesterol acyltransferase promotes oxidized LDL/oxysterol-induced apoptosis in macrophages. *Journal of lipid research*. **46**(9), pp.1933-1943.

Friedenreich, C.M. 2010. The role of physical activity in breast cancer etiology. In: *Seminars in oncology*: Elsevier, pp.297-302.

Fuda, H., Javitt, N.B., Mitamura, K., Ikegawa, S. and Strott, C.A. 2007. Oxysterols are substrates for cholesterol sulfotransferase. *Journal of lipid research*. **48**(6), pp.1343-1352.

Fuda, H., Lee, Y.C., Shimizu, C., Javitt, N.B. and Strott, C.A. 2002. Mutational analysis of human hydroxysteroid sulfotransferase SULT2B1 isoforms reveals that exon 1B of the SULT2B1 gene produces cholesterol sulfotransferase, whereas exon 1A yields pregnenolone sulfotransferase. *Journal of Biological Chemistry*. **277**(39), pp.36161-36166.

Fukuchi, J., Kokontis, J.M., Hiipakka, R.A., Chuu, C.-p. and Liao, S. 2004. Antiproliferative effect of liver X receptor agonists on LNCaP human prostate cancer cells. *Cancer research*. **64**(21), pp.7686-7689.

Gabitova, L., Restifo, D., Gorin, A., Manocha, K., Handorf, E., Yang, D.-H., Cai, K.Q., Klein-Szanto, A.J., Cunningham, D. and Kratz, L.E. 2015. Endogenous sterol metabolites regulate growth of EGFR/KRAS-dependent tumors via LXR. *Cell reports*. **12**(11), pp.1927-1938.

Gabrilovich, D.I., Corak, J., Ciernik, I.F., Kavanaugh, D. and Carbone, D.P. 1997. Decreased antigen presentation by dendritic cells in patients with breast cancer. *Clinical Cancer Research*. **3**(3), pp.483-490.

Gagliano, T., Shah, K., Gargani, S., Lao, L., Alsaleem, M., Chen, J., Ntafis, V., Huang, P., Ditsiou, A. and Vella, V. 2020. PIK3C δ expression by fibroblasts promotes triple-negative breast cancer progression. *The Journal of clinical investigation*. **130**(6), pp.3188-3204.

Galon, J., Costes, A., Sanchez-Cabo, F., Kirilovsky, A., Mlecnik, B., Lagorce-Pagès, C., Tosolini, M., Camus, M., Berger, A. and Wind, P. 2006. Type, density, and location of immune cells within human colorectal tumors predict clinical outcome. *Science*. **313**(5795), pp.1960-1964.

Gao, J.H., He, L.H., Yu, X.H., Zhao, Z.W., Wang, G., Zou, J., Wen, F.J., Zhou, L., Wan, X.J., Zhang, D.W. and Tang, C.K. 2019. CXCL12 promotes atherosclerosis by downregulating ABCA1 expression via the CXCR4/GSK3 β / β -catenin(T120)/TCF21 pathway. *J Lipid Res*. **60**(12), pp.2020-2033.

Gao, Y., Xu, D., Li, H., Xu, J., Pan, Y., Liao, X., Qian, J., Hu, Y. and Yu, G. 2021. Avasimibe Dampens Cholangiocarcinoma Progression by Inhibiting FoxM1-AKR1C1 Signaling. *Frontiers in oncology*. **11**, p1788.

Gelissen, I.C., Rye, K.A., Brown, A.J., Dean, R.T. and Jessup, W. 1999. Oxysterol efflux from macrophage foam cells: the essential role of acceptor phospholipid. *J Lipid Res*. **40**(9), pp.1636-1646.

Geng, F., Cheng, X., Wu, X., Yoo, J.Y., Cheng, C., Guo, J.Y., Mo, X., Ru, P., Hurwitz, B., Kim, S.-H., Otero, J., Pudevalli, V., Lefai, E., Ma, J., Nakano, I., Horbinski, C., Kaur, B., Chakravarti, A. and Guo, D. 2016. Inhibition of SOAT1 Suppresses Glioblastoma Growth via Blocking SREBP-1-Mediated Lipogenesis. *Clinical cancer research : an official journal of the American Association for Cancer Research*. **22**(21), pp.5337-5348.

Giordano, C., La Camera, G., Gelsomino, L., Barone, I., Bonofiglio, D., Andò, S. and Catalano, S. 2020. The Biology of Exosomes in Breast Cancer Progression: Dissemination, Immune Evasion and Metastatic Colonization. *Cancers*. **12**(8), p2179.

Giudetti, A.M., De Domenico, S., Ragusa, A., Lunetti, P., Gaballo, A., Franck, J., Simeone, P., Nicolardi, G., De Nuccio, F., Santino, A., Capobianco, L., Lanuti, P., Fournier, I., Salzet, M., Maffia, M. and Vergara, D. 2019. A specific lipid metabolic profile is associated with the epithelial mesenchymal transition program. *Biochimica et Biophysica Acta (BBA) - Molecular and Cell Biology of Lipids*. **1864**(3), pp.344-357.

Goldstein, I., Rivlin, N., Shoshana, O.-y., Ezra, O., Madar, S., Goldfinger, N. and Rotter, V. 2013. Chemotherapeutic agents induce the expression and activity of their clearing enzyme CYP3A4 by activating p53. *Carcinogenesis*. **34**(1), pp.190-198.

González, L., Eiro, N., Fernandez-Garcia, B., González, L.O., Dominguez, F. and Vizoso, F.J. 2016. Gene expression profile of normal and cancer-associated fibroblasts according to intratumoral inflammatory cells phenotype from breast cancer tissue. *Molecular Carcinogenesis*. **55**(11), pp.1489-1502.

Gottesman, M.M., Fojo, T. and Bates, S.E. 2002. Multidrug resistance in cancer: role of ATP-dependent transporters. *Nature Reviews Cancer*. **2**(1), pp.48-58.

Gouirand, V., Guillaumond, F. and Vasseur, S. 2018. Influence of the tumor microenvironment on cancer cells metabolic reprogramming. *Frontiers in oncology*. **8**, p117.

Granucci, F., Foti, M. and Ricciardi-Castagnoli, P. 2005. Dendritic Cell Biology. *Advances in Immunology*. Academic Press, pp.193-233.

Gregorczyk, S., Kang, Y., Brandt, D., Kolm, P., Singer, G. and Perry, R.R. 1996. p-Glycoprotein expression as a predictor of breast cancer recurrence. *Annals of surgical oncology*. **3**(1), pp.8-14.

Griffiths, W.J., Abdel-Khalik, J., Crick, P.J., Yutuc, E. and Wang, Y. 2016a. New methods for analysis of oxysterols and related compounds by LC–MS. *The Journal of steroid biochemistry and molecular biology*. **162**, pp.4-26.

Griffiths, W.J., Abdel-Khalik, J., Hearn, T., Yutuc, E., Morgan, A.H. and Wang, Y. 2016b. Current trends in oxysterol research. *Biochemical Society Transactions*. **44**(2), pp.652-658.

Griffiths, W.J., Crick, P.J., Meljon, A., Theofilopoulos, S., Abdel-Khalik, J., Yutuc, E., Parker, J.E., Kelly, D.E., Kelly, S.L. and Arenas, E. 2019. Additional pathways of sterol metabolism: Evidence from analysis of Cyp27a1–/– mouse brain and plasma. *Biochimica et Biophysica Acta (BBA)-Molecular and Cell Biology of Lipids*. **1864**(2), pp.191-211.

Group, B.I.G.C., Mouridsen, H., Giobbie-Hurder, A., Goldhirsch, A., Thürlimann, B., Paridaens, R., Smith, I., Mauriac, L., Forbes, J.F., Price, K.N., Regan, M.M., Gelber, R.D. and Coates, A.S. 2009. Letrozole therapy alone or in sequence with tamoxifen in women with breast cancer. *The New England journal of medicine*. **361**(8), pp.766-776.

Guarisch-Sousa, R., Monteiro, J.S., Alecrim, L.C., Michaloski, J.S., Cardeal, L.B., Ferreira, E.N., Carraro, D.M., Nunes, D.N., Dias-Neto, E. and Reimand, J. 2019. A transcriptome-based signature of pathological angiogenesis predicts breast cancer patient survival. *PLoS genetics*. **15**(12), pe1008482.

Guerra, N., Tan, Y.X., Joncker, N.T., Choy, A., Gallardo, F., Xiong, N., Knoblaugh, S., Cado, D., Greenberg, N.R. and Raulet, D.H.J.I. 2008. NKG2D-deficient mice are defective in tumor surveillance in models of spontaneous malignancy. **28**(4), pp.571-580.

Guestini, F., Ono, K., Miyashita, M., Ishida, T., Ohuchi, N., Nakagawa, S., Hirakawa, H., Tamaki, K., Ohi, Y. and Rai, Y. 2019. Impact of Topoisomerase II α , PTEN, ABCC1/MRP1, and KI67 on triple-negative breast cancer patients treated with neoadjuvant chemotherapy. *Breast cancer research and treatment*. **173**(2), pp.275-288.

Gui, Y., Aguilar-Mahecha, A., Krzemien, U., Hosein, A., Buchanan, M., Lafleur, J., Pollak, M., Ferrario, C. and Basik, M. 2019. Metastatic breast carcinoma-associated fibroblasts have enhanced protumorigenic properties related to increased IGF2 expression. *Clinical Cancer Research*. **25**(23), pp.7229-7242.

Guo, L., Cui, H., Zhao, G., Liu, R., Li, Q., Zheng, M., Guo, Y. and Wen, J. 2018. Intramuscular preadipocytes impede differentiation and promote lipid deposition of muscle satellite cells in chickens. *BMC genomics*. **19**(1), pp.1-14.

Gura, T., Hu, G. and Veis, A. 1996. Posttranscriptional aspects of the biosynthesis of type 1 collagen pro-alpha chains: The effects of posttranslational modifications on synthesis pauses during elongation of the Pro α 1 (I) chain. *Journal of cellular biochemistry*. **61**(2), pp.194-215.

Hagerty, R., Butow, P., Ellis, P., Lobb, E., Pendlebury, S., Leigh, N., Goldstein, D., Lo, S.K. and Tattersall, M. 2004. Cancer patient preferences for communication of prognosis in the metastatic setting. *Journal of clinical oncology*. **22**(9), pp.1721-1730.

Hanson, A.N. and Bentley, J.P. 1983. Quantitation of Type I to type III collagen ratios in small samples of human tendon, blood vessels, and atherosclerotic plaque. *Analytical Biochemistry*. **130**(1), pp.32-40.

Hansson, M., Ellis, E., Hunt, M.C., Schmitz, G. and Babiker, A. 2003. Marked induction of sterol 27-hydroxylase activity and mRNA levels during differentiation of human cultured monocytes into macrophages. *Biochimica et Biophysica Acta (BBA)-Molecular Cell Research*. **1593**(2-3), pp.283-289.

Hao, M., Hou, S., Li, W., Li, K., Xue, L., Hu, Q., Zhu, L., Chen, Y., Sun, H. and Ju, C. 2020. Combination of metabolic intervention and T cell therapy enhances solid tumor immunotherapy. *Science Translational Medicine*. **12**(571).

Harmsen, S., Meijerman, I., Beijnen, J. and Schellens, J. 2007. The role of nuclear receptors in pharmacokinetic drug–drug interactions in oncology. *Cancer treatment reviews*. **33**(4), pp.369-380.

Harry, D., Morris, H. and McINTYRE, N. 1971. Cholesterol biosynthesis in transplantable hepatomas: evidence for impairment of uptake and storage of dietary cholesterol. *Journal of lipid research*. **12**(3), pp.313-317.

Hasebe, T., Sasaki, S., Imoto, S. and Ochiai, A. 2000. Proliferative activity of intratumoral fibroblasts is closely correlated with lymph node and distant organ metastases of invasive ductal carcinoma of the breast. *The American journal of pathology*. **156**(5), pp.1701-1710.

Held, P. 2018. Using phenol red to assess pH in tissue culture media. *BioTek Appl. Note1*. pp.1-7.

Henderson, V.C., Demko, N., Hakala, A., MacKinnon, N., Federico, C.A., Fergusson, D. and Kimmelman, J. 2015. A meta-analysis of threats to valid clinical inference in preclinical research of sunitinib. *Elife*. **4**, pe08351.

Hennigs, A., Riedel, F., Gondos, A., Sinn, P., Schirmacher, P., Marmé, F., Jäger, D., Kauczor, H.-U., Stieber, A., Lindel, K., Debus, J., Golatta, M., Schütz, F., Sohn, C., Heil, J. and Schneeweiss, A. 2016. Prognosis of breast cancer molecular subtypes in routine clinical care: A large prospective cohort study. *BMC cancer*. **16**(1), pp.734-734.

Herber, D.L., Cao, W., Nefedova, Y., Novitskiy, S.V., Nagaraj, S., Tyurin, V.A., Corzo, A., Cho, H.-I., Celis, E. and Lennox, B.J.N.m. 2010. Lipid accumulation and dendritic cell dysfunction in cancer. **16**(8), p880.

Hinz, B., Celetta, G., Tomasek, J.J., Gabbiani, G. and Chaponnier, C. 2001. Alpha-smooth muscle actin expression upregulates fibroblast contractile activity. *Mol Biol Cell*. **12**(9), pp.2730-2741.

Hinz, B., Dugina, V., Ballestrem, C., Wehrle-Haller, B. and Chaponnier, C. 2003. Alpha-smooth muscle actin is crucial for focal adhesion maturation in myofibroblasts. *Molecular biology of the cell*. **14**(6), pp.2508-2519.

Hoerer, S., Schmid, A., Heckel, A., Budzinski, R.-M. and Nar, H. 2003. Crystal Structure of the Human Liver X Receptor β Ligand-binding Domain in Complex with a Synthetic Agonist. *Journal of Molecular Biology*. **334**(5), pp.853-861.

Hoffman, W., Lakkis, F.G. and Chalasani, G. 2016. B Cells, Antibodies, and More. *Clinical journal of the American Society of Nephrology : CJASN*. **11**(1), pp.137-154.

Honzumi, S., Shima, A., Hiroshima, A., Koieyama, T., Ubukata, N. and Terasaka, N. 2010. LXRA regulates human CETP expression in vitro and in transgenic mice. *Atherosclerosis*. **212**(1), pp.139-145.

Howell, A., Cuzick, J., Baum, M., Buzdar, A., Dowsett, M., Forbes, J.F., Hocht-Boes, G., Houghton, J., Locker, G.Y. and Tobias, J.S. 2005. Results of the ATAC (Arimidex, Tamoxifen, Alone or in Combination) trial after completion of 5 years' adjuvant treatment for breast cancer. *Lancet*. **365**(9453), pp.60-62.

Howlander, N., et al., . 2020. SEER*Explorer. Breast cancer-SEER incidence rates by age at diagnosis, by sex, 2013-2017. *National Cancer Institute. Bethesda, MD. Accessed on January 29, 2021. <https://seer.cancer.gov/explorer/>, 2021.*

Hu, J., Kinn, J., Zirakzadeh, A., Sherif, A., Norstedt, G., Wikström, A. and Winqvist, O. 2013. The effects of chemotherapeutic drugs on human monocyte-derived dendritic cell

differentiation and antigen presentation. *Clinical & Experimental Immunology*. **172**(3), pp.490-499.

Hu, X., Li, S., Wu, J., Xia, C. and Lala, D.S. 2003. Liver X Receptors Interact with Corepressors to Regulate Gene Expression. *Molecular Endocrinology*. **17**(6), pp.1019-1026.

Huang, J., Lee, S.-J., Kang, S., Choi, M.H. and Im, D.-S. 2020. 7α , 25-Dihydroxycholesterol Suppresses Hepatocellular Steatosis through GPR183/EBI2 in Mouse and Human Hepatocytes. *Journal of Pharmacology and Experimental Therapeutics*. **374**(1), pp.142-150.

Huang, Y., Jin, Q., Su, M., Ji, F., Wang, N., Zhong, C., Jiang, Y., Liu, Y., Zhang, Z., Yang, J., Wei, L., Chen, T. and Li, B. 2017. Leptin promotes the migration and invasion of breast cancer cells by upregulating ACAT2. *Cell Oncol (Dordr)*. **40**(6), pp.537-547.

Hutchinson, S.A., Lianto, P., Moore, J.B., Hughes, T.A. and Thorne, J.L. 2019a. Phytosterols inhibit side-chain oxysterol mediated activation of LXR in breast cancer cells. *International journal of molecular sciences*. **20**(13), p3241.

Hutchinson, S.A., Lianto, P., Roberg-Larsen, H., Battaglia, S., Hughes, T.A. and Thorne, J.L. 2019b. ER-Negative Breast Cancer Is Highly Responsive to Cholesterol Metabolite Signalling. *Nutrients*. **11**(11), p2618.

Hutchinson, S.A. and Thorne, J.L. 2019. A Stable Luciferase Reporter System to Characterize LXR Regulation by Oxysterols and Novel Ligands. *Lipid-Activated Nuclear Receptors*. Springer, pp.15-32.

Hutchinson, S.A., Websdale, A., Cioccoloni, G., Røberg-Larsen, H., Lianto, P., Kim, B., Rose, A., Soteriou, C., Pramanik, A. and Wastall, L.M. 2021. Liver x receptor alpha drives chemoresistance in response to side-chain hydroxycholesterols in triple negative breast cancer. *Oncogene*. pp.1-12.

Ignatova, I.D., Angdisen, J., Moran, E. and Schulman, I.G. 2013a. Differential regulation of gene expression by LXRs in response to macrophage cholesterol loading. *Molecular endocrinology (Baltimore, Md.)*. **27**(7), pp.1036-1047.

Ignatova, I.D., Angdisen, J., Moran, E. and Schulman, I.G. 2013b. Differential Regulation of Gene Expression by LXRs in Response to Macrophage Cholesterol Loading. *Molecular Endocrinology*. **27**(7), pp.1036-1047.

Ikenoya, M., Yoshinaka, Y., Kobayashi, H., Kawamine, K., Shibuya, K., Sato, F., Sawanobori, K., Watanabe, T. and Miyazaki, A. 2007. A selective ACAT-1 inhibitor, K-604, suppresses fatty streak lesions in fat-fed hamsters without affecting plasma cholesterol levels. *Atherosclerosis*. **191**(2), pp.290-297.

Inasu, M., Bendahl, P.-O., Fernö, M., Malmström, P., Borgquist, S. and Kimbung, S. 2021. High CYP27A1 expression is a biomarker of favorable prognosis in premenopausal patients with estrogen receptor positive primary breast cancer. *NPJ Breast Cancer*. **7**(1), pp.1-11.

Insull Jr, W., Koren, M., Davignon, J., Sprecher, D., Schrott, H., Keilson, L.M., Brown, A.S., Dujovne, C.A., Davidson, M.H. and McLain, R. 2001. Efficacy and short-term safety of a new ACAT inhibitor, avasimibe, on lipids, lipoproteins, and apolipoproteins, in patients with combined hyperlipidemia. *Atherosclerosis*. **157**(1), pp.137-144.

Janowski, B.A., Grogan, M.J., Jones, S.A., Wisely, G.B., Kliewer, S.A., Corey, E.J. and Mangelsdorf, D.J. 1999. Structural requirements of ligands for the oxysterol liver X receptors LXR α and LXR β . *Proceedings of the National Academy of Sciences*. **96**(1), pp.266-271.

Javitt, N.B., Lee, Y.C., Shimizu, C., Fuda, H. and Strott, C.A. 2001. Cholesterol and Hydroxycholesterol Sulfotransferases: Identification, Distinction from Dehydroepiandrosterone Sulfotransferase, and Differential Tissue Expression. *Endocrinology*. **142**(7), pp.2978-2984.

- Jia, B., Chen, B., Long, H., Rong, T. and Su, X. 2020. Tumor volume is more reliable to predict nodal metastasis in non-small cell lung cancer of 3.0 cm or less in the greatest tumor diameter. *World Journal of Surgical Oncology*. **18**(1), p168.
- Jia, Y., Domenico, J., Takeda, K., Han, J., Wang, M., Armstrong, M., Reisdorph, N., O'Connor, B.P., Lucas, J.J. and Gelfand, E.W. 2013. Steroidogenic enzyme Cyp11a1 regulates Type 2 CD8+ T cell skewing in allergic lung disease. *Proceedings of the National Academy of Sciences*. p201216671.
- Jiang, Y., Sun, A., Zhao, Y., Ying, W., Sun, H., Yang, X., Xing, B., Sun, W., Ren, L. and Hu, B. 2019. Proteomics identifies new therapeutic targets of early-stage hepatocellular carcinoma. *Nature*. **567**(7747), pp.257-261.
- Jiang, Y.J., Kim, P., Elias, P.M. and Feingold, K.R. 2005. LXR and PPAR activators stimulate cholesterol sulfotransferase type 2 isoform 1b in human keratinocytes. *Journal of lipid research*. **46**(12), pp.2657-2666.
- Jones, S., Holmes, F.A., O'Shaughnessy, J., Blum, J.L., Vukelja, S.J., McIntyre, K.J., Phippen, J.E., Bordelon, J.H., Kirby, R.L. and Sandbach, J. 2009. Docetaxel with cyclophosphamide is associated with an overall survival benefit compared with doxorubicin and cyclophosphamide: 7-year follow-up of US Oncology Research Trial 9735. *Journal of Clinical Oncology*. **27**(8), pp.1177-1183.
- Jones, S.E.S., Michael A, Holmes, F.A.O.S., Joyce A, Blum, J.L.V., Svetislava, McIntyre, K.J.P., John E, Bordelon, J.H.K., Robert, Sandbach, J.H., William J, Khandelwal, P.N., Angel G, Richards, D.A.A., Stephen P, Mennel, R.G.B., Kristi A and Meyer, W.G.A., Lina. 2006. Phase III trial comparing doxorubicin plus cyclophosphamide with docetaxel plus cyclophosphamide as adjuvant therapy for operable breast cancer. *Journal of Clinical Oncology*. **24**(34), pp.5381-5387.
- Jue, T.R., Sena, E.S., Macleod, M.R., McDonald, K.L. and Hirst, T.C. 2018. A systematic review and meta-analysis of topoisomerase inhibition in pre-clinical glioma models. *Oncotarget*. **9**(13), p11387.
- Juhász, A., Rimanoczy, A., Boda, K., Vincze, G., Szilávik, G., Zana, M., Bjelik, A., Pakaski, M., Bodi, N. and Palotas, A. 2005. CYP46 T/C polymorphism is not associated with Alzheimer's dementia in a population from Hungary. *Neurochemical research*. **30**(8), pp.943-948.
- K Tiwari, A., Sodani, K., Dai, C.-L., R Ashby, C. and Chen, Z.-S. 2011. Revisiting the ABCs of multidrug resistance in cancer chemotherapy. *Current pharmaceutical biotechnology*. **12**(4), pp.570-594.
- Kabat, G.C., Kim, M., Phipps, A.I., Li, C.I., Messina, C.R., Wactawski-Wende, J., Kuller, L., Simon, M.S., Yasmeen, S., Wassertheil-Smoller, S. and Rohan, T.E. 2011. Smoking and alcohol consumption in relation to risk of triple-negative breast cancer in a cohort of postmenopausal women. *Cancer causes & control : CCC*. **22**(5), pp.775-783.
- Kajimura, S. 2017. Advances in the understanding of adipose tissue biology. *Nature Reviews Endocrinology*. **13**, p69.
- Kannenbergh, F., Gorzelniak, K., Jäger, K., Fobker, M., Rust, S., Repa, J., Roth, M., Björkhem, I. and Walter, M. 2013. Characterization of cholesterol homeostasis in telomerase-immortalized Tangier disease fibroblasts reveals marked phenotype variability. *Journal of Biological Chemistry*. **288**(52), pp.36936-36947.
- Kassam, F., Enright, K., Dent, R., Dranitsaris, G., Myers, J., Flynn, C., Fralick, M., Kumar, R. and Clemons, M. 2009. Survival outcomes for patients with metastatic triple-negative breast cancer: implications for clinical practice and trial design. *Clin Breast Cancer*. **9**(1), pp.29-33.

Kawai, O., Ishii, G., Kubota, K., Murata, Y., Naito, Y., Mizuno, T., Aokage, K., Saijo, N., Nishiwaki, Y. and Gemma, A. 2008. Predominant infiltration of macrophages and CD8+ T cells in cancer nests is a significant predictor of survival in stage IV nonsmall cell lung cancer. *Cancer: Interdisciplinary International Journal of the American Cancer Society*. **113**(6), pp.1387-1395.

Kazlauskas, A. and Cooper, J.A. 1990. Phosphorylation of the PDGF receptor beta subunit creates a tight binding site for phosphatidylinositol 3 kinase. *The EMBO journal*. **9**(10), pp.3279-3286.

Kelley, K.W., Nakao-Inoue, H., Molofsky, A.V. and Oldham, M.C. 2018. Variation among intact tissue samples reveals the core transcriptional features of human CNS cell classes. *Nature neuroscience*. **21**(9), pp.1171-1184.

Kennecke, H., Yerushalmi, R., Woods, R., Cheang, M.C.U., Voduc, D., Speers, C.H., Nielsen, T.O. and Gelmon, K. 2010. Metastatic behavior of breast cancer subtypes. *Journal of clinical oncology*. **28**(20), pp.3271-3277.

Kim, B., Fatayer, H., Hanby, A.M., Horgan, K., Perry, S.L., Valleley, E.M., Verghese, E.T., Williams, B.J., Thorne, J.L. and Hughes, T.A. 2013. Neoadjuvant chemotherapy induces expression levels of breast cancer resistance protein that predict disease-free survival in breast cancer. *PLoS One*. **8**(5).

Kim, H.M., Jung, W.H. and Koo, J.S. 2015. Expression of cancer-associated fibroblast related proteins in metastatic breast cancer: an immunohistochemical analysis. *Journal of Translational Medicine*. **13**(1), p222.

Kim, R., Kawai, A., Wakisaka, M., Funaoka, Y., Yasuda, N., Hidaka, M., Morita, Y., Ohtani, S., Ito, M. and Arihiro, K. 2019. A potential role for peripheral natural killer cell activity induced by preoperative chemotherapy in breast cancer patients. *Cancer Immunology, Immunotherapy*. **68**(4), pp.577-585.

Kimbung, S., Chang, C.-y., Bendahl, P.-O., Dubois, L., Thompson, J.W., McDonnell, D.P. and Borgquist, S. 2017. Impact of 27-hydroxylase (CYP27A1) and 27-hydroxycholesterol in breast cancer. *Endocrine-related cancer*. **24**(7), pp.339-349.

Kimura, T., Nada, S., Takegahara, N., Okuno, T., Nojima, S., Kang, S., Ito, D., Morimoto, K., Hosokawa, T. and Hayama, Y. 2016. Polarization of M2 macrophages requires Lamtor1 that integrates cytokine and amino-acid signals. *Nature communications*. **7**(1), pp.1-17.

Kloudova, A., Brynychova, V., Vaclavikova, R., Vrana, D., Gatek, J., Mrhalova, M., Kodet, R. and Soucek, P. 2017. Expression of oxysterol pathway genes in oestrogen-positive breast carcinomas. *Clinical endocrinology*. **86**(6), pp.852-861.

Kloudova-Spalenkova, A., Ueng, Y.-F., Wei, S., Kopeckova, K., Guengerich, F.P. and Soucek, P. 2020. Plasma oxysterol levels in luminal subtype breast cancer patients are associated with clinical data. *The Journal of Steroid Biochemistry and Molecular Biology*. **197**, p105566.

Koboldt, D., Fulton, R., McLellan, M., Schmidt, H., Kalicki-Veizer, J., McMichael, J., Fulton, L., Dooling, D., Ding, L. and Mardis, E. 2012. Comprehensive molecular portraits of human breast tumours. *Nature*. **490**(7418), pp.61-70.

Kong, A.-N.T., Yang, L., Meihui, M., Tao, D. and Bjornsson, T.D. 1992. Molecular cloning of the alcohol/hydroxysteroid form (hSTa) of sulfotransferase from human liver. *Biochemical and biophysical research communications*. **187**(1), pp.448-454.

Konishi, H., Okajima, H., Okada, Y., Yamamoto, H., Fukai, K. and Watanabe, H. 1991. High levels of cholesteryl esters, progesterone and estradiol in the testis of aging male Fischer 344 rats: feminizing Leydig cell tumors. *Chemical and pharmaceutical bulletin*. **39**(2), pp.501-504.

Kopcow, H.D., Eriksson, M., Mselle, T.F., Damrauer, S., Wira, C.R., Sentman, C.L. and Strominger, J.L. 2010. Human decidual NK cells from gravid uteri and NK cells from cycling endometrium are distinct NK cell subsets. *Placenta*. **31**(4), pp.334-338.

Krammer, J., Pinker-Domenig, K., Robson, M.E., Gönen, M., Bernard-Davila, B., Morris, E.A., Mangino, D.A. and Jochelson, M.S. 2017. Breast cancer detection and tumor characteristics in BRCA1 and BRCA2 mutation carriers. *Breast cancer research and treatment*. **163**(3), pp.565-571.

Kumar, A.S., Benz, C.C., Shim, V., Minami, C.A., Moore, D.H. and Esserman, L.J. 2008. Estrogen receptor–Negative breast Cancer Is less likely to arise among lipophilic statin users. *Cancer Epidemiology and Prevention Biomarkers*. **17**(5), pp.1028-1033.

Kurebayashi, J., Otsuki, T., Kunisue, H., Tanaka, K., Yamamoto, S. and Sonoo, H. 2000. Expression levels of estrogen receptor- α , estrogen receptor- β , coactivators, and corepressors in breast cancer. *Clinical Cancer Research*. **6**(2), pp.512-518.

Kwan, M.L., Habel, L.A., Flick, E.D., Quesenberry, C.P. and Caan, B. 2008. Post-diagnosis statin use and breast cancer recurrence in a prospective cohort study of early stage breast cancer survivors. *Breast cancer research and treatment*. **109**(3), pp.573-579.

La Marca, V., Maresca, B., Spagnuolo, M.S., Cigliano, L., Dal Piaz, F., Di Iorio, G. and Abrescia, P. 2016. Lecithin-cholesterol acyltransferase in brain: Does oxidative stress influence the 24-hydroxycholesterol esterification? *Neuroscience Research*. **105**, pp.19-27.

Lacombe, A.M.F., Soares, I.C., Mariani, B.M.d.P., Nishi, M.Y., Bezerra-Neto, J.E., Charchar, H.d.S., Brondani, V.B., Tanno, F., Srougi, V. and Chambo, J.L. 2020. Sterol O-acyl transferase 1 as a prognostic marker of adrenocortical carcinoma. *Cancers*. **12**(1), p247.

Laffitte, B.A., Joseph, S.B., Walczak, R., Pei, L., Wilpitz, D.C., Collins, J.L. and Tontonoz, P. 2001a. Autoregulation of the human liver X receptor alpha promoter. *Mol Cell Biol*. **21**(22), pp.7558-7568.

Laffitte, B.A., Repa, J.J., Joseph, S.B., Wilpitz, D.C., Kast, H.R., Mangelsdorf, D.J. and Tontonoz, P. 2001b. LXRs control lipid-inducible expression of the apolipoprotein E gene in macrophages and adipocytes. *Proceedings of the National Academy of Sciences of the United States of America*. **98**(2), pp.507-512.

Lakomy, D., Rébé, C., Sberna, A.L., Masson, D., Gautier, T., Chevriaux, A., Raveneau, M., Ogier, N., Nguyen, A.T., Gambert, P., Grober, J., Bonnotte, B., Solary, E. and Lagrost, L. 2009. Liver X receptor-mediated induction of cholesteryl ester transfer protein expression is selectively impaired in inflammatory macrophages. *Arterioscler Thromb Vasc Biol*. **29**(11), pp.1923-1929.

Lange, Y., Steck, T.L., Ye, J., Lanier, M.H., Molugu, V. and Ory, D. 2009. Regulation of fibroblast mitochondrial 27-hydroxycholesterol production by active plasma membrane cholesterol. *J Lipid Res*. **50**(9), pp.1881-1888.

Lappano, R., Recchia, A.G., De Francesco, E.M., Angelone, T., Cerra, M.C., Picard, D. and Maggiolini, M. 2011. The cholesterol metabolite 25-hydroxycholesterol activates estrogen receptor α -mediated signaling in cancer cells and in cardiomyocytes. *PloS one*. **6**(1), pe16631.

Lau, J., Ioannidis, J.P., Terrin, N., Schmid, C.H. and Olkin, I. 2006. The case of the misleading funnel plot. *Bmj*. **333**(7568), pp.597-600.

Lavie, O., Barnett-Griness, O., Narod, S. and Rennert, G. 2008. The risk of developing uterine sarcoma after tamoxifen use. *International Journal of Gynecologic Cancer*. **18**(2).

Lavinsky, R.M., Jepsen, K., Heinzl, T., Torchia, J., Mullen, T.-M., Schiff, R., Del-Rio, A.L., Ricote, M., Ngo, S. and Gemsch, J. 1998. Diverse signaling pathways modulate nuclear

receptor recruitment of N-CoR and SMRT complexes. *Proceedings of the National Academy of Sciences*. **95**(6), pp.2920-2925.

Lavrnja, I., Smiljanic, K., Savic, D., Mladenovic-Djordjevic, A., Tesovic, K., Kanazir, S. and Pekovic, S. 2017. Expression profiles of cholesterol metabolism-related genes are altered during development of experimental autoimmune encephalomyelitis in the rat spinal cord. *Scientific reports*. **7**(1), pp.1-14.

Le Cornet, C., Walter, B., Sookthai, D., Johnson, T.S., Kühn, T., Herpel, E., Kaaks, R. and Fortner, R.T. 2020. Circulating 27-hydroxycholesterol and breast cancer tissue expression of CYP27A1, CYP7B1, LXR- β , and ER β : results from the EPIC-Heidelberg cohort. *Breast Cancer Research*. **22**(1), pp.1-10.

Lee, H., Lee, H.J., Song, I.H., Bang, W.S., Heo, S.-H., Gong, G. and Park, I.A. 2018. CD11c-positive dendritic cells in triple-negative breast cancer. *in vivo*. **32**(6), pp.1561-1569.

Lee, H.J., Li, J., Vickman, R.E., Li, J., Liu, R., Durkes, A.C., Elzey, B.D., Yue, S., Liu, X., Ratliff, T.L. and Cheng, J.-X. 2018. Cholesterol Esterification Inhibition Suppresses Prostate Cancer Metastasis by Impairing the Wnt/ β -catenin Pathway. *Molecular cancer research : MCR*. **16**(6), pp.974-985.

Lee, J.H., Kim, H.M. and Koo, J.S. 2018. Differential Expression of Cancer-Associated Fibroblast-Related Proteins in Ductal Carcinoma in situ According to Molecular Subtype and Stromal Histology. *Pathobiology*. **85**(5-6), pp.311-321.

Lee, K.N., Jackson, K.W., Christiansen, V.J., Chung, K.H. and McKee, P.A. 2004. A novel plasma proteinase potentiates α 2-antiplasmin inhibition of fibrin digestion. *Blood*. **103**(10), pp.3783-3788.

Lee, L.J., Alexander, B., Schnitt, S.J., Comander, A., Gallagher, B., Garber, J.E. and Tung, N. 2011. Clinical outcome of triple negative breast cancer in BRCA1 mutation carriers and noncarriers. *Cancer*. **117**(14), pp.3093-3100.

Lee, S.S.-Y., Li, J., Tai, J.N., Ratliff, T.L., Park, K. and Cheng, J.-X. 2015. Avasimibe encapsulated in human serum albumin blocks cholesterol esterification for selective cancer treatment. *ACS nano*. **9**(3), pp.2420-2432.

Lehmann, Bauer, J.A., Chen, X., Sanders, M.E., Chakravarthy, A.B., Shyr, Y. and Pietsenpol, J.A. 2011. Identification of human triple-negative breast cancer subtypes and preclinical models for selection of targeted therapies. *The Journal of clinical investigation*. **121**(7), pp.2750-2767.

Lehmann, Kliewer, S.A., Moore, L.B., Smith-Oliver, T.A., Oliver, B.B., Su, J.-L., Sundseth, S.S., Winegar, D.A., Blanchard, D.E. and Spencer, T.A. 1997. Activation of the nuclear receptor LXR by oxysterols defines a new hormone response pathway. *Journal of Biological Chemistry*. **272**(6), pp.3137-3140.

Lehmann, J.M., Kliewer, S.A., Moore, L.B., Smith-Oliver, T.A., Oliver, B.B., Su, J.-L., Sundseth, S.S., Winegar, D.A., Blanchard, D.E. and Spencer, T.A. 1997. Activation of the nuclear receptor LXR by oxysterols defines a new hormone response pathway. *Journal of Biological Chemistry*. **272**(6), pp.3137-3140.

Lei, J., Wang, H., Zhu, D., Wan, Y. and Yin, L. 2020. Combined effects of avasimibe immunotherapy, doxorubicin chemotherapy, and metal-organic frameworks nanoparticles on breast cancer. *Journal of cellular physiology*. **235**(5), pp.4814-4823.

Leonessa, F. and Clarke, R. 2003. ATP binding cassette transporters and drug resistance in breast cancer. *Endocrine-related cancer*. **10**(1), pp.43-73.

Levy, D., de Melo, T.C., Oliveira, B.A., Paz, J.L., de Freitas, F.A., Reichert, C.O., Rodrigues, A. and Bydlowski, S.P. 2019. 7-Ketocholesterol and cholestane-triol increase expression of

- SMO and LXR α signaling pathways in a human breast cancer cell line. *Biochemistry and Biophysics Reports*. **19**, p100604.
- Li, C., Yang, L., Zhang, D. and Jiang, W. 2016. Systematic review and meta-analysis suggest that dietary cholesterol intake increases risk of breast cancer. *Nutrition Research*. **36**(7), pp.627-635.
- Li, J., Daly, E., Campioli, E., Wabitsch, M. and Papadopoulos, V. 2014. De novo synthesis of steroids and oxysterols in adipocytes. *Journal of Biological Chemistry*. **289**(2), pp.747-764.
- Li, J., Daly, E., Campioli, E., Wabitsch, M. and Papadopoulos, V. 2014. De novo synthesis of steroids and oxysterols in adipocytes. *J Biol Chem*. **289**(2), pp.747-764.
- Li, J., Gu, D., Lee, S.S.Y., Song, B., Bandyopadhyay, S., Chen, S., Konieczny, S.F., Ratliff, T.L., Liu, X., Xie, J. and Cheng, J.X. 2016. Abrogating cholesterol esterification suppresses growth and metastasis of pancreatic cancer. *Oncogene*. **35**(50), pp.6378-6388.
- Li, J., Qu, X., Tian, J., Zhang, J.-T. and Cheng, J.-X. 2018. Cholesterol esterification inhibition and gemcitabine synergistically suppress pancreatic ductal adenocarcinoma proliferation. *PLOS ONE*. **13**(2), pe0193318.
- Li, J., Ren, S., Piao, H.-l., Wang, F., Yin, P., Xu, C., Lu, X., Ye, G., Shao, Y. and Yan, M. 2016. Integration of lipidomics and transcriptomics unravels aberrant lipid metabolism and defines cholesteryl oleate as potential biomarker of prostate cancer. *Scientific reports*. **6**(1), pp.1-11.
- Li, K., Fazekasova, H., Wang, N., Sagoo, P., Peng, Q., Khamri, W., Gomes, C., Sacks, S.H., Lombardi, G. and Zhou, W. 2011. Expression of complement components, receptors and regulators by human dendritic cells. *Molecular immunology*. **48**(9-10), pp.1121-1127.
- Li, M., Yang, Y., Wei, J., Cun, X., Lu, Z., Qiu, Y., Zhang, Z. and He, Q. 2018. Enhanced chemo-immunotherapy against melanoma by inhibition of cholesterol esterification in CD8(+) T cells. *Nanomedicine*. **14**(8), pp.2541-2550.
- Li, X., Pandak, W.M., Erickson, S.K., Ma, Y., Yin, L., Hylemon, P. and Ren, S. 2007. Biosynthesis of the regulatory oxysterol, 5-cholesten-3 β , 25-diol 3-sulfate, in hepatocytes. *Journal of lipid research*. **48**(12), pp.2587-2596.
- Li, Y., Liang, Y., Sang, Y., Song, X., Zhang, H., Liu, Y., Jiang, L. and Yang, Q. 2018. MiR-770 suppresses the chemo-resistance and metastasis of triple negative breast cancer via direct targeting of STMN1. *Cell Death & Disease*. **9**(1), p14.
- Li-Hawkins, J., Lund, E.G., Bronson, A.D. and Russell, D.W. 2000. Expression cloning of an oxysterol 7 α -hydroxylase selective for 24-hydroxycholesterol. *Journal of Biological Chemistry*. **275**(22), pp.16543-16549.
- Lianto, P., Hutchinson, S.A., Moore, J.B., Hughes, T.A. and Thorne, J.L. 2021. Characterisation and prognostic value of LXR splice variants in triple negative breast cancer. *iScience*. p103212.
- Liaw A, G.R., Maechler M, Huber W, Warnes G. 2020. heatmap.2{gplots} R documentation: Enhanced Heat Map.
- Lin, Y.-C., Ma, C., Hsu, W.-C., Lo, H.-F. and Yang, V.C. 2007. Molecular interaction between caveolin-1 and ABCA1 on high-density lipoprotein-mediated cholesterol efflux in aortic endothelial cells. *Cardiovascular Research*. **75**(3), pp.575-583.
- Lindström, L.S., Yau, C., Czene, K., Thompson, C.K., Hoadley, K.A., van't Veer, L.J., Balassanian, R., Bishop, J.W., Carpenter, P.M., Chen, Y.-Y., Datnow, B., Hasteh, F., Krings, G., Lin, F., Zhang, Y., Nordenskjöld, B., Stål, O., Benz, C.C., Fornander, T., Borowsky, A.D., Esserman, L.J. and Group, S.T. 2018. Intratumor Heterogeneity of the Estrogen Receptor and

the Long-term Risk of Fatal Breast Cancer. *JNCI: Journal of the National Cancer Institute*. **110**(7), pp.726-733.

Linn, S., Giaccone, G., Van Diest, P., Blokhuis, W., van Der Valk, P., Van Kalken, C., Kuiper, C., Pinedo, H. and Baak, J. 1995. Prognostic relevance of P-glycoprotein expression in breast cancer. *Annals of Oncology*. **6**(7), pp.679-685.

Liu, C., Yang, X.V., Wu, J., Kuei, C., Mani, N.S., Zhang, L., Yu, J., Sutton, S.W., Qin, N. and Banie, H. 2011a. Oxysterols direct B-cell migration through EBI2. *Nature*. **475**(7357), pp.519-523.

Liu, C., Yang, X.V., Wu, J., Kuei, C., Mani, N.S., Zhang, L., Yu, J., Sutton, S.W., Qin, N. and Banie, H.J.N. 2011b. Oxysterols direct B-cell migration through EBI2. **475**(7357), p519.

Liu, J.Y., Fu, W.Q., Zheng, X.J., Li, W., Ren, L.W., Wang, J.H., Yang, C. and Du, G.H. 2021. Avasimibe exerts anticancer effects on human glioblastoma cells via inducing cell apoptosis and cell cycle arrest. *Acta Pharmacol Sin*. **42**(1), pp.97-107.

Liu, W., Chakraborty, B., Safi, R., Kazmin, D., Chang, C.-y. and McDonnell, D.P. 2021. Dysregulated cholesterol homeostasis results in resistance to ferroptosis increasing tumorigenicity and metastasis in cancer. *Nature Communications*. **12**(1), p5103.

Liu, Y., Wang, Y., Hao, S., Qin, Y. and Wu, Y. 2021. Knockdown of sterol O-acyltransferase 1 (SOAT1) suppresses SCD1-mediated lipogenesis and cancer procession in prostate cancer. *Prostaglandins & Other Lipid Mediators*. **153**, p106537.

Liu, Y., Wei, Z., Ma, X., Yang, X., Chen, Y., Sun, L., Ma, C., Miao, Q.R., Hajjar, D.P. and Han, J. 2018. 25-Hydroxycholesterol activates the expression of cholesterol 25-hydroxylase in an LXR-dependent mechanism. *Journal of lipid research*. **59**(3), pp.439-451.

Liu, Y., Wei, Z., Ma, X., Yang, X., Chen, Y., Sun, L., Ma, C., Miao, Q.R., Hajjar, D.P., Han, J. and Duan, Y. 2018. 25-Hydroxycholesterol activates the expression of cholesterol 25-hydroxylase in an LXR-dependent mechanism. *J Lipid Res*. **59**(3), pp.439-451.

Long, J., Chen, P., Lin, J., Bai, Y., Yang, X., Bian, J., Lin, Y., Wang, D., Yang, X. and Zheng, Y. 2019. DNA methylation-driven genes for constructing diagnostic, prognostic, and recurrence models for hepatocellular carcinoma. *Theranostics*. **9**(24), p7251.

Loos, M., Storz, R., Müller, W. and Lemmel, E.-M. 1981. Immunofluorescence studies on the subcomponents of the first component of complement (C1): detection of C1q and C1s in different cells of biopsy material and on human as well as on guinea pig peritoneal macrophages. *Immunobiology*. **158**(3), pp.213-224.

Lou, X., Toresson, G., Benod, C., Suh, J.H., Philips, K.J., Webb, P. and Gustafsson, J.-A. 2014. Structure of the retinoid X receptor α -liver X receptor β (RXR α -LXR β) heterodimer on DNA. *Nature structural & molecular biology*. **21**(3), pp.277-281.

Louault, K., Bonneaud, T.L., Séveno, C., Gomez-Bougie, P., Nguyen, F., Gautier, F., Bourgeois, N., Loussouarn, D., Kerdraon, O., Barillé-Nion, S., Jézéquel, P., Campone, M., Amiot, M., Juin, P.P. and Souazé, F. 2019. Interactions between cancer-associated fibroblasts and tumor cells promote MCL-1 dependency in estrogen receptor-positive breast cancers. *Oncogene*. **38**(17), pp.3261-3273.

Lu, D., Zhou, X., Yao, L., Liu, C., Jin, F. and Wu, Y. 2014. Clinical implications of the interleukin 27 serum level in breast cancer. *Journal of investigative medicine*. **62**(3), pp.627-631.

Lu, M., Hu, X.-H., Li, Q., Xiong, Y., Hu, G.-J., Xu, J.-J., Zhao, X.-N., Wei, X.-X., Chang, C.C.Y., Liu, Y.-K., Nan, F.-J., Li, J., Chang, T.-Y., Song, B.-L. and Li, B.-L. 2013. A specific cholesterol metabolic pathway is established in a subset of HCCs for tumor growth. *Journal of molecular cell biology*. **5**(6), pp.404-415.

- Lu, M., Hu, X.H., Li, Q., Xiong, Y., Hu, G.J., Xu, J.J., Zhao, X.N., Wei, X.X., Chang, C.C., Liu, Y.K., Nan, F.J., Li, J., Chang, T.Y., Song, B.L. and Li, B.L. 2013. A specific cholesterol metabolic pathway is established in a subset of HCCs for tumor growth. *J Mol Cell Biol.* **5**(6), pp.404-415.
- Lu, R., Hu, X., Zhou, J., Sun, J., Zhu, A.Z., Xu, X., Zheng, H., Gao, X., Wang, X. and Jin, H. 2016. COPS5 amplification and overexpression confers tamoxifen-resistance in ER α -positive breast cancer by degradation of NCoR. *Nature communications.* **7**(1), pp.1-13.
- Lu, R., Tsuboi, T., Okumura-Noji, K., Iwamoto, N. and Yokoyama, S. 2016. Caveolin-1 facilitates internalization and degradation of ABCA1 and probucol oxidative products interfere with this reaction to increase HDL biogenesis. *Atherosclerosis.* **253**, pp.54-60.
- Lund, E.G., Guileyardo, J.M. and Russell, D.W. 1999. cDNA cloning of cholesterol 24-hydroxylase, a mediator of cholesterol homeostasis in the brain. *Proceedings of the National Academy of Sciences.* **96**(13), pp.7238-7243.
- Lund, E.G., Kerr, T.A., Sakai, J., Li, W.P. and Russell, D.W. 1998. cDNA cloning of mouse and human cholesterol 25-hydroxylases, polytopic membrane proteins that synthesize a potent oxysterol regulator of lipid metabolism. *J Biol Chem.* **273**(51), pp.34316-34327.
- Luo, J., Hendryx, M., Manson, J.E., Figueiredo, J.C., LeBlanc, E.S., Barrington, W., Rohan, T.E., Howard, B.V., Reding, K., Ho, G.Y., Garcia, D.O. and Chlebowski, R.T. 2019. Intentional Weight Loss and Obesity-Related Cancer Risk. *JNCI Cancer Spectr.* **3**(4), ppkz054.
- Luo, Y., Liu, L., Li, X. and Shi, Y. 2020. Avasimibe inhibits the proliferation, migration and invasion of glioma cells by suppressing linc00339. *Biomedicine & Pharmacotherapy.* **130**, p110508.
- Luo, Y. and Tall, A.R. 2000. Sterol upregulation of human CETP expression in vitro and in transgenic mice by an LXR element. *J Clin Invest.* **105**(4), pp.513-520.
- Ma, Y., Wang, Y., Xu, Z., Wang, Y., Fallon, J.K. and Liu, F. 2017. Extreme low dose of 5-fluorouracil reverses MDR in cancer by sensitizing cancer associated fibroblasts and down-regulating P-gp. *PLoS One.* **12**(6), pe0180023.
- Mahmoud, S., Lee, A., Paish, E., Macmillan, R., Ellis, I. and Green, A. 2012. Tumour-infiltrating macrophages and clinical outcome in breast cancer. *Journal of clinical pathology.* **65**(2), pp.159-163.
- Mak, P.A., Laffitte, B.A., Desrumaux, C., Joseph, S.B., Curtiss, L.K., Mangelsdorf, D.J., Tontonoz, P. and Edwards, P.A. 2002. Regulated expression of the apolipoprotein E/C-I/C-IV/C-II gene cluster in murine and human macrophages. A critical role for nuclear liver X receptors alpha and beta. *J Biol Chem.* **277**(35), pp.31900-31908.
- Maksimenko, J., Irmejs, A., Nakazawa-Miklasevica, M., Melbarde-Gorkusa, I., Trofimovics, G., Gardovskis, J. and Miklasevics, E. 2014. Prognostic role of BRCA1 mutation in patients with triple-negative breast cancer. *Oncology letters.* **7**(1), pp.278-284.
- Manthravadi, S., Shrestha, A. and Madhusudhana, S. 2016. Impact of statin use on cancer recurrence and mortality in breast cancer: A systematic review and meta-analysis. *Int J Cancer.* **139**(6), pp.1281-1288.
- Mantovani, A., Sica, A., Sozzani, S., Allavena, P., Vecchi, A. and Locati, M. 2004. The chemokine system in diverse forms of macrophage activation and polarization. *Trends in immunology.* **25**(12), pp.677-686.
- Mantovani, A., Sozzani, S., Locati, M., Allavena, P. and Sica, A. 2002. Macrophage polarization: tumor-associated macrophages as a paradigm for polarized M2 mononuclear phagocytes. *Trends in immunology.* **23**(11), pp.549-555.

Mast, N., Anderson, K.W., Johnson, K.M., Phan, T.T.N., Guengerich, F.P. and Pikuleva, I.A. 2017a. In vitro cytochrome P450 46A1 (CYP46A1) activation by neuroactive compounds. *The Journal of biological chemistry*. **292**(31), pp.12934-12946.

Mast, N., Anderson, K.W., Lin, J.B., Li, Y., Turko, I.V., Tatsuoka, C., Bjorkhem, I. and Pikuleva, I.A. 2017b. Cytochrome P450 27A1 deficiency and regional differences in brain sterol metabolism cause preferential cholesterol accumulation in the cerebellum. *Journal of Biological Chemistry*. **292**(12), pp.4913-4924.

Mast, N., Lin, J.B. and Pikuleva, I.A. 2015. Marketed Drugs Can Inhibit Cytochrome P450 27A1, a Potential New Target for Breast Cancer Adjuvant Therapy. *Molecular pharmacology*. **88**(3), pp.428-436.

Masuda, H., Baggerly, K.A., Wang, Y., Zhang, Y., Gonzalez-Angulo, A.M., Meric-Bernstam, F., Valero, V., Lehmann, B.D., Pietenpol, J.A., Hortobagyi, G.N., Symmans, W.F. and Ueno, N.T. 2013. Differential response to neoadjuvant chemotherapy among 7 triple-negative breast cancer molecular subtypes. *Clinical cancer research : an official journal of the American Association for Cancer Research*. **19**(19), pp.5533-5540.

Matsumoto, K., Fujiwara, Y., Nagai, R., Yoshida, M. and Ueda, S. 2008. Expression of two isozymes of acyl-coenzyme A: cholesterol acyltransferase-1 and -2 in clear cell type renal cell carcinoma. *Int J Urol*. **15**(2), pp.166-170.

Mavaddat, N., Barrowdale, D., Andrulis, I.L., Domchek, S.M., Eccles, D., Nevanlinna, H., Ramus, S.J., Spurdle, A., Robson, M. and Sherman, M. 2012. Pathology of breast and ovarian cancers among BRCA1 and BRCA2 mutation carriers: results from the Consortium of Investigators of Modifiers of BRCA1/2 (CIMBA). *Cancer Epidemiology and Prevention Biomarkers*. **21**(1), pp.134-147.

Mechetner, E.B. and Roninson, I.B. 1992. Efficient inhibition of P-glycoprotein-mediated multidrug resistance with a monoclonal antibody. *Proceedings of the National Academy of Sciences*. **89**(13), pp.5824-5828.

Menegaz, R., Michelin, M., Etchebehere, R., Fernandes, P. and Murta, E. 2008. Peri- and intratumoral T and B lymphocytic infiltration in breast cancer. *European journal of gynaecological oncology*. **29**(4), p321.

Menke, J.G., Macnaul, K.L., Hayes, N.S., Baffic, J., Chao, Y.S., Elbrecht, A., Kelly, L.J., Lam, M.H., Schmidt, A., Sahoo, S., Wang, J., Wright, S.D., Xin, P., Zhou, G., Moller, D.E. and Sparrow, C.P. 2002. A novel liver X receptor agonist establishes species differences in the regulation of cholesterol 7 α -hydroxylase (CYP7 α). *Endocrinology*. **143**(7), pp.2548-2558.

Mentoor, I., Engelbrecht, A.-M., van de Vyver, M., van Jaarsveld, P.J. and Nell, T. 2021. The paracrine effects of adipocytes on lipid metabolism in doxorubicin-treated triple negative breast cancer cells. *Adipocyte*. **10**(1), pp.505-523.

Meuwese, M.C., de Groot, E., Duivenvoorden, R., Trip, M.D., Ose, L., Maritz, F.J., Basart, D.C.G., Kastelein, J.J.P., Habib, R., Davidson, M.H., Zwinderman, A.H., Schwocho, L.R., Stein, E.A. and Captivate Investigators, f.t. 2009. ACAT Inhibition and Progression of Carotid Atherosclerosis in Patients With Familial Hypercholesterolemia: The CAPTIVATE Randomized Trial. *JAMA*. **301**(11), pp.1131-1139.

Millar, E.K., Browne, L.H., Beretov, J., Lee, K., Lynch, J., Swarbrick, A. and Graham, P.H. 2020. Tumour Stroma Ratio Assessment Using Digital Image Analysis Predicts Survival in Triple Negative and Luminal Breast Cancer. *Cancers*. **12**(12), p3749.

Millis, S.Z., Gatalica, Z., Winkler, J., Vranic, S., Kimbrough, J., Reddy, S. and O'Shaughnessy, J.A. 2015. Predictive biomarker profiling of > 6000 breast cancer patients shows

- heterogeneity in TNBC, with treatment implications. *Clinical breast cancer*. **15**(6), pp.473-481. e473.
- Min, H.-K., Kapoor, A., Fuchs, M., Mirshahi, F., Zhou, H., Maher, J., Kellum, J., Warnick, R., Contos, Melissa J. and Sanyal, Arun J. 2012. Increased Hepatic Synthesis and Dysregulation of Cholesterol Metabolism Is Associated with the Severity of Nonalcoholic Fatty Liver Disease. *Cell Metabolism*. **15**(5), pp.665-674.
- Mittempergher, L., Saghatchian, M., Wolf, D.M., Michiels, S., Canisius, S., Dessen, P., Delalogue, S., Lazar, V., Benz, S.C. and Tursz, T. 2013. A gene signature for late distant metastasis in breast cancer identifies a potential mechanism of late recurrences. *Molecular oncology*. **7**(5), pp.987-999.
- Moestue, S.A., Borgan, E., Huuse, E.M., Lindholm, E.M., Sitter, B., Børresen-Dale, A.-L., Engebraaten, O., Mælandsmo, G.M. and Gribbestad, I.S. 2010. Distinct choline metabolic profiles are associated with differences in gene expression for basal-like and luminal-like breast cancer xenograft models. *BMC cancer*. **10**(1), p433.
- Moorman, A.M., Vink, R., Heijmans, H.J., van der Palen, J. and Kouwenhoven, E.A. 2012. The prognostic value of tumour-stroma ratio in triple-negative breast cancer. *European Journal of Surgical Oncology (EJSO)*. **38**(4), pp.307-313.
- Morisaki, M., Shikita, M. and Ikekawa, N. 1985. [20] Side-chain cleavage of cholesterol by gas chromatography-mass spectrometry in a selected ion monitoring mode. *Methods in Enzymology*. Academic Press, pp.352-364.
- Munajat, I., Zulmi, W., Norazman, M.Z. and Wan Faisham, W.I. 2008. Tumour volume and lung metastasis in patients with osteosarcoma. *J Orthop Surg (Hong Kong)*. **16**(2), pp.182-185.
- Muraro, E., Comaro, E., Talamini, R., Turchet, E., Miolo, G., Scalone, S., Militello, L., Lombardi, D., Spazzapan, S., Perin, T., Massarut, S., Crivellari, D., Dolcetti, R. and Martorelli, D. 2015. Improved Natural Killer cell activity and retained anti-tumor CD8+ T cell responses contribute to the induction of a pathological complete response in HER2-positive breast cancer patients undergoing neoadjuvant chemotherapy. *Journal of Translational Medicine*. **13**(1), p204.
- Nahta, R., Yu, D., Hung, M.-C., Hortobagyi, G.N. and Esteva, F.J. 2006. Mechanisms of disease: understanding resistance to HER2-targeted therapy in human breast cancer. *Nature clinical practice Oncology*. **3**(5), pp.269-280.
- Naing, A., Fu, S., Habra, M.A., Chugh, R., Kebebew, E., Russell, J., Welshans, D., Fassnacht, M., Kroiss, M. and Goebeler, M.-E. 2015. *ATR-101 phase 1 clinical study for adrenocortical carcinoma*. American Society of Clinical Oncology.
- Naito, A.T., Sumida, T., Nomura, S., Liu, M.-L., Higo, T., Nakagawa, A., Okada, K., Sakai, T., Hashimoto, A. and Hara, Y. 2012. Complement C1q activates canonical Wnt signaling and promotes aging-related phenotypes. *Cell*. **149**(6), pp.1298-1313.
- Nakasone, E.S., Askautrud, H.A., Kees, T., Park, J.-H., Plaks, V., Ewald, A.J., Fein, M., Rasch, M.G., Tan, Y.-X. and Qiu, J. 2012. Imaging tumor-stroma interactions during chemotherapy reveals contributions of the microenvironment to resistance. *Cancer cell*. **21**(4), pp.488-503.
- Nelson, E.R., Wardell, S.E., Jasper, J.S., Park, S., Suchindran, S., Howe, M.K., Carver, N.J., Pillai, R.V., Sullivan, P.M. and Sondhi, V. 2013. 27-Hydroxycholesterol links hypercholesterolemia and breast cancer pathophysiology. *Science*. **342**(6162), pp.1094-1098.
- Nelson, E.R., Wardell, S.E., Jasper, J.S., Park, S., Suchindran, S., Howe, M.K., Carver, N.J., Pillai, R.V., Sullivan, P.M., Sondhi, V., Umetani, M., Geradts, J. and McDonnell, D.P. 2013. 27-

Hydroxycholesterol links hypercholesterolemia and breast cancer pathophysiology. *Science*. **342**(6162), pp.1094-1098.

Nieman, K.M., Romero, I.L., Van Houten, B. and Lengyel, E. 2013. Adipose tissue and adipocytes support tumorigenesis and metastasis. *Biochimica et Biophysica Acta (BBA)-Molecular and Cell Biology of Lipids*. **1831**(10), pp.1533-1541.

Noblejas-López, M.d.M., Morcillo-García, S., Nieto-Jiménez, C., Nuncia-Cantarero, M., Gyórfy, B., Galan-Moya, E.M., Pandiella, A. and Ocaña, A. 2018. Evaluation of transcriptionally regulated genes identifies NCOR1 in hormone receptor negative breast tumors and lung adenocarcinomas as a potential tumor suppressor gene. *PloS one*. **13**(11), pe0207776.

Nong, C., Zou, M., Xue, R., Bai, L., Liu, L., Jiang, Z., Sun, L., Huang, X., Zhang, L. and Wang, X. 2020. The role of invariant natural killer T cells in experimental xenobiotic-induced cholestatic hepatotoxicity. *Biomedicine & Pharmacotherapy*. **122**, p109579.

Norlin, M., Toll, A., Björkhem, I. and Wikvall, K. 2000. 24-Hydroxycholesterol is a substrate for hepatic cholesterol 7 α -hydroxylase (CYP7A). *Journal of lipid research*. **41**(10), pp.1629-1639.

Norlin, M., von Bahr, S., Björkhem, I. and Wikvall, K. 2003a. On the substrate specificity of human CYP27A1 implications for bile acid and cholestanol formation. *Journal of lipid research*. **44**(8), pp.1515-1522.

Norlin, M., von Bahr, S., Björkhem, I. and Wikvall, K. 2003b. On the substrate specificity of human CYP27A1: implications for bile acid and cholestanol formation. *Journal of lipid research*. **44**(8), pp.1515-1522.

Nowakowska, M.K., Lei, X., Thompson, M.T., Shaitelman, S.F., Wehner, M.R., Woodward, W.A., Giordano, S.H. and Nead, K.T. 2021. Association of statin use with clinical outcomes in patients with triple-negative breast cancer. *Cancer*. **127**(22), pp.4142-4150.

O'Leary, J.G., Goodarzi, M., Drayton, D.L. and von Andrian, U.H. 2006. T cell- and B cell-independent adaptive immunity mediated by natural killer cells. *Nat Immunol*. **7**(5), pp.507-516.

Ohshiro, T., Matsuda, D., Sakai, K., Degirolamo, C., Yagyu, H., Rudel, L.L., Ōmura, S., Ishibashi, S. and Tomoda, H. 2011. Pyripyropene A, an acyl-coenzyme A: cholesterol acyltransferase 2-selective inhibitor, attenuates hypercholesterolemia and atherosclerosis in murine models of hyperlipidemia. *Arteriosclerosis, thrombosis, and vascular biology*. **31**(5), pp.1108-1115.

Oishi, Y., Spann, N.J., Link, V.M., Muse, E.D., Strid, T., Edillor, C., Kolar, M.J., Matsuzaka, T., Hayakawa, S. and Tao, J. 2017. SREBP1 contributes to resolution of pro-inflammatory TLR4 signaling by reprogramming fatty acid metabolism. *Cell metabolism*. **25**(2), pp.412-427.

Oka, H., Emori, Y., Hayashi, Y. and Nomoto, K. 2000. Breakdown of Th cell immune responses and steroidogenic CYP11A1 expression in CD4+ T cells in a murine model implanted with B16 melanoma. *Cellular immunology*. **206**(1), pp.7-15.

Olsen, C.J., Moreira, J., Lukanidin, E.M. and Ambartsumian, N.S. 2010. Human mammary fibroblasts stimulate invasion of breast cancer cells in a three-dimensional culture and increase stroma development in mouse xenografts. *BMC Cancer*. **10**, p444.

Olsson, J.M., Eriksson, L.C. and Dallner, G. 1991. Lipid compositions of intracellular membranes isolated from rat liver nodules in Wistar rats. *Cancer research*. **51**(14), pp.3774-3780.

Oni, T.E., Biffi, G., Baker, L.A., Hao, Y., Tonelli, C., Somerville, T.D., Deschênes, A., Belleau, P., Hwang, C.-i. and Sánchez-Rivera, F.J. 2020. SOAT1 promotes mevalonate pathway dependency in pancreatic cancer. *Journal of Experimental Medicine*. **217**(9).

Oni, T.E., Biffi, G., Baker, L.A., Hao, Y., Tonelli, C., Somerville, T.D.D., Deschênes, A., Belleau, P., Hwang, C.I., Sánchez-Rivera, F.J., Cox, H., Brosnan, E., Doshi, A., Lumia, R.P., Khaledi, K., Park, Y., Trotman, L.C., Lowe, S.W., Krasnitz, A., Vakoc, C.R. and Tuveson, D.A. 2020. SOAT1 promotes mevalonate pathway dependency in pancreatic cancer. *J Exp Med*. **217**(9).

Onitilo, A.A., Engel, J.M., Greenlee, R.T. and Mukesh, B.N. 2009. Breast cancer subtypes based on ER/PR and Her2 expression: comparison of clinicopathologic features and survival. *Clinical medicine & research*. **7**(1-2), pp.4-13.

Oshi, M., Asaoka, M., Tokumaru, Y., Angarita, F.A., Yan, L., Matsuyama, R., Zsiros, E., Ishikawa, T., Endo, I. and Takabe, K. 2020. Abundance of regulatory T cell (Treg) as a predictive biomarker for neoadjuvant chemotherapy in triple-negative breast cancer. *Cancers*. **12**(10), p3038.

Ou, Z., Wada, T., Gramignoli, R., Li, S., Strom, S.C., Huang, M. and Xie, W. 2011. MicroRNA hsa-miR-613 Targets the Human LXR α Gene and Mediates a Feedback Loop of LXR α Autoregulation. *Molecular endocrinology*. **25**(4), pp.584-596.

Ouyang, G., Yi, B., Pan, G. and Chen, X. 2020. A robust twelve-gene signature for prognosis prediction of hepatocellular carcinoma. *Cancer Cell International*. **20**, pp.1-18.

Özmen, H.K. and Askin, S. 2013. Lecithin: cholesterol acyltransferase and Na⁺-K⁺-ATPase activity in patients with breast cancer. *Journal of breast cancer*. **16**(2), pp.159-163.

Pan, J., Zhang, Q., Palen, K., Wang, L., Qiao, L., Johnson, B., Sei, S., Shoemaker, R.H., Lubet, R.A., Wang, Y. and You, M. 2019. Potentiation of Kras peptide cancer vaccine by avasimibe, a cholesterol modulator. *EBioMedicine*. **49**, pp.72-81.

Pan, Y., Yuan, Y., Liu, G. and Wei, Y. 2017. P53 and Ki-67 as prognostic markers in triple-negative breast cancer patients. *PLoS One*. **12**(2), pe0172324.

Park, H.-M., Kim, H., Kim, D.W., Yoon, J.-H., Kim, B.-G. and Cho, J.-Y. 2020. Common plasma protein marker LCAT in aggressive human breast cancer and canine mammary tumor. *BMB reports*. **53**(12), p664.

Park, S., Shimizu, C., Shimoyama, T., Takeda, M., Ando, M., Kohno, T., Katsumata, N., Kang, Y.-K., Nishio, K. and Fujiwara, Y. 2006. Gene expression profiling of ATP-binding cassette (ABC) transporters as a predictor of the pathologic response to neoadjuvant chemotherapy in breast cancer patients. *Breast cancer research and treatment*. **99**(1), pp.9-17.

Park, S.Y., Kim, H.M. and Koo, J.S. 2015. Differential expression of cancer-associated fibroblast-related proteins according to molecular subtype and stromal histology in breast cancer. *Breast cancer research and treatment*. **149**(3), pp.727-741.

Parker, J.S., Mullins, M., Cheang, M.C., Leung, S., Voduc, D., Vickery, T., Davies, S., Fauron, C., He, X. and Hu, Z. 2009. Supervised risk predictor of breast cancer based on intrinsic subtypes. *Journal of clinical oncology*. **27**(8), p1160.

Pasanen, I., Lehtonen, S., Sormunen, R., Skarp, S., Lehtilahti, E., Pietilä, M., Sequeiros, R.B., Lehenkari, P. and Kuvaja, P. 2016. Breast cancer carcinoma-associated fibroblasts differ from breast fibroblasts in immunological and extracellular matrix regulating pathways. *Experimental cell research*. **344**(1), pp.53-66.

Pattanayak, S.P., Sunita, P. and Mazumder, P.M. 2014. Restorative effect of *Dendrophthoe falcata* (Lf) Ettingsh on lipids, lipoproteins, and lipid-metabolizing enzymes in DMBA-induced mammary gland carcinogenesis in Wistar female rats. *Comparative Clinical Pathology*. **23**(4), pp.1013-1022.

Paulus, P., Stanley, E.R., Schäfer, R., Abraham, D. and Aharinejad, S. 2006. Colony-stimulating factor-1 antibody reverses chemoresistance in human MCF-7 breast cancer xenografts. *Cancer research*. **66**(8), pp.4349-4356.

Pelon, F., Bourachot, B., Kieffer, Y., Magagna, I., Mermet-Meillon, F., Bonnet, I., Costa, A., Givel, A.-M., Attieh, Y., Barbazan, J., Bonneau, C., Fuhrmann, L., Descroix, S., Vignjevic, D., Silberzan, P., Parrini, M.C., Vincent-Salomon, A. and Mehta-Grigoriou, F. 2020. Cancer-associated fibroblast heterogeneity in axillary lymph nodes drives metastases in breast cancer through complementary mechanisms. *Nature Communications*. **11**(1), p404.

Peng, X.-X., Tiwari, A.K., Wu, H.-C. and Chen, Z.-S. 2012. Overexpression of P-glycoprotein induces acquired resistance to imatinib in chronic myelogenous leukemia cells. *Chinese journal of cancer*. **31**(2), pp.110-118.

Phung, M.T., Tin, S.T. and Elwood, J.M. 2019. Prognostic models for breast cancer: a systematic review. *BMC cancer*. **19**(1), p230.

Pikuleva, I.A., Babiker, A., Waterman, M.R. and Björkhem, I. 1998. Activities of recombinant human cytochrome P450c27 (CYP27) which produce intermediates of alternative bile acid biosynthetic pathways. *Journal of Biological Chemistry*. **273**(29), pp.18153-18160.

Plat, J., Nichols, J.A. and Mensink, R.P. 2005. Plant sterols and stanols: effects on mixed micellar composition and LXR (target gene) activation. *Journal of lipid research*. **46**(11), pp.2468-2476.

Playdon, M.C., Bracken, M.B., Sanft, T.B., Ligibel, J.A., Harrigan, M. and Irwin, M.L. 2015. Weight gain after breast cancer diagnosis and all-cause mortality: systematic review and meta-analysis. *JNCI: Journal of the National Cancer Institute*. **107**(12).

Pommier, A., Alves, G., Viennois, E., Bernard, S., Communal, Y., Sion, B., Marceau, G., Damon, C., Mouzat, K. and Caira, F. 2010. Liver X Receptor activation downregulates AKT survival signaling in lipid rafts and induces apoptosis of prostate cancer cells. *Oncogene*. **29**(18), pp.2712-2723.

Popiolek, M., Izumi, Y., Hopper, A.T., Dai, J., Miller, S., Shu, H.-J., Zorumski, C.F. and Mennerick, S. 2020. Effects of CYP46A1 inhibition on long-term-depression in hippocampal slices ex vivo and 24S-hydroxycholesterol levels in mice in vivo. *Frontiers in molecular neuroscience*. **13**.

Prat, A., Parker, J.S., Karginova, O., Fan, C., Livasy, C., Herschkowitz, J.I., He, X. and Perou, C.M. 2010. Phenotypic and molecular characterization of the claudin-low intrinsic subtype of breast cancer. *Breast Cancer Research*. **12**(5), pR68.

Preuss, I., Ludwig, M.-G., Baumgarten, B., Bassilana, F., Gessier, F., Seuwen, K. and Sailer, A.W. 2014. Transcriptional regulation and functional characterization of the oxysterol/EBI2 system in primary human macrophages. *Biochemical and Biophysical Research Communications*. **446**(3), pp.663-668.

Protani, M., Coory, M. and Martin, J.H. 2010. Effect of obesity on survival of women with breast cancer: systematic review and meta-analysis. *Breast Cancer Research and Treatment*. **123**(3), pp.627-635.

Qian, H.W., Zhao, X., Yan, R.H., Yao, X., Gao, S., Sun, X., Du, X.M., Yang, H.Y., Wong, C.C.L. and Yan, N. 2020. Structural basis for catalysis and substrate specificity of human ACAT1. *Nature*. **581**(7808), pp.333-+.

Qin, Y.-Y., Li, H., Guo, X.-J., Ye, X.-F., Wei, X., Zhou, Y.-H., Zhang, X.-J., Wang, C., Qian, W. and Lu, J. 2011. Adjuvant chemotherapy, with or without taxanes, in early or operable breast cancer: a meta-analysis of 19 randomized trials with 30698 patients. *PLoS One*. **6**(11), pe26946.

Qiu, Y., Wang, J., Lei, J. and Roeder, K. 2021. Identification of cell-type-specific marker genes from co-expression patterns in tissue samples. *Bioinformatics*. **37**(19), pp.3228-3234.

Raal, F.J., Marais, A.D., Klepack, E., Lovalvo, J., McLain, R. and Heinonen, T. 2003. Avasimibe, an ACAT inhibitor, enhances the lipid lowering effect of atorvastatin in subjects with homozygous familial hypercholesterolemia. *Atherosclerosis*. **171**(2), pp.273-279.

Rakha, E.A., Reis-Filho, J.S., Baehner, F., Dabbs, D.J., Decker, T., Eusebi, V., Fox, S.B., Ichihara, S., Jacquemier, J. and Lakhani, S.R. 2010. Breast cancer prognostic classification in the molecular era: the role of histological grade. *Breast cancer research*. **12**(4), pp.1-12.

Rakovitch, E., Nofech-Mozes, S., Hanna, W., Narod, S., Thiruchelvam, D., Saskin, R., Spayne, J., Taylor, C. and Paszat, L. 2012. HER2/neu and Ki-67 expression predict non-invasive recurrence following breast-conserving therapy for ductal carcinoma in situ. *British Journal of Cancer*. **106**(6), pp.1160-1165.

Ramirez, M.I., Millien, G., Hinds, A., Cao, Y., Seldin, D.C. and Williams, M.C. 2003. T1 α , a lung type I cell differentiation gene, is required for normal lung cell proliferation and alveolus formation at birth. *Developmental Biology*. **256**(1), pp.62-73.

Rayes, J., Lax, S., Wichaiyo, S., Watson, S.K., Di, Y., Lombard, S., Grygielska, B., Smith, S.W., Skordilis, K. and Watson, S.P. 2017. The podoplanin-CLEC-2 axis inhibits inflammation in sepsis. *Nature Communications*. **8**(1), p2239.

Reid, K. 1986. Activation and control of the complement system. *Essays in biochemistry*. **22**, pp.27-68.

Ren, J., Franklin, E.T. and Xia, Y. 2017. Uncovering structural diversity of unsaturated fatty acyls in cholesteryl esters via photochemical reaction and tandem mass spectrometry. *Journal of The American Society for Mass Spectrometry*. **28**(7), pp.1432-1441.

Ren, M., Xu, H., Xia, H., Tang, Q. and Bi, F. 2021. Simultaneously targeting SOAT1 and CPT1A ameliorates hepatocellular carcinoma by disrupting lipid homeostasis. *Cell death discovery*. **7**(1), pp.1-15.

Reome, J.B., Hylind, J.C., Dutton, R.W. and Dobrzanski, M.J. 2004. Type 1 and type 2 tumor infiltrating effector cell subpopulations in progressive breast cancer. *Clinical immunology*. **111**(1), pp.69-81.

Repa, J.J. and Mangelsdorf, D.J. 2000. The role of orphan nuclear receptors in the regulation of cholesterol homeostasis. *Annual review of cell and developmental biology*. **16**(1), pp.459-481.

Richardsen, E., Uglehus, R., Due, J., Busch, C. and Busund, L.T. 2008. The prognostic impact of M-CSF, CSF-1 receptor, CD68 and CD3 in prostatic carcinoma. *Histopathology*. **53**(1), pp.30-38.

Riihilä, P., Viikklepp, K., Nissinen, L., Farshchian, M., Kallajoki, M., Kivisaari, A., Meri, S., Peltonen, J., Peltonen, S. and Kähäri, V.M. 2020. Tumour-cell-derived complement components C1r and C1s promote growth of cutaneous squamous cell carcinoma. *British Journal of Dermatology*. **182**(3), pp.658-670.

Roberg-Larsen, H., Lund, K., Seterdal, K.E., Solheim, S., Vehus, T., Solberg, N., Krauss, S., Lundanes, E. and Wilson, S.R. 2017. Mass spectrometric detection of 27-hydroxycholesterol in breast cancer exosomes. *The Journal of steroid biochemistry and molecular biology*. **169**, pp.22-28.

Rody, A., Holtrich, U., Pusztai, L., Liedtke, C., Gaetje, R., Ruckhaeberle, E., Solbach, C., Hanker, L., Ahr, A., Metzler, D., Engels, K., Karn, T. and Kaufmann, M. 2009. T-cell metagene predicts a favorable prognosis in estrogen receptor-negative and HER2-positive breast cancers. *Breast Cancer Research*. **11**(2), pR15.

Ronco, A., De Stefani, E., Boffetta, P., Deneo-Pellegrini, H., Mendilaharsu, M. and Leborgne, F. 1999. Vegetables, fruits, and related nutrients and risk of breast cancer: a case-control study in Uruguay. *Nutrition and cancer*. **35**(2), pp.111-119.

Rosenau, W. and Moon, H.D. 1961. Lysis of homologous cells by sensitized lymphocytes in tissue culture. *Journal of the National Cancer Institute*. **27**(2), pp.471-483.

Rothberg, K.G., Heuser, J.E., Donzell, W.C., Ying, Y.-S., Glenney, J.R. and Anderson, R.G. 1992. Caveolin, a protein component of caveolae membrane coats. *Cell*. **68**(4), pp.673-682.

Roumenina, L.T., Daugan, M.V., Noé, R., Petitprez, F., Vano, Y.A., Sanchez-Salas, R., Becht, E., Meilleroux, J., Le Clec'h, B. and Giraldo, N.A. 2019. Tumor cells hijack macrophage-produced complement C1q to promote tumor growth. *Cancer immunology research*. **7**(7), pp.1091-1105.

Rousset, X., Vaisman, B., Amar, M., Sethi, A.A. and Remaley, A.T. 2009. Lecithin: cholesterol acyltransferase: from biochemistry to role in cardiovascular disease. *Current opinion in endocrinology, diabetes, and obesity*. **16**(2), p163.

Rowe, A.H., Armann, C.A., Edwards, J.Y., Sawyez, C.G., Morand, O.H., Hegele, R.A. and Huff, M.W. 2003. Enhanced synthesis of the oxysterol 24 (S), 25-epoxycholesterol in macrophages by inhibitors of 2, 3-oxidosqualene: lanosterol cyclase: a novel mechanism for the attenuation of foam cell formation. *Circulation research*. **93**(8), pp.717-725.

Ruggieri, S. and Fallani, A. 1979. Lipid composition of Yoshida ascites hepatoma and of livers and blood plasma from host and normal rats. *Lipids*. **14**(4), pp.323-333.

Ruggieri, S., Fallani, A. and Tombaccini, D. 1976. Effect of essential fatty acid deficiency on the lipid composition of the Yoshida ascites hepatoma (AH 130) and of the liver and blood plasma from host and normal rats. *Journal of lipid research*. **17**(5), pp.456-466.

Rühl, R., Krzyżosiak, A., Niewiadomska-Cimicka, A., Rochel, N., Szeles, L., Vaz, B., Wietrzych-Schindler, M., Álvarez, S., Szklenar, M., Nagy, L., de Lera, A.R. and Krężel, W. 2015. 9-cis-13,14-Dihydroretinoic Acid Is an Endogenous Retinoid Acting as RXR Ligand in Mice. *PLoS genetics*. **11**(6), pp.e1005213-e1005213.

Russo, L., Muir, L., Geletka, L., Delproposto, J., Baker, N., Flesher, C., O'Rourke, R. and Lumeng, C.N. 2020. Cholesterol 25-hydroxylase (CH25H) as a promoter of adipose tissue inflammation in obesity and diabetes. *Molecular metabolism*. **39**, p100983.

Rye, I.H., Trinh, A., Sætersdal, A.B., Nebdal, D., Lingjærde, O.C., Almendro, V., Polyak, K., Børresen-Dale, A.L., Helland, Å. and Markowitz, F. 2018. Intratumor heterogeneity defines treatment-resistant HER 2+ breast tumors. *Molecular oncology*. **12**(11), pp.1838-1855.

Sabatier, R., Finetti, P., Guille, A., Adelaide, J., Chaffanet, M., Viens, P., Birnbaum, D. and Bertucci, F. 2014. Claudin-low breast cancers: clinical, pathological, molecular and prognostic characterization. *Molecular Cancer*. **13**(1), p228.

Sahi, J., Milad, M.A., Zheng, X., Rose, K.A., Wang, H., Stilgenbauer, L., Gilbert, D., Jolley, S., Stern, R.H. and LeCluyse, E.L. 2003. Avasimibe induces CYP3A4 and multiple drug resistance protein 1 gene expression through activation of the pregnane X receptor. *Journal of Pharmacology and Experimental Therapeutics*. **306**(3), pp.1027-1034.

Saint-Pol, J., Candela, P., Boucau, M.-C., Fenart, L. and Gosselet, F. 2013. Oxysterols decrease apical-to-basolateral transport of Aβ peptides via an ABCB1-mediated process in an in vitro Blood-brain barrier model constituted of bovine brain capillary endothelial cells. *Brain research*. **1517**, pp.1-15.

Santana, M.A. and Esquivel-Guadarrama, F. 2006. Cell Biology of T Cell Activation and Differentiation. *International Review of Cytology*. Academic Press, pp.217-274.

Saucier, S.E., Kandutsch, A., Taylor, F.R., Spencer, T., Phirwa, S. and Gayen, A. 1985. Identification of regulatory oxysterols, 24 (S), 25-epoxycholesterol and 25-hydroxycholesterol, in cultured fibroblasts. *Journal of Biological Chemistry*. **260**(27), pp.14571-14579.

Saucier, S.E., Kandutsch, A.A., Taylor, F.R., Spencer, T.A., Phirwa, S. and Gayen, A.K. 1985. Identification of regulatory oxysterols, 24(S),25-epoxycholesterol and 25-hydroxycholesterol, in cultured fibroblasts. *J Biol Chem*. **260**(27), pp.14571-14579.

Sawada, N., Sakaki, T., Ohta, M. and Inouye, K. 2000. Metabolism of vitamin D3 by human CYP27A1. *Biochemical and biophysical research communications*. **273**(3), pp.977-984.

Sawyers, C.L. 1999. Chronic myeloid leukemia. *New England Journal of Medicine*. **340**(17), pp.1330-1340.

Scarlett, U.K., Rutkowski, M.R., Rauwerdink, A.M., Fields, J., Escovar-Fadul, X., Baird, J., Cubillos-Ruiz, J.R., Jacobs, A.C., Gonzalez, J.L. and Weaver, J.J.J.o.E.M. 2012. Ovarian cancer progression is controlled by phenotypic changes in dendritic cells. **209**(3), pp.495-506.

Schacht, V., Ramirez, M.I., Hong, Y.K., Hirakawa, S., Feng, D., Harvey, N., Williams, M., Dvorak, A.M., Dvorak, H.F., Oliver, G. and Detmar, M. 2003. T1alpha/podoplanin deficiency disrupts normal lymphatic vasculature formation and causes lymphedema. *Embo j*. **22**(14), pp.3546-3556.

Schatteman, G.C., Morrison-Graham, K., van Koppen, A., Weston, J.A. and Bowen-Pope, D.F. 1992. Regulation and role of PDGF receptor alpha-subunit expression during embryogenesis. *Development*. **115**(1), pp.123-131.

Schiraldi, M., Raucci, A., Muñoz, L.M., Livoti, E., Celona, B., Venereau, E., Apuzzo, T., De Marchis, F., Pedotti, M., Bachi, A., Thelen, M., Varani, L., Mellado, M., Proudfoot, A., Bianchi, M.E. and Ugucioni, M. 2012. HMGB1 promotes recruitment of inflammatory cells to damaged tissues by forming a complex with CXCL12 and signaling via CXCR4. *The Journal of experimental medicine*. **209**(3), pp.551-563.

Segala, G., David, M., de Medina, P., Poirot, M.C., Serhan, N., Vergez, F., Mougel, A., Saland, E., Carayon, K. and Leignadier, J. 2017. Dendrogenin A drives LXR to trigger lethal autophagy in cancers. *Nature communications*. **8**(1), pp.1-17.

Sevov, M., Elfineh, L. and Cavelier, L.B. 2006. Resveratrol regulates the expression of LXR- α in human macrophages. *Biochemical and biophysical research communications*. **348**(3), pp.1047-1054.

Shang, L., Hattori, M., Fleming, G., Jaskowiak, N., Hedeker, D., Olopade, O.I. and Huo, D. 2021. Impact of post-diagnosis weight change on survival outcomes in Black and White breast cancer patients. *Breast Cancer Research*. **23**(1), p18.

Shao, W., Kuhn, C., Mayr, D., Ditsch, N., Kailuwait, M., Wolf, V., Harbeck, N., Mahner, S., Jeschke, U. and Cavaillès, V. 2021. Cytoplasmic LXR expression is an independent marker of poor prognosis for patients with early stage primary breast cancer. *Journal of Cancer Research and Clinical Oncology*. pp.1-10.

Sheng, X., Parmentier, J.-H., Tucci, J., Pei, H., Cortez-Toledo, O., Dieli-Conwright, C.M., Oberley, M.J., Neely, M., Orgel, E. and Louie, S.G. 2017. Adipocytes sequester and metabolize the chemotherapeutic daunorubicin. *Molecular Cancer Research*.

Shepherd, J.H., Hyslop, T., Fan, C., Martinez, A.F., Parker, J., Hoadley, K., Hu, Z., Li, Y., Soloway, M. and Spears, P. 2021. *Abstract PD9-03: Genomic analysis of the CALGB 40603 (Alliance) neoadjuvant trial in TNBC identifies immune features associated with pathological complete response and event-free survival*. AACR.

Shi, S.-Z., Lee, E.-J., Lin, Y.-J., Chen, L., Zheng, H.-Y., He, X.-Q., Peng, J.-Y., Noonepalle, S.K., Shull, A.Y., Pei, F.C., Deng, L.-B., Tian, X.-L., Deng, K.-Y., Shi, H. and Xin, H.-B. 2019. Recruitment of monocytes and epigenetic silencing of intratumoral CYP7B1 primarily contribute to the accumulation of 27-hydroxycholesterol in breast cancer. *American journal of cancer research*. **9**(10), pp.2194-2208.

Shinde, A.V., Humeres, C. and Frangogiannis, N.G. 2017. The role of α -smooth muscle actin in fibroblast-mediated matrix contraction and remodeling. *Biochimica et biophysica acta. Molecular basis of disease*. **1863**(1), pp.298-309.

Sigmundsdottir, H., Pan, J., Debes, G.F., Alt, C., Habtezion, A., Soler, D. and Butcher, E.C. 2007. DCs metabolize sunlight-induced vitamin D3 to 'program' T cell attraction to the epidermal chemokine CCL27. *Nature immunology*. **8**(3), p285.

Sjöström, M., Lundstedt, D., Hartman, L., Holmberg, E., Killander, F., Kovács, A., Malmström, P., Niméus, E., Rönnerman, E.W. and Fernö, M. 2017. Response to radiotherapy after breast-conserving surgery in different breast cancer subtypes in the swedish breast cancer group 91 radiotherapy randomized clinical trial. *Journal of Clinical Oncology*. **35**(28), pp.3222-3229.

Smeland, H.Y.H., Askeland, C., Wik, E., Knutsvik, G., Molven, A., Edelmann, R.J., Reed, R.K., Warren, D.J., Gullberg, D. and Stuhr, L. 2020. Integrin $\alpha 11\beta 1$ is expressed in breast cancer stroma and associates with aggressive tumor phenotypes. *The Journal of Pathology: Clinical Research*. **6**(1), pp.69-82.

Smith, D.C., Kroiss, M., Kebebew, E., Habra, M.A., Chugh, R., Schneider, B.J., Fassnacht, M., Jafarinasabian, P., Ijzerman, M.M. and Lin, V.H. 2020a. A phase 1 study of nevanimibe HCl, a novel adrenal-specific sterol O-acyltransferase 1 (SOAT1) inhibitor, in adrenocortical carcinoma. *Investigational New Drugs*. pp.1-9.

Smith, D.C., Kroiss, M., Kebebew, E., Habra, M.A., Chugh, R., Schneider, B.J., Fassnacht, M., Jafarinasabian, P., Ijzerman, M.M. and Lin, V.H. 2020b. A phase 1 study of nevanimibe HCl, a novel adrenal-specific sterol O-acyltransferase 1 (SOAT1) inhibitor, in adrenocortical carcinoma. *Investigational new drugs*. **38**(5), pp.1421-1429.

Smith, D.C., Kroiss, M., Kebebew, E., Habra, M.A., Chugh, R., Schneider, B.J., Fassnacht, M., Jafarinasabian, P., Ijzerman, M.M., Lin, V.H., Mohideen, P. and Naing, A. 2020. A phase 1 study of nevanimibe HCl, a novel adrenal-specific sterol O-acyltransferase 1 (SOAT1) inhibitor, in adrenocortical carcinoma. *Investigational New Drugs*. **38**(5), pp.1421-1429.

Smith, I.E., Dowsett, M., Ebbs, S.R., Dixon, J.M., Skene, A., Blohmer, J.U., Ashley, S.E., Francis, S., Boeddinghaus, I. and Walsh, G. 2005. Neoadjuvant treatment of postmenopausal breast cancer with anastrozole, tamoxifen, or both in combination: the Immediate Preoperative Anastrozole, Tamoxifen, or Combined with Tamoxifen (IMPACT) multicenter double-blind randomized trial. *J Clin Oncol*. **23**(22), pp.5108-5116.

Solheim, S., Hutchinson, S.A., Lundanes, E., Wilson, S.R., Thorne, J.L. and Roberg-Larsen, H. 2019. Fast liquid chromatography-mass spectrometry reveals side chain oxysterol heterogeneity in breast cancer tumour samples. *The Journal of steroid biochemistry and molecular biology*.

Soliman, N.A. and Yussif, S.M. 2016. Ki-67 as a prognostic marker according to breast cancer molecular subtype. *Cancer biology & medicine*. **13**(4), p496.

Song, B.-L., Wang, C.-H., Yao, X.-M., Yang, L., Zhang, W.-J., Wang, Z.-Z., Zhao, X.-N., Yang, J.-B., Qi, W. and Yang, X.-Y. 2006. Human acyl-CoA: cholesterol acyltransferase 2 gene expression in intestinal Caco-2 cells and in hepatocellular carcinoma. *Biochemical Journal*. **394**(3), pp.617-626.

Soroosh, P., Wu, J., Xue, X., Song, J., Sutton, S.W., Sablad, M., Yu, J., Nelen, M.I., Liu, X. and Castro, G. 2014. Oxysterols are agonist ligands of ROR γ t and drive Th17 cell differentiation. *Proceedings of the National Academy of Sciences*. **111**(33), pp.12163-12168.

Sozen, E., Yazgan, B., Sahin, A., Ince, U. and Ozer, N.K. 2018. High cholesterol diet-induced changes in oxysterol and scavenger receptor levels in heart tissue. *Oxidative medicine and cellular longevity*. **2018**.

Stål, O., Sullivan, S., Wingren, S., Skoog, L., Rutqvist, L.E., Carstensen, J.M. and Nordenskjöld, B. 1995. c-erbB-2 expression and benefit from adjuvant chemotherapy and radiotherapy of breast cancer. *European Journal of Cancer*. **31**(13), pp.2185-2190.

Steyerberg, E.W., Moons, K.G., van der Windt, D.A., Hayden, J.A., Perel, P., Schroter, S., Riley, R.D., Hemingway, H., Altman, D.G. and Group, P. 2013. Prognosis Research Strategy (PROGRESS) 3: prognostic model research. *PLoS Med*. **10**(2), pe1001381.

Stiles, A.R., Kozlitina, J., Thompson, B.M., McDonald, J.G., King, K.S. and Russell, D.W. 2014. Genetic, anatomic, and clinical determinants of human serum sterol and vitamin D levels. *Proceedings of the National Academy of Sciences*. **111**(38), pp.E4006-E4014.

Strushkevich, N., MacKenzie, F., Cherkesova, T., Grabovec, I., Usanov, S. and Park, H.-W. 2011. Structural basis for pregnenolone biosynthesis by the mitochondrial monooxygenase system. *Proceedings of the National Academy of Sciences*. **108**(25), pp.10139-10143.

Subbaiah, P.V., Liu, M. and Witt, T.R. 1997. Impaired cholesterol esterification in the plasma in patients with breast cancer. *Lipids*. **32**(2), pp.157-162.

Sun, X., Mao, Y., Wang, J., Zu, L., Hao, M., Cheng, G., Qu, Q., Cui, D., Keller, E.T., Chen, X., Shen, K. and Wang, J. 2014. IL-6 secreted by cancer-associated fibroblasts induces tamoxifen resistance in luminal breast cancer. *Oncogene*.

Sunryd, J.C., Cheon, B., Graham, J.B., Giorda, K.M., Fissore, R.A. and Hebert, D.N. 2014. TMTC1 and TMTC2 are novel endoplasmic reticulum tetratricopeptide repeat-containing adapter proteins involved in calcium homeostasis. *J Biol Chem*. **289**(23), pp.16085-16099.

Suon, S., Zhao, J., Villarreal, S.A., Anumula, N., Liu, M., Carangia, L.M., Renger, J.J. and Zerbinatti, C.V. 2010. Systemic treatment with liver X receptor agonists raises apolipoprotein E, cholesterol, and amyloid- β peptides in the cerebral spinal fluid of rats. *Molecular Neurodegeneration*. **5**(1), p44.

Svensson, S., Östberg, T., Jacobsson, M., Norström, C., Stefansson, K., Hallén, D., Johansson, I.C., Zachrisson, K., Ogg, D. and Jendeberg, L. 2003. Crystal structure of the heterodimeric complex of LXRA and RXR β ligand-binding domains in a fully agonistic conformation. *The EMBO journal*. **22**(18), pp.4625-4633.

Szedlacsek, S.E., Wasowicz, E., Hulea, S.A., Nishida, H.I., Kummerow, F.A. and Nishida, T. 1995. Esterification of oxysterols by human plasma lecithin-cholesterol acyltransferase. *Journal of Biological Chemistry*. **270**(20), pp.11812-11819.

Tabas, I., Chen, L.L., Clader, J.W., McPhail, A.T., Burnett, D.A., Bartner, P., Das, P.R., Pramanik, B.N., Puar, M.S. and Feinmark, S.J. 1990. Rabbit and human liver contain a novel pentacyclic triterpene ester with acyl-CoA: cholesterol acyltransferase inhibitory activity. *Journal of Biological Chemistry*. **265**(14), pp.8042-8051.

Talley, D.J., Sadowski, J.A., Boler, S.A. and Li, J.J. 1983. Changes in lipid profiles of estrogen-induced and transplanted renal carcinomas in Syrian hamsters. *International journal of cancer*. **32**(5), pp.617-621.

Tam, S.-P., Mok, L., Chimini, G., Vasa, M. and Deeley, R.G. 2006. ABCA1 mediates high-affinity uptake of 25-hydroxycholesterol by membrane vesicles and rapid efflux of oxysterol by intact cells. *American Journal of Physiology-Cell Physiology*. **291**(3), pp.C490-C502.

Tardif, J.-C., Grégoire, J., L'Allier, P.L., Anderson, T.J., Bertrand, O., Reeves, F., Title, L.M., Alfonso, F., Schampaert, E. and Hassan, A. 2004. Effects of the acyl coenzyme A: cholesterol acyltransferase inhibitor avasimibe on human atherosclerotic lesions. *Circulation*. **110**(21), pp.3372-3377.

Tartter, P.I., Papatestas, A.E., Ioannovich, J., Mulvihill, M.N., Lesnick, G. and Aufses Jr, A.H. 1981. Cholesterol and obesity as prognostic factors in breast cancer. *Cancer*. **47**(9), pp.2222-2227.

Tchou, J., Kossenkov, A.V., Chang, L., Satija, C., Herlyn, M., Showe, L.C. and Puré, E. 2012. Human breast cancer associated fibroblasts exhibit subtype specific gene expression profiles. *BMC medical genomics*. **5**(1), p39.

Terasaka, N., Miyazaki, A., Kasanuki, N., Ito, K., Ubukata, N., Koieyama, T., Kitayama, K., Tanimoto, T., Maeda, N. and Inaba, T. 2007. ACAT inhibitor pactimibe sulfate (CS-505) reduces and stabilizes atherosclerotic lesions by cholesterol-lowering and direct effects in apolipoprotein E-deficient mice. *Atherosclerosis*. **190**(2), pp.239-247.

Thirunavukkarasu, C., Selvedhiran, K., Prince Vijaya Singh, J., Senthilnathan, P. and Sakthisekaran, D. 2003. Effect of sodium selenite on lipids and lipid-metabolizing enzymes in N-nitrosodiethylamine-induced hepatoma-bearing rats. *The Journal of Trace Elements in Experimental Medicine: The Official Publication of the International Society for Trace Element Research in Humans*. **16**(1), pp.1-15.

Thorne, J.L., Battaglia, S., Baxter, D.E., Hayes, J.L., Hutchinson, S.A., Jana, S., Millican-Slater, R.A., Smith, L., Teske, M.C. and Wastall, L.M. 2018. MiR-19b non-canonical binding is directed by HuR and confers chemosensitivity through regulation of P-glycoprotein in breast cancer. *Biochimica et Biophysica Acta (BBA)-Gene Regulatory Mechanisms*. **1861**(11), pp.996-1006.

Toledo, E., Salas-Salvadó, J., Donat-Vargas, C., Buil-Cosiales, P., Estruch, R., Ros, E., Corella, D., Fitó, M., Hu, F.B. and Arós, F. 2015. Mediterranean diet and invasive breast cancer risk among women at high cardiovascular risk in the PREDIMED trial: a randomized clinical trial. *JAMA internal medicine*. **175**(11), pp.1752-1760.

Treilleux, I., Blay, J.-Y., Bendriss-Vermare, N., Ray-Coquard, I., Bachelot, T., Guastalla, J.-P., Bremond, A., Goddard, S., Pin, J.-J. and Barthelemy-Dubois, C. 2004. Dendritic cell infiltration and prognosis of early stage breast cancer. *Clinical Cancer Research*. **10**(22), pp.7466-7474.

Trunova, G.V., Makarova, O.V., Diatropov, M.E., Bogdanova, I.M., Mikchailova, L.P. and Abdulaeva, S.O. 2011. Morphofunctional characteristic of the immune system in BALB/c and C57BL/6 mice. *Bull Exp Biol Med*. **151**(1), pp.99-102.

Tsukamoto, F., Shiba, E., Taguchi, T., Sugimoto, T., Watanabe, T., Kim, S.J., Tanji, Y., Kimoto, Y., Izukura, M. and Ai, S.-I. 1997. Immunohistochemical detection of P-glycoprotein in breast cancer and its significance as a prognostic factor. *Breast cancer*. **4**(4), p259.

Uhlen, M., Zhang, C., Lee, S., Sjöstedt, E., Fagerberg, L., Bidkhori, G., Benfeitas, R., Arif, M., Liu, Z. and Edfors, F. 2017a. A pathology atlas of the human cancer transcriptome. *Science*. **357**(6352): <https://www.proteinatlas.org/ENSG00000167780-SOAT2/cell>.

Uhlen, M., Zhang, C., Lee, S., Sjöstedt, E., Fagerberg, L., Bidkhori, G., Benfeitas, R., Arif, M., Liu, Z. and Edfors, F. 2017b. A pathology atlas of the human cancer transcriptome. *Science*. **357**(6352): <https://www.proteinatlas.org/ENSG00000057252-SOAT1/cell>.

Ulven, S.M., Dalen, K.T., Gustafsson, J.A. and Nebb, H.I. 2004. Tissue-specific autoregulation of the LXRA gene facilitates induction of apoE in mouse adipose tissue. *J Lipid Res*. **45**(11), pp.2052-2062.

Van Emburgh, B.O., Hu, J.J., Levine, E.A., Mosley, L.J., Case, L.D., Lin, H.Y., Knight, S.N., Perrier, N.D., Rubin, P. and Sherrill, G.B. 2008. Polymorphisms in drug metabolism genes, smoking, and p53 mutations in breast cancer. *Molecular Carcinogenesis: Published in cooperation with the University of Texas MD Anderson Cancer Center*. **47**(2), pp.88-99.

van Heushen, G.P.H., van der Krift, T.P., Hostetler, K.Y. and Wirtz, K.W. 1983. Effect of nonspecific phospholipid transfer protein on cholesterol esterification in microsomes from Morris hepatomas. *Cancer research*. **43**(9), pp.4207-4210.

Vandermoere, F., El Yazidi-Belkoura, I., Adriaenssens, E., Lemoine, J. and Hondermarck, H. 2005. The antiapoptotic effect of fibroblast growth factor-2 is mediated through nuclear factor-kappaB activation induced via interaction between Akt and IkappaB kinase-beta in breast cancer cells. *Oncogene*. **24**(35), pp.5482-5491.

Vanier, M.T., Wenger, D.A., Comly, M.E., Rousson, R., Brady, R.O. and Pentchev, P.G. 1988. Niemann-Pick disease group C: clinical variability and diagnosis based on defective cholesterol esterification: A collaborative study on 70 patients. *Clinical genetics*. **33**(5), pp.331-348.

Varol, C., Mildner, A. and Jung, S. 2015. Macrophages: development and tissue specialization. *Annual review of immunology*. **33**, pp.643-675.

Veena, K., Shanthi, P. and Sachdanandam, P. 2006. The biochemical alterations following administration of Kalpaamruthaa and Semecarpus anacardium in mammary carcinoma. *Chemico-biological interactions*. **161**(1), pp.69-78.

Vega, G.L., Weiner, M.F., Lipton, A.M., von Bergmann, K., Lütjohann, D., Moore, C. and Svetlik, D. 2003. Reduction in Levels of 24S-Hydroxycholesterol by Statin Treatment in Patients With Alzheimer Disease. *Archives of Neurology*. **60**(4), pp.510-515.

Velling, T., Kusche-Gullberg, M., Sejersen, T. and Gullberg, D. 1999. cDNA cloning and chromosomal localization of human alpha(11) integrin. A collagen-binding, I domain-containing, beta(1)-associated integrin alpha-chain present in muscle tissues. *J Biol Chem*. **274**(36), pp.25735-25742.

Verghese, E.T., Shenoy, H., Cookson, V.J., Green, C.A., Howarth, J., Partanen, R., Pollock, S., Waterworth, A., Speirs, V. and Hughes, T.A. 2011. Epithelial–mesenchymal interactions in breast cancer: evidence for a role of nuclear localized β -catenin in carcinoma-associated fibroblasts. *Histopathology*. **59**(4), pp.609-618.

Vermeulen, A. 1976. The hormonal activity of the postmenopausal ovary. *The Journal of Clinical Endocrinology & Metabolism*. **42**(2), pp.247-253.

Viale, G., Newell, A.E.H., Walker, E., Harlow, G., Bai, I., Russo, L., Dell’Orto, P. and Maisonneuve, P. 2019. Ki-67 (30-9) scoring and differentiation of Luminal A-and Luminal B-like breast cancer subtypes. *Breast cancer research and treatment*. **178**(2), pp.451-458.

Vigne, S., Chalmin, F., Duc, D., Clottu, A.S., Apetoh, L., Lobaccaro, J.-M.A., Christen, I., Zhang, J. and Pot, C. 2017. IL-27-induced type 1 regulatory T-cells produce oxysterols that constrain IL-10 production. *Frontiers in immunology*. **8**, p1184.

Vona-Davis, L., Rose, D.P., Hazard, H., Howard-McNatt, M., Adkins, F., Partin, J. and Hobbs, G. 2008. Triple-negative breast cancer and obesity in a rural Appalachian population. *Cancer Epidemiology and Prevention Biomarkers*. **17**(12), pp.3319-3324.

Wang, H., Yin, Y., Li, W., Zhao, X., Yu, Y., Zhu, J., Qin, Z., Wang, Q., Wang, K. and Lu, W. 2012. Over-expression of PDGFR- β promotes PDGF-induced proliferation, migration, and angiogenesis of EPCs through PI3K/Akt signaling pathway. *PloS one*. **7**(2), pe30503.

Wang, L., Liu, Y. and Yu, G. 2019. Avasimibe inhibits tumor growth by targeting FoxM1-AKR1C1 in osteosarcoma. *OncoTargets and therapy*. **12**, pp.815-823.

Wang, X.M., Kim, H.P., Nakahira, K., Ryter, S.W. and Choi, A.M.K. 2009. The Heme Oxygenase-1/Carbon Monoxide Pathway Suppresses TLR4 Signaling by Regulating the Interaction of TLR4 with Caveolin-1. *The Journal of Immunology*. **182**(6), pp.3809-3818.

Wang, Y.Y., Attané, C., Milhas, D., Dirat, B., Dauvillier, S., Guerard, A., Gilhodes, J., Lazar, I., Alet, N. and Laurent, V. 2017. Mammary adipocytes stimulate breast cancer invasion through metabolic remodeling of tumor cells. *JCI insight*. **2**(4).

Wang, Z., Yang, X., Chen, L., Zhi, X., Lu, H., Ning, Y., Yeong, J., Chen, S., Yin, L., Wang, X. and Li, X. 2017. Upregulation of hydroxysteroid sulfotransferase 2B1b promotes hepatic oval cell proliferation by modulating oxysterol-induced LXR activation in a mouse model of liver injury. *Archives of Toxicology*. **91**(1), pp.271-287.

Warnes GR, B.B., Bonebakker L, Gentleman R, Huber W, Liaw A, Lumley T, Maechler M, Magnusson A, Moeller S, Schwartz M, Venables B. 2020. gplots: Various R programming tools for plotting data2013. R package version 2.12.1.

Weber, C.E., Kothari, A.N., Wai, P.Y., Li, N.Y., Driver, J., Zapf, M.A.C., Franzen, C.A., Gupta, G.N., Osipo, C., Zlobin, A., Syn, W.K., Zhang, J., Kuo, P.C. and Mi, Z. 2015. Osteopontin mediates an MZF1–TGF- β 1-dependent transformation of mesenchymal stem cells into cancer-associated fibroblasts in breast cancer. *Oncogene*. **34**(37), pp.4821-4833.

Websdale, A., Kiew, Y., Chalmers, P., Chen, X., Cioccoloni, G., Hughes, T.A., Luo, X., Mwarzi, R., Poirot, M., Røberg-Larsen, H., Wu, R., Xu, M., Zulyniak, M.A. and Thorne, J.L. 2021. Pharmacologic and genetic inhibition of cholesterol esterification enzymes reduces tumour burden: a systematic review and meta-analysis of preclinical models. *Biochemical Pharmacology*. p114731.

Wei, L., Lu, X., Weng, S., Zhu, S. and Chen, Y. 2021. Cholesteryl Ester Promotes Mammary Tumor Growth in MMTV-PyMT Mice and Activates Akt-mTOR Pathway in Tumor Cells. *Biomolecules*. **11**(6), p853.

Wendel, M., Galani, I.E., Suri-Payer, E. and Cerwenka, A.J.C.r. 2008. Natural killer cell accumulation in tumors is dependent on IFN- γ and CXCR3 ligands. **68**(20), pp.8437-8445.

Wielinga, P.R., Westerhoff, H.V. and Lankelma, J. 2000. The relative importance of passive and P-glycoprotein mediated anthracycline efflux from multidrug-resistant cells. *European journal of biochemistry*. **267**(3), pp.649-657.

Williams, R.J., McCarthy, A.D. and Sutherland, C.D. 1989. Esterification and absorption of cholesterol: in vitro and in vivo observations in the rat. *Biochimica et Biophysica Acta (BBA) - Lipids and Lipid Metabolism*. **1003**(2), pp.213-216.

Wood, R., Chumbler, F. and Wiegand, R.D. 1978. Effect of dietary cyclopropene fatty acids on the octadecenoates of individual lipid classes of rat liver and hepatoma. *Lipids*. **13**(4), pp.232-238.

Wright, H.J., Hou, J., Xu, B., Cortez, M., Potma, E.O., Tromberg, B.J. and Razorenova, O.V. 2017. CDCP1 drives triple-negative breast cancer metastasis through reduction of lipid-droplet abundance and stimulation of fatty acid oxidation. *Proceedings of the National Academy of Sciences of the United States of America*. **114**(32), pp.E6556-E6565.

Wu, C.-Y., Chen, Y.-J., Ho, H.J., Hsu, Y.-C., Kuo, K.N., Wu, M.-S. and Lin, J.-T. 2012. Association between nucleoside analogues and risk of hepatitis B virus–related hepatocellular carcinoma recurrence following liver resection. *Jama*. **308**(18), pp.1906-1913.

Wu, Q., Ishikawa, T., Sirianni, R., Tang, H., McDonald, J.G., Yuhanna, I.S., Thompson, B., Girard, L., Mineo, C. and Brekken, R.A. 2013. 27-Hydroxycholesterol promotes cell-autonomous, ER-positive breast cancer growth. *Cell reports*. **5**(3), pp.637-645.

Wu, Q., Ishikawa, T., Sirianni, R., Tang, H., McDonald, J.G., Yuhanna, I.S., Thompson, B., Girard, L., Mineo, C., Brekken, R.A., Umetani, M., Euhus, D.M., Xie, Y. and Shaul, P.W. 2013. 27-Hydroxycholesterol promotes cell-autonomous, ER-positive breast cancer growth. *Cell Rep.* **5**(3), pp.637-645.

Wu, S.Z., Roden, D.L., Wang, C., Holliday, H., Harvey, K., Cazet, A.S., Murphy, K.J., Pereira, B., Al-Eryani, G. and Bartonicek, N. 2020. Stromal cell diversity associated with immune evasion in human triple-negative breast cancer. *The EMBO Journal.* **39**(19), pe104063.

Xiong, H., Yan, T., Zhang, W., Shi, F., Jiang, X., Wang, X., Li, S., Chen, Y., Chen, C. and Zhu, Y. 2018. miR-613 inhibits cell migration and invasion by downregulating Daam1 in triple-negative breast cancer. *Cellular signalling.* **44**, pp.33-42.

Xiong, K., Wang, G., Peng, T., Zhou, F., Chen, S., Liu, W., Ju, L., Xiao, Y., Qian, K. and Wang, X. 2021. The cholesterol esterification inhibitor avasimibe suppresses tumour proliferation and metastasis via the E2F-1 signalling pathway in prostate cancer. *Cancer Cell International.* **21**(1), p461.

Xu, H., Xia, H., Zhou, S., Tang, Q. and Bi, F. 2021. Cholesterol activates the Wnt/PCP-YAP signaling in SOAT1-targeted treatment of colon cancer. *Cell death discovery.* **7**(1), pp.1-13.

Xu, M., Zhou, H., Tan, K.C.B., Guo, R., Shiu, S.W.M. and Wong, Y. 2009. ABCG1 mediated oxidized LDL-derived oxysterol efflux from macrophages. *Biochemical and Biophysical Research Communications.* **390**(4), pp.1349-1354.

Yamada, A., Ishikawa, T., Ota, I., Kimura, M., Shimizu, D., Tanabe, M., Chishima, T., Sasaki, T., Ichikawa, Y. and Morita, S. 2013. High expression of ATP-binding cassette transporter ABCB11 in breast tumors is associated with aggressive subtypes and low disease-free survival. *Breast cancer research and treatment.* **137**(3), pp.773-782.

Yamaguchi, J., Moriuchi, H., Ueda, T., Kawashita, Y., Hazeyama, T., Tateishi, M., Aoki, S., Uchihashi, K. and Nakamura, M. 2021. Active behavior of triple-negative breast cancer with adipose tissue invasion: a single center and retrospective review. *BMC Cancer.* **21**(1), p434.

Yamamuro, D., Yamazaki, H., Osuga, J.-i., Okada, K., Wakabayashi, T., Takei, A., Takei, S., Takahashi, M., Nagashima, S. and Holleboom, A.G. 2020. Esterification of 4 β -hydroxycholesterol and other oxysterols in human plasma occurs independently of LCAT. *Journal of lipid research.* **61**(9), pp.1287-1299.

Yang, B., Radcliff, C., Hughes, D., Kelemen, S. and Rizzo, V. 2011. p190 RhoGTPase-activating protein links the β 1 integrin/caveolin-1 mechanosignaling complex to RhoA and actin remodeling. *Arteriosclerosis, thrombosis, and vascular biology.* **31**(2), pp.376-383.

Yang, C., McDonald, J.G., Patel, A., Zhang, Y., Umetani, M., Xu, F., Westover, E.J., Covey, D.F., Mangelsdorf, D.J. and Cohen, J.C. 2006. Sterol intermediates from cholesterol biosynthetic pathway as liver X receptor ligands. *Journal of Biological Chemistry.* **281**(38), pp.27816-27826.

Yang, Q., Goding, S., Hokland, M. and Basse, P. 2006. Antitumor activity of NK cells. *Immunologic research.* **36**(1), pp.13-25.

Yang, W., Bai, Y., Xiong, Y., Zhang, J., Chen, S., Zheng, X., Meng, X., Li, L., Wang, J., Xu, C., Yan, C., Wang, L., Chang, C.C.Y., Chang, T.-Y., Zhang, T., Zhou, P., Song, B.-L., Liu, W., Sun, S.-c., Liu, X., Li, B.-I. and Xu, C. 2016. Potentiating the antitumour response of CD8(+) T cells by modulating cholesterol metabolism. *Nature.* **531**(7596), pp.651-655.

Yantsevich, A.V., Dichenko, Y.V., MacKenzie, F., Mukha, D.V., Baranovsky, A.V., Gilep, A.A., Usanov, S.A. and Strushkevich, N.V. 2014. Human steroid and oxysterol 7 α -hydroxylase CYP 7B1: substrate specificity,azole binding and misfolding of clinically relevant mutants. *The FEBS journal.* **281**(6), pp.1700-1713.

Yao, S., Sucheston, L.E., Millen, A.E., Johnson, C.S., Trump, D.L., Nesline, M.K., Davis, W., Hong, C.-C., McCann, S.E. and Hwang, H. 2011. Pretreatment serum concentrations of 25-hydroxyvitamin D and breast cancer prognostic characteristics: a case-control and a case-series study. *PLoS one*. **6**(2), pe17251.

Ye, J.-H., Wang, X.-H., Shi, J.-J., Yin, X., Chen, C., Chen, Y., Wu, H.-Y., Jiong, S., Sun, Q., Zhang, M., Shi, X.-B., Zhou, G.-R., Hassan, S., Feng, J.-F., Xu, X.-Y. and Zhang, W.-J. 2021. Tumor-associated macrophages are associated with response to neoadjuvant chemotherapy and poor outcomes in patients with triple-negative breast cancer. *Journal of Cancer*. **12**(10), pp.2886-2892.

Yuan, Z.-Y., Luo, R.-Z., Peng, R.-J., Wang, S.-S. and Xue, C. 2014. High infiltration of tumor-associated macrophages in triple-negative breast cancer is associated with a higher risk of distant metastasis. *Oncotargets and therapy*. **7**, p1475.

Yue, S., Li, J., Lee, S.-Y., Lee, Hyeon J., Shao, T., Song, B., Cheng, L., Masterson, Timothy A., Liu, X., Ratliff, Timothy L. and Cheng, J.-X. 2014. Cholesteryl Ester Accumulation Induced by PTEN Loss and PI3K/AKT Activation Underlies Human Prostate Cancer Aggressiveness. *Cell Metabolism*. **19**(3), pp.393-406.

Zhang, J., Larsson, O. and Sjövall, J. 1995. 7 α -Hydroxylation of 25-hydroxycholesterol and 27-hydroxycholesterol in human fibroblasts. *Biochimica et Biophysica Acta (BBA)-Lipids and Lipid Metabolism*. **1256**(3), pp.353-359.

Zhang, M., Qiu, L., Zhang, Y., Xu, D., Zheng, J.C. and Jiang, L. 2017. CXCL12 enhances angiogenesis through CXCR7 activation in human umbilical vein endothelial cells. *Scientific Reports*. **7**(1), p8289.

Zhang, Q., Yang, J., Bai, J. and Ren, J. 2018. Reverse of non-small cell lung cancer drug resistance induced by cancer-associated fibroblasts via a paracrine pathway. *Cancer science*. **109**(4), pp.944-955.

Zhang, Y., Repa, J.J., Gauthier, K. and Mangelsdorf, D.J. 2001. Regulation of lipoprotein lipase by the oxysterol receptors, LXRalpha and LXRbeta. *J Biol Chem*. **276**(46), pp.43018-43024.

Zhao, L., Liu, Y., Zhao, F., Jin, Y., Feng, J., Geng, R., Sun, J., Kang, L., Yu, L. and Wei, Y. 2020. Inhibition of cholesterol esterification enzyme enhances the potency of human chimeric antigen receptor T cells against pancreatic carcinoma. *Molecular Therapy-Oncolytics*. **16**, pp.262-271.

Zhou, J., Wang, X.-H., Zhao, Y.-X., Chen, C., Xu, X.-Y., Sun, Q., Wu, H.-Y., Chen, M., Sang, J.-F., Su, L., Tang, X.-Q., Shi, X.-B., Zhang, Y., Yu, Q., Yao, Y.-Z. and Zhang, W.-J. 2018. Cancer-Associated Fibroblasts Correlate with Tumor-Associated Macrophages Infiltration and Lymphatic Metastasis in Triple Negative Breast Cancer Patients. *Journal of Cancer*. **9**(24), pp.4635-4641.

Zhu, K., Pan, Q., Zhang, X., Kong, L.-Q., Fan, J., Dai, Z., Wang, L., Yang, X.-R., Hu, J., Wan, J.-L., Zhao, Y.-M., Tao, Z.-H., Chai, Z.-T., Zeng, H.-Y., Tang, Z.-Y., Sun, H.-C. and Zhou, J. 2013. MiR-146a enhances angiogenic activity of endothelial cells in hepatocellular carcinoma by promoting PDGFRA expression. *Carcinogenesis*. **34**(9), pp.2071-2079.

Zhu, Y., Chen, C.-Y., Li, J., Cheng, J.-X., Jang, M. and Kim, K.-H. 2018. In vitro exploration of ACAT contributions to lipid droplet formation during adipogenesis [S]. *Journal of lipid research*. **59**(5), pp.820-829.